

Cover Page



Universiteit Leiden



The handle <http://hdl.handle.net/1887/25491> holds various files of this Leiden University dissertation

Author: Vorst, Joost van der

Title: Near-infrared fluorescence-guided surgery : pre-clinical validation and clinical translation

Issue Date: 2014-05-01

Near-infrared fluorescence-guided surgery

Pre-clinical validation and clinical translation

Joost van der Vorst

© J.R. van der Vorst, 2014

ISBN/EAN: 978-90-6464-766-6

Cover design: Flavoureyes, www.flavoureyes.com

Design and lay-out: Ferdinand van Nispen, www.citroenvlinder-dtp.nl, Bilthoven

Printed by: GVO drukkers & vormgevers B.V. | Ponsen & Looijen, Ede

The author of this thesis is a MD-medical research trainee funded by The Netherlands Organisation for Health Research and Development (grant nr. 92003593). The research described in this thesis was financially supported by the Center for Translational Molecular Medicine (CTMM, DeCoDe and MUSIS projects), the Dutch Cancer Society (UL 2010-4732), Foundation "Michaël van Vloten", Foundation "De Drie Lichten", Leiden University Fund (LUF).

Financial support by Krijnen Medical, Amgen, Percuros, Chipsoft, PerkinElmer, Bayer, Guerbet, Astellas Pharma, Intuitive Surgical, Convatec, Welmed, Erbe, Karl Storz, OnTarget, ABN Amro, Pfizer, Oldelft, PI Medical Diagnostics, the Dutch Society of Gastroenterology, stichting Wetenschappelijk Onderzoek Heelkunde Groene Hart Ziekenhuis and het doelfonds beeldverwerking van de Bontiusstichting for the printing of this thesis is gratefully acknowledged.

Near-infrared fluorescence-guided surgery

Pre-clinical validation and clinical translation

Proefschrift

ter verkrijging van
de graad van Doctor aan de Universiteit Leiden,
op gezag van Rector Magnificus prof.mr. C.J.J.M. Stolker,
volgens besluit van het College voor Promoties
te verdedigen op donderdag 1 mei 2014
klokke 15:00 uur

door

Joost Renier van der Vorst

geboren te Geldrop in 1984

Promotiecommissie

Promotor: Prof. dr. C.J.H. van de Velde

Co-promotor: Dr. A.L. Vahrmeijer

Overige leden: Prof. dr. C.W.G.M. Löwik
Prof. dr. B.P.F. Lelieveldt
Prof. dr. V.T.H.B.M. Smit
Prof. dr. C.H.C. Dejong (Universiteit van Maastricht)

CONTENTS

Chapter 1	General introduction and outline of thesis	9
Part I:	Pre-clinical validation of near-infrared fluorescence guided surgery	19
Chapter 2	Near-infrared fluorescence imaging of liver metastases in rats using indocyanine green	21
Chapter 3	Intraoperative fluorescence delineation of head and neck cancer with a fluorescent anti-epidermal growth factor receptor nanobody	35
Chapter 4	Near-infrared fluorescence imaging of both colorectal cancer and ureters using a low-dose integrin targeted probe	57
Part II:	Clinical translation: Sentinel lymph node imaging	73
Chapter 5	Optimization of near-infrared fluorescent sentinel lymph node mapping for vulvar cancer	75
Chapter 6	Optimization of near-infrared fluorescent sentinel lymph node mapping in cervical cancer patients	87
Chapter 7	Randomized comparison of near-infrared fluorescence lymphatic tracers for sentinel lymph node mapping of cervical cancer	101
Chapter 8	Dose optimization for near-infrared fluorescence sentinel lymph node mapping in patients with melanoma	115
Chapter 9	Near-infrared fluorescence sentinel lymph node mapping of the oral cavity in head and neck cancer patients.	131
Chapter 10	Randomized comparison of near-infrared fluorescence imaging using indocyanine green and ^{99m} technetium with or without patent blue for the sentinel lymph node procedure in breast cancer patients	141

Part III:	Clinical translation: Solid tumor imaging	157
Chapter 11	Near-infrared fluorescence-guided resection of colorectal liver metastases	161
Chapter 12	Near-infrared fluorescence imaging in patients undergoing pancreaticoduodenectomy	175
Chapter 13	Intraoperative near-infrared fluorescence imaging of parathyroid adenomas using low-dose methylene blue	191
Chapter 14	Near-infrared fluorescence imaging of a solitary fibrous tumor of the pancreas using methylene blue	205
Part IV		215
Chapter 15	Summary and Future Perspectives	217
	Nederlandse samenvatting	230
	List of Publications	235
	Curriculum Vitae	240
	Dankwoord	241

Chapter 1

General introduction and outline of thesis

Adapted from:

Vahrmeijer AL, Hutteman M, van der Vorst JR, van de Velde CJ, Frangioni JV. Image-guided cancer surgery using near-infrared fluorescence, *Nat Rev Clin Oncol*. 2013 Sep;10(9):507-18

Verbeek FP, van der Vorst JR, Schaafsma BE, Hutteman M, Bonsing BA, van Leeuwen FW, Frangioni JV, van de Velde CJ, Swijnenburg RJ, Vahrmeijer AL. Intraoperative near-infrared fluorescence imaging in hepato-pancreatobiliary surgery, *J Hepatobiliary Pancreat Sci*. 2012 Nov;19(6):626-37

Schaafsma BE, Mieog JS, Hutteman M, van der Vorst JR, Kuppen PJ, Löwik CW, Frangioni JV, van de Velde CJ, Vahrmeijer AL. The clinical use of indocyanine green as a near-infrared fluorescent contrast agent for image-guided oncologic surgery. *J Surg Oncol*. 2011 Sep 1;104(3):323-32

Paradigm shifts in surgery arise when surgeons are empowered to perform surgery faster, better, and/or less expensively than current standards. For most solid tumors, surgical resection remains the only curative treatment. Improvements in preoperative imaging techniques have made a meaningful impact on cancer patient care. However, the determination of a safe resection margin and the assessment of distant metastases during surgery can be challenging since only a limited number of tools are available intraoperatively. For certain indications such as colorectal liver metastases, intraoperative ultrasound is being used to identify tumors.¹ However, during most cancer surgeries, the eyes and hands of the surgeon remain the dominant “imaging modalities” used to decide which tissue needs to be resected, i.e., malignant cells, and which tissue needs to be avoided, i.e., normal cells. Palpation and visual inspection are not always sufficient for discriminating between tissue types, though, leading to irradical resections or unnecessary removal of healthy tissue. Unfortunately, this results in relatively high occurrence of irradical tumor resections and high recurrence rates. In breast cancer, for example, many of which are non-palpable, margin positivity rates range from 5 to 49%^{2,3} and local recurrence rates following breast-conservative therapy of 6.7 to 11% are reported.⁴ Furthermore, the identification of vital structures (e.g. nerves, ureters, bile ducts) during surgery, which is imperative to minimize comorbidity, can be challenging. These gaps in surgical techniques and surgical management of cancer patients show that there is a need for imaging modalities that can provide surgeons with real-time visual information during surgery about the location of tissues to be resected and tissues to be spared.

Near-infrared fluorescence optical imaging

Medical imaging is generally based on and also used for obtaining contrast between tissues of interest and surrounding tissues. In this perspective, two different contrast methods can be distinguished: endogenous and exogenous contrast methods. Endogenous contrast methods use natural optical properties of tissue where exogenous contrast methods necessitate the administration of contrast agents. A typical example of a endogenous contrast method is measuring the oxygenation status of tissue by using the absorbing properties of by oxygen saturated hemoglobin or using ultrasound waves for the detection of liver metastases. However, with regards to tumor imaging or imaging of vital structures, endogenous contrast methods often suffer from low sensitivity, specificity and low resolution. For this purpose, exogenous contrast methods are more feasible in most cases.

Exogenous methods using fluorescence are based on the administration of a contrast agent with fluorescent properties (a fluorophore). Over the past several years, intraoperative imaging using invisible near-infrared (NIR) fluorescent light has entered the surgical theatre to fill the gap between preoperative imaging and intraoperative reality.⁵⁻⁷ Near-infrared (NIR) fluorescence optical imaging is a technique that is based on the use of fluorophores and invisible light ranging from 700 to 900 nm in wavelength. Whereas visible light penetrates tissue on a micron scale, NIR light (700 nm - 900 nm) can travel millimeters, up to centimeters, through tissue.⁸ Because tissue exhibits almost no autofluorescence in the NIR spectrum, the signal-to-background can be maximized using NIR fluorescent contrast agents, creating “white stars in a black sky”.^{9,10} In addition, it does not use ionizing radiation, making it an inherently safe technique provided that attention is paid to laser illumination levels. And, as NIR light is invisible to the human eye, it does not alter the look of the surgical field, thus minimizing the learning curve. Specialized intraoperative imaging systems for open surgery¹¹⁻¹⁷, laparoscopy^{18,19}, thoracoscopy^{20,21}, and robotic surgery^{22,23} have recently become available for clinical trials. Using these systems, NIR fluorescent contrast agents can be visualized with acquisition times in the millisecond range, enabling real-time guidance during surgery (Figure 1).

Sentinel lymph node imaging

Sentinel lymph node (SLN) mapping, introduced for the management of cutaneous melanoma by Morton et al.²⁴, is nowadays standard-of-care in a variety of cancers, including breast cancer and cutaneous melanoma. Currently, most centers perform SLN mapping using a radioactive tracer, a visible blue dye such as isosulfan blue or patent blue, or a combination of the two. Although in most cases acceptable results are obtained using these methods, they both have some drawbacks. Visible blue dyes stain the patient and the surgical field and cannot be visualized below the surface of tissue. Thereby, tattooing of the skin can last for months after surgery. Radioactive tracers expose patients and caregivers to ionizing radiation, are expensive, and imaging suffers from poor spatial and temporal resolution. For SLN mapping using NIR fluorescence imaging, contrast agents are injected at a low concentration with no staining of the surgical field, no ionizing radiation is used, and an improvement is observed over blue dyes in terms of depth sensitivity.

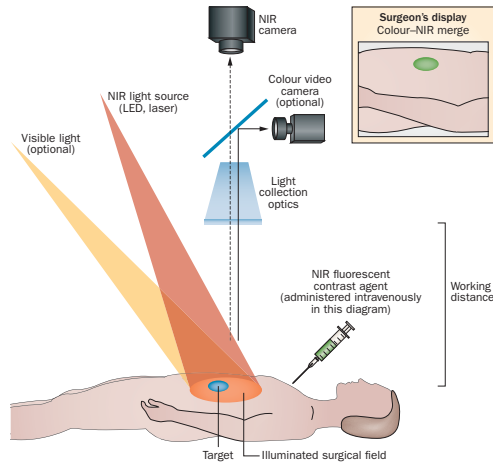


Figure 1 - The mechanics of NIR fluorescence imaging

The mechanics of NIR fluorescence imaging. NIR fluorescent contrast agents are administered intravenously, topically or intraparenchymally. During surgery, the agent is visualized using an NIR fluorescence imaging system of the desired form factor (above the surgical field for open surgery, or encased within a fiberscope for minimally-invasive and robotic surgery). All systems must have adequate NIR excitation light, collection optics, filtration and a camera sensitive to NIR fluorescence emission light. An optimal imaging system includes simultaneous visible (white) light illumination of the surgical field, which can be merged with the generated NIR fluorescence images. The surgeon's display can be one of several form factors, including a standard computer monitor, goggles or a wall projector. Current imaging systems operate at a sufficient working distance that enables the surgeon to operate and illuminates a sizable surgical field. Abbreviations: LED, light-emitting diode; NIR, near-infrared.

For SLN mapping, targeted contrast agents are not necessary. Since indocyanine green (ICG) is the only 800 nm NIR fluorescent contrast agent that is approved for sentinel lymph node mapping by the Food and Drug Administration (FDA) or the European Medicines Agency (EMA), many SLN studies were undertaken as soon as the first intraoperative imaging systems became available. Numerous clinical studies have shown feasibility of NIR fluorescence imaging using ICG for the SLN procedure in breast cancer^{15,25}, gastrointestinal cancers^{26,27}, prostate cancer¹⁹ and other tumor types²⁸. A few research groups premixed ICG with human serum albumin (HSA; complex is ICG:HSA) to improve retention in the first draining lymph node and to increase fluorescence. However, no advantage of using ICG:HSA over ICG alone was shown in breast cancer²⁵, cervical cancer²⁹ and vulvar cancer³⁰. Another approach is the combined use of radioactive nanocolloids and ICG. This combination permits preoperative planning and intraoperative localization of deeply located SLNs with direct optical guidance by a single lymphatic tracer. Several proof of principle studies showed the feasibility of using the ICG-^{99m}Tc-nanocolloid^{19,28,31}.

Tumor imaging

One of the key applications in cancer surgery is intraoperative tumor visualization. In order to visualize tumors using NIR fluorescence imaging, a contrast agent should accumulate in or around a tumor. To date, NIR fluorescent contrast agents specific for many different targets have been developed, including agents for cancer cells³²⁻³⁴, sentinel lymph nodes^{28,35,36}, neurological diseases^{37,38}, cardiovascular diseases^{39,40}, skeletal processes⁴¹, renally cleared agents for ureter imaging⁴², and hepatically cleared agents for bile duct imaging^{43,44}. Optically-active nerve cell agents have also been described, but are yet to achieve NIR wavelengths.^{45,46} Although a variety of tumor specific NIR fluorescent contrast agents have been applied preclinically, none of these has obtained full clinical approval by either the FDA or EMA.

Intraoperative NIR fluorescence imaging depends on the availability of a NIR fluorescent contrast agent and an intraoperative imaging system to visualize the otherwise invisible contrast agent during surgery.⁷ As stated before, ICG is the only 800 nm NIR fluorescent contrast agent that is approved for near-infrared fluorescence imaging. Methylene blue (MB) has been applied clinically for many years as a visible (dark blue) contrast agent. As MB was introduced into clinical practice in an era where no formal approval was needed, no evaluation by the FDA, EMA, or comparable authorities has been performed, but it remains widely used. When sufficiently diluted, MB acts as a 700 nm fluorophore. ICG is clinically used to test the clearance capacity of the liver and MB is used for the macroscopic identification of ureters and parathyroid glands. These agents can be successfully deployed using naturally occurring mechanisms of the human body, which result in accumulation of the agent. Using ICG and MB first-in-human intraoperative tumor imaging studies have been published in various cancer types.⁴⁷⁻⁵¹ A disadvantage of both fluorophores however is the inability to conjugate them to tissue-specific ligands such as an antibody or peptide. Novel NIR fluorophores have been developed which can be easily conjugated to targeting ligands (antibodies, nanobodies, peptides) using straightforward chemistry techniques and have optimized fluorescent properties. Using these 'targeting' fluorophores, several preclinical studies have been performed to identify tumors during surgery.

OUTLINE OF THE THESIS

This thesis is divided in three parts; **Part I** focuses on preclinical validation of NIR fluorescence imaging of solid tumors and tumor metastases, **Part II** describes the clinical use and optimization of NIR fluorescence for the sentinel lymph node procedure and **Part III** describes the clinical introduction of NIR fluorescent imaging of solid tumors.

Part I, chapter 2 describes the intraoperative use of indocyanine green (ICG) administered at different time-points in different doses for NIR fluorescence imaging of colorectal liver metastases in an experimental rat model. **Chapter 3** describes the use of a NIR fluorescent nanobody targeting the EGF-receptor in an experimental orthotopic tongue tumor mouse model. **Chapter 4** shows the successful use of the novel cRGD-ZW800-1 probe in a subcutaneous and orthotopic colon cancer mouse model.

Part II shows the use of NIR fluorescence imaging and ICG premixed with human serum albumin (complex: ICG:HSA) for SLN mapping in vulvar cancer in **chapter 5** and cervical cancer in **chapter 6**. A randomized comparison of ICG with or without premixing with HSA in cervical cancer patients was reported in **chapter 7**. **Chapter 8** demonstrates the use of ICG:HSA and NIR fluorescence in melanoma patients. **Chapter 9** shows the use of NIR fluorescence imaging for SLN mapping in head and neck cancer patients. **Chapter 10** demonstrates a randomized comparison of using ICG with or without patent blue for SLN mapping in breast cancer patients.

Part III, chapter 11 reports the clinical use of NIR fluorescence imaging and ICG to identify occult otherwise missed colorectal liver metastases during surgery. **Chapter 12** demonstrates the attempt to intraoperatively visualize pancreatic tumors after an intravenous injection of ICG. Besides, NIR fluorescence imaging of bile ducts was explored. **Chapter 13** describes the use of NIR fluorescence and methylene blue for the intraoperative identification of parathyroid adenomas. **Chapter 14** describes a patient suffering from a solitary fibrous tumor of the pancreas, which was intraoperatively clearly visualized using NIR fluorescence and methylene blue for the first time in literature.

Finally, all results are summarized and discussed and future perspectives are given in **chapter 15**.

REFERENCES

1. Kruskal JB, Kane RA. Intraoperative US of the liver: techniques and clinical applications. *Radiographics* 2006; 26:1067-1084.
2. Rizzo M, Iyengar R, Gabram SG et al. The effects of additional tumor cavity sampling at the time of breast-conserving surgery on final margin status, volume of resection, and pathologist workload. *Ann Surg Oncol* 2010; 17:228-234.
3. McLaughlin SA. Surgical management of the breast: breast conservation therapy and mastectomy. *Surg Clin North Am* 2013; 93:411-428.
4. Clarke M, Collins R, Darby S et al. Effects of radiotherapy and of differences in the extent of surgery for early breast cancer on local recurrence and 15-year survival: an overview of the randomised trials. *Lancet* 2005; 366:2087-2106.
5. Schaafsma BE, Mieog JS, Hutteman M et al. The clinical use of indocyanine green as a near-infrared fluorescent contrast agent for image-guided oncologic surgery. *J Surg Oncol* 2011; 104:323-332.
6. Verbeek FP, van der Vorst JR, Schaafsma BE et al. Image-guided hepatopancreatobiliary surgery using near-infrared fluorescent light. *J Hepatobiliary Pancreat Sci* 2012; 19:626-637.
7. Gioux S, Choi HS, Frangioni JV. Image-guided surgery using invisible near-infrared light: fundamentals of clinical translation. *Mol Imaging* 2010; 9:237-255.
8. Chance B. Near-infrared images using continuous, phase-modulated, and pulsed light with quantitation of blood and blood oxygenation. *Ann N Y Acad Sci* 1998; 838:29-45.
9. Frangioni JV. In vivo near-infrared fluorescence imaging. *Curr Opin Chem Biol* 2003; 7:626-634.
10. Vahrmeijer AL, Hutteman M, van der Vorst JR et al. Image-guided cancer surgery using near-infrared fluorescence. *Nat Rev Clin Oncol* 2013.
11. Phillips BT, Lanier ST, Conkling N et al. Intraoperative perfusion techniques can accurately predict mastectomy skin flap necrosis in breast reconstruction: results of a prospective trial. *Plast Reconstr Surg* 2012; 129:778e-788e.
12. Hirche C, Engel H, Kolios L et al. An experimental study to evaluate the fluobeam 800 imaging system for fluorescence-guided lymphatic imaging and sentinel node biopsy. *Surg Innov* 2013; 20:516-523.
13. Gotoh K, Yamada T, Ishikawa O et al. A novel image-guided surgery of hepatocellular carcinoma by indocyanine green fluorescence imaging navigation. *J Surg Oncol* 2009; 100:75-79.
14. Troyan SL, Kianzad V, Gibbs-Strauss SL et al. The FLARE intraoperative near-infrared fluorescence imaging system: a first-in-human clinical trial in breast cancer sentinel lymph node mapping. *Ann Surg Oncol* 2009; 16:2943-2952.
15. Mieog JS, Troyan SL, Hutteman M et al. Toward optimization of imaging system and lymphatic tracer for near-infrared fluorescent sentinel lymph node mapping in breast cancer. *Ann Surg Oncol* 2011; 18:2483-2491.
16. Crane LM, Themelis G, Pleijhuis RG et al. Intraoperative multispectral fluorescence imaging for the detection of the sentinel lymph node in cervical cancer: a novel concept. *Mol Imaging Biol* 2011; 13:1043-1049.
17. Yamauchi K, Nagafuji H, Nakamura T et al. Feasibility of ICG fluorescence-guided sentinel node biopsy in animal models using the HyperEye Medical System. *Ann Surg Oncol* 2011; 18:2042-2047.
18. Cahill RA, Anderson M, Wang LM et al. Near-infrared (NIR) laparoscopy for intraoperative lymphatic road-mapping and sentinel node identification during definitive surgical resection of early-stage colorectal neoplasia. *Surg Endosc* 2011.
19. van der Poel HG, Buckle T, Brouwer OR et al. Intraoperative laparoscopic fluorescence guidance to the sentinel lymph node in prostate cancer patients: clinical proof of concept of an integrated functional imaging approach using a multimodal tracer. *Eur Urol* 2011; 60:826-833.
20. Moroga T, Yamashita S, Tokuiishi K et al. Thoracoscopic segmentectomy with intraoperative evaluation of sentinel nodes for stage I non-small cell lung cancer. *Ann Thorac Cardiovasc Surg* 2012; 18:89-94.
21. Yamashita S, Tokuiishi K, Anami K et al. Video-assisted thoracoscopic indocyanine green fluorescence imaging system shows sentinel lymph nodes in non-small-cell lung cancer. *J Thorac Cardiovasc Surg* 2011; 141:141-144.

22. Borofsky MS, Gill IS, Hemal AK et al. Near-infrared fluorescence imaging to facilitate super-selective arterial clamping during zero-ischaemia robotic partial nephrectomy. *BJU Int* 2013; 111:604-610.
23. Spinoglio G, Priora F, Bianchi PP et al. Real-time near-infrared (NIR) fluorescent cholangiography in single-site robotic cholecystectomy (SSRC): a single-institutional prospective study. *Surg Endosc* 2013; 27:2156-2162.
24. Morton DL, Wen DR, Wong JH et al. Technical details of intraoperative lymphatic mapping for early stage melanoma. *Arch Surg* 1992; 127:392-399.
25. Hutteman M, Mieog JS, van der Vorst JR et al. Randomized, double-blind comparison of indocyanine green with or without albumin premixing for near-infrared fluorescence imaging of sentinel lymph nodes in breast cancer patients. *Breast Cancer Res Treat* 2011; 127:163-170.
26. Schaafsma BE, Verbeek FP, van der Vorst JR et al. Ex vivo sentinel node mapping in colon cancer combining blue dye staining and fluorescence imaging. *J Surg Res* 2013; 183:253-257.
27. Tajima Y, Yamazaki K, Masuda Y et al. Sentinel node mapping guided by indocyanine green fluorescence imaging in gastric cancer. *Ann Surg* 2009; 249:58-62.
28. Brouwer OR, Klop WM, Buckle T et al. Feasibility of Sentinel Node Biopsy in Head and Neck Melanoma Using a Hybrid Radioactive and Fluorescent Tracer. *Ann Surg Oncol* 2011; 19:1988-1994.
29. Schaafsma BE, van der Vorst JR, Gaarenstroom KN et al. Randomized comparison of near-infrared fluorescence lymphatic tracers for sentinel lymph node mapping of cervical cancer. *Gynecol Oncol* 2012; 127:126-130.
30. Schaafsma BE, Verbeek FP, Peters AA et al. Near-infrared fluorescence sentinel lymph node biopsy in vulvar cancer: a randomised comparison of lymphatic tracers. *BJOG* 2013; 120:758-764.
31. Schaafsma BE, Verbeek FP, Rietbergen DD et al. Clinical trial of combined radio- and fluorescence-guided sentinel lymph node biopsy in breast cancer. *Br J Surg* 2013; 100:1037-1044.
32. Weissleder R, Tung CH, Mahmood U et al. In vivo imaging of tumors with protease-activated near-infrared fluorescent probes. *Nat Biotechnol* 1999; 17:375-378.
33. Choi HS, Gibbs SL, Lee JH et al. Targeted zwitterionic near-infrared fluorophores for improved optical imaging. *Nat Biotechnol* 2013; 31:148-153.
34. Olson ES, Jiang T, Aguilera TA et al. Activatable cell penetrating peptides linked to nanoparticles as dual probes for in vivo fluorescence and MR imaging of proteases. *Proc Natl Acad Sci U S A* 2010; 107:4311-4316.
35. Ohnishi S, Lomnes SJ, Laurence RG et al. Organic alternatives to quantum dots for intraoperative near-infrared fluorescent sentinel lymph node mapping. *Mol Imaging* 2005; 4:172-181.
36. Emerson DK, Limmer KK, Hall DJ et al. A receptor-targeted fluorescent radiopharmaceutical for multiple-reporter sentinel lymph node imaging. *Radiology* 2012; 265:186-193.
37. Hyde D, de KR, MacLaurin SA et al. Hybrid FMT-CT imaging of amyloid-beta plaques in a murine Alzheimer's disease model. *Neuroimage* 2009; 44:1304-1311.
38. Pham W, Zhao BQ, Lo EH et al. Crossing the blood-brain barrier: a potential application of myristoylated polyarginine for in vivo neuroimaging. *Neuroimage* 2005; 28:287-292.
39. Sosnovik DE, Nahrendorf M, Deliollanis N et al. Fluorescence tomography and magnetic resonance imaging of myocardial macrophage infiltration in infarcted myocardium in vivo. *Circulation* 2007; 115:1384-1391.
40. Deguchi JO, Aikawa M, Tung CH et al. Inflammation in atherosclerosis: visualizing matrix metalloproteinase action in macrophages in vivo. *Circulation* 2006; 114:55-62.
41. Wunder A, Straub RH, Gay S et al. Molecular imaging: novel tools in visualizing rheumatoid arthritis. *Rheumatology (Oxford)* 2005; 44:1341-1349.
42. Verbeek FP, van der Vorst JR, Schaafsma BE et al. Intraoperative near infrared fluorescence guided identification of the ureters using low dose methylene blue: a first in human experience. *J Urol* 2013; 190:574-579.
43. Figueiredo JL, Siegel C, Nahrendorf M et al. Intraoperative near-infrared fluorescent cholangiography (NIRFC) in mouse models of bile duct injury. *World J Surg* 2010; 34:336-343.
44. Verbeek FP, Schaafsma BE, Tummers QR et al. Optimization of near-infrared fluorescence cholangiography for open and laparoscopic surgery. *Surg Endosc* 2013.

45. Whitney MA, Crisp JL, Nguyen LT et al. Fluorescent peptides highlight peripheral nerves during surgery in mice. *Nat Biotechnol* 2011; 29:352-356.
46. Gibbs-Strauss SL, Vooght C, Fish KM et al. Molecular imaging agents specific for the annulus fibrosus of the intervertebral disk. *Mol Imaging* 2010; 9:128-140.
47. Ishizawa T, Fukushima N, Shibahara J et al. Real-time identification of liver cancers by using indocyanine green fluorescent imaging. *Cancer* 2009; 115:2491-2504.
48. Hwang SW, Malek AM, Schapiro R et al. Intraoperative use of indocyanine green fluorescence videography for resection of a spinal cord hemangioblastoma. *Neurosurgery* 2010; 67:ons300-ons303.
49. Ferroli P, Acerbi F, Albanese E et al. Application of intraoperative indocyanine green angiography for CNS tumors: results on the first 100 cases. *Acta Neurochir Suppl* 2011; 109:251-257.
50. Hojo M, Arakawa Y, Funaki T et al. Usefulness of Tumor Blood Flow Imaging by Intraoperative Indocyanine Green Videoangiography in Hemangioblastoma Surgery. *World Neurosurg* 2013.
51. van der Vorst JR, Schaafsma BE, Hutteman M et al. Near-infrared fluorescence-guided resection of colorectal liver metastases. *Cancer* 2013; 119:3411-3418.

Part I:

Pre-clinical validation of
near-infrared fluorescence
guided surgery

Chapter 2

Near-Infrared fluorescence imaging of liver metastases in rats using indocyanine green

van der Vorst JR, Hutteman M, Mieog JS, de Rooij KE, Kaijzel EL, Lowik CW,
Putter H, Kuppen PJ, Frangioni JV, van de Velde CJ and Vahrmeijer AL

J Surg Res. 2012 May 15;174(2):266-71

ABSTRACT

Background

Near-infrared (NIR) fluorescence imaging using indocyanine green (ICG) is a promising technique to obtain real-time assessment of the extent and number of colorectal liver metastases during surgery. The current study aims to optimize dosage and timing of ICG administration.

Material and methods

Liver tumors were induced in 18 male WAG/Rij rats by subcapsular inoculation of CC531 rat colorectal cancer cells into three distinct liver lobes. Rats were divided in 2 groups: imaging after 24 and 48 hours or 72 and 96 hours after intravenous ICG administration. In each time group, rats were allocated to three dose groups: 0.04, 0.08, or 0.16 mg ICG. Intraoperative imaging and *ex vivo* measurements were performed using Mini-FLARE™ and confirmed by fluorescence microscopy. Fluorescence intensity was quantified using the Mini-FLARE software and the difference between tumor signal and liver signal (tumor-to-liver ratio; TLR) was calculated.

Results

In all 18 rats, all colorectal liver metastases (N = 34), some as small as 1.2 mm, were identified using ICG and the Mini-FLARE™ imaging system. Average tumor-to-liver ratio (TLR) over all groups was 3.0 ± 1.2 . TLR was significantly higher in the 72 h time group compared to other time points. ICG dose did not significantly influence TLR, but a trend was found favoring the 0.08 mg dose group. Fluorescence microscopy demonstrated a clear fluorescent rim around the tumor.

Conclusions

This study demonstrates that colorectal cancer liver metastases can be clearly identified during surgery using ICG and the Mini-FLARE™ imaging system, with optimal timing of 72 h post-injection and an optimal dose of 0.08 mg (0.25 mg/kg) ICG. NIR fluorescence imaging has the potential to improve intraoperative detection of micrometastases and thus the completeness of resection.

INTRODUCTION

With a worldwide annual incidence of approximately 1 million cases and an annual mortality of over 500,000 cases, colorectal cancer is the second cause of cancer death worldwide.¹ The survival of patients with colorectal carcinoma is mostly determined by the occurrence of distant metastases. Approximately 30% of patients with CRC eventually develop liver metastases.^{2,3} When metastases are confined to the liver and are resectable, surgical resection can offer a 5-year survival rate of 35-40%.^{3,4} Despite improved surgical techniques, preoperative imaging modalities and improved chemotherapy regimens, intrahepatic recurrence rates vary from 11-26%.⁵⁻⁸ This is possibly due to an inadequate assessment of the extent of disease before and during liver surgery. Currently, the most frequently used imaging modalities to make this assessment are computed tomography (CT) and intraoperative ultrasonography (IOUS). However, even with the combined use of these modalities, 6-20 % of liver metastases can not be identified.⁹⁻¹¹ In particular, the detection of small (< 5 mm) liver metastases and superficially located liver metastases appears to be difficult.¹¹ New imaging modalities are necessary to facilitate a more complete assessment of the extent of disease.

Near-infrared (NIR) fluorescence imaging is a promising technique to intraoperatively assess the extent of colorectal liver metastases. Recently, Ishizawa and colleagues¹² have shown that primary hepatocellular carcinoma and colorectal liver metastases could be identified using NIR fluorescence imaging and the NIR fluorescent agent indocyanine green (ICG). Colorectal liver metastases could be identified by a fluorescent rim around the metastases. They hypothesized that this distinct fluorescent pattern is probably based on biliary excretion disorders in the surrounding normal liver tissue that is compressed by expanding pressure of the tumor. In their study of 49 patients, a fixed dose of 0.5 mg/kg ICG was administered preoperatively as part of a routine ICG clearance test, which is commonly used in Asia to plan the safe extent of hepatectomy. The interval between administration of ICG and surgery varied between 1 to 7 days. Consequently, the optimal dose of ICG and time of administration before surgery remain unclear.

The goal of our study was to determine the optimal ICG dose and administration time before surgery, using a syngeneic rat model of colorectal cancer metastases in conjunction with the Mini-FLARE™ image-guided surgery system.

MATERIAL AND METHODS

Animal model

The colorectal cancer rat CC531 cell line was used for this study. The cell line and the induction of liver metastases have been described previously.¹³ In short, cells were cultured in RPMI 1640 supplemented with 2 mM L-glutamine (Gibco, Invitrogen Ltd, Carlsbad, USA), 10% heat-inactivated fetal calf serum, 100 U/ml penicillin and 0.1 mg/ml streptomycin sulfate. In order to induce liver metastases, CC531-syngeneic male WAG/Rij rats (Harlan, Horst, the Netherlands) weighing approximately 300-350 g underwent median laparotomy and the liver was mobilized and exposed. Subsequently, 125,000 CC531 cells (in 50 μ l PBS) were subcapsularly inoculated into the left and right main liver lobes and the right accessory liver lobe.¹³ Four weeks after inoculation, metastases ranging from 1.2 to 13.4 mm in size had originated in the liver.

The weight of the animals was followed throughout the experiment to monitor their general health state. Throughout tumor inoculation, injection of ICG and imaging, the animals were anesthetized with 5% isoflurane for induction and 2% isoflurane for maintenance in oxygen with a flow of 0.8 L/min. During anesthesia, the respiration rate was constantly monitored. For postoperative analgesia, the analgesic buprenorphine (0.1 mg/kg) was used. The Animal Welfare Committee of the Leiden University Medical Center approved the experiments. All animals were housed in the animal facility of the Leiden University Medical Center. Pellet food and fresh tap water were provided *ad libitum*.

NIR fluorescent contrast agent

The clinically available NIR fluorescent contrast agent ICG (Pulsion Medical Systems, Munich, Germany) was used. Three ICG dose groups were tested: 0.04, 0.08 and 0.16 mg. Before injection, ICG powder was resuspended in 200 μ L sterile water.

Intraoperative NIR fluorescence imaging system

Imaging of liver metastases was performed using the Mini-FLARE™ imaging system (Trojan et al., manuscript under review), which is a miniaturized version of the FLARE™ imaging system.¹⁴ Briefly, the system consists of two wavelength-isolated light sources: a “white” light source, generating 26,600 lx of 400-650 nm light and a “near infrared” light source, generating 7.7 mW/cm² of 760 nm light. Color video and NIR fluorescence images are simultaneously acquired and displayed in real-time using custom optics and software that separate the color video and NIR fluorescence

images. A pseudo-colored (lime green) merged image of the color video and NIR fluorescence images is also displayed. The imaging head is attached to a flexible gooseneck arm, which permits positioning of the imaging head virtually anywhere over the surgical field, and at extreme angles.

Experimental design

In a time-dependent and dose-dependent experiment, NIR fluorescence imaging was performed in 18 tumor-bearing rats. To minimize surgery-related trauma and distress, rats were divided in two groups: imaging after 24 and 48 hours, and imaging after 72 and 96 hours of ICG administration. In each time group, rats were allocated to three dose groups of 0.04, 0.08, or 0.16 mg ICG, which was administered intravenously via the penile vein. Each dose group contained 3 rats. ICG dose levels were chosen based on clinically relevant doses using human body weight and correspond to doses of 10, 20 and 40 mg of ICG. The imaging time-points were chosen based on Ishizawa et al.¹² who reported NIR fluorescence imaging is preferably performed at least 24 hours after ICG administration. Furthermore, for clinical translation, these time-points must be logistically acceptable to use in a clinical setting. For intraoperative imaging, the liver and other intra-abdominal organs were exposed after median laparotomy. After the first intraoperative imaging session (24 or 72 hours after ICG administration), the abdomen was closed in two layers and the animal was imaged again 24 hours later. At all time-points, tumor fluorescence and fluorescence of abdominal organs was measured.

Data analysis

NIR fluorescence data generated with the Mini-FLARE™ system were analyzed using the Mini-FLARE™ software package. Regions-of-interest were drawn on the outline of the tumor, liver, kidney, spleen, stomach, small bowel, colon and bladder as traced manually by visual interpretation on the white light image. Subsequently, fluorescence intensity was automatically calculated and exported to statistical analysis software.

Fluorescence microscopy

After intraoperative imaging experiments at 48 or 96 hours, the liver was excised completely for *ex vivo* fluorescence measurements. Subsequently, liver tumors were sliced in two to examine internal fluorescent patterns using the Mini-FLARE™ system. Excised tumor slices were snap-frozen on dry ice and stored at -80°C or were fixed in 10% buffered formalin overnight, washed in 70% ethanol and subsequently

embedded in paraffin. Frozen tissue sections were measured for fluorescence using the Nuance multispectral imager (CRi, Woburn, MA) mounted on a Leica DM IRE2 inverted microscope (Leica, Wetzlar, Germany) and subsequently stained with hematoxylin and eosin. White light images were created using the same microscope and subsequently merged with fluorescence images.

Statistical analysis

Statistical analysis and generation of graphs were performed using GraphPad Prism Software (version 5.01, La Jolla, USA) and SPSS (version 17.0). Fluorescence intensity and tumor size were reported as mean and standard deviation. To test differences between dose groups and time groups, repeated measures ANOVA was used with rat as random factor and dose, time, and dose by time interaction as fixed effects. When the dose by time interaction was not significant, it was subsequently removed from the model. Comparisons between doses and between time points were performed using least square difference (LSD) adjustment for multiple testing. Statistical tests were two-tailed and $p < 0.05$ was considered significant.

RESULTS

Intraoperative detection of colorectal liver metastases

In 18 rats, syngeneic colorectal liver metastases were induced using the colorectal cancer rat cell line CC531. The mean number of metastases per rat was 1.8 ± 0.8 (range 1 – 3). The mean size of the liver metastases was 5.2 ± 0.3 mm (range 1.2 – 13.4 mm). In all 18 rats, all colorectal liver metastases ($N = 34$) were identified using ICG and the Mini-FLARE™ imaging system (Fig. 1).

Dose of ICG and time of intraoperative imaging

To determine the influence of ICG dosage and time of imaging, rats were allocated to three dose groups and imaged at four time points and tumor-to-liver ratios (TLRs) were calculated. At all time-points (24, 48, 72 and 96 hours) and in all dose groups (0.04, 0.08 and 0.16 mg), fluorescence intensity of liver metastases was significantly higher than the fluorescent intensity of normal liver tissue ($P < 0.001$). Average TLR over all groups was 3.0 ± 1.2 . The highest average TLR (4.3 ± 1.8) was reached in the 0.08 mg dose group and 72 h after intravenous administration (Fig. 2C).

Repeated measures ANOVA was used to test for differences in TLR between dose and time groups. There was a significant effect of time ($P < 0.001$),

but the effects of dose ($P = 0.12$) and dose by time interaction ($P = 0.91$) were not significant. Dose by time interaction was therefore removed from the model. Consequently, the model included rat as random factor and dose and time as fixed effects. This model showed that the TLR was significantly higher in the 72 h time group compared to the 24 h ($P < 0.001$), 48 h ($P = 0.001$) and 96 h ($P = 0.004$) time groups (Fig. 2D). Also, the TLR was significantly higher in the 96 h time group compared to the 24 h group ($P = 0.049$). ICG dose did not significantly influence TLRs, but a trend was found favoring the 0.08 mg dose group (0.08 vs. 0.04, $P = 0.06$; 0.08 vs. 0.16, $P = 0.09$).

Biodistribution of Indocyanine Green

Fluorescent intensity of the metastases, liver, kidney, stomach, spleen, small bowel, colon and bladder was measured at all time points and in all dose groups (data not shown).

Repeated measures ANOVA was used to test for differences in fluorescent intensity of the liver (Fig. 2A) and liver metastases (Fig. 2B) between dose and time groups. Dose by time interaction did not significantly effect liver signal ($P = 0.1$) and metastases signal ($P = 0.125$) and was therefore removed from the model. There was a significant effect of time on both liver signal ($P < 0.001$) and liver metastases signal ($P < 0.001$). No significant effect of dose was found on liver signal ($P = 0.061$) and metastases signal ($P = 0.152$). This model showed that liver signal and metastases signal were both significantly higher in the 24 h group compared to all other time-points ($P < 0.001$).

NIR fluorescence intensity of all organs except for the stomach, colon and the small bowel, was lower or equal to the liver signal. Fluorescence intensity of the stomach, colon and small bowel was significantly higher compared to other organs and had a maximum at 48 and 72 hours.

Microscopic distribution of ICG in liver metastases

To determine the precise location of ICG in the vicinity of the tumor, sliced liver metastases were examined for internal fluorescent patterns using the Mini-FLARE™ system. In all liver metastases a clear fluorescent rim around the tumor was found. Frozen tissue sections were examined using the Nuance multispectral imager (CRi, Woburn, MA) mounted on a Leica DM IRE2 inverted microscope (Leica, Wetzlar, Germany). A clear fluorescent rim was found in stromal tissue in the transition area between tumor and normal liver tissue in all liver metastases. In this area, multiple cell types that are involved in tissue inflammation (e.g. granulocytes, lymphocytes) were found (Fig 3).

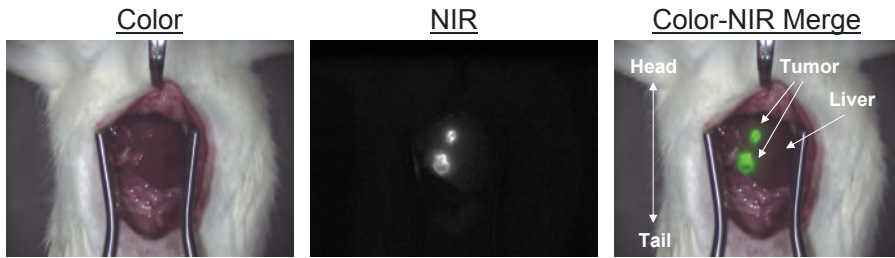


Figure 1 – Intraoperative detection of colorectal liver metastases using NIR fluorescence. Shown are a color image (left), a NIR fluorescence image (middle) and a pseudo-colored green merge (right) of two CC531 colorectal liver metastases intraoperatively detected using NIR fluorescence in a male rat 72 h after injection of 0.08 mg indocyanine green.

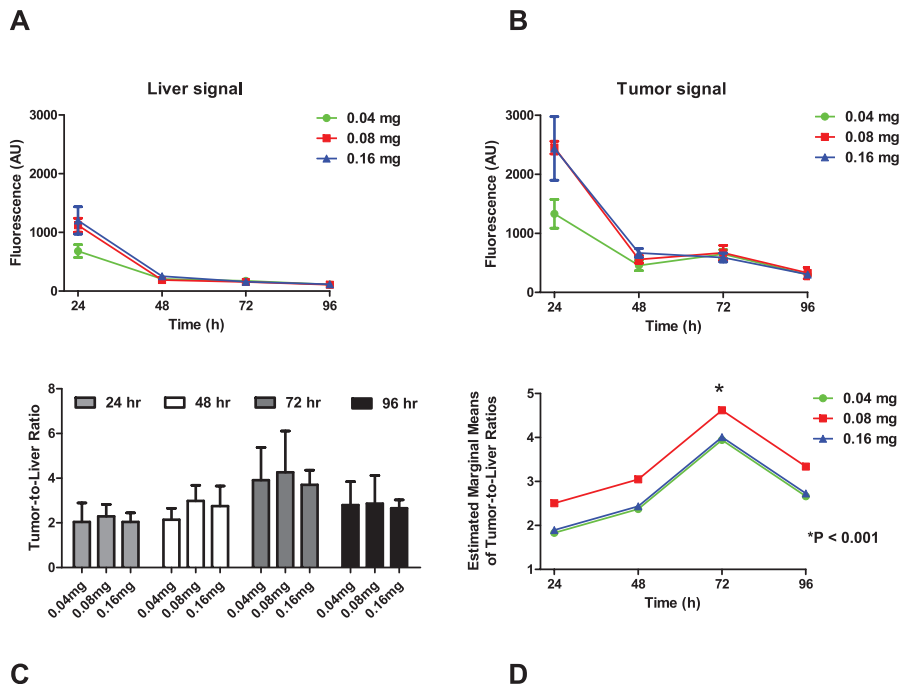


Figure 2 – Dose of ICG and timing of intraoperative imaging

A. Fluorescent intensity of the liver in 18 rats injected with 0.04, 0.08 or 0.16 after 24, 48, 72 and 96 h.

B. Fluorescent intensity of all liver tumors (N = 34) in 18 rats injected with 0.04, 0.08 or 0.16 mg ICG after 24, 48, 72 and 96 h.

C. Average tumor-to-liver ratios and standard deviations are plotted for all liver metastases (N = 34) in 18 rats injected with 0.04, 0.08 or 0.16 mg ICG after 24, 48, 72 and 96 h.

D. Estimated marginal means of tumor-to-liver ratio for rats injected with 0.04, 0.08 or 0.16 mg ICG after 24, 48, 72 and 96 h using the repeated measures ANOVA and least square difference (LSD) adjustment for multiple testing. This model showed that the tumor-to-liver ratio was significantly higher in the 72 h time group compared to the 24 h ($P < 0.001$), 48 h ($P = 0.001$) and 96 h ($P = 0.004$) time groups. ICG dose did not significantly influence tumor-to-liver ratios, but a trend was found favoring the 0.08 mg dose group (0.08 vs. 0.04, $P = 0.06$; 0.08 vs. 0.16, $P = 0.09$).

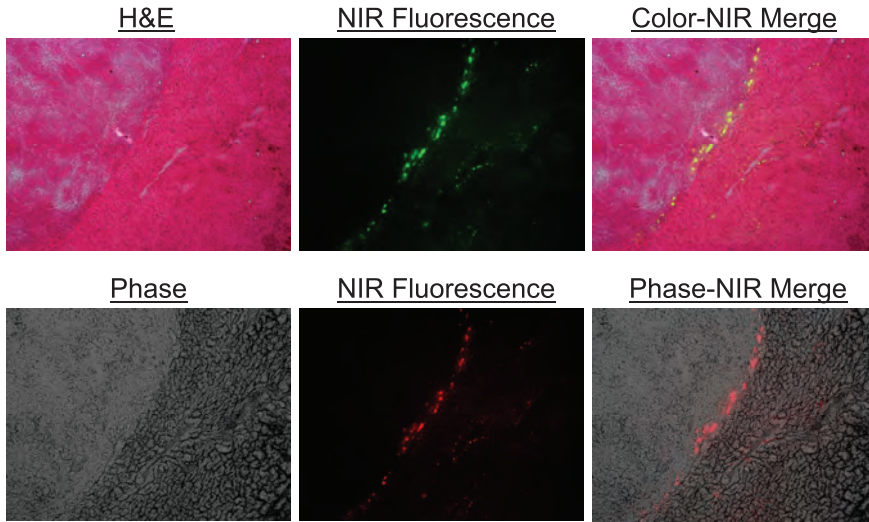


Figure 3 – Fluorescent microscopy of a colorectal liver metastasis

Shown are a hematoxylin and eosin staining (top left), a pseudo-colored green NIR fluorescence image (top middle) and pseudo-colored green merge (top right) of a 20 μm frozen tissue section of a colorectal liver metastasis. Furthermore, a phase image (bottom left), a pseudo-colored red NIR fluorescence image (bottom middle) and a pseudo-colored red merge (bottom right) of a 20 μm frozen tissue section of a colorectal liver metastasis is shown. The fluorescent rim in stromal tissue in the transition area between tumor and normal liver tissue can be clearly identified.

DISCUSSION

In the present study, significant differences in TLR were shown between four different time points after ICG administration, with an optimal time of imaging of 72 h after ICG administration. No significant effects were found with regard to dose level; however, a trend was shown favoring 0.08 mg. Moreover, all liver metastases, even as small as 1.2 mm, could be clearly identified during liver surgery using clinically available ICG and the Mini-FLARE™ system in this syngeneic rat model.

Highest TLRs were reached 72 h after ICG administration. Fluorescence intensity of the liver and the liver metastases were also examined separately. Fluorescent intensity of the liver decreased strongly after 24 h and was not dose dependent. Fluorescent intensity of the liver metastases also decreased strongly at 48 h, but a small, non-significant peak was found at 72 h. This small peak can be explained by the re-uptake of ICG in the small bowel as part of the enterohepatic circulation and subsequent passage through the bowel tract, hence the highest TLR at 72 h.

Regarding ICG dosage, a trend was found favoring the 0.08 mg ICG group. Extrapolating to human body weight, this dose corresponds to a dose of 20 mg ICG, which is frequently used in a clinical setting. To optimize this technique in clinical practice, a dose-finding study is imperative. As ICG is already clinically available and FDA-approved, a straightforward translation of our results to the clinic can be made.

It is known that a substantial part of liver metastases, mainly the small (< 5 mm) and superficially located, can not be identified using conventional imaging modalities such as CT or IOUS. Size of metastases in the present study varied from 1.2 to 13.4 mm of which 50 % were smaller than 5 mm. This emphasizes that ICG fluorescence in liver surgery might be of great value in detecting small colorectal liver metastases. As the currently used preclinical animal model only generated colorectal liver metastases, future clinical studies will have to determine the ability of this technique to discriminate between malignant and benign lesions of the liver.

Since maximum penetration depth of NIR fluorescence is currently up to 1 cm, identification of non-superficially situated liver metastases will be more challenging. Therefore, intraoperative ICG fluorescence must be regarded as a complement on currently used conventional imaging modalities as IOUS and CT. Improvements in imaging systems, NIR fluorescence contrast agents and software and reduction in background fluorescence may facilitate NIR fluorescence imaging of deeper located metastases.

The currently used technique to detect liver metastases using NIR fluorescence and ICG is based on the clearance capacity of the liver. It has been described that in patients with a cirrhotic liver, or in patients pretreated with chemotherapy, the liver function and clearing capacity can be reduced. A reduced liver function could also affect the clearance of ICG, which can result in a higher background signal and therefore lower contrast. However, it has been shown that even cirrhotic livers have an extensive clearance capacity.¹⁵ This implies that the currently used technique can probably be used in subjects with a reduced liver function. Though, in these patients, the optimal time interval between ICG administration and imaging could be longer. Future clinical studies have to elaborate on this topic.

A recent development in liver surgery is the introduction of laparoscopic surgery. NIR fluorescence can be of great value, also in laparoscopic surgery, since palpation of the liver is not possible and the surgeon can only rely on visual inspection and preoperative imaging. To anticipate on this potential new

application, laparoscopic NIR fluorescence camera systems are presently being developed and tested.^{16,17}

In summary, this study demonstrates clear identification of colorectal liver metastases during surgery using the clinically available NIR fluorescent agent ICG and the Mini-FLARE™ system. Imaging 72 h after administration of 0.08 mg ICG provided the highest TLRs. In particular, the ability to detect small (< 5 mm) and superficially located metastases can be of great value during liver surgery. When the current intraoperative identification of colorectal liver metastases can be improved using this technique, the resection can potentially be performed more accurately and preoperatively missed metastases can be involved in surgical decision making.

REFERENCES

1. Parkin DM, Bray F, Ferlay J et al. Global cancer statistics, 2002. *CA Cancer J Clin* 2005; 55:74-108.
2. Manfredi S, Lepage C, Hatem C et al. Epidemiology and management of liver metastases from colorectal cancer. *Ann Surg* 2006; 244:254-259.
3. Ruers T, Bleichrodt RP. Treatment of liver metastases, an update on the possibilities and results. *Eur J Cancer* 2002; 38:1023-1033.
4. Simmonds PC, Primrose JN, Colquitt JL et al. Surgical resection of hepatic metastases from colorectal cancer: a systematic review of published studies. *Br J Cancer* 2006; 94:982-999.
5. Wei AC, Greig PD, Grant D et al. Survival after hepatic resection for colorectal metastases: a 10-year experience. *Ann Surg Oncol* 2006; 13:668-676.
6. Pawlik TM, Scoggins CR, Zorzi D et al. Effect of surgical margin status on survival and site of recurrence after hepatic resection for colorectal metastases. *Ann Surg* 2005; 241:715-22, discussion.
7. Abdalla EK, Vauthey JN, Ellis LM et al. Recurrence and outcomes following hepatic resection, radiofrequency ablation, and combined resection/ablation for colorectal liver metastases. *Ann Surg* 2004; 239:818-825.
8. Karanjia ND, Lordan JT, Fawcett WJ et al. Survival and recurrence after neo-adjuvant chemotherapy and liver resection for colorectal metastases: a ten year study. *Eur J Surg Oncol* 2009; 35:838-843.
9. Leen E, Ceccotti P, Moug SJ et al. Potential value of contrast-enhanced intraoperative ultrasonography during partial hepatectomy for metastases: an essential investigation before resection? *Ann Surg* 2006; 243:236-240.
10. Sahani DV, Kalva SP, Tanabe KK et al. Intraoperative US in patients undergoing surgery for liver neoplasms: comparison with MR imaging. *Radiology* 2004; 232:810-814.
11. Nomura K, Kadoya M, Ueda K et al. Detection of hepatic metastases from colorectal carcinoma: comparison of histopathologic features of anatomically resected liver with results of preoperative imaging. *J Clin Gastroenterol* 2007; 41:789-795.
12. Ishizawa T, Fukushima N, Shibahara J et al. Real-time identification of liver cancers by using indocyanine green fluorescent imaging. *Cancer* 2009; 115:2491-2504.
13. Vahrmeijer AL, van Dierendonck JH, Schutrups J et al. Potentiation of the cytostatic effect of melphalan on colorectal cancer hepatic metastases by infusion of buthionine sulfoximine (BSO) in the rat: enhanced tumor glutathione depletion by infusion of BSO in the hepatic artery. *Cancer Chemother Pharmacol* 1999; 44:111-116.
14. Troyan SL, Kianzad V, Gibbs-Strauss SL et al. The FLARE intraoperative near-infrared fluorescence imaging system: a first-in-human clinical trial in breast cancer sentinel lymph node mapping. *Ann Surg Oncol* 2009; 16:2943-2952.
15. Bloemen JG, Olde Damink SW, Venema K et al. Short chain fatty acids exchange: Is the cirrhotic, dysfunctional liver still able to clear them? *Clin Nutr* 2010; 29:365-369.
16. Matsui A, Tanaka E, Choi HS et al. Real-time intra-operative near-infrared fluorescence identification of the extrahepatic bile ducts using clinically available contrast agents. *Surgery* 2010; 148:87-95.
17. van der Pas MH, van Dongen GA, Cailler F et al. Sentinel node procedure of the sigmoid using indocyanine green: feasibility study in a goat model. *Surg Endosc* 2010; 24:2182-2187.

Chapter 3

Intraoperative fluorescence delineation of head and neck cancer with a fluorescent anti-epidermal growth factor receptor nanobody

van Driel PB¹, van der Vorst JR¹, Verbeek FP, Oliveira S, Snoeks TJ, Keereweer S,
Chan B, Boonstra MC, Frangioni JV, van Bergen en Henegouwen PM,
Vahrmeijer AL, Lowik CW

¹Both authors contributed equally to this work and share first-authorship

Int J Cancer. 2013 Nov 13

ABSTRACT:

Background

Intraoperative near-infrared (NIR) fluorescence imaging is a technology with high potential to provide the surgeon with real-time visualization of tumors during surgery. This study explores the feasibility for clinical translation of an epidermal growth factor receptor (EGFR) targeting nanobody for intraoperative imaging and resection of orthotopic tongue tumors and cervical lymph node metastases.

Material and Methods

The anti-EGFR nanobody 7D12 and the negative control nanobody R2 were conjugated to the NIR fluorophore IRDye800CW (7D12-800CW and R2-800CW). Orthotopic tongue tumors were induced in nude mice using the OSC-19-luc2-cGFP cell line. Tumor bearing mice were injected with 25 μ g 7D12-800CW, R2-800CW or 11 μ g 800CW. Subsequently, other mice were injected with 50 μ g or 75 μ g of 7D12-800CW. The FLARE imaging system and the IVIS spectrum were used to identify, delineate and resect the primary tumor and cervical lymph node metastases.

Results

All tumors could be clearly identified using 7D12-800CW. A significantly higher tumor-to-background ratio (TBR) was observed in mice injected with 7D12-800CW compared to mice injected with R2-800CW and 800CW. The highest average TBR (2.00 ± 0.34 and 2.72 ± 0.17 for FLARE and IVIS spectrum, respectively) was observed 24 hours after administration of the EGFR-specific nanobody. After injection of 75 μ g 7D12-800CW cervical lymph node metastases could be clearly detected. Orthotopic tongue tumors and cervical lymph node metastases in a mouse model were clearly identified intraoperatively using a recently developed fluorescent EGFR targeting nanobody.

Conclusion

Translation of this approach to the clinic would potentially improve the rate of radical surgical resections.

INTRODUCTION

In oncology, a range of noninvasive imaging modalities, including X-ray, ultrasonography, computed tomography (CT) and magnetic resonance imaging (MRI), enable early detection, staging, and treatment evaluation of cancer. However, in most cases surgeons still discriminate healthy tissue from cancerous tissue by means of visual inspection and palpation during surgery. Given the fact that adequate tumor free margins are of paramount importance for patient prognosis and outcome, and that irradical resections still frequently occur, novel imaging modalities are needed. Despite the primary objective of achieving macroscopic clearance of 1 cm in the surgical management of oropharyngeal or oral squamous cell carcinoma (OSCC), the presence of tumor positive margins has been reported in 16% of patients.¹ Numerous reports have indicated that involved margins imply deteriorated prognoses.² On the other hand, applying wider surgical margins will result in functional impairment in most cases.^{3,4} Therefore, clearer delineation of the tumor during surgery may improve the number of radical resections, thus increasing patients' survival rates while maintaining postoperative functionality.

Near-infrared (NIR) fluorescence imaging is a novel imaging technique that provides the surgeon with real-time visualization of tumors during surgery.⁵⁻⁷ In the NIR region (650 – 800 nm), less absorption of light by tissue components allows much deeper penetration of light. Furthermore, lower fluorescence from endogenous fluorophores decreases the non-specific background signal. As the human eye is not sensitive to NIR fluorescent light, a specific NIR fluorescence imaging system is needed to visualize the fluorescence signal. At the same time, since NIR light is invisible to the human eye, it will not alter the surgical field.⁸

One of the main challenges in intraoperative fluorescence imaging lies in the development, validation and clinical introduction of a tumor specific agent. Being widely overexpressed in OSCC, the epidermal growth factor receptor (EGFR) serves as an interesting target for intraoperative fluorescence imaging.^{9,10} The EGFR is a transmembrane glycoprotein that is involved in DNA synthesis and cell proliferation. Overexpression contributes to oncogenesis by proliferation, dedifferentiation, inhibition of apoptosis, invasiveness and lack of adhesion dependence.¹¹ Furthermore, EGFR overexpression is often associated with a poor prognosis for patients with OSCC.¹²

For tumor targeting using molecular imaging techniques, antibodies are promising as they can be raised specifically against practically any molecular

target. Nevertheless, due to their large hydrodynamic diameter, intact antibodies accumulate in the liver. Moreover, long half-life in the bloodstream and slow blood clearance via the liver results in high contrast images only several days after injection. A very appealing alternative is the use of nanobodies.¹³ Nanobodies are the smallest functional antigen-binding fragments derived from naturally-occurring heavy-chain only antibodies.¹⁴ They show very specific binding to their targets and their size of approximately 15 kDa ensures efficient distribution and tissue penetration, as well as rapid clearance from the body.¹⁵⁻¹⁷

This study assesses the feasibility of intraoperative fluorescence delineation of orthotopic OSCC and microscopic lymph node metastases, using an anti-EGFR nanobody and a clinically available fluorescence camera system. For this, the anti-EGFR nanobody 7D12 was conjugated to the NIR fluorophore IRDye800CW.¹⁸, as previously described by Oliveira et al.¹⁷. Tumor accumulation and specificity of 7D12-800CW was compared to the negative control nanobody R2-800CW and to 800CW alone.

MATERIAL and METHODS

Cell lines and culture

Two human cell lines were used. For the animal studies, the metastatic oral squamous cell carcinoma (OSCC) line OSC-19 was used. The OSC19 cell line was established in Japan with cells from a patient with a well-differentiated squamous cell carcinoma of the tongue that metastasized to a cervical lymph node.¹⁹ Luc2 luciferase from pGL4.10 plasmid (Promega, Madison, WI, USA) was cloned into the multiple cloning site (MCS) of the lentiviral vector pCDH-EF1-MCS-T2A-copGFP (Biotac, Heidelberg, Germany) using specific primers with the corresponding restriction sites. OSC-19 cells were transduced by self-inactivating lentiviral vectors as previously described²⁰ and positive cell clones selected by limit dilution to create a stable luciferase 2 (luc2) and green fluorescent protein (GFP) expressing OSC-19-Luc2-copGFP cell line. The cells were grown *in vitro* in Dulbecco's Modified Eagle's Medium (DMEM, Invitrogen, Carlsbad, CA, USA) containing 4.5 g D-Glucose/L, 110 mg sodium pyruvate/L, 580 mg L-glutamine/L supplemented with 10% fetal bovine serum (FCS; Lonza, Basel, Swiss), 100 IU/mL penicillin, 100 µg/mL streptomycin (Invitrogen), 1x Minimal Essential Medium (MEM) Non-Essential Amino Acids solution and 1x MEM vitamin solution (Invitrogen). The human colorectal cancer cell line SW620 was used as an EGFR

negative control. This cell line was cultured in Leibovitz's L-15 medium (Invitrogen) containing 300 mg L-glutamine/L supplemented with 10% FetalClone II (Hyclone, Logan, UT, USA) 100 IU/mL penicillin, 100 µg/mL streptomycin (Invitrogen) and 20 mM HEPES (Invitrogen). All cell lines were grown in a humidified incubator at 37°C and 5% CO₂. Cells were regularly checked for *Mycoplasma* infection by PCR.

Nanobodies and Conjugation to IRDye800CW

Two nanobodies were used: 7D12 and R2. The EGFR specific nanobody 7D12 binds to the ectodomain of the EGFR.^{18,21} EGFR specificity of 7D12-800CW *in vitro* and *in vivo* was reported earlier.¹⁷ The nanobody R2 was used as a non-EGFR specific control.^{22,23} Both nanobodies have a molecular weight of approximately 15 kDa and show similar *in vivo* biodistribution.^{17,18,24} The generation of the nanobodies 7D12 and R2 was described previously.^{18,23} Induction of protein expression and purification of nanobodies from the periplasmic space of *Escherichia coli* were performed as described by Roovers et al.²⁵ Conjugation of both nanobodies to the NIR fluorophore IRDye800CW was performed as described by Oliveira et al.¹⁷ Briefly, the IRDye800CW N-hydroxysuccinimide ester (LI-COR, Lincoln, NE, USA) was added to the protein in a 4-fold molar excess and was incubated for two hours at room temperature. Removal of the unconjugated fluorophore was accomplished by using two Zeba Spin Desalting columns (Thermo Fisher Scientific, Perbio Science Nederland B.B., Ettenleur, the Netherlands) per protein in two sequential steps. The fluorescent nanobodies, i.e. 7D12-800CW and R2-800CW, were characterized as previously described¹⁷, namely for their conjugation efficiency and these parameters were in agreement with previous values, i.e. 0.5 and 1.1, respectively.

EGFR expression

OSC-19 and SW620 cells were cultured until subconfluence. Cells were detached with trypsin and adjusted at 1×10^5 cells/tube in ice cold PBS, 10% FCS (Lonza, Basel, Swiss) and 1% sodium azide. The anti-EGFR monoclonal antibody sc-120 alexa fluor 647 (Santa Cruz biotechnology, Santa Cruz, CA, USA) or non-specific normal mouse IgG_{2a} alexa fluor 647 (Santa Cruz) were added and cells were incubated in the dark on ice for 30 minutes. After incubation, cells were washed three times in ice cold PBS and resuspended in ice cold PBS, containing 10% FCS (Lonza) and 1% sodium azide. Flow cytometry of alexa fluor 647 labeled cells was performed using the BD LSR II (BD biosciences, San Jose, CA, USA). EGFR expression was estimated as the geometric mean of fluorescence intensity measured in 10.000 viable cells. The experiment was performed in duplicate.

Binding study

A binding assay was performed to confirm the specificity of the EGFR binding of 7D12-800CW. A black 96-well plate (Greiner bio-one, Frickenhausen, Deutschland) was used in which 20.000 OSC-19-luc2-cGFP and SW620 cells were seeded per well. After one day, cells were washed with binding medium (DMEM supplemented with 25 mM Hepes and 1% BSA, at pH 7.2). 7D12-800CW (7D12), R2-800CW (R2) and IRDye800CW carboxylate (800CW, LI-COR, Lincoln, NE, USA) were added in triplicate in a concentration range of 0 to 50 nM. R2-800CW and IRDye800CW carboxylate were used as negative controls. The cells were incubated for 2 hours in the dark on a rocker at 4°C and afterwards washed two times with binding medium. Bound proteins were directly observed with the Odyssey scanner (LI-COR), scanning at 800 nm. Directly after these measurements cells were fixed with 4% paraformaldehyde and incubated with TO-PRO-3 (Invitrogen) at 1:5000 for 15 minutes. Again cells were washed twice and the plate was imaged using the 700nm channel of the Odyssey (LI-COR) to detect TO-PRO3 fluorescence. Nucleus staining was performed to correct the fluorescence signal for the amount of cells enabling direct comparison of fluorescence signal of both cell lines.

Fluorescence imaging systems

Real-time fluorescence imaging of primary tumor and lymph node metastases was performed using the FLARE imaging system.²⁶ Briefly, This imaging system consists of three wavelength-isolated light sources: a 400-650 nm light source generating 40.000 lux (white light), a 656-678 nm light source generating 4 mW/cm² (700 nm) and a 745 – 779 nm light source generating 14 mW/cm² (800 nm). The imaging head, attached to a flexible gooseneck arm, enables real-time image acquisition from all three cameras. Color, NIR fluorescence and pseudo-colored (lime green) merged images are displayed in real time. Next to the FLARE imaging system, the IVIS spectrum (Caliper Life Science, Hopkinton, MA, USA) was used to visualize primary tumors and metastases. Data analysis of FLARE and IVIS spectrum data was performed using image J and the *Living Image* software from xenogen version 3.2 (Caliper LS) respectively. Multiple regions of interest (ROI) were drawn in the tumor and in adjacent normal tissue of the tongue and divided by each other to calculate TBRs.

Animal model

Nude Balb/c female mice (Charles River laboratories, l'Arbresle, France), aged 4 – 6 weeks, were housed in individually ventilated cages and provided with food and sterilized water ad libitum. Animal experiments were approved by the local animal welfare committee of the Leiden University Medical Center.

Orthotopic tongue tumors were submucosally induced in the tip of the tongue through injection of 40.000 OSC-19-luc2-cGFP cells, diluted in 20 μ L phosphate-buffered saline (PBS). Mice body weight was monitored twice a week and tumor growth was monitored twice a week by bioluminescence (BLI) measurements and visual inspection of the tongue. BLI signal, being the most sensitive imaging method for the detection of tumor cells²⁷, served as an *in vivo* control for the tumor specific fluorescence of the nanobodies. Imaging procedures were performed under isoflurane gas anesthesia. Weight measurements and tongue inspections were performed to monitor general health during the experiments. Mice were sacrificed by injection of high doses ketamine/xylazine.

Fluorescence measurements

Twenty days after injection of tumor cells, mice ($n = 9$) were randomly divided into three groups and received a systemic injection of 25 μ g 7D12-800CW (1.6 nmol, 64 nmol/kg), 25 μ g R2-800CW (1.5 nmol, 60 nmol/kg) or 11 μ g 800CW carboxylate (1 nmol, 40 nmol/kg, LI-COR). For the two nanobodies, a previous study reported 25 μ g to be the optimal dose.¹⁷ Fluorescent images were acquired at 0.5, 1, 2, 4, 8, 24 and 48 hours after injection.

For the detection of microscopic cervical lymph node metastases two additional concentrations of 50 and 75 μ g 7D12-800CW were injected ($n = 4$). Mice were sacrificed at 24 hours after injection and overlying skin of the cervical region was removed for gross examination. Whole-body fluorescence imaging was performed and the tongue and cervical lymph nodes were subsequently resected.

Histology and fluorescence microscopy

After *ex vivo* fluorescent measurements, the resected tongues were cut in two. One half was frozen on dry ice, the other half fixed in 4% formalin overnight and embedded in paraffin blocks. Cervical lymph nodes on both sides were resected. The left lymph node was frozen on dry ice, the right lymph node paraffin embedded and fixed in 4% formalin overnight. Tissue was sectioned at 10 μ m and imaged using the Odyssey (LI-COR). All images were acquired using the same settings but

the images (i.e. brightness and contrast) of the control probes were altered to show any fluorescence and emphasize the difference in localization between specific and non-specific probes. To confirm the presence of tumor cells, fluorescence microscopy (Nikon eclipse e800, Nikon, Amsterdam, the Netherlands) of the GFP fluorescence signal emitted by OSC-19-luc2-cGFP cells was performed on frozen tissue slices. Histologic sections were stained with standard hematoxylin-eosin stain (HE). As expected, fluorescence of GFP could not be detected in paraffin embedded sections. Therefore, the presence of smaller cervical lymph node metastases in paraffin sections was confirmed by staining the cervical lymph node sections with anti-human wide-spectrum cytokeratin staining (Abcam inc., Cambridge, MA, USA).

Statistical analysis

For statistical analysis, SPSS statistical software package (Version 16.0, Chicago, IL) was used. TBR's were calculated by dividing the fluorescent signal of the tumor by fluorescent signal of surrounding tissue. TBR was reported in mean and standard deviation. To compare TBR between dose groups and time points, and to assess the relation between dose and time, a mixed model analysis was used. When a significant difference was detected, a one-way ANOVA was used to post-test for differences between separate dose groups and/or time points. The one-way ANOVA was corrected using the Bonferroni correction. $P < 0.05$ was considered significant. Differences between the FLARE and IVIS imaging systems were tested with an unpaired T-test.

RESULTS

In vitro results

The specificity of the EGFR targeting nanobody for the squamous cell carcinoma of the tongue, that metastasizes to cervical lymph nodes, was first validated *in vitro*. For that purpose, we started with the evaluation of the EGFR expression in the OSC-19-luc2-cGFP cell line. Direct staining of the cell surface epitope of the EGFR of OSC-19-luc2-cGFP cells caused an increase in fluorescence intensity, as shown by a shift to the right through flow cytometry analyses, compared to the non-specific antibody (Fig 1A). Next, as a control to the EGFR overexpressing OSC-19-luc2-cGFP cell line, we assessed the EGFR expression in the human colon carcinoma cell line SW620, a cell line that has no overexpression of the EGFR. In contrast to OSC-19-luc2-cGFP, the FACS data of this cell line revealed no increase in fluorescence intensity, thus confirming the absence of EGFR expression in the SW620 cell line (Fig 1B).

Both these cell lines were employed to confirm the specificity of the EGFR targeting nanobody 7D12-800CW, which was compared to the non-EGFR specific nanobody R2-800CW and to 800CW alone. The IRDye800CW-conjugated probes were produced and characterized as described by Oliveira et al.¹⁷ Consistently, after purification of the conjugates through removal of unconjugated fluorophores, a small percentage of the 800CW unconjugated fluorophore (less than 7.5 % of the 800CW conjugated fraction) was still present (data not shown) and the fluorophore to protein molar ratio of 7D12-800CW and R2-800CW after random conjugation was 0.5 and 1.1 respectively.

The cell assay, performed at 4°C to prevent internalization and investigate binding only, clearly demonstrated an EGFR specific binding of 7D12-800CW in OSC-19-luc2-cGFP cells that proved to be concentration dependent (Fig 1C). With R2-800CW and 800CW, although slightly concentration dependent, significantly less fluorescence intensity was observed (Fig 1C). In the EGFR negative cell line no significant differences in fluorescence intensity between 7D12-800CW and R2-800CW were observed. Altogether, these results confirm the specificity of 7D12-800CW for binding to EGFR and show that both the negative control R2-800CW and the 800CW alone do not associate with these cells (Fig 1C and 1D).

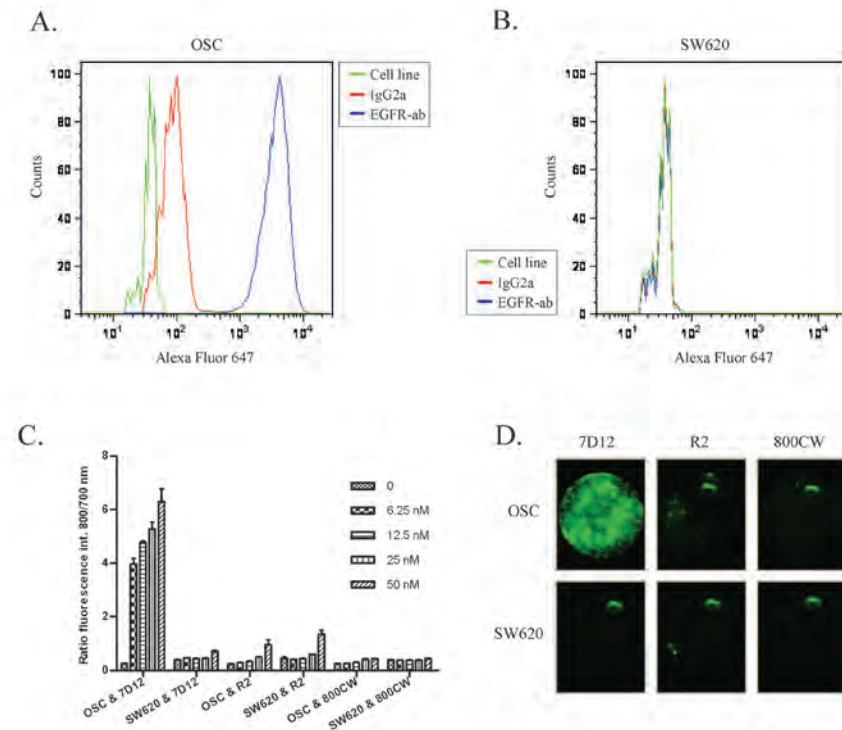


Figure 1 – EGFR expression and binding assay: Flow cytometry was performed using OSC-19-luc2-cGFP and SW620 without antibody (green), with an EGFR specific antibody conjugated to alexa fluor 647 (blue) and with an isotype control normal mouse IgG2a conjugated to alexa fluor 647 (red). 7D12-800CW binds to human epidermal growth factor receptor expressed on OSC19-luc2-cGFP cells.

A. The EGFR is highly expressed on the surface of OSC-19-luc2-cGFP cells.

B. No expression of EGFR was found on the surface of SW620 cells.

C. The human EGFR expressing OSC cells and EGFR negative SW620 cells were incubated with different concentrations of 7D12-800CW, R2-800CW and 800CW. The ratio of the fluorophore bound protein and the fluorescence intensity of TO-PRO-3 was plotted to correct for the amount of cells. Every concentration was performed in triplicate. Error bars indicate the standard deviation.

D. Images were acquired with the Odyssey Scanner (LICOR). OSC and SW620 cells were incubated with 50 nM 7D12, R2 and 800CW. OSC = OSC-19-luc2-cGFP.

Animal model

Within three weeks after orthotopic inoculation of OSC-19-luc2-cGFP cells in the tip of the tongue, all mice developed a primary tongue tumor and cervical lymph node metastases (a typical example is shown in Fig 2A), observed during regular visual inspection and confirmed by the increase in mean bioluminescence signal (Fig 2B)

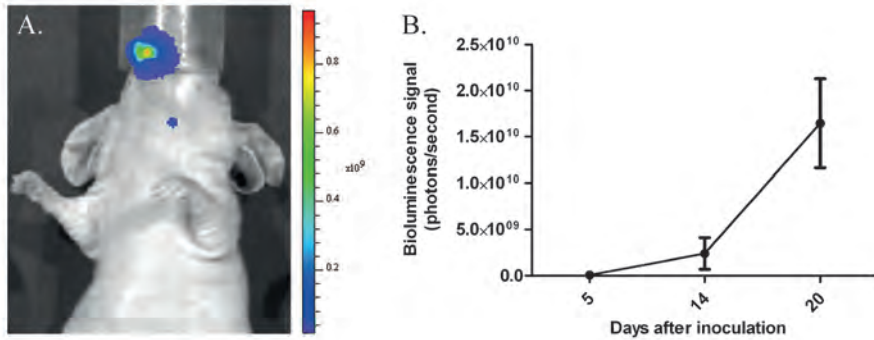


Figure 2 - Tumor growth followed by imaging bioluminescence:

A. Bioluminescent image after injection of OSC-19-luc2-cGFP cells. Primary tongue tumor and lymph node metastasis are shown.

B. Increase of tumor growth (measured in bioluminescence signal) as a function of time.

In vivo NIR Fluorescence Imaging of primary tumors

Three weeks after tumor cell inoculation, mice were injected intravenously with 25 μg of 7D12-800CW, R2-800CW or 11 μg 800CW (for equivalent fluorescence to 7D12-800CW). To assess the feasibility of a possible clinical translation, fluorescence images were taken with both the preclinical, highly sensitive IVIS spectrum camera as well as with the FLARE intraoperative imaging system. As demonstrated in Figure 3A, all tumors of the animals that were injected with 7D12-800CW could be clearly identified through NIR fluorescence using both imaging modalities. No adequate tumor-to-background ratios were observed in the control mice injected with R2-800CW or 800CW (Fig 3B), which is in agreement with the results obtained in vitro (Fig 1). Using the IVIS imaging system, a mixed model showed significant differences in TBRs between three study groups and between time points ($p < 0.0001$ and $p < 0.0001$, respectively) (Fig 4A). Post-testing using a one-way ANOVA showed significant differences between the 7D12-800CW and the R2-800CW ($p < 0.0001$) study groups and between the 7D12-800CW and 800CW ($p < 0.0001$) study groups. No significant difference was found between R2-800CW and 800CW ($p > 0.999$). The highest TBR (2.72 ± 0.17) was measured at 24 hours after administration of 7D12-800CW. Using the FLARE imaging system, a mixed model showed significant differences in TBRs between the three study groups and between time points ($p = 0.041$ and $p < 0.0001$, respectively) (Fig 4B). Post-testing using a one-way ANOVA showed significant differences between the 7D12-800CW and the R2-800CW study groups ($p = 0.05$) and between the 7D12-800CW and 800CW study groups ($p = 0.002$). No significant difference was found between R2-800CW and

800CW ($p = 0.77$). The highest TBR (2.00 ± 0.34) was measured at 24 hours after administration of 7D12-800CW. The highest TBR measured with the IVIS imaging system was significantly higher compared to the highest TBR measured with the FLARE imaging system ($p = 0.03$).

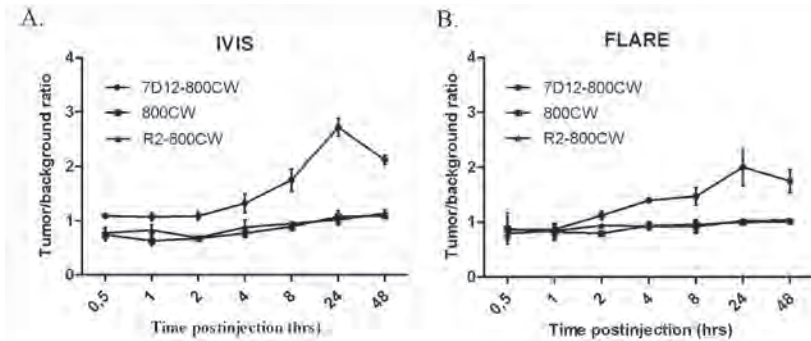


Figure 4 - Intraoperative tumor to background ratios over time: The tumor to background ratio of 7D12-800CW is significantly higher compared to those of R2-800CW and 800CW. Tumor to background ratios were calculated from 0.5 hours to 48 hours after injection. Error bars indicate the standard deviation. Tumor to background ratios were plotted for the IVIS-Spectrum (A) and the FLARE imaging system (B).

Ex vivo fluorescence imaging and histology of primary tumors

In cryo sections, fluorescent imaging of the GFP that was transduced in the OSC-19 cells confirmed the presence of tumor cells in the tongue (Fig 5). After fluorescent imaging (GFP and NIR fluorescence), sections were stained with HE. Even sub-millimeter islands of tumor cells, confirmed with GFP fluorescence, co-localized with the fluorescence of 7D12-800CW, as measured with the Odyssey Scanner (Fig 5). No co-localization was observed in the tongue specimens of mice injected with R2-800CW or 800CW, which is in agreement with our observations *in vivo* (Fig 3B).

In vivo and ex vivo fluorescence imaging and histology of cervical lymph nodes

In contrast to the primary tumor, microscopic cervical lymph node metastases were not grossly visible. In fact, a dose of 75 μg of 7D12-800CW only gave a weak fluorescence signal through the skin using the IVIS, but, importantly, a strong fluorescence with both imaging systems could be detected when the skin was removed (Fig 6). This highlights the potential of this imaging modality in the intraoperative context.

During *ex vivo* imaging, the fluorescence of GFP that was transfected in the OSC-19-luc2-cGFP cells confirmed the presence of cervical lymph node metastases in the tissue specimen and could be colocalized to the fluorescent signal of 7D12-800CW. As expected, due to bleaching and the washing steps, no GFP fluorescence was found in the paraffin sections of the cervical lymph nodes. Nevertheless,

immunohistochemical analysis, using a wide spectrum anti-cytokeratin staining, confirmed the presence of tumor cells. As shown in Figure 6, the fluorescence signal of 7D12-800CW co-localizes with the tumor cells in the cervical lymph node.

DISCUSSION

In the present study, the EGFR targeting nanobody conjugated to 800CW was used to delineate orthotopic OSCC tumor margins during surgery. After 2 hours post injection tumors could already be clearly delineated. The highest TBR was obtained 24 hours after injection. Furthermore, a significant difference in TBR was observed between mice injected with 7D12-800CW, and mice injected with the control nanobodyR2-800CW or with 800CW alone.

NIR fluorescent optical imaging is an imaging technique with high potential to obtain real-time information about the presence, location and dimensions of tumor tissue so that adequate tumor free margins can be obtained after resection.²⁸⁻³⁰ Although the first clinical trial has recently been performed²⁹, it remains challenging to find a suitable fluorescent probe which can be detected with a sensitive NIR-fluorescent imaging system.

The first challenge to NIR fluorescence imaging is the optimal fluorescent probe. An ideal fluorescent probe should distribute well, have a high affinity towards its target and a fast clearance from the bloodstream, to allow efficient accumulation at the tumor and rapid acquisition of images with high contrast. Furthermore, no accumulation in the liver is desirable and the ability to adequately penetrate the tissue of interest is of great importance. The EGFR serves as a very interesting target in head and neck cancer as the majority of these cancers overexpress this receptor.^{10,31} In a previous study we used recombinant human EGFR ligands conjugated to 800CW to target head and neck tumors.³² Although efficient in targeting head and neck tumors, recombinant human EGFR ligands can potentially activate this receptor, which promotes its malignant phenotype. In other studies, cetuximab conjugated to Cy5.5 and panitumumab conjugated to 800CW are used to image head and neck tumors.^{9,33} Conventional antibodies, however, show slower blood clearance (up to several days), higher accumulation in the liver and limited tumor penetration compared to nanobodies.¹⁷ For these reasons, we have selected a nanobody as our probe for this study.

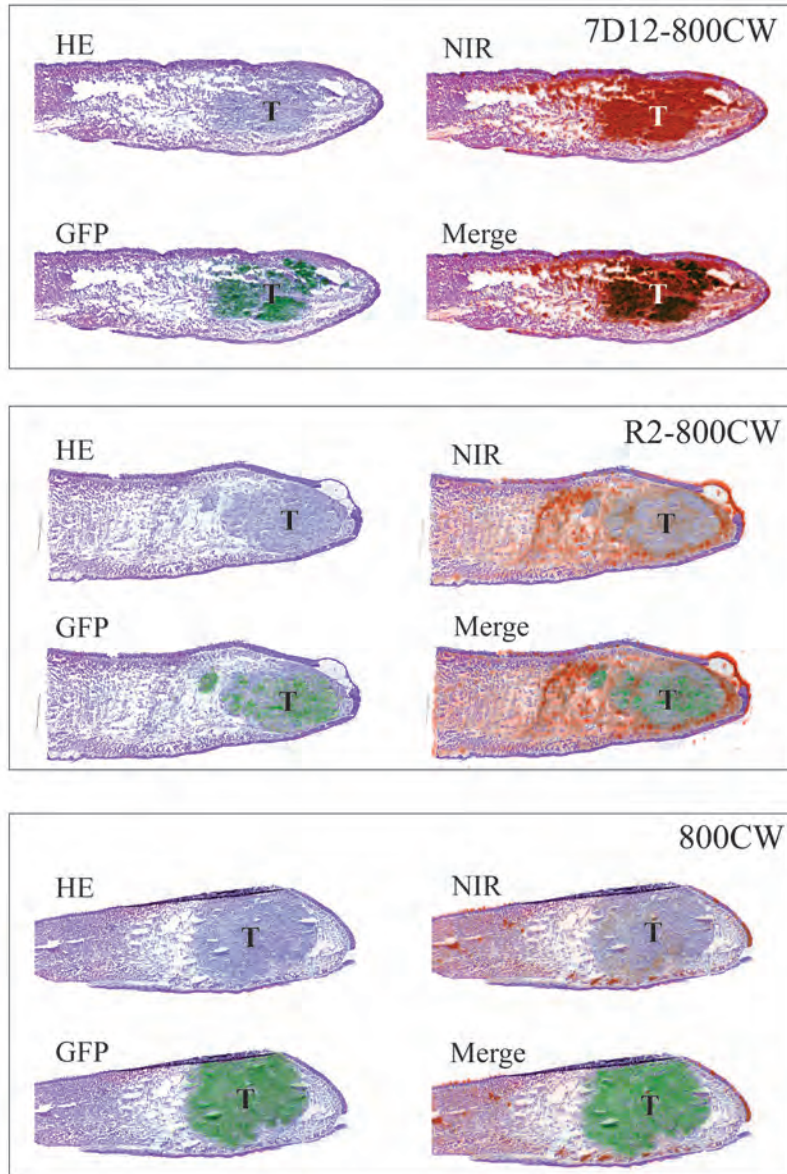


Figure 5 - Histology and fluorescence imaging of orthotopic primary tongue tumors: Shown are hematoxylin and eosin (HE) stainings, HE and GFP fluorescence overlays, HE and NIR fluorescence overlays and HE, NIR and GFP fluorescence overlays. In the 7D12-800CW tissue specimen, a clear overlap between NIR and GFP (indicating tumor cells) fluorescence was observed. In the R2-800CW and 800CW specimens, no overlap between NIR and GFP fluorescence was observed. Brightness and contrast of the images of R2-800CW and 800CW was altered to show fluorescence and emphasize the localization in tissue.

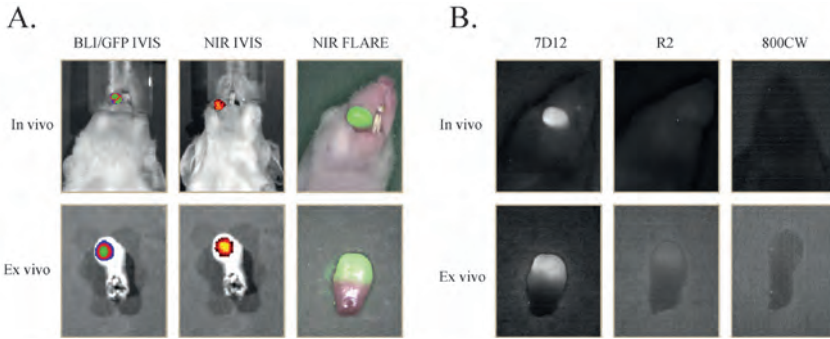


Figure 3 – Multimodal *in vivo* and *ex vivo* imaging of an orthotopic tongue tumor: 7D12 is specifically taken up in the oral squamous cell carcinoma of the tongue. Mice bearing OSC-19-luc2-cGFP human xenografts were intravenously injected with 25µg of 7D12, R2 and 800CW. After 24 hours fluorescent images were obtained with the IVIS spectrum and the intraoperative camera system (FLARE).

A. *In vivo*: bioluminescence brightfield merge image (left), NIR fluorescence brightfield merge IVIS image of 7D12-800CW (middle) and NIR fluorescence color merge FLARE image (right) *Ex vivo*: GFP brightfield merge image (left), NIR fluorescence brightfield merge IVIS image of 7D12-800CW (middle) and NIR fluorescence color merge FLARE image (right)

B. *In vivo*: Fluorescent imaging of a tongue tumor 24 hours after administration of 7D12-800CW (left), R2-800CW (middle) and 800CW (right). *Ex vivo*: Fluorescent imaging of a tongue tumor 24 hours after administration of 7D12-800CW (left), R2-800CW (middle) and 800CW (right). Images were obtained with the intraoperative camera system (FLARE)

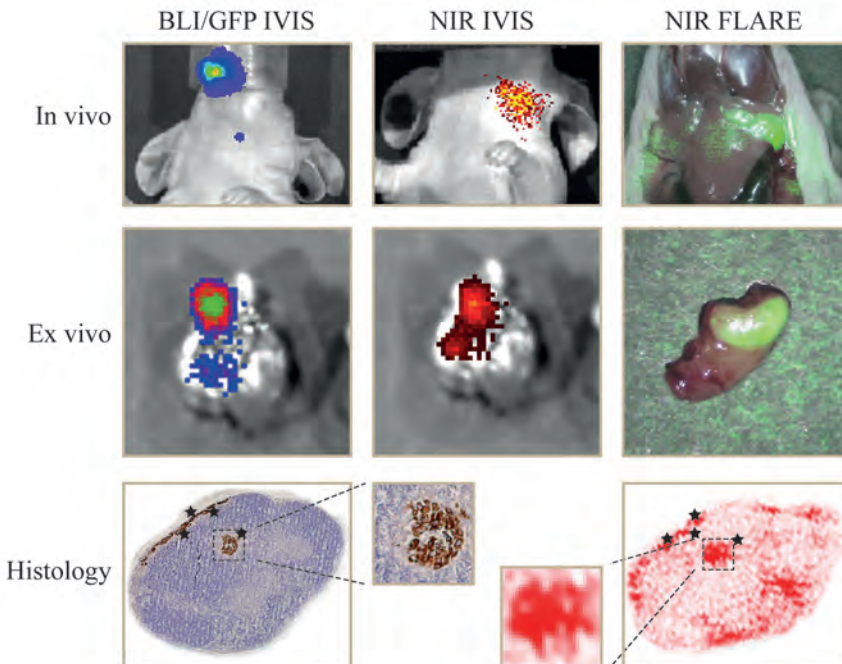


Figure 6 – *In vivo*, *ex vivo* and histological fluorescence imaging of cervical lymph nodes:

In vivo: bioluminescence brightfield merge image (left), NIR fluorescence brightfield merge IVIS image of 7D12-800CW (middle) and NIR fluorescence color merge FLARE image (right)

Ex vivo: GFP brightfield merge image (left), NIR fluorescence brightfield merge IVIS image of 7D12-800CW (middle) and NIR fluorescence color merge FLARE image (right)

Histology: Shown are a hematoxylin and eosin (HE) staining combined with a cytokeratin staining (left) and NIR fluorescence image (right) of a cervical lymph node of a mice injected with 7D12-800CW. A clear overlap between NIR fluorescence and the brown cytokeratin staining (indicating tumor cells) was observed.

Next to the ideal probe, the extent to which a tumor can be visualized during surgery is highly depending on the NIR fluorescent imaging system. Gioux et al.³⁴ have reviewed the technical requirements for an intraoperative imaging system. To assess the feasibility of translating our results into clinical experiments, we used the clinically available FLARE™ imaging system. This system is able to adequately detect microscopic disease intraoperatively and has proven its clinical use in over 25 clinical trials.^{26,35} Using the IVIS spectrum we were able to measure bioluminescence and confirm the presence of tumor cells *ex vivo*, by imaging GFP fluorescence of the transfected OSC-19-luc2-cGFP cells. Furthermore, fluorescence measurements obtained with the IVIS spectrum, i.e. a closed ('black box') preclinical imaging system, were compared with the measurements of the clinically available FLARE™ imaging system. This comparison showed a significant difference in TBR favoring the IVIS spectrum on the optimal imaging time point (24hr post injection). This difference can be explained by the fact that the IVIS spectrum is, in contrary to the FLARE imaging system, a 'black box' imager with less daylight interfering and subsequently less background fluorescence. However, since this device obviously cannot be used intraoperatively, the FLARE imaging system is an adequate alternative as the average TBR was over 2.

In previous studies, we used the EGFR targeted nanobody 7D12 conjugated to 800CW to image subcutaneous A431 tumor xenografts, which have high EGFR expression.¹⁷ Undoubtedly, the host microenvironment has great influence on tumor biology that affects parameters such as angiogenesis, growth, invasion, metastasis and lymphangiogenesis. Therefore, an orthotopic model is clinically a more relevant model with great importance to assess the ability of a probe for fluorescence delineation of tumors and its possible translation to the clinic. In this study, we successfully tested the potentiality of intraoperative fluorescence delineation of orthotopic OSCC and microscopic lymph node metastases using a clinically available fluorescence imaging system. Based on these results we conclude that clinical translation of 7D12-800CW may be possible, using the FLARE imaging system in the intraoperative set-up.

A sufficient TBR is required to distinguish tumor from normal tissue³⁰ The

small molecular weight of 7D12 allows fast detection of the tumor due to rapid distribution and fast clearance of unbound molecules. Oliveira et al.¹⁷ reported tumor detection from 30 minutes after injection onwards. In the present study, using both the FLARE and IVIS spectrum, the tumor could be sufficiently detected 2 hours post injection. The use of an orthotopic model in the tongue that differs in angiogenesis, lymphangiogenesis and interstitial pressure from a subcutaneous A431 tumor, could perhaps explain these variations. Nevertheless, the highest average tumor to background ratio (2.72 IVIS spectrum vs 2.0 FLARE) was obtained 24 hours after injection, which is in agreement with what was previously reported in the subcutaneous tumor model.¹⁷ Although nanobodies distribute and bind to their targets very rapidly, the background signal is relatively high during the first hours. Monovalent nanobodies are not efficiently internalized and therefore bound nanobody can un-bind over a certain period of time.³⁶ The 7D12-800CW washout from normal tissue occurs faster than the release from its receptor in the tumor. As a result the TBR will increase over time until an optimal TBR is reached. After that, release of nanobody from its receptor will result in a decrease in TBR. A decreased TBR in our study was seen after 48 hours.

Cryosections of the tongue confirmed the tumor specific fluorescence by colocalization of the fluorescent signal of 7D12-800CW and the fluorescence of the GFP transfected OSC-19 cells. In the cryosections of mice injected with R2-800CW some fluorescence was detected, but there was no colocalization of NIR and GFP fluorescence. R2-800CW fluorescence mainly originated from the area surrounding the tumor. A possible explanation for the non-EGFR specific presence of R2-800CW could be the enhanced permeability and retention that is seen in many tumors.³⁷ Fluorescence could not be detected in the cryo sections of tongues of mice injected with 800CW alone.

When translating 7D12-800CW to the clinic, the specific binding of the nanobody to human EGFR could result in higher background fluorescence and therefore lower contrast. Importantly, Oliveira et al.¹⁷ demonstrated the ability of 7D12-800CW to distinguish between different expression levels of EGFR *in vitro*. This implies that 7D12 could differentiate tumor tissue with high EGFR expression from normal tissue without overexpression of EGFR.

The prognosis of patients with head and neck cancer is largely dependent on lymph node involvement.^{38,39} A sentinel lymph node (SLN) procedure could prevent elective neck dissections that are frequently performed for adequate staging and local control. Furthermore, despite the analysis by a trained pathologist, (micro)

metastases and occult tumor cells in lymph nodes can be missed by standard histopathological examination. Limited examination of one lymph node could increase the accuracy of staging in head and neck cancer. Recently van der Vorst et al.⁴⁰ demonstrated the feasibility to detect draining lymph nodes in head and neck cancers using the nonspecific fluorescent tracer ICG:HSA. The fluorescent tracer however, quickly migrated to lymph nodes beyond the SLN. This present study demonstrates the feasibility of specific targeting of cervical lymph node metastases. A dose of 75 µg of 7D12-800CW clearly allowed delineation of the primary tumor and identification of the cervical lymph node metastases after removal of the skin. Histology showed clear co-localization of the NIR fluorescence of 7D12-800CW and the cytokeratin staining, that confirmed the presence of tumor cells. Compared to the primary tumor however, an increase of nonspecific background signal was observed. Also, the smaller the tumor or metastases, the lower the fluorescent signal. Furthermore, the influence of optical properties on the light propagation through tissue can result in a blurred delineation of smaller tumors. Altogether, these aspects rendered visualization of the metastases slightly difficult, which was significantly improved by removal of the skin. Further research is needed to explore which is the minimum size of lymph node metastases that can be detected using 7D12-800CW. Intraoperative detection of lymph node metastases would be a better alternative to the non-specific SLN procedure. First, the efficiency of an intraoperative histopathological diagnosis on fresh-frozen sections could be increased by examination of the fluorescence positive lymph node. Eventually, the procedure might even prevent intraoperative pathologic analysis of fresh-frozen tissue sections.

In conclusion, the present study reports a recently developed fluorescent EGFR targeting nanobody, which clearly allowed the identification of orthotopic tongue tumors and cervical lymph node metastases in a mouse model. These results highlight the potential of this nanobody for clinical translation in the context of surgical management of oropharyngeal or OSCC.

REFERENCES

1. McMahon J, O'Brien CJ, Pathak I et al. Influence of condition of surgical margins on local recurrence and disease-specific survival in oral and oropharyngeal cancer. *Br J Oral Maxillofac Surg* 2003; 41:224-231.
2. Iseli TA, Lin MJ, Tsui A et al. Are wider surgical margins needed for early oral tongue cancer? *J Laryngol Otol* 2012; 126:289-294.
3. Looser KG, Shah JP, Strong EW. The significance of "positive" margins in surgically resected epidermoid carcinomas. *Head Neck Surg* 1978; 1:107-111.
4. Loree TR, Strong EW. Significance of positive margins in oral cavity squamous carcinoma. *Am J Surg* 1990; 160:410-414.
5. Weissleder R, Pittet MJ. Imaging in the era of molecular oncology. *Nature* 2008; 452:580-589.
6. Frangioni JV. New technologies for human cancer imaging. *J Clin Oncol* 2008; 26:4012-4021.
7. Keereweer S, Kerrebijn JD, van Driel PB et al. Optical Image-guided Surgery-Where Do We Stand? *Mol Imaging Biol* 2011; 13:199-207.
8. Adams KE, Ke S, Kwon S et al. Comparison of visible and near-infrared wavelength-excitable fluorescent dyes for molecular imaging of cancer. *J Biomed Opt* 2007; 12:024017.
9. Heath CH, Deep NL, Sweeny L et al. Use of panitumumab-IRDye800 to image microscopic head and neck cancer in an orthotopic surgical model. *Ann Surg Oncol* 2012; 19:3879-3887.
10. Pomerantz RG, Grandis JR. The epidermal growth factor receptor signaling network in head and neck carcinogenesis and implications for targeted therapy. *Semin Oncol* 2004; 31:734-743.
11. Yarden Y. The EGFR family and its ligands in human cancer: signalling mechanisms and therapeutic opportunities. *Eur J Cancer* 2001; 37 Suppl 4:S3-S8.
12. Laimer K, Spizzo G, Gastl G et al. High EGFR expression predicts poor prognosis in patients with squamous cell carcinoma of the oral cavity and oropharynx: a TMA-based immunohistochemical analysis. *Oral Oncol* 2007; 43:193-198.
13. Muyldermans S, Atarhouch T, Saldanha J et al. Sequence and structure of VH domain from naturally occurring camel heavy chain immunoglobulins lacking light chains. *Protein Eng* 1994; 7:1129-1135.
14. Hamers-Casterman C, Atarhouch T, Muyldermans S et al. Naturally occurring antibodies devoid of light chains. *Nature* 1993; 363:446-448.
15. Cortez-Retamozo V, Lauwereys M, Hassanzadeh GG et al. Efficient tumor targeting by single-domain antibody fragments of camels. *Int J Cancer* 2002; 98:456-462.
16. De GE, Saerens D, Muyldermans S et al. Antibody repertoire development in camelids. *Dev Comp Immunol* 2006; 30:187-198.
17. Sabrina Oliveira, Guus A.M.S.van Dongen, Marijke Stigter-van Walsum et al. Rapid Visualization of Human Tumor Xenografts through Optical Imaging with a Near-infrared Fluorescent Anti-Epidermal Growth Factor Receptor Nanobody. *Molecular Imaging* 2011.
18. Gaikam LO, Huang L, Cavellers V et al. Comparison of the biodistribution and tumor targeting of two ^{99m}Tc-labeled anti-EGFR nanobodies in mice, using pinhole SPECT/micro-CT. *J Nucl Med* 2008; 49:788-795.
19. Yokoi T, Yamaguchi A, Odajima T et al. Establishment and characterization of a human cell line derived from a squamous cell carcinoma of the tongue. *Tumor Research* 1988;43-57.
20. Carlotti F, Bazuine M, Kekarainen T et al. Lentiviral vectors efficiently transduce quiescent mature 3T3-L1 adipocytes. *Mol Ther* 2004; 9:209-217.
21. Roovers RC, Vosjan MJ, Laeremans T et al. A biparatopic anti-EGFR nanobody efficiently inhibits solid tumour growth. *Int J Cancer* 2011; 129:2013-2024.
22. van der Linden R, de GB, Stok W et al. Induction of immune responses and molecular cloning of the heavy chain antibody repertoire of Lama glama. *J Immunol Methods* 2000; 240:185-195.
23. Dolk E, van VC, Perez JM et al. Induced refolding of a temperature denatured llama heavy-chain antibody fragment by its antigen. *Proteins* 2005; 59:555-564.
24. Oliveira S, Cohen R, Walsum MS et al. A novel method to quantify IRDye800CW fluorescent antibody probes ex vivo in tissue distribution studies. *EJNMMI Res* 2012; 2:50.

25. Roovers RC, Laeremans T, Huang L et al. Efficient inhibition of EGFR signaling and of tumour growth by antagonistic anti-EGFR Nanobodies. *Cancer Immunol Immunother* 2007; 56:303-317.
26. Troyan SL, Kianzad V, Gibbs-Strauss SL et al. The FLARE intraoperative near-infrared fluorescence imaging system: a first-in-human clinical trial in breast cancer sentinel lymph node mapping. *Ann Surg Oncol* 2009; 16:2943-2952.
27. Kim JB, Urban K, Cochran E et al. Non-invasive detection of a small number of bioluminescent cancer cells in vivo. *PLoS One* 2010; 5:e9364.
28. Mieog JS, Hutteman M, van der Vorst JR et al. Image-guided tumor resection using real-time near-infrared fluorescence in a syngeneic rat model of primary breast cancer. *Breast Cancer Res Treat* 2010.
29. van Dam GM, Crane LM, Themelis G et al. Intraoperative tumor-specific fluorescence imaging in ovarian cancer by folate receptor-alpha targeting: first in-human results. *Nat Med* 2011; Sep 18;17(10):1315-9.
30. Keereweer S, Sterenborg HJ, Kerrebijn JD et al. Image-guided surgery in head and neck cancer: current practice and future directions of optical imaging. *Head Neck* 2012; 34:120-126.
31. Grandis JR, Tweardy DJ. Elevated levels of transforming growth factor alpha and epidermal growth factor receptor messenger RNA are early markers of carcinogenesis in head and neck cancer. *Cancer Res* 1993; 53:3579-3584.
32. Keereweer S, Kerrebijn JD, Mol IM et al. Optical imaging of oral squamous cell carcinoma and cervical lymph node metastasis. *Head Neck* 2012; 34:1002-1008.
33. Gleysteen JP, Duncan RD, Magnuson JS et al. Fluorescently labeled cetuximab to evaluate head and neck cancer response to treatment. *Cancer Biol Ther* 2007; 6:1181-1185.
34. Gioux S, Choi HS, Frangioni JV. Image-guided surgery using invisible near-infrared light: fundamentals of clinical translation. *Mol Imaging* 2010; 9:237-255.
35. Mieog JS, Troyan SL, Hutteman M et al. Toward optimization of imaging system and lymphatic tracer for near-infrared fluorescent sentinel lymph node mapping in breast cancer. *Ann Surg Oncol* 2011; 18:2483-2491.
36. Heukers R, Vermeulen JF, Fereidouni F et al. Endocytosis of EGFR requires its kinase activity and N-terminal transmembrane dimerization motif. *J Cell Sci* 2013; 126:4900-4912.
37. Keereweer S, Mol IM, Kerrebijn JD et al. Targeting integrins and enhanced permeability and retention (EPR) effect for optical imaging of oral cancer. *J Surg Oncol* 2012; 105:714-718.
38. Leemans CR, Tiwari R, Nauta JJ et al. Regional lymph node involvement and its significance in the development of distant metastases in head and neck carcinoma. *Cancer* 1993; 71:452-456.
39. Layland MK, Sessions DG, Lenox J. The influence of lymph node metastasis in the treatment of squamous cell carcinoma of the oral cavity, oropharynx, larynx, and hypopharynx: N0 versus N+. *Laryngoscope* 2005; 115:629-639.
40. van der Vorst JR, Schaafsma BE, Verbeek FP et al. Near-infrared fluorescence sentinel lymph node mapping of the oral cavity in head and neck cancer patients. *Oral Oncol* 2012.

Chapter 4

Near-infrared fluorescent imaging of both colorectal cancer and ureters using a low-dose integrin targeted probe

Verbeek FP¹, van der Vorst JR¹, Tummers QR, Boonstra MC, de Rooij KE, Lowik CW, Valentijn RP, van de Velde CJ, Frangioni JV, Choi H, Vahrmeijer AL

¹Both authors contributed equally to this work and share first-authorship.

ABSTRACT

Background

Irradical tumor resections and iatrogenic ureteral injury remain a significant problem during lower abdominal surgery. The aim of the current study was to intraoperatively identify both colorectal tumors and ureters in subcutaneous and orthotopic animal models using cRGD-ZW800-1 and NIR fluorescence.

Material and Methods

The zwitterionic fluorophore ZW800-1 was conjugated to the tumor specific peptide cRGD (targeting integrins) and to the α -specific peptide cRAD. One nmol cRGD-ZW800-1, cRAD-ZW800-1, or ZW800-1 alone was injected in mice bearing subcutaneous HT-29 human colorectal tumors. Subsequently, cRGD-ZW800-1 was injected at dosages of 0.25 and 1 nmol in mice bearing orthotopic HT-29 tumors transfected with luciferase2. In vivo biodistribution and ureteral visualization were investigated in rats. Fluorescence was measured intraoperatively at several time points after probe administration using the FLARE imaging system.

Results

Both subcutaneous and orthotopic tumors could be clearly identified using cRGD-ZW800-1. A significantly higher signal-to-background ratio (SBR) was observed in mice injected with cRGD-ZW800-1 (2.42 ± 0.77) compared to mice injected with cRAD-ZW800-1 or ZW800-1 alone (1.21 ± 0.19 and 1.34 ± 0.19 , respectively) when measured at 24 h after probe administration. The clearance of cRGD-ZW800-1 permitted visualization of the ureters and also generated minimal background fluorescence in the gastrointestinal tract.

Conclusions

This study appears to be the first to demonstrate both clear tumor demarcation and ureteral visualization after a single intravenous injection of a targeted NIR fluorophore. As a low dose of cRGD-ZW800-1 provided clear tumor identification, clinical translation of these results should be possible.

INTRODUCTION

In cancer surgery, positive resection margins remain one of the biggest problems, resulting in a high number of recurrences and poor prognosis. In contrast to the many imaging modalities that can be used preoperatively for diagnosis, staging, and surgical planning (CT, MRI, SPECT, PET), real-time, intraoperative imaging modalities to assess the extent of disease and to determine adequate resection margins are lacking. In most cases, surgeons still have to rely only on palpation and visual inspection to discriminate between tumor tissue and normal tissue.¹ Since this situation has not been changed for many decades, there remains a need for a diagnostic tool that can discriminate tumor tissue from normal tissue in real time during surgery.

In addition, iatrogenic ureteral injury is a rare, but serious complication of lower abdominal surgery, with a reported incidence rate varying from 0.7% up to 10%.²⁻⁴ Ureteral identification can be challenging, especially in patients with previous surgery or inflammation, and during minimally invasive procedures. Early identification of ureteral damage permits direct repair and is of paramount importance to reduce morbidity and preservation of renal function.

Near-infrared (NIR) fluorescence guided surgery is a novel technique that enables real-time visualization of tumors and vital structures (i.e. ureters) using light in the NIR spectrum.⁵⁻⁷ The use of NIR light has the advantages of being less absorbed by tissue and being invisible to the human eye. This results in high tissue penetration without altering the look of the surgical field. By conjugating NIR fluorescent dyes to tumor specific ligands, intraoperative NIR fluorescent tumor detection and demarcation can be achieved. During the last decade, many tumor-specific ligands, such as antibodies, nanobodies, and peptides have been used for this purpose, all with their own advantages and disadvantages.⁸⁻¹¹ Furthermore, multiple fluorescent dyes have been tested to optimize fluorescent intensity, biodistribution, and clearance.¹²⁻¹⁵ In addition, Metildi et. al. recently showed the ability to visualize sub-millimeter tumor deposits along the cecal wall in a patient-derived orthotopic nude mouse model using a chimeric CEA antibody and visible fluorescence.¹⁶

The present study evaluates the use of a low dose fluorescent dye ZW800-1 conjugated to the cyclic RGD peptide (cRGD) targeting integrin for colorectal tumor imaging and ureteral visualization.¹⁵ RGD is a small peptide that targets integrin $\alpha 5\beta 1$, $\alpha 8\beta 1$, $\alpha v\beta 1$, $\alpha v\beta 3$, $\alpha v\beta 5$, $\alpha v\beta 6$, $\alpha v\beta 8$ and $\alpha 11\beta 3$.¹⁷⁻²⁰ Integrins are

cell-surface transmembrane heterodimeric glycoproteins that are involved in cell adhesion, matrix interaction, and cell signaling pathways²¹; integrin $\alpha_v\beta_3$ plays a key role in the early phase of tumor angiogenesis, tumor cell migration, and is overexpressed in various cancer types, including colorectal and breast cancer²². Moreover, an intermediate to high expression of $\alpha_v\beta_3$ is observed on the (neo) vasculature of colon carcinoma in about 75% of patients with colon cancer.^{23,24} cRGD-ZW800-1 has recently been developed and validated by our group using in vitro and in vivo assays with melanoma, breast, liver and lung cancer cell lines¹⁵. In addition, recent preclinical studies demonstrated successful identification of breast, colon, lung, ovarian, and glioblastoma cancers by targeting $\alpha_v\beta_3$ integrin.²⁵⁻²⁹ Furthermore, a number of clinical studies successfully showed integrin $\alpha_v\beta_3$ targeting using ¹⁸F-galacto-RGD and PET imaging in breast cancer and malignant gliomas.^{28,30-32}

ZW800-1 is a recently developed zwitterionic fluorescent dye which is cleared rapidly by the kidneys, has a high quantum yield, and was engineered for high hydrophilicity.³³ ZW800-1 has a net charge of 0 after conjugation to a targeting ligand with a net charge of -1 prior to conjugation, an absorption peak of approximately 772 nm, and an emission peak of 788 nm in fetal bovine serum. ZW800-1 is freely filtered by the kidney and is exclusively eliminated from the body by the kidneys. As such, non-specific background signal in the intestines is low, making it valuable for colorectal tumor imaging, and simultaneously, ureteral visualization is enabled. To maximize renal clearance of the conjugate, the hydrophilic variant RGDyK was chosen for conjugation to ZW800-1.³⁴

The aim of the current study was to evaluate the ability to visualize both colorectal cancer and ureters using NIR fluorescence and a single injection of cRGD-ZW800-1.

MATERIAL AND METHODS

Ethical standards and animal care

All animal experiments were approved for animal health, ethics, and research by the Animal Welfare Committee of Leiden University Medical Center, the Netherlands. All animals received humane care and maintenance in compliance with the “Code of Practice Use of Laboratory Animals in Cancer Research” (Inspectie W&V, July 1999). All animals were housed in the animal facility of the Leiden University Medical Center. Pellet food and fresh tap water were provided ad libitum. The weight of the animals was followed throughout the experiment to monitor their general health state. Throughout tumor inoculation, imaging, and surgical procedures, the animals were anesthetized with 5% isoflurane for induction and 2% isoflurane for maintenance in oxygen with a flow of 0.8 L/min and placed on an animal bed with an integrated nose mask.

Tumor models

Subcutaneous colon tumors were induced in 6 week-old CD1-Foxn1^{nu} female mice (Charles River Laboratories, Wilmington, MA, USA) weighing 25 - 35 g by subcutaneous injection at 4 sites with 5×10^5 HT29-luc2 cells in 40 μ L RPMI1640 medium per site. Tumor growth was monitored longitudinally using a digital caliper and with bioluminescence imaging (BLI) after an intraperitoneal injection of 150 mg/kg of D-luciferin solution (SynChem, Inc., Elk Grove Village, IL) in PBS in a total volume of 50 μ L 10 minutes prior to imaging using the IVIS Spectrum imaging system (Caliper LifeSciences, Hopkinton, MA, USA). In order to induce orthotopic tumors, subcutaneously growing HT29-luc2 colon tumors were harvested and subsequently transplanted onto the cecum of a healthy mouse, according to the model described by Tseng et al.³⁵ (fig. 4a). Briefly, the cecal wall was slightly incised to facilitate tumor cell infiltration and small tumor fragments (approximately 2 mm) were transplanted on the cecal wall using a 6-0 suture. Tumor growth was monitored using BLI.

In Vivo biodistribution and ureteral visualization

The ability to visualize gastrointestinal tumors in close proximity to other organs was investigated in nude mice bearing orthotopic HT29 tumors. As cRGD-ZW800-1 is cleared renally, a single intravenous injection could potentially also permit ureteral visualization. However, it showed to be challenging to visualize the ureter

in nude mice weighing only 25-35 g. Therefore, to validate in vivo biodistribution and ureteral visualization, cRGD-ZW800-1 was also administered to male WAG/Rij rats (Harlan, Horst, The Netherlands) weighing approximately 300–350 g.

NIR fluorescence imaging

When tumors were measured 5 mm in diameter, the fluorescent probe was injected. 1 nmol cRGD-ZW800-1 (N = 3), 1 nmol cRAD-ZW800-1 (N = 3), or 1 nmol ZW800-1 (N = 3) was injected intravenously in mice bearing subcutaneous tumors. NIR fluorescent signal was measured at 0.3, 0.5, 1, 2, 4, 8, 24, and 48 h after injection using the FLARE imaging system and signal-to-background ratios were calculated. Subsequently, cRGD-ZW800-1 was injected at dosages of 1 and 0.25 nmol in mice with orthotopically transplanted cecal tumors (N = 6). To observe in vivo biodistribution and ureteral visualization, 30 nmol cRGD-ZW800-1 was injected intravenously in 3 Wag/Rij rats. After injection, NIR fluorescent signal of the liver, small bowel, colon, kidney, and bladder was measured over time. NIR fluorescence measurements were performed using the FLARE imaging system as described before ³⁶.

Histological analysis

Subcutaneous tumors were surgically removed and processed. Snap frozen tissue was sectioned at 6 μ m and was scanned on the Odyssey Infrared Imaging System (LI-COR Biosciences, Lincoln, NE) using the 800 nm channel. Subsequently sections were stained using a hematoxylin and eosin to make an overlay.

Statistical Analysis

For statistical analysis, SPSS statistical software package (Version 17.0, Chicago, IL) was used. To generate graphs, GraphPad Prism Software (Version 5.01, La Jolla, CA) was used. Signal-to-background ratios (SBR) were calculated by dividing the fluorescent signal of the tumor by fluorescent signal of surrounding tissue. SBR was reported in mean and standard deviation. To compare SBRs between dose groups and time points, and to assess the relation between dose and time, a mixed model analysis was used. When a significant difference was detected, a one-way ANOVA was used to post-test for differences between separate dose groups and/or time points. The one-way ANOVA was corrected using the Bonferroni correction. $P < 0.05$ was considered significant.

RESULTS

NIR fluorescent probe

cRGD and cRAD were conjugated to ZW800-1 as described in the supplementary data (Fig. 1). Purity (> 98%) was confirmed by analytical reversed-phase HPLC (770 nm absorbance) and MALDI-TOF.

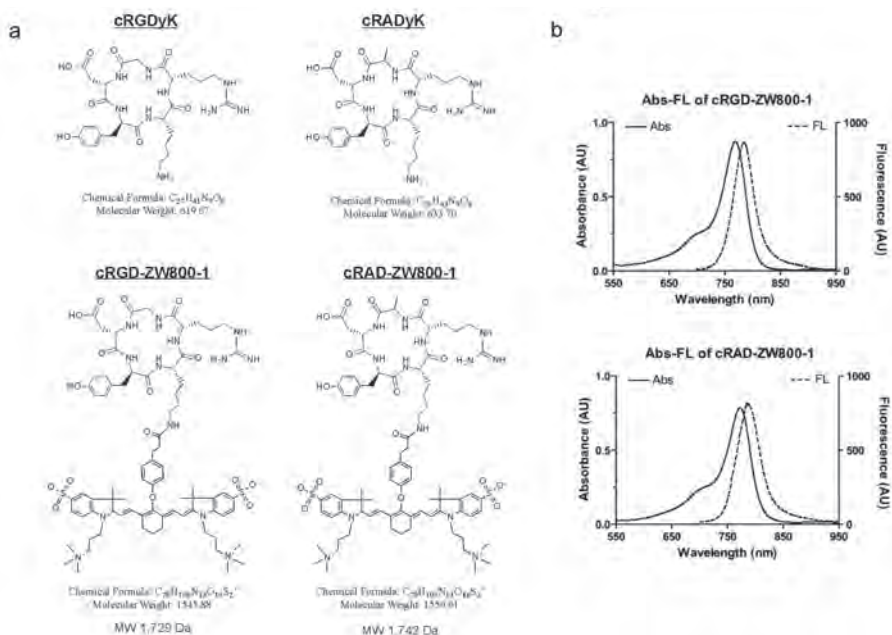


Figure 1 - Structure formulas and optical properties: a: Chemical structures and formulae of cRGDyK and cRADyK before and after conjugation to ZW800-1. b: Optical property measurements of cRGD-ZW800-1 and cRAD-ZW800-1.

Intraoperative NIR Fluorescence Imaging Mice with Subcutaneous tumors

Three weeks after inoculation, mice were injected intravenously with cRGD-ZW800-1, cRAD-ZW800-1, or ZW800-1 alone. All subcutaneous tumors of mice could be clearly identified after injection of cRGD-ZW800-1 using NIR fluorescence (SBR at 24 h after injection was 2.42 ± 0.77 ; Fig. 2). No adequate tumor-to-background ratios were observed in the control mice injected with cRAD-ZW800-1 (SBR was 1.21 ± 0.19 at 24 h after injection) or ZW800-1 alone (SBR was 1.34 ± 0.19 at 24 h after injection). Using a mixed-model analysis, differences in SBRs between 3 study groups and between time points were significant ($P = 0.006$ and $P < 0.0001$,

respectively; Fig. 2). Post-testing using a one-way ANOVA showed significant differences between the cRGD-ZW800-1 and the cRAD-ZW800-1 ($P < 0.0001$) study groups and between the cRGD-ZW800-1 and ZW800-1 alone ($P < 0.0001$) study groups. No significant difference was found between cRAD-ZW800-1 and ZW800-1 alone ($P = 1.0$). The highest SBRs were measured at 8 (2.33 ± 0.68) and 24 h (2.42 ± 0.77) after administration of cRGD-ZW800-1.

Histological analysis

Using the Odyssey Infrared Imaging System, clear differences were observed between 3 study groups. An increased fluorescent signal was observed in tumors harvested from mice in which cRGD-ZW800-1 was injected and a weak fluorescent signal was measured in tumors harvested from mice in the control groups (cRAD-ZW800-1 and ZW800-1 alone) (Fig. 3).

Intraoperative NIR Fluorescence Imaging in Mice with Orthotopic Tumors

In 6 mice with orthotopically transplanted colon tumors, tumor growth was assessed using BLI (Fig. 4b). After 30 days, BLI measurements showed approximately 5.0×10^6 counts and cRGD-ZW800-1 was administered intravenously. cRGD-ZW800-1 was administered at dosages of 1 (N = 3) and 0.25 nmol (N = 3) (Fig. 4c). In all mice, tumors could be adequately differentiated from surrounding healthy bowel tissue (Fig. 4c and d). Average SBR in these mice was 2.62 ± 0.17 and 1.75 ± 0.36 for the 1 and 0.25 nmol dose groups respectively.

In vivo Biodistribution and Ureteral Visualization in Rats

To assess the potential use of cRGD-ZW800-1 for both intraoperative detection of gastrointestinal tumors and ureteral identification, the NIRF intensity of abdominal organs was quantified over time in 3 male Wag/Rij rats. After administration of cRGD-ZW800-1 intravenously, medial laparotomy was performed and signal in liver, small bowel, colon, kidney, and bladder was measured. Time points were 0, 0.1, 0.5, 1, 2, 3, 4, 8, and 24 h after intravenous administration (fig. 5). Average fluorescence intensities (normalized arbitrary units, AU) at $t = 2$ hour, were: $594 (\pm 163)$, $599 (\pm 65)$, $443 (\pm 169)$, $6172 (\pm 3250)$ and $21714 (\pm 2102)$ for the liver, small bowel, colon, kidney, and bladder respectively. Figure 5a shows an example in which the ureters could clearly be visualized, 30 minutes after injection of cRGD-ZW800-1.

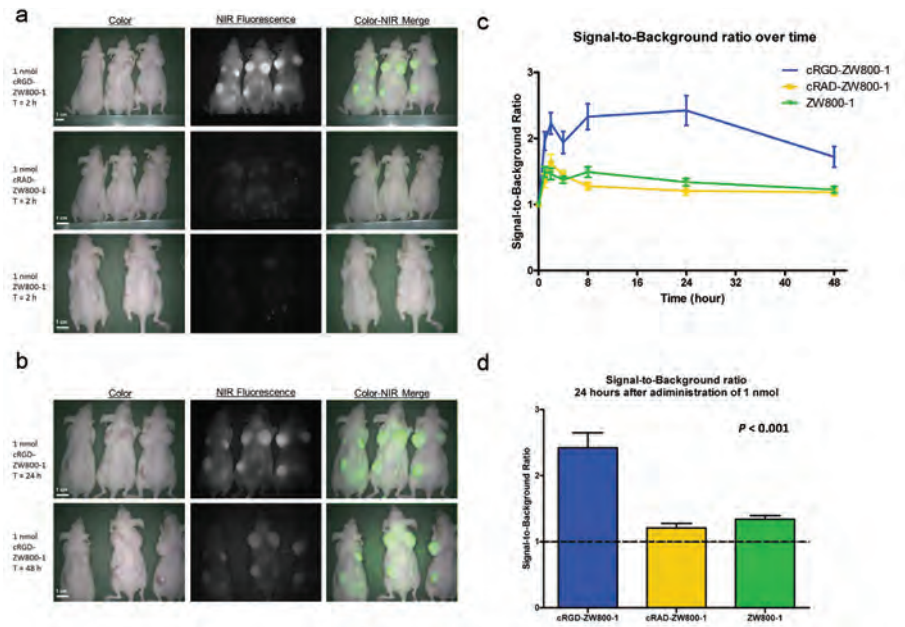


Figure 2 – In vivo NIR fluorescence imaging of mice bearing subcutaneous tumors: a: NIR fluorescence imaging of mice bearing subcutaneous HT-29-Luc2 tumors 2 h after administration of 1 nmol cRGD-ZW800-1 (upper row), 1 nmol RAD-ZW800-1 (middle row), and 1 nmol ZW800-1 (lower row). b: NIR fluorescence imaging of the same cRGD-ZW800-1 mice 24 and 48 h after dye administration. Scale bars represent 1 cm. c: Tumor-to-background ratios over time. Plotted are the tumor-to-background ratios (mean, SEM) of cRGD-ZW800-1 (blue line), cRAD-ZW800-1 (yellow), and ZW800-1 alone (green). d: Signal-to-background ratio (mean, SEM) 24 h after administration of 1 nmol of fluorophore.

DISCUSSION

The present study reports the use of a ligand (cRGD) conjugated to ZW800-1 that targets integrins in low dosage range for NIR fluorescence imaging during surgery. cRGD-ZW800-1 was successfully used in both subcutaneous and orthotopic mouse models to identify malignant cells. Because contrast agents can accumulate in tumors via enhanced permeability and retention (EPR)³⁷⁻⁴¹, 2 negative control groups (cRAD-ZW800-1 and ZW800-1 alone) were included to confirm specificity of the fluorescent signal in tumors.

With regards to an oncologic resection, in which all tumor cells need to be resected, a specific NIR fluorescent signal is vital. We aimed to develop a fluorescent agent with a low non-specific tumor accumulation component and high specific targeting. Choi et al. recently published the use of the targeted zwitterionic near-infrared fluorophore cRGD-ZW800-1 and compared it with commercially available

fluorophores.¹⁵ It was shown that cRGD-ZW800-1 outperformed the commercially available dyes in vitro for immunocytochemistry, histopathology and immunoblotting and in vivo for image-guided surgery. However, as this was not the design of the study, no negative controls were used in in vivo image-guided surgery models. Therefore, the current study aimed to test the specificity of cRGD-ZW800-1. Mice injected with cRAD-ZW800-1 or ZW800-1 alone showed no tumor signal both during in vivo imaging using the FLARE imaging system and ex vivo imaging using the Odyssey imaging system. Since cRGD-ZW800-1 and cRAD-ZW800-1 are comparable with regards to size, charge, and solubility, it can be stated that it's highly probable that the cRGD-ZW800-1 signal is specific.

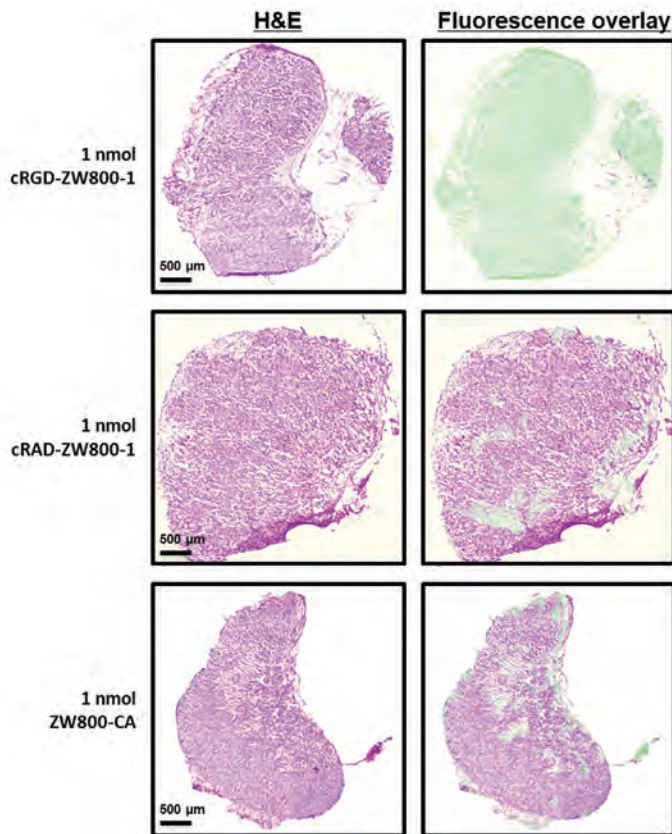


Figure 3 – Fluorescence microscopy: Shown are hematoxylin and eosin (H&E) staining (left column) with a pseudo-colored green NIR fluorescence overlay (Odyssey, right column) of a 5 µm tissue section of a subcutaneously growing colon tumor using a 5 X objective. A high fluorescent signal was observed after cRGD-ZW800-1 administration using the Odyssey compared to cRAD-ZW800-1 and ZW800-1. Scale bars represent 500 µm.

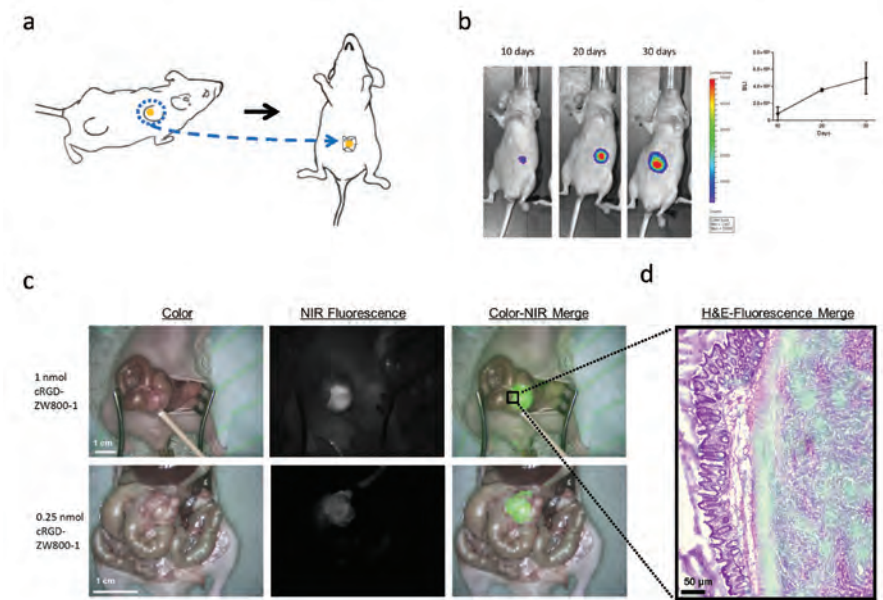


Figure 4 Intraoperative imaging of orthotopic colon tumors: a: Schematic overview of the induction of an orthotopic tumor model. Subcutaneously growing HT29-luc2 colon tumors were resected and transplanted onto the cecum of a healthy mouse. b: tumor growth monitoring using noninvasive bioluminescence imaging. c: Shown are 2 examples of cRGD-ZW800-1 administered intravenously, which allowed clear tumor identification using NIR fluorescence in orthotopic colon tumor bearing mice. cRGD-ZW800-1 was injected at dosages of 1 nmol and 0.25 nmol. Scale bars represent 1 cm. d: H&E and fluorescence overlay of the border between tumor and normal colon tissue.

Imaging in the peritoneal cavity can be challenging, mostly due to high levels of background fluorescence when tracers are cleared by the liver. In this study, high tumor-to-background ratios were observed in the orthotopic tumor model due to the low hepatic clearance and the resulting low fluorescent signal in the gastrointestinal tract.

Since cRGD-ZW800-1 is cleared renally, it permits ureteral visualisation in addition to tumor imaging. Noninvasive detection of the ureters using NIR fluorescence has several advantages over conventional ureteral stent placing as it can be used within minutes after dye administration during both open and laparoscopic surgery. Besides, placement of ureteral stents is an invasive procedure that harbors an increased risk of complications such as ureteral perforation, urinary tract infection, and acute renal failure. Clinical feasibility to identify the ureters using NIR imaging has recently been demonstrated.⁴² Using cRGD-ZW800-1 for both tumor and ureter imaging during lower abdominal procedures, surgical outcome could

be greatly improved, while reducing morbidity. Furthermore, this technique will be of even greater value in laparoscopic surgery as no tactile information can be used. To date, several laparoscopic imaging systems are commercially available, however, further technical developments are in progress to facilitate optimal real-time NIR fluorescence guidance in relation to surgical anatomy.^{43,44}

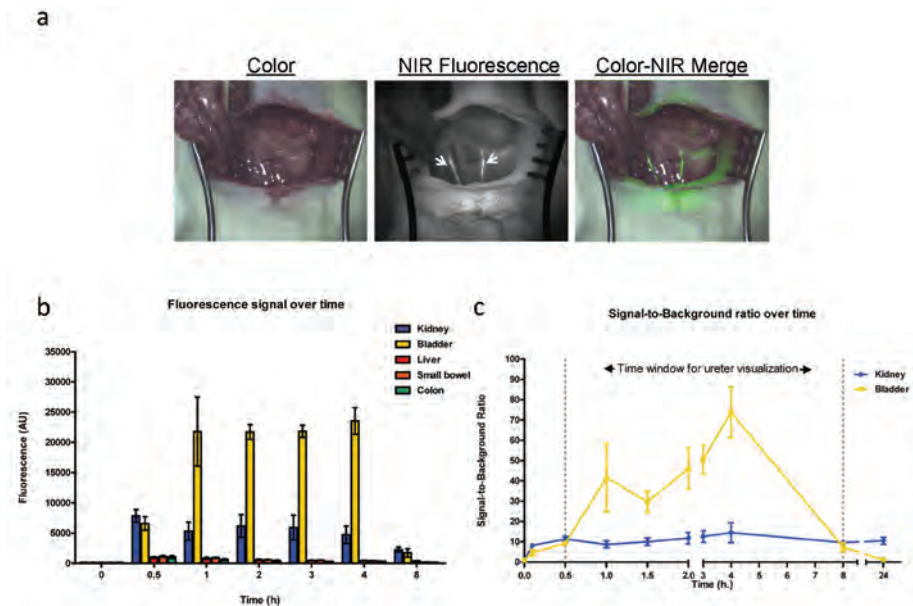


Figure 5 – In vivo biodistribution and ureteral visualization in rats: a: Both ureters (arrowheads) could clearly be observed after injection of cRGD-ZW800-1 using NIR fluorescence imaging. b: Fluorescence intensity of abdominal organs was measured using the Mini-FLARE camera system in 3 rats at several time points. c: Signal-to-background ratio of both kidney and ureter is shown over time. Based on these curves the ideal window for ureter visualization appears to lie between 10 min and 8 h. Bars represent mean \pm SEM.

Since cRGD has been extensively used for clinical imaging studies^{45,46}, toxicity and safety data are more available when compared to newly synthesized ligands. In these clinical studies, galacto-cRGD was conjugated to fluorodeoxyglucose (¹⁸F). However, as cRGD (yK) is more hydrophilic compared to galacto-RGD, the cRGDyK variant was used in this study and will be used for clinical translation.

Another advantage of cRGD-ZW800-1 is that it permits clear tumor and ureteral visualization at low dosages compared to current FDA/EMA approved NIR fluorophores (ICG and Methylene blue). When the dosages used in mice and rats are converted by body surface area, 0.25, 1, and 30 nmol is equivalent to a total human dose of 0.096, 0.39, and 1.33 mg respectively. These dosages are much lower compared to the commonly used amounts of ICG (10-25 mg) and methylene

blue (15-60 mg). In addition, a dose of 0.25 nmol in mice corresponds to a human equivalent dose of < 100 µg, which is below the FDA threshold for micro-dosing and portends more rapid clinical translation.^{47,48}

In conclusion, the present study reports the use of a recently developed fluorescent probe with minimal background uptake in the gastrointestinal tract. cRGD-ZW800-1 showed clear uptake in both a subcutaneous and an orthotopic colon cancer mouse model. Moreover, as cRGD-ZW800-1 is cleared renally, ureteral visualization is feasible after a single injection. As a low probe dose was used, clinical translation of these results is possible.

REFERENCES

1. Vahrmeijer AL, Frangioni JV. Seeing the invisible during surgery. *Br J Surg* 2011; 98:749-750.
2. Selzman AA, Spirnak JP. Iatrogenic ureteral injuries: a 20-year experience in treating 165 injuries. *J Urol* 1996; 155:878-881.
3. Delacroix SE, Jr., Winters JC. Urinary tract injuries: recognition and management. *Clin Colon Rectal Surg* 2010; 23:221.
4. Preston JM. Iatrogenic ureteric injury: common medicolegal pitfalls. *BJU Int* 2000; 86:313-317.
5. Frangioni JV. In vivo near-infrared fluorescence imaging. *Curr Opin Chem Biol* 2003; 7:626-634.
6. Vahrmeijer AL, Hutteman M, van der Vorst JR et al. Image-guided cancer surgery using near-infrared fluorescence. *Nat Rev Clin Oncol* 2013.
7. Pleijhuis RG, Graafland M, de VJ et al. Obtaining adequate surgical margins in breast-conserving therapy for patients with early-stage breast cancer: current modalities and future directions. *Ann Surg Oncol* 2009; 16:2717-2730.
8. Oliveira S, van Dongen GA, Stigter-van WM et al. Rapid visualization of human tumor xenografts through optical imaging with a near-infrared fluorescent anti-epidermal growth factor receptor nanobody. *Mol Imaging* 2012; 11:33-46.
9. Themelis G, Harlaar NJ, kelder W et al. Enhancing surgical vision by using real-time imaging of alphavbeta3-integrin targeted near-infrared fluorescent agent. *Ann Surg Oncol* 2011; 18:3506-3513.
10. Heath CH, Deep NL, Sweeny L et al. Use of panitumumab-IRDye800 to image microscopic head and neck cancer in an orthotopic surgical model. *Ann Surg Oncol* 2012; 19:3879-3887.
11. Metildi CA, Tang CM, Kaushal S et al. In Vivo Fluorescence Imaging of Gastrointestinal Stromal Tumors Using Fluorophore-Conjugated Anti-KIT Antibody. *Ann Surg Oncol* 2013.
12. van der Vorst JR, Hutteman M, Mieog JS et al. Near-Infrared Fluorescence Imaging of Liver Metastases in Rats using Indocyanine Green. *J Surg Res* 2011; 174:271.
13. Keereweer S, Mol IM, Vahrmeijer AL et al. Dual wavelength tumor targeting for detection of hypopharyngeal cancer using near-infrared optical imaging in an animal model. *Int J Cancer* 2012; 131:1633-1640.
14. Wu Y, Cai W, Chen X. Near-infrared fluorescence imaging of tumor integrin alpha v beta 3 expression with Cy7-labeled RGD multimers. *Mol Imaging Biol* 2006; 8:226-236.
15. Choi HS, Gibbs SL, Lee JH et al. Targeted zwitterionic near-infrared fluorophores for improved optical imaging. *Nat Biotechnol* 2013; 31:148-153.
16. Metildi CA, Kaushal S, Luiken GA et al. Fluorescently labeled chimeric anti-CEA antibody improves detection and resection of human colon cancer in a patient-derived orthotopic xenograft (PDOX) nude mouse model. *J Surg Oncol* 2013.
17. Bunschoten A, Buckle T, Visser N et al. Multimodal interventional molecular imaging of tumor margins and distant metastases using the integrin $\alpha_v\beta_3$ expression. *ChemBioChem* 2012; May 7;13(7):1039-45.
18. Tucker GC. Integrins: molecular targets in cancer therapy. *Curr Oncol Rep* 2006; 8:96-103.
19. Barczyk M, Carracedo S, Gullberg D. Integrins. *Cell Tissue Res* 2010; 339:269-280.
20. Ruoslahti E. RGD and other recognition sequences for integrins. *Annu Rev Cell Dev Biol* 1996; 12:697-715.
21. Hood JD, Cheresch DA. Role of integrins in cell invasion and migration. *Nat Rev Cancer* 2002; 2:91-100.
22. Vonlaufen A, Wiedle G, Borisch B et al. Integrin alpha(v)beta(3) expression in colon carcinoma correlates with survival. *Mod Pathol* 2001; 14:1126-1132.
23. Vonlaufen A, Wiedle G, Borisch B et al. Integrin alpha(v)beta(3) expression in colon carcinoma correlates with survival. *Mod Pathol* 2001; 14:1126-1132.
24. Max R, Gerritsen RR, Nooijen PT et al. Immunohistochemical analysis of integrin alpha v beta 3 expression on tumor-associated vessels of human carcinomas. *Int J Cancer* 1997; 71:320-324.
25. Axelsson R, Bach-Gansmo T, Castell-Conesa J et al. An open-label, multicenter, phase 2a study to assess the feasibility of imaging metastases in late-stage cancer patients with the alpha(v)beta(3)-selective angiogenesis imaging agent (99m)Tc-NC100692. *Acta Radiol* 2010; 51:40-46.

26. Huang R, Vider J, Kovar JL et al. Integrin alphavbeta3-Targeted IRDye 800CW Near-Infrared Imaging of Glioblastoma. *Clin Cancer Res* 2012.
27. Edwards WB, Akers WJ, Ye Y et al. Multimodal imaging of integrin receptor-positive tumors by bioluminescence, fluorescence, gamma scintigraphy, and single-photon emission computed tomography using a cyclic RGD peptide labeled with a near-infrared fluorescent dye and a radionuclide. *Mol Imaging* 2009; 8:101-110.
28. Beer AJ, Kessler H, Wester HJ et al. PET Imaging of Integrin alphaVbeta3 Expression. *Theranostics* 2011; 1:48-57.
29. Harlaar NJ, Kelder W, Sarantopoulos A et al. Real-time near infrared fluorescence (NIRF) intra-operative imaging in ovarian cancer using an alpha(v)beta(3)-integrin targeted agent. *Gynecol Oncol* 2013; 128:590-595.
30. Beer AJ, Haubner R, Sarbia M et al. Positron emission tomography using [18F]Galacto-RGD identifies the level of integrin alpha(v)beta3 expression in man. *Clin Cancer Res* 2006; 12:3942-3949.
31. Beer AJ, Niemeyer M, Carlsen J et al. Patterns of alphavbeta3 expression in primary and metastatic human breast cancer as shown by 18F-Galacto-RGD PET. *J Nucl Med* 2008; 49:255-259.
32. Schnell O, Krebs B, Carlsen J et al. Imaging of integrin alpha(v)beta(3) expression in patients with malignant glioma by [18F] Galacto-RGD positron emission tomography. *Neuro Oncol* 2009; 11:861-870.
33. Choi HS, Nasr K, Alyabyev S et al. Synthesis and in vivo fate of zwitterionic near-infrared fluorophores. *Angew Chem Int Ed Engl* 2011; 50:6258-6263.
34. Pohle K, Notni J, Bussemer J et al. 68Ga-NODAGA-RGD is a suitable substitute for (18)F-Galacto-RGD and can be produced with high specific activity in a cGMP/GRP compliant automated process. *Nucl Med Biol* 2012; 39:777-784.
35. Tseng W, Leong X, Engleman E. Orthotopic mouse model of colorectal cancer. *J Vis Exp* 2007;484.
36. Troyan SL, Kianzad V, Gibbs-Strauss SL et al. The FLARE intraoperative near-infrared fluorescence imaging system: a first-in-human clinical trial in breast cancer sentinel lymph node mapping. *Ann Surg Oncol* 2009; 16:2943-2952.
37. Intes X, Ripoll J, Chen Y et al. In vivo continuous-wave optical breast imaging enhanced with Indocyanine Green. *Med Phys* 2003; 30:1039-1047.
38. Keereweer S, Mol IM, Kerrebijn JD et al. Targeting integrins and enhanced permeability and retention (EPR) effect for optical imaging of oral cancer. *J Surg Oncol* 2012; 105:714-718.
39. Arias JL. Drug targeting strategies in cancer treatment: an overview. *Mini Rev Med Chem* 2011; 11:1-17.
40. Maeda H, Wu J, Sawa T et al. Tumor vascular permeability and the EPR effect in macromolecular therapeutics: a review. *J Control Release* 2000; 65:271-284.
41. Fang J, Nakamura H, Maeda H. The EPR effect: Unique features of tumor blood vessels for drug delivery, factors involved, and limitations and augmentation of the effect. *Adv Drug Deliv Rev* 2011; 63:136-151.
42. Verbeek FP, van der Vorst JR, Schaafsma BE et al. Intraoperative near infrared fluorescence guided identification of the ureters using low dose methylene blue: a first in human experience. *J Urol* 2013; 190:574-579.
43. Sherwinter DA. Identification of anomalous biliary anatomy using near-infrared cholangiography. *J Gastrointest Surg* 2012; 16:1814-1815.
44. Verbeek FP, Schaafsma BE, Tummers QR et al. Optimization of near-infrared fluorescence cholangiography for open and laparoscopic surgery. *Surg Endosc* 2013.
45. Beer AJ, Haubner R, Goebel M et al. Biodistribution and pharmacokinetics of the alphavbeta3-selective tracer 18F-galacto-RGD in cancer patients. *J Nucl Med* 2005; 46:1333-1341.
46. Haubner R, Wester HJ, Weber WA et al. Noninvasive imaging of alpha(v)beta3 integrin expression using 18F-labeled RGD-containing glycopeptide and positron emission tomography. *Cancer Res* 2001; 61:1781-1785.
47. U.S. Department of Health and Human Services, Center for Drug Evaluation and Research. Guidance for industry, investigators, and reviewers exploratory IND studies. Rockville, Md: U.S. Department of Health and Human Services 2006.
48. Scheuer W, van Dam GM, Dobosz M et al. Drug-based optical agents: infiltrating clinics at lower risk. *Sci Transl Med* 2012; 4:134ps11.

Part II:

Clinical translation:
Sentinel lymph node
imaging

Chapter 5

Optimization of near-infrared fluorescent sentinel lymph node mapping for vulvar cancer

Hutteman M¹, van der Vorst JR¹, Gaarenstroom K, Peters AA, Mieog JS
Schaafsma BE, Kuppen PJ, Frangioni JV, van de Velde CJ

¹Both authors contributed equally to this work and share first authorship

Am J Obstet Gynecol. 2012 Jan;206(1)

ABSTRACT

Objectives

Near-infrared (NIR) fluorescence imaging has the potential to improve sentinel lymph node (SLN) mapping in vulvar cancer, which was assessed in the current study. Furthermore, dose optimization of indocyanine green adsorbed to human serum albumin (ICG:HSA) was performed.

Material and Methods

Nine vulvar cancer patients underwent the standard SLN procedure using ^{99m}technetium-nanocolloid and patent blue. In addition, intraoperative imaging was performed after peritumoral injection of 1.6 mL of 500, 750 or 1000 μ M of ICG:HSA.

Results

NIR fluorescence SLN mapping was successful in all patients. A total of 14 SLNs (average 1.6, range 1-4) were detected: 14 radioactive (100%), 11 blue (79%), and 14 NIR fluorescent (100%).

Conclusions

This study demonstrates feasibility and accuracy of SLN mapping using ICG:HSA. Considering safety, cost, and pharmacy preferences, an ICG:HSA concentration of 500 μ M appears optimal for SLN mapping in vulvar cancer.

INTRODUCTION

Vulvar cancer is a relatively rare disease with an annual incidence of approximately 4000 cases in the United States, resulting in 900 deaths per year.¹ Tumor size and invasion into adjacent tissues are important factors for staging vulvar cancers, but nodal status remains the single most important prognosticator.² Radical vulvectomy with en bloc inguinofemoral lymphadenectomy has been replaced in the surgical treatment of vulvar cancer by radical wide local excision or radical vulvectomy with inguinofemoral lymphadenectomy using separate groin incisions.³ The latter modification has significantly decreased surgery-related morbidity.³ However, 30% to 70% of patients treated with full inguinofemoral lymphadenectomy still suffer from lymphedema.⁴⁻⁶ Only 27% of patients with clinically stage I or II vulvar cancer have tumor positive lymph nodes; therefore, approximately 70% of patients undergo unnecessary lymphadenectomy.⁶

The sentinel lymph node (SLN) biopsy, as introduced in the management of cutaneous melanoma by Morton,⁷ was first described in vulvar cancer by Levenback in 1994.⁸ The SLN procedure in vulvar cancer patients has been validated in multicenter trials and its introduction in regular clinical practice has marked a significant reduction in lymphedema, wound infection, and wound dehiscence.^{9,10} Currently, the procedure usually involves a combination of a radioactive colloid and a blue dye. However, the use of radiotracers requires complex logistics including the involvement of a nuclear medicine physician and the transport of radioactivity, and is therefore not available in all clinics. Moreover, blue dyes cannot be visualized when the lymph nodes and lymphatic channels are covered by tissue, such as skin or fat.

The use of invisible near-infrared (NIR) light (700-900 nm) has several characteristics that can be advantageous in the SLN procedure, which include relatively high penetration into living tissue (millimeters to centimeters), when compared to blue dyes, and the lack of ionizing radiation.¹¹ Indocyanine green (ICG) is one of only 2 clinically available NIR fluorescent agents and is currently the most optimal agent for SLN mapping.¹² In several studies, intraoperative imaging systems in combination with ICG have been used for the SLN procedure for various types of cancer.¹³⁻¹⁸ The lymphatic channels and SLNs in vulvar cancer are often located in a relatively superficial location in the groin when compared to other tumors; therefore, NIR fluorescence imaging could be particularly useful for this indication. Indeed, Crane et al. reported the successful use of ICG alone at

a concentration of 645 μM , in conjunction with an intraoperative imaging system for the SLN procedure in vulvar cancer.¹⁹ In that study involving 10 patients, 26 of 29 SLNs (90%) were detected *in vivo* by NIR fluorescence. Furthermore, lymphatic channels could be visualized in 5 of 16 groins (31%) containing SLNs.

Preclinical evidence demonstrated that premixing of ICG with human serum albumin (HSA, complex is ICG:HSA) increases the fluorescence intensity and hydrodynamic diameter of ICG, resulting in better retention in the SLN.²⁰ The aims of the current study were to assess the use of NIR fluorescence imaging using ICG:HSA and the Mini-FLARE intraoperative imaging system for the SLN procedure in vulvar cancer and to optimize ICG:HSA dose.

MATERIAL AND METHODS

Preparation of Indocyanine Green Adsorbed to Human Serum Albumin

ICG (25 mg vials) was purchased from Pulsion Medical Systems (Munich, Germany) and resuspended in 10 mL of sterile water for injection for the 500 μM group, or in 5 mL of sterile water for injection for the 750 μM and 1000 μM groups, to yield stock solutions of 3.2 mM and 6.4 mM, respectively. Various amounts of this stock solution were transferred to a 50 cc vial of Cealb (20% human serum albumin [HSA] solution; Sanquin, Amsterdam, The Netherlands) to yield ICG in HSA (ICG:HSA) at a final concentration of 500 μM , 750 μM , or 1000 μM .

Intraoperative NIR Fluorescence Imaging

SLN mapping was performed using the Mini-FLARE image-guided surgery system as described in detail previously.¹⁴ Briefly, the system consists of 2 wavelength separated light sources: a "white" LED light source, generating 26,600 lx of 400 to 650 nm light to illuminate the surgical field and an NIR LED light source, generating 7.7 mW / cm^2 of fluorescence excitation light. White light and NIR fluorescence images are acquired simultaneously and displayed in real time, using custom designed optics and software. A pseudo-colored (lime green) image of NIR fluorescence superimposed over the white light image is also displayed, to provide the NIR fluorescence signal in proper anatomical context.

Clinical Trial

The current dose escalation clinical trial was approved by the Medical Ethics Committee of the Leiden University Medical Center and was performed in concordance with the ethical standards of the Helsinki Declaration of 1975. Nine consecutive patients that planned to undergo a SLN procedure for squamous cell vulvar carcinoma were included in this study between June 2010 and January 2011. All patients had clinically FIGO stage I vulvar cancer with a unifocal carcinoma measuring less than 4 cm in diameter, not encroaching the vagina, anus or urethra and with negative inguinofemoral nodes as determined by palpation and ultrasonography. Exclusion criteria were pregnancy, lactation or an allergy to iodine, shellfish, or indocyanine green.

All patients gave informed consent and were anonymized. Patients received the standard-of-care SLN procedure.⁹ For our institution, this implies peritumoral injections of 60-100 MBq ^{99m}technetium-nanocolloid on the afternoon of the day before, or the morning prior to surgery. Before the start of the operation, 1 mL total of patent blue V (Guerbet, France) was injected at 4 sites peritumorally. Immediately after injection of patent blue, 1.6 mL total of ICG:HSA was injected as 4 injections at the same location as the patent blue injections. After surgical scrub, the Mini-FLARE imaging head was positioned at approximately 30 cm above the surgical field. The NIR fluorescence signal was measured percutaneously, prior to skin incision, and continuously during the surgical procedure. Throughout the procedure, the surgeon was continuously provided with real-time NIR fluorescence image guidance. When the SLN could not be found easily by NIR fluorescence, the handheld gamma probe could be used for the localization of SLNs. Relative brightness of the SLNs was determined by measuring signal-to-background ratios (SBR), that is the NIR fluorescence signal of the SLN divided by a directly adjacent region. Excised sentinel lymph nodes were analyzed *ex vivo* for NIR fluorescence and radioactivity and were routinely analyzed by histopathological frozen section analysis. SLNs were fixed in formalin and embedded in paraffin for hematoxylin, eosin, and immunohistopathological staining for AE1/AE3 at multiple levels, with an interval of 250 μ m, according to the GROningen International Study on Sentinel nodes in Vulvar cancer (GROINSS-V) study protocol.⁹

Statistical Analysis

For statistical analysis, SPSS statistical software package (Version 17.0, Chicago, IL) was used. Graphs were generated using GraphPad Prism Software (Version 5.01, La Jolla, CA). To compare the SBR between concentration groups, a one-way analysis

of variance (ANOVA) was performed with pairwise comparison with least square difference (LSD) adjustment for multiple comparisons. Assumption of homogeneity of variances was assessed using Levene's test. All statistical tests were two-tailed and $P < 0.05$ was considered significant.

RESULTS

Patient and Tumor Characteristics

Nine consecutive patients with vulvar cancer undergoing SLN mapping were included in this study. Patients and tumor characteristics are described in Table 1. Median body mass index (BMI) was 27 (range 23-45), median age was 50 years (range 30-72 years), and median tumor size was 13 mm (range 4-22 mm). In 6 patients, the tumor was laterally located and in 3 patients the tumor was located on, or near, the midline.

Table 1 – Patient and Tumor Characteristics

Patient	Dose (μM)	Age (Years)	BMI	Tumor Localization	Tumor Size (mm)
1	500	72	33	Right	22
2	500	30	22	Right	10
3	500	67	26	Left	10
4	750	37	29	Midline	17
5	750	42	45	Left	22
6	750	37	23	Right	20
7	1000	72	27	Midline	6
8	1000	50	26	Midline	4
9	1000	74	32	Left	13

Abbreviation: BMI = body mass index

Intraoperative NIR Fluorescence Imaging

Average time between ICG:HSA injection and skin incision was 19 ± 4 minutes. In all patients ($N = 9$), NIR fluorescence imaging using the Mini-FLARE system enabled visualization of one or more SLNs (Figure 1). Average time between skin incision and resection of the first SLN was 13 ± 5 minutes. A total of 14 SLNs were detected, all of which were radioactive and fluorescent (Table 2). Four SLNs from 3 patients did not have blue staining from patent blue. After all NIR fluorescent nodes were resected, the surgical field was systematically inspected for remaining radioactivity

or blue nodes. No additional nodes were found that were not detected by NIR fluorescence. No adverse reactions associated with the use of ICG:HSA or the Mini-FLARE imaging system were observed.

Table 2 – SLN Identification Results

Patient	Number of SLN detected	Radiocolloid	Blue	NIR Fluorescence	SLN+	Percutaneous Visualization
1	2 (1 left, 1 right)	2	2	2	0	Unilateral
2	1 (right)	1	1	1	0	Yes
3	1 (left)	1	1	1	1	Yes
4	2 (1 right, 1 left)	2	1	2	0	Unilateral
5	1 (left)	1	1	1	0	No
6	1 (right)	1	1	1	0	Yes
7	1 (left)	1	0	1	0	Yes
8	4 (2 left, 2 right)	4	3	4	0	Yes
9	1 (left)	1	1	1	1	No
Total	14	14 (100%)	11 (79%)	14 (100%)	2	8 of 12 groins

Abbreviations: SLN+ = number of SLNs containing tumor cells

The Effect of Lymphatic Tracer Dose on SLN Brightness

The effect of injected lymphatic tracer dose on fluorescence brightness was determined by comparing SBRs between concentration groups. Mean SBRs of the SLNs were 12.3 ± 2.9 , 16.6 ± 4.3 , and 9.5 ± 4.3 for the 500, 750 and 1000 μM concentration groups, respectively (Figure 2). A one-way ANOVA showed no significant effect of concentration on SBR ($P = 0.16$), and pairwise comparison with LSD adjustment for multiple comparison showed no difference between the individual concentration and SBR, although a trend was found for a decreased SBR of the 1000 μM group when compared to the 750 μM group ($P = 0.07$). However, due to the small sample size, the current pilot study may not have sufficient power to detect significant differences in dose groups.

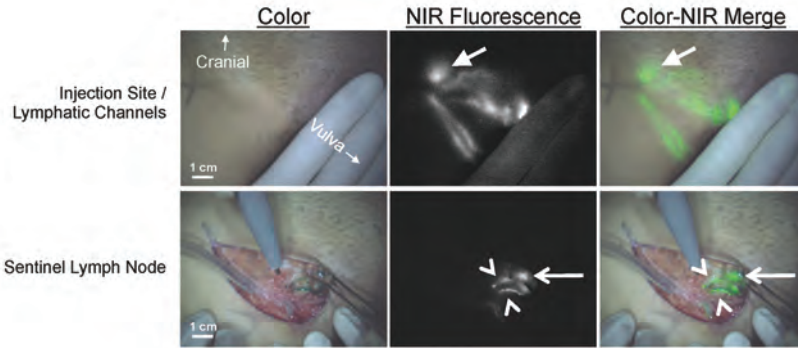


Figure 1 – Sentinel lymph node mapping using NIR fluorescence imaging in vulvar cancer: Peritumoral injection of 1.6 mL of 500 μM ICG:HSA (injection site covered by hand) identifies lymphatic channels, which converge in a SLN (arrow) that can be seen percutaneously (top row). Identification of the SLN (arrow) and 2 afferent lymphatic channels (arrowheads) is demonstrated using NIR fluorescence imaging 17 min after injection of ICG:HSA (bottom row). Camera exposure times were 100 msec (top row) and 45 msec (bottom row). Scale bars represent 1 cm.

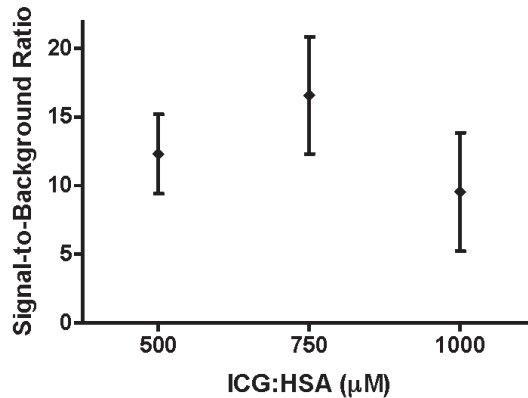


Figure 2 – Optimization of ICG:HSA dose: Signal-to-background ratio (mean \pm S.D.) of vulvar SLNs (ordinate) is plotted as a function of injected dose of ICG:HSA (abscissa). The SBRs of the 500, 750, and 1000 μM concentration groups were not significantly different, although a trend was found favoring 750 μM over 1000 μM ($P = 0.07$).

Percutaneous Visualization of Lymphatic Channels

The mean BMI of patients in which lymphatic channels were visualized percutaneously to all SLN containing groins (N = 5 patients) was 24.8 ± 2.2 . In patients with bilateral SLNs in which percutaneous visualization was possible for the groin (N = 2 patients), the mean BMI was 31.0 ± 2.8 , and in patients where percutaneous visualization of lymphatic channels was not possible (N = 2 patients), the mean BMI was 38.5 ± 9.2 . A one-way ANOVA showed a significant difference in the BMIs between these 3 groups ($P = 0.024$). A pairwise comparison with LSD adjustment for multiple comparison showed a significantly higher BMI for the group in which percutaneous visualization of lymphatic channels was not possible, when compared to the group in which percutaneous visualization of lymphatic channels was possible ($P = 0.009$).

DISCUSSION

The current study showed feasibility and accuracy of SLN mapping in vulvar cancer using ICG:HSA and the Mini-FLARE imaging system. In all 9 cases, the Mini-FLARE permitted the gynecologist to perform SLN mapping under direct image-guidance after skin incision. The flexible gooseneck of the Mini-FLARE could be used to position the system at any required location over the surgical field, which ensured no interference with the procedure. Indeed, no additional time was needed to complete the procedure, with an average time between skin incision and resection of the first SLN of 13 ± 5 minutes.

All radioactive SLNs could also be detected by NIR fluorescence. This higher detectability compared to the study by Crane et al. that utilized ICG alone¹⁹ may be due to improved brightness of ICG:HSA over ICG, better retention in the SLN, better imaging system performance, an optimized tradeoff between injection concentration and tracer dilution within lymphatic channels, or a combination thereof.¹⁴ In contrast, 4 out of 14 SLNs could not be detected by patent blue, which is comparable to previous findings.^{10,19,21} Lymphatic channels could be visualized in the majority of patients prior to skin incision. This aided the gynecologist in determining the location of the incision and facilitated a more efficient identification of SLNs. In the patients where percutaneous visualization of lymphatic channels was not possible, a higher BMI was observed when compared to patients where the lymphatic channels could be visualized percutaneously. Crane et al. observed similar findings.¹⁹ Future studies will have to determine whether NIR fluorescence imaging can replace radiocolloids in the SLN procedure in vulvar cancer, which could potentially be feasible only in non-obese patients. This could be

particularly beneficial in clinics where radiotracers are not available. Furthermore, as the patient population in Western societies tends to suffer from increasingly higher BMIs, the penetration depth has to be increased for NIR fluorescence imaging to be a generally usable imaging modality. To accomplish this, current research is focusing on improved fluorophores (some of which are currently in the process of clinical approval²²) and improved camera systems using optimized detection techniques to maximize the depth at which a fluorophore can be detected.^{23,24}

In the current study, no significant differences in NIR fluorescence signal were observed between the different concentrations that were administered. However, a trend was observed showing a decline of signal in the 1000 mM group, which is in line with previously reported results in breast cancer.¹⁴ A decrease of fluorescence signal with an increase in concentration can be explained by an effect in fluorescence quenching.¹² Fluorescence quenching occurs when the concentration of a fluorophore is too high, causing molecules to absorb the emitted light of other nearby molecules, thereby effectively attenuating the fluorescence signal. In the current study, ICG was adsorbed to HSA prior to injection. Preclinical work has shown premixing to increase the fluorescence brightness of ICG and improve retention in the SLN.²⁰ Flow to higher tier nodes seemed to have been avoided, as no additional NIR fluorescent nodes were identified that were not radioactive. An ongoing study is investigating whether the albumin is actually needed for optimal SLN mapping in vulvar cancer. When the optimal imaging parameters have been determined, larger trials can be performed to assess patient benefit.

In conclusion, the current study demonstrates the feasibility of SLN mapping in vulvar cancer patients using ICG:HSA and the Mini-FLARE image-guided surgery system. The preferred dose can be determined by local preparation preferences because no differences between tested doses were observed. In general, a dose of 500 mM seemed to be optimal, as it requires minimal manipulation of ICG and albumin volumes.

REFERENCES

1. Jemal A, Siegel R, Xu J, Ward E. Cancer statistics, 2010. *CA Cancer J Clin* 2010;60:277-300.
2. Hacker NF. Revised FIGO staging for carcinoma of the vulva. *Int J Gynaecol Obstet* 2009;105:105-06.
3. Ansink A, Van Der Velden J. Surgical interventions for early squamous cell carcinoma of the vulva. *Cochrane database of systematic reviews (Online)* 2000:CD002036.
4. Gaarenstroom KN, Kenter GG, Trimbos JB, et al. Postoperative complications after vulvectomy and inguinofemoral lymphadenectomy using separate groin incisions. *Int J Gynecol Cancer* 2003;13:522-27.
5. Rouzier R, Haddad B, Dubernard G, Dubois P, Paniel BJ. Inguinofemoral dissection for carcinoma of the vulva: effect of modifications of extent and technique on morbidity and survival. *J Am Coll Surg* 2003;196:442-50.
6. De Hullu JA, Van Der Zee AG. Surgery and radiotherapy in vulvar cancer. *Crit Rev Oncol Hematol* 2006;60:38-58.
7. Morton DL, Wen DR, Wong JH, et al. Technical details of intraoperative lymphatic mapping for early stage melanoma. *Arch Surg* 1992;127:392-99.
8. Levenback C, Burke TW, Gershenson DM, Morris M, Malpica A, Ross MI. Intraoperative lymphatic mapping for vulvar cancer. *Obstet Gynecol* 1994;84:163-67.
9. Van Der Zee AG, Oonk MH, De Hullu JA, et al. Sentinel node dissection is safe in the treatment of early-stage vulvar cancer. *J Clin Oncol* 2008;26:884-89.
10. Hampf M, Hantschmann P, Michels W, Hillemanns P, German Multicenter Study G. Validation of the accuracy of the sentinel lymph node procedure in patients with vulvar cancer: results of a multicenter study in Germany. *Gynecol Oncol* 2008;111:282-88.
11. Frangioni JV. In vivo near-infrared fluorescence imaging. *Curr Opin Chem Biol* 2003;7:626-34.
12. Gioux S, Choi HS, Frangioni JV. Image-guided surgery using invisible near-infrared light: fundamentals of clinical translation. *Mol Imaging* 2010;9:237-55.
13. Hojo T, Nagao T, Kikuyama M, Akashi S, Kinoshita T. Evaluation of sentinel node biopsy by combined fluorescent and dye method and lymph flow for breast cancer. *Breast* 2010.
14. Mieog JS, Troyan SL, Hutteman M, et al. Towards Optimization of Imaging System and Lymphatic Tracer for Near-Infrared Fluorescent Sentinel Lymph Node Mapping in Breast Cancer. *Ann Surg Oncol* 2011.
15. Troyan SL, Kianzad V, Gibbs-Strauss SL, et al. The FLARE intraoperative near-infrared fluorescence imaging system: a first-in-human clinical trial in breast cancer sentinel lymph node mapping. *Ann Surg Oncol* 2009;16:2943-52.
16. Murawa D, Hirche C, Dresel S, Hunerbein M. Sentinel lymph node biopsy in breast cancer guided by indocyanine green fluorescence. *Br J Surg* 2009;96:1289-94.
17. Crane LM, Themelis G, Pleijhuis RG, et al. Intraoperative Multispectral Fluorescence Imaging for the Detection of the Sentinel Lymph Node in Cervical Cancer: A Novel Concept. *Mol Imaging Biol* 2010.
18. Fujiwara M, Mizukami T, Suzuki A, Fukamizu H. Sentinel lymph node detection in skin cancer patients using real-time fluorescence navigation with indocyanine green: preliminary experience. *J Plast Reconstr Aesthet Surg* 2009;62:e373-e78.
19. Crane LM, Themelis G, Arts HJ, et al. Intraoperative near-infrared fluorescence imaging for sentinel lymph node detection in vulvar cancer: First clinical results. *Gynecol Oncol* 2010.
20. Ohnishi S, Lomnes SJ, Laurence RG, Gogbashian A, Mariani G, Frangioni JV. Organic alternatives to quantum dots for intraoperative near-infrared fluorescent sentinel lymph node mapping. *Mol Imaging* 2005;4:172-81.
21. Rob L, Robova H, Pluta M, et al. Further data on sentinel lymph node mapping in vulvar cancer by blue dye and radiocolloid Tc99. *Int J Gynecol Cancer* 2007;17:147-53.
22. Marshall MV, Draney D, Sevick-Muraca EM, Olive DM. Single-dose intravenous toxicity study of IRDye 800CW in Sprague-Dawley rats. *Mol Imaging Biol* 2010;12:583-94.
23. Gioux S, Mazhar A, Cuccia DJ, Durkin AJ, Tromberg BJ, Frangioni JV. Three-dimensional surface profile intensity correction for spatially modulated imaging. *J Biomed Opt* 2009;14:034045.
24. Kumar AT, Raymond SB, Bacskai BJ, Boas DA. Comparison of frequency-domain and time-domain fluorescence lifetime tomography. *Opt Lett* 2008;33:470-72.

Chapter 6

Optimization of near-infrared fluorescent sentinel lymph node mapping in cervical cancer patients

van der Vorst JR¹, Hutteman M¹, Gaarenstroom K, Peters AA, Mieog JS,
Schaafsma BE, Kuppen PJ, Frangioni JV, van de Velde CJ, Vahrmeijer AL

¹Both authors contributed equally to this work and share first authorship.

ABSTRACT

Background

In early cervical cancer, a total pelvic lymphadenectomy is the standard of care even though most patients have negative nodes and thus undergo lymphadenectomy unnecessarily. Although the value of sentinel lymph node mapping in early stage cervical cancer has not yet been established, near-infrared (NIR) fluorescence imaging is a promising technique to perform this procedure. NIR fluorescence imaging is based on invisible NIR light and can provide high sensitivity, high-resolution, and real-time image-guidance during surgery.

Material and Methods

Clinical trial subjects were 9 consecutive cervical cancer patients undergoing total pelvic lymphadenectomy. Prior to surgery, 1.6 mL of indocyanine green adsorbed to human serum albumin (ICG:HSA) was injected transvaginally and submucosally in 4 quadrants around the tumor. Patients were allocated to 500, 750, or 1,000 μM ICG:HSA concentration groups. The Mini-FLARE™ imaging system was used for NIR fluorescence detection and quantitation.

Results

Sentinel lymph nodes were identified in all 9 patients. An average of 3.4 ± 1.2 sentinel lymph nodes was identified per patient. No differences in signal to background of the sentinel lymph nodes between the 500, 750, and 1,000 μM dose groups were found ($P = 0.73$). In 2 patients, tumor-positive lymph nodes were found. In both patients, tumor-positive lymph nodes confirmed by pathology were also NIR fluorescent.

Conclusion

This study demonstrated preliminary feasibility to successfully detect sentinel lymph nodes in cervical cancer patients using ICG:HSA and the Mini-FLARE™ imaging system. When considering safety, cost-effectiveness, and pharmacy preferences, an ICG:HSA concentration of 500 μM was optimal for sentinel lymph node mapping in cervical cancer patients.

INTRODUCTION

Approximately 11,000 women are diagnosed with cervical cancer annually in the United States, resulting in over 4,000 deaths per year.¹ Cervical cancer is also the most common cause of cancer-related death in women in developing countries.² The prognosis of cervical cancer patients depends on tumor stage and tumor size, but nodal status remains the single most important prognostic factor. The surgical treatment of invasive cervical cancer depends upon the FIGO stage of the patient at time of diagnosis.³ In early stage cervical cancer, a radical hysterectomy is performed in combination with a bilateral pelvic lymphadenectomy to detect lymphatic spread. Nodal tumor involvement occurs in up to 27% of early stage cervical cancer patients⁴ and in these patients, radiotherapy or chemoradiation is the primary treatment of choice.⁵ Therefore, a total lymphadenectomy is performed unnecessarily in a substantial fraction of patients, exposing them to the risk of lymphedema and surgical injuries.

SLN mapping and biopsy is an accepted procedure for vulvar cancer, cutaneous melanomas, and breast cancer; however, its reliability for clinical use in the treatment of early stage cervical cancer has not yet been established.^{6,7} Research on the use of the SLN procedure in early stage cervical cancer patients has been extensively described using a blue dye, a radiocolloid such as ^{99m}Technetium (^{99m}Tc), or a combination of both with various results.^{8,9} Van de Lande et al. published a literature review involving over 800 patients with cervical cancer in which they described detection rates of 84%, 88%, and 97% when using blue dye alone, ^{99m}Tc alone, or a combination of both, respectively.¹⁰ Regarding the sensitivity to detect the SLNs, ^{99m}Tc, alone or in combination with blue dye, yielded the highest pooled sensitivity (92%, range 79%-98%); however, this was not significantly higher than the pooled sensitivity of blue dye alone (82%, range 67%-92%).

Due to the midline position of the cervix, it often has a bilateral multifarious drainage pattern, which makes the SLN procedure in cervical cancer patients more challenging than in breast cancer patients, for example. The main lymphatic drainage patterns have been described previously¹¹, and several studies have shown that satisfactory SLN detection in cervical cancer is established when SLNs are detected on both sides of the pelvis. Of note, status of a SLN on one side of the pelvis does not predict the nodal status of the other side.¹²

NIR fluorescence imaging is a technique that can be used in real time during surgery. This technique uses invisible near-infrared light that can be visualized using specialized camera systems.¹³ NIR fluorescence imaging has several advantages, such as relatively high tissue penetration (up to 5 millimeters without special techniques), low autofluorescence, and the lack of ionizing radiation.¹⁴ Recent preclinical and clinical studies have demonstrated that near-infrared (NIR) fluorescence imaging using the NIR fluorescence agent indocyanine green (ICG) enables real-time intraoperative visualization of lymphatic channels and detection of the SLNs in various forms of cancer without the need for radioactivity.¹⁵ Furthermore, previous preclinical work has demonstrated that adsorption of ICG to human serum albumin (HSA, complex is ICG:HSA) increases the fluorescence intensity and the hydrodynamic diameter, thereby providing improved detection and better retention in the SLN.¹⁶

Crane et al. recently described that the use of NIR fluorescence imaging in cervical cancer patients is technically feasible.¹⁷ ICG was injected after laparotomy. In this pilot study, a detection rate of 60% was reached, bilateral SLNs were detected in 30% of patients and 1 of 2 patients who had nodal involvement was false-negative.

The aim of the current study was to assess the intraoperative use of NIR fluorescence imaging using ICG:HSA and the Mini-FLARE™ imaging system in SLN biopsy in cervical cancer patients. A secondary goal was to optimize the dose of the ICG:HSA NIR fluorescent lymphatic tracer.

MATERIAL AND METHODS

Preparation of Indocyanine Green Adsorbed to Human Serum Albumin

ICG (25 mg vials) was purchased from Pulsion Medical Systems (Munich, Germany) and was resuspended in 10 cc of sterile water for injection to yield a 2.5-mg/ml (3.2 mM) stock solution for the 500- μ M concentration group. Of this solution, 7.8 cc was transferred to a 50-cc vial of Cealb (20% human serum albumin (HSA) solution; Sanquin, Amsterdam, The Netherlands) to yield ICG in HSA (ICG:HSA) at a final concentration of 500 μ M. ICG (25 mg vials) was resuspended in 5 cc of sterile water for injection to yield a 5.0 mg/ml (6.4 mM) for the 750- μ M and 1,000- μ M concentration groups. Of this solution, 5.8 cc or 7.8 cc was transferred to a 50-cc vial of Cealb (20% human serum albumin (HSA) solution) to yield ICG in HSA (ICG:HSA) at a final concentration of 750 μ M or 1,000 μ M, respectively.

Intraoperative NIR Imaging System (Mini-FLARE™)

SLN mapping was performed using the Mini-FLARE™ image-guided surgery system as described by Mieog et al.¹⁵ Briefly, the system consists of 2 wavelength-isolated light sources: a “white” light source, generating 26,600 lx of 400-650 nm light and a “near-infrared” light source, generating 7.7 mW/cm² of 760 nm light. Color video and NIR fluorescence images are simultaneously acquired and displayed in real time using custom optics and software that separate the color video and NIR fluorescence images. A pseudo-colored (lime green) merged image of the color video and NIR fluorescence images is also displayed. The imaging head is attached to a flexible gooseneck arm, which permits positioning of the imaging head virtually anywhere over the surgical field, and at extreme angles. For intraoperative use, the imaging head and imaging system pole stand are wrapped in a sterile shield and drape (Medical Technique Inc., Tucson, AZ).

Clinical Trial

The single-institution clinical trial was approved by the Medical Ethics Committee of the Leiden University Medical Center and was performed in accordance with the ethical standards of the Helsinki Declaration of 1975. A total of 9 consecutive patients with cervical cancer that planned to undergo a radical abdominal trachelectomy or a radical hysterectomy and a total pelvic lymphadenectomy were included. All patients provided informed consent and were anonymized. Exclusion criteria were pregnancy, lactation or an allergy to iodine, shellfish, or indocyanine green. All procedures were performed by 2 gynecologists who were assisted by experienced researchers. Before the start of surgery, 1.6 mL ICG:HSA (concentration: 500, 750 or 1,000 µM) was transvaginally injected submucosally in 4 quadrants around the cervical tumor using a 21G, 1½ inch needle. Directly after the ICG:HSA injection, surgical scrub and sterile covering of the operation field commenced, and a laparotomy was performed. Before the systematic pelvic lymphadenectomy was performed, all standard locations (along the external iliac vessels and the hypogastric artery, along the common iliac artery, the obturator fossa and the lateral parametrium) were examined for NIR fluorescence using the Mini-FLARE™ imaging system. Fluorescent hotspots exhibiting a signal-to-background ratio (SBR) ≥ 1.1 *in vivo* were considered positive by NIR fluorescence. All fluorescent hotspots were denominated as SLNs and were subsequently resected and measured for fluorescence *ex vivo*. Then, the systemic pelvic lymphadenectomy was performed and all resected LNs were also measured for fluorescence *ex vivo*.

Lymphadenectomy consisted of removal of all lymph node-bearing fatty tissue along the external iliac vessels, the common iliac artery, the hypogastric artery, and from the obturator fossa¹⁸. Also, the area lateral to and underneath the superior vesical arteries (lateral parametrium) was cleared from the lymphatic tissue. The radical hysterectomy and abdominal trachelectomy were performed according to the standard procedure. In case of a radical trachelectomy, histopathological frozen analysis was performed and when nodes were found to contain metastases, a hysterectomy was performed in addition. Afterwards, all resected lymph nodes were examined by routine histopathological analysis, and lymph nodes were fixed in formalin and embedded in paraffin for routine hematoxylin and eosin staining. SLNs and non-SLNs were examined separately.

Statistical Analysis

For statistical analysis and to generate graphs, GraphPad Prism Software (Version 5.01, La Jolla, CA) was used. Differences in SBR between concentration groups were tested with a one-way analysis of variance (ANOVA) with subsequent pairwise comparisons corrected according to the Bonferroni correction. Assumption of equal variances was confirmed using Levene's test. All statistical tests were two-tailed and $P < 0.05$ was considered significant.

RESULTS

Patient and Tumor Characteristics

Patient and tumor characteristics are described in Table 1. Nine patients with stage Ib cervical cancer undergoing primary surgery were included in the study. Of these patients, median BMI was 21 (range 18-35), median age was 40 years (range 29-77 years), and median tumor size was 3.05 cm (range 0.7-11 cm). One patient presented with an exophytic cervical tumor measuring 11 cm in length and 4 cm in width protruding into the vagina. Five patients underwent a radical hysterectomy and 3 patients underwent a radical trachelectomy. In one patient, extensive endometriosis precluded radical hysterectomy. In this patient, the uterus was left in situ, but a pelvic lymphadenectomy was performed.

Table 1 - Patient and Tumor Characteristics

Patient no.	ICG:HSA Dose (μ M)	Age (Years)	BMI	FIGO Stage	Type of Surgery	Tumor Type	Tumor Size (cm)
1	500	35	35	IB1	Radical Trachelectomy	Adenosquamous	2.5
2	500	43	26	IB2	Radical Hysterectomy	Squamous	4.5
3	500	77	21	IB2	Radical Hysterectomy	Squamous	11.0
4	750	46	30	IB1	No resection	Squamous	n/a
5	750	59	21	IB1	Radical Hysterectomy	Squamous	4.2
6	750	29	22	IB1	Radical Trachelectomy	Squamous	2.5
7	1000	30	18	IB1	Radical Trachelectomy	Squamous	1.0
8	1000	40	20	IB1	Radical Hysterectomy	Squamous	0.7
9	1000	34	21	IB1	Radical Hysterectomy	Squamous	3.6

Intraoperative NIR Fluorescence Imaging

In all patients (N = 9), NIR fluorescence imaging enabled identification of 1 or more fluorescent hotspots. An example of the NIR fluorescence images of the procedure in cervical cancer is shown in Figure 1. Average time between injection of ICG:HSA and NIR fluorescence imaging was 51 ± 18 min. A total of 31 fluorescent hotspots were detected. On average, 3.4 ± 1.2 (range 1-5) fluorescent hotspots per patient were identified by NIR fluorescence (Table 2). Within these hotspots, a total of 41 lymph nodes were found after histopathological examination, yielding an average of 4.6 ± 2.1 true lymph nodes per patient. In 3 fluorescent hotspots, adipose tissue only, with no lymph tissue present, was found after histopathological examination. An average of 25.1 lymph nodes (range 10-39) per patient were harvested. Histological analysis showed that 2 of 9 patients had metastases in a total of 3 SLNs. No other lymph node metastases were observed.

Localization of Sentinel Lymph Nodes

A total of 31 fluorescent hotspots were confirmed to be SLNs. All SLNs were pelvic nodes and were identified along the left (n = 8) and right (n = 6) external iliac vessels, the right common iliac vessels (n = 4), the left (n = 5) and right (n = 4) obturator fossa, and the left (n = 2) and right (n = 2) lateral parametrium. Table 2 provides exact locations for all SLNs. In 8 of 9 patients, bilateral SLNs were found. After histological confirmation, 3 positive SLNs were found in 2 patients. In the first patient, the positive SLNs were located in the left lateral parametrium and along the right external iliac vessels. In the second patient, the positive SLN was located along the left external iliac vessels.

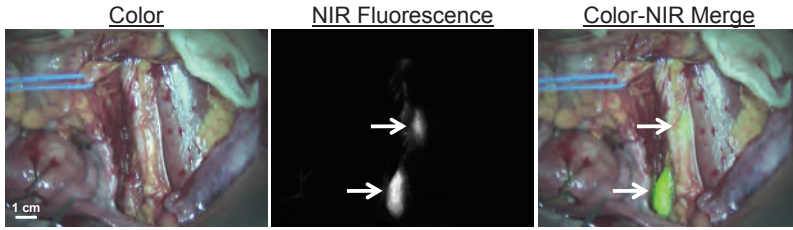


Figure 1 – NIR Fluorescence-Based SLN mapping using ICG:HSA and Mini-FLARE™: Identification of 2 SLNs (arrows), located along the left iliac vessels, with NIR fluorescence imaging is demonstrated in a cervical cancer patient, 45 min after administration of 750 μM ICG:HSA. Camera exposure time was 100 msec. Scale bar represents 1 cm.

Ex vivo imaging of lymph nodes

All lymph nodes were examined for fluorescence *ex vivo* using the Mini-FLARE™ imaging system. In 4 of 9 patients additional fluorescent hotspots (N=10) were identified, which were not identified during *in vivo* NIR fluorescence imaging (Table 2). Within 8 of these 10 hotspots, a total of 10 lymph nodes were found after histopathological examination and within 2 of 10 these hotspots, adipose tissue only, with no lymph node tissue present, was found after histopathological examination. The hotspots that contained lymph nodes were harvested along the left (n = 1) and the right (n = 1) external iliac vessels, and the left (n = 1) and the right (n = 5) obturator fossa. The hotspots that contained only adipose tissue were harvested along the left (n = 1) and the right (n = 1) external iliac vessels. No additional metastases were found during *ex vivo* analysis.

Optimization of ICG:HSA Dose

In all dose groups (500, 750, and 1,000 μM), fluorescence intensity of the SLN was significantly higher than the fluorescence intensity of surrounding tissue ($P < 0.001$). Mean SBRs of the SLNs were 10.1 ± 1.2 , 10.3 ± 1.2 and 12.0 ± 5.7 for the 500 μM , 750 μM , and 1,000 μM dose groups, respectively (Figure 2). A one-way ANOVA test showed no significant differences in SBRs of SLNs between the different dose groups ($P = 0.76$).

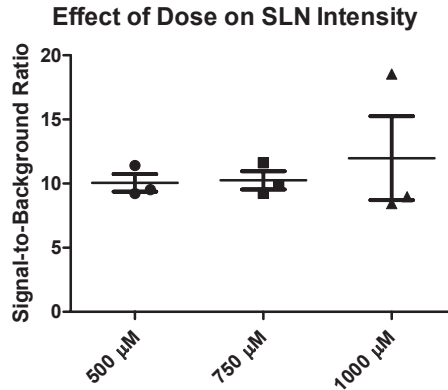


Figure 2 – Brightness of SLNs as a Function of ICG:HSA Dose: Signal-to-background ratio (mean \pm S.D) of the SLNs (ordinate) as a function of injected dose of ICG:HSA (abscissa). Statistical comparisons are as follows: The SBRs of the 500, 750, and 1,000 μ M concentration groups were not significantly different.

DISCUSSION

The current study showed the feasibility of the SLN procedure in early stage cervical cancer patients using ICG:HSA and the Mini-FLARE™ imaging system. The Mini-FLARE™ imaging system that was used in the current study displays NIR fluorescence signal, color signal, and a merge of both and illuminates the surgical field with white light. This enabled the gynecologist to perform the SLN detection and resection under direct image guidance. The imaging head of the Mini-FLARE™ system is attached to a flexible gooseneck arm, which permitted flexible positioning of the imaging head at extreme angles over the surgical field. This is of particular importance in large abdominal surgery. During all procedures, intraoperative imaging using this imaging system was successful and uneventful.

No differences in SBR of the SLNs between the 500, 750, and 1,000 μ M dose groups were found. The location of the NIR fluorescent SLNs was in concordance with formerly published drainage patterns.¹¹ Furthermore, bilateral SLNs were found in 8 of 9 patients. The 3 tumor-positive SLNs (in 2 patients) were located along the left external iliac vessels ($n = 1$), the right external iliac vessels ($n = 1$), and in the left lateral parametrium ($n = 1$). Identification of a parametrial SLN is rather remarkable because there is presently no consensus on removal of parametrial lymph nodes during total pelvic lymphadenectomy.¹⁹⁻²² Although larger clinical trials will be required to answer this question, from this study we can at least conclude that parametrial lymph nodes are identifiable using ICG:HSA and Mini-FLARE™.

The detection rate of SLNs in our pilot-study was 100% and this detection rate is in concordance with a prospective, multicenter cohort study of 590 patients that examined SLN mapping in cervical cancer patients and observed a detection rate of 93.5% when a combination of patent blue and radiocolloids was used.²³ In the current study, on average, a total of 3.4 SLNs were identified per patient intraoperatively, which is also consistent with previously published data.^{8,9} In the recently published study by Crane et al.¹⁷ on NIR fluorescence SLN mapping in cervical cancer patients, ICG was injected after laparotomy and NIR fluorescence measurements were made directly after injection. Furthermore, ICG was diluted in patent blue prior to injection. These differences in study design along with the use of a different imaging system hinder a direct comparison of the results.

The optimal time interval between injection of ICG:HSA and NIR fluorescence imaging is still unknown. Nevertheless, timing of imaging could be of great importance in terms of detection rate, sensitivity, and SBRs of SLNs. The mean interval between administration of ICG:HSA and NIR fluorescence measurements in the current study was 51 min. This time interval was relatively long because the ICG:HSA injection was performed prior to surgery, followed by surgical scrub and operation time to expose the iliac vessels. During surgery, no more than several minutes were needed for SLN detection and resection.

Ex vivo NIR fluorescence imaging of total lymphadenectomy specimens detected 10 additional fluorescent hotspots in 4 of 9 patients. Detection of these additional fluorescent hotspots during *ex vivo* imaging could possibly be explained by the relatively long time interval between ICG:HSA administration and performance of the total lymphadenectomy. Although ICG:HSA has an improved hydrodynamic diameter compared to ICG alone, passage through the SLN to second tier nodes can still possibly occur if the time interval is long enough. An alternative explanation for the additional *ex vivo* detected fluorescent hotspots is that these hotspots were missed *in vivo* due to technical limitations, as for example, the limited penetration depth (millimeters) for NIR fluorescent light. Future larger studies are needed to optimize timing and to evaluate the importance of additional fluorescent hotspots that are missed *in vivo* and are detected in the resection specimen. Nevertheless, to bypass this pitfall, the development of new lymphatic tracers that are retained in the SLN without flowing through to higher tier nodes is imperative to optimize NIR fluorescence SLN mapping in cervical cancer.

In the current study, fluorescent hotspots were found *in vivo* ($n = 3$) and *ex vivo* ($n = 2$) that did not contain lymphatic tissue but consisted of adipose tissue, which is

Table 2 – Results from *In Vivo* and *Ex Vivo* SLN Imaging

Patient no.	NIR Hotspots <i>In Vivo</i>	Additional NIR Hotspots <i>Ex Vivo</i>	T Total LNs Harvested	Tumor-Positive SLNs		False-Negatives	Location of NIR Fluorescent SLNs	Injection-Imaging Interval (min)	Bilateral SLNs Identified
				From Pathology	Fluorescent				
1	3	3	15	0	0	n/a	Left (1) and right (1) external iliac, left obturator (1)	94	Yes
2	4	0	36	2	2	0	Left (1) and right (1) parametrium, right external iliac (1), right common iliac (1)	35	Yes
3	3	0	17	0	0	n/a	Left external iliac (1) left obturator (2)	43	Yes
4	3	1	23	0	0	n/a	Left (1) and right (1) external iliac, left obturator (1)	44	Yes
5	4	0	39	0	0	n/a	Left (1) and right (1) external iliac, right parametrium (1), right common iliac (1)	40	Yes
6	5	0	33	0	0	n/a	Left (1) and right (1) external iliac, right common iliac (1), left obturator (1), left parametrium (1)	44	Yes
7	1	0	16	0	0	n/a	Right obturator (1)	41	No
8	5	2	37	0	0	n/a	Left (1) and right (1) external iliac, right common iliac (1) obturator right (2)	62	Yes
9	3	4	10	1	1	0	Left (2) and right (1) external iliac	58	Yes
31	10	10	226	3	3	0		Average = 51 ± 18	

not an uncommon observation in the SLN procedure. A plausible explanation for these fluorescent hotspots is that fluorescent lymph fluid can exit the lymphatic channel, due to extensive manipulation during surgery or anatomical aberrations, for example. If detection of a relatively small number of these hotspots does not obfuscate the identification of the true SLNs, this phenomenon does not negatively influence the SLN procedure.

In a recently published dose-finding clinical study performed by our group using NIR fluorescence SLN mapping in breast cancer patients, an optimal ICG:HSA dose range between 400 and 800 μM was found.¹⁵ In the 1,000 μM ICG:HSA dose group, the fluorescent intensity and the SBR of the SLNs decreased, most probably caused by an effect known as fluorescence quenching.²⁴ In the current study, no differences were found in SBRs between the 500, 750, and 1,000 μM dose groups. This lack of difference combined with pharmacy preferences, safety, previous results, and costs make a dose of 500 μM most convenient to perform the SLN procedure in cervical cancer patients.

As in other areas of surgery, the use of laparoscopy is expanding in cancer surgery. Lymphadenectomies are being performed laparoscopically as standard of care in several centers. NIR fluorescence may also be of great value in laparoscopic surgery because palpation is not possible and the surgeon can only rely on visual inspection and preoperative imaging. To implement NIR fluorescence in laparoscopic surgery, laparoscopic NIR fluorescence camera systems are currently being developed and tested.²⁵

In conclusion, we assessed the potential value of NIR fluorescence imaging in SLN mapping in early stage cervical cancer patients. Although sample size was small, this study showed a high SLN detection rate (100%) and no false-negative lymph nodes. However, to prove actual patient benefit and to assess sensitivity more precisely, larger clinical trials will be necessary.

REFERENCES

1. Jemal A, Siegel R, Ward E et al. Cancer statistics, 2009. *CA Cancer J Clin* 2009; 59:225-249.
2. Ferlay J, Bray F, Pisani P et al. *GLOBOCAN: Cancer Incidence, Mortality and Prevalence Worldwide*. Lyon: IARC Press; 2001.
3. Hacker NF. Revised FIGO staging for carcinoma of the vulva. *Int J Gynaecol Obstet* 2009; 105:105-106.
4. Horn LC, Hentschel B, Fischer U et al. Detection of micrometastases in pelvic lymph nodes in patients with carcinoma of the cervix uteri using step sectioning: Frequency, topographic distribution and prognostic impact. *Gynecol Oncol* 2008; 111:276-281.
5. Green J, Kirwan J, Tierney J et al. Concomitant chemotherapy and radiation therapy for cancer of the uterine cervix. *Cochrane Database Syst Rev* 2005; CD002225.
6. Van Der Zee AG, Oonk MH, De Hullu JA et al. Sentinel node dissection is safe in the treatment of early-stage vulvar cancer. *J Clin Oncol* 2008; 26:884-889.
7. Morton DL, Wen DR, Wong JH et al. Technical details of intraoperative lymphatic mapping for early stage melanoma. *Arch Surg* 1992; 127:392-399.
8. Levenback C, Coleman RL, Burke TW et al. Lymphatic mapping and sentinel node identification in patients with cervix cancer undergoing radical hysterectomy and pelvic lymphadenectomy. *J Clin Oncol* 2002; 20:688-693.
9. Marchiole P, Buenerd A, Scoazec JY et al. Sentinel lymph node biopsy is not accurate in predicting lymph node status for patients with cervical carcinoma. *Cancer* 2004; 100:2154-2159.
10. van de Lande J, Torrenge B, Raijmakers PG et al. Sentinel lymph node detection in early stage uterine cervix carcinoma: a systematic review. *Gynecol Oncol* 2007; 106:604-613.
11. Ercoli A, Delmas V, Iannone V et al. The lymphatic drainage of the uterine cervix in adult fresh cadavers: anatomy and surgical implications. *Eur J Surg Oncol* 2010; 36:298-303.
12. Silva LB, Silva-Filho AL, Traiman P et al. Sentinel node detection in cervical cancer with (99m)Tc-phytate. *Gynecol Oncol* 2005; 97:588-595.
13. Vahrmeijer AL, Frangioni JV. Seeing the invisible during surgery. *Br J Surg* 2011; 98:749-750.
14. Frangioni JV. *In vivo* near-infrared fluorescence imaging. *Curr Opin Chem Biol* 2003; 7:626-634.
15. Mieog JS, Troyan SL, Hutteman M et al. Towards Optimization of Imaging System and Lymphatic Tracer for Near-Infrared Fluorescent Sentinel Lymph Node Mapping in Breast Cancer. *Ann Surg Oncol* 2011; 18:2483-2491.
16. Ohnishi S, Lomnes SJ, Laurence RG et al. Organic alternatives to quantum dots for intraoperative near-infrared fluorescent sentinel lymph node mapping. *Mol Imaging* 2005; 4:172-181.
17. Crane LM, Themelis G, Pleijhuis RG et al. Intraoperative Multispectral Fluorescence Imaging for the Detection of the Sentinel Lymph Node in Cervical Cancer: A Novel Concept. *Mol Imaging Biol* 2010.
18. Pieterse QD, Kenter GG, Gaarenstroom KN et al. The number of pelvic lymph nodes in the quality control and prognosis of radical hysterectomy for the treatment of cervical cancer. *Eur J Surg Oncol* 2007; 33:216-221.
19. Bader AA, Winter R, Haas J et al. Where to look for the sentinel lymph node in cervical cancer. *Am J Obstet Gynecol* 2007; 197:678-7.
20. Steed H, Capstick V, Schepansky A et al. Early cervical cancer and parametrial involvement: is it significant? *Gynecol Oncol* 2006; 103:53-57.
21. Winter R, Haas J, Reich O et al. Parametrial spread of cervical cancer in patients with negative pelvic lymph nodes. *Gynecol Oncol* 2002; 84:252-257.
22. Photopulos GJ, Zwaag RV. Class II radical hysterectomy shows less morbidity and good treatment efficacy compared to class III. *Gynecol Oncol* 1991; 40:21-24.
23. Altgassen C, Hertel H, Brandstadt A et al. Multicenter validation study of the sentinel lymph node concept in cervical cancer: AGO Study Group. *J Clin Oncol* 2008; 26:2943-2951.
24. Gioux S, Choi HS, Frangioni JV. Image-guided surgery using invisible near-infrared light: fundamentals of clinical translation. *Mol Imaging* 2010; 9:237-255.
25. van der Poel HG, Buckle T, Brouwer OR et al. Intraoperative Laparoscopic Fluorescence Guidance to the Sentinel Lymph Node in Prostate Cancer Patients: Clinical Proof of Concept of an Integrated Functional Imaging Approach Using a Multimodal Tracer. *Eur Urol* 2011; 60:826-33.

Chapter 7

Randomized comparison of near-infrared fluorescence lymphatic tracers for sentinel lymph node mapping of cervical cancer

Schaafsma BE¹, van der Vorst JR¹, Gaarenstroom KA, Peters AA, Verbeek FP, de Kroon CD, Trimbos JB, Poelgeest MI, Frangioni JV, Vahrmeijer AL

¹Both authors contributed equally to this work and share first authorship.

Gynecol Oncol. 2012 Oct;127(1):126-30

ABSTRACT

Background

Near-infrared fluorescence imaging using indocyanine green (ICG) has recently been introduced as a novel technique for sentinel lymph node (SLN) mapping in early-stage cervical cancer. Although preclinical research has shown that ICG adsorbed to human serum albumin (ICG:HSA) improves its performance, the need for HSA has not yet been confirmed in cervical cancer patients. The current randomized study aims to determine whether ICG:HSA offers advantages over using ICG alone.

Material and Methods

Eighteen consecutive early-stage cervical cancer patients scheduled to undergo pelvic lymphadenectomy were included. Prior to surgery, 1.6 mL of 500 μ M ICG:HSA or 500 μ M ICG alone was injected transvaginally in 4 quadrants around the tumor. The Mini-FLARE imaging system was used for intraoperative NIR fluorescence detection and quantitation.

Results

SLNs were identified intraoperatively in 78% of the patients. Patient and tumor characteristics were equally distributed over both treatment groups. No significant difference in signal-to-background ratio (9.3 vs. 10.1, $P = .72$) or average number of detected SLNs (2.9 vs 2.7, $P = .84$) was found between the ICG:HSA group and the ICG alone group, respectively.

Conclusion

In conclusion, this double-blind, randomized trial showed no advantage of ICG:HSA over ICG alone for the SLN procedure in early-stage cervical cancer. Further optimization is required to improve the intraoperative detection rate.

INTRODUCTION

As part of surgical management in early-stage cervical cancer, bilateral pelvic lymphadenectomy is considered standard of care. However, pelvic lymphadenectomy is associated with complications, such as lymphedema, the risk of nerve injury, and lymphocyst formation.¹ Because lymph node involvement occurs in approximately 12% to 22% of early-stage cervical cancer patients, the majority of patients do not benefit from a pelvic lymphadenectomy, but may suffer from its complications.^{2,3} Over the last decades, the sentinel lymph node (SLN) concept has proven to be feasible and safe in vulvar cancer, melanoma, and breast cancer for selecting patients who would benefit from lymphadenectomy. In addition, the SLN can be used for ultra staging to aid in the identification of micrometastases.⁴ However, due to the bilateral multifarious drainage pattern of the cervix, the SLN procedure is more challenging in cervical cancer patients than in breast cancer patients, for example. SLN biopsy in early-stage cervical cancer patients has been extensively described using blue dye, a radiocolloid, or a combination of both, with various results.⁵

Intraoperative near-infrared (NIR) fluorescence imaging using indocyanine green (ICG) has emerged as a novel technique for SLN detection in cervical cancer patients.⁶⁻¹⁰ NIR fluorescence imaging has several advantages, such as a relatively high tissue penetration and low autofluorescence. ICG is currently the only clinically available NIR lymphatic tracer. However, due to its relatively low fluorescence brightness (quantum yield) and its small hydrodynamic diameter, it is not an optimal lymphatic tracer. Preclinical work has demonstrated that adsorption of ICG to human serum albumin (HSA, complex is ICG:HSA), by simply mixing it, increases the fluorescence intensity (a threefold) and hydrodynamic diameter.¹¹ These advantages could provide improved detection and retention of the tracer in the SLN. On the other hand, the use of albumin adds cost and complexity to the procedure. Moreover, the use of human blood products, such as HSA, poses regulatory hurdles in certain countries, such as the United States. The aim of this double-blind randomized trial was to confirm feasibility of NIR fluorescence imaging for SLN mapping in cervical cancer and to assess whether ICG alone could render the same fluorescence intensity in the SLNs as ICG:HSA.

MATERIAL AND METHODS

Preparation of Indocyanine Green adsorbed to Human Serum Albumin

Indocyanine green (25-mg vials) was purchased from Pulsion Medical Systems (Munich, Germany) and was resuspended in 10 cc of sterile water. To obtain a 500 μM final concentration, 7.8 mL of the 3.2-mM ICG solution was diluted in 42.8 mL of sterile water for injection or 42.8 ml of Cealb (20% human serum albumin, Sanquin, Amsterdam, The Netherlands) for the preparation of ICG alone or ICG:HSA, respectively. A dose of 500 μM was chosen based on previous studies that showed that the optimal dose of ICG:HSA lies between 400 and 800 μM and has the benefit of minimal manipulation of ICG and albumin volumes.^{6,12}

Intraoperative Near-Infrared Imaging System (Mini-FLARE)

SLN mapping was performed using the Mini-Fluorescence-Assisted Resection and Exploration (Mini-FLARE) image-guided surgery system as described previously¹². Briefly, the system consists of 2 wavelength isolated light sources: a “white” light source, generating 26,600 lx of 400–650 nm light, and a “near-infrared” light source, generating 7.7 mW/cm² of 760 nm light. Color video and NIR fluorescence images are simultaneously acquired and displayed in real time using custom optics and software that separate the color video and NIR fluorescence images. A pseudo-colored (lime green) merged image of the color video and NIR fluorescence images is also displayed. The imaging head is attached to a flexible gooseneck arm, which permits positioning of the imaging head at extreme angles virtually anywhere over the surgical field. For intraoperative use, the imaging head and imaging system pole stand are wrapped in a sterile shield and drape (Medical Technique Inc., Tucson, AZ).

Clinical Trial

The double-blind, randomized, noninferiority trial comparing ICG:HSA with ICG alone was approved by the Medical Ethics Committee of the Leiden University Medical Center and was performed in accordance with the ethical standards of the Helsinki Declaration of 1975. All patients planning to undergo a total pelvic lymphadenectomy for early stage cervical cancer were eligible for participation in the study. Exclusion criteria were pregnancy, lactation, or an allergy to iodine, shellfish, or indocyanine green. All patients gave informed consent and were anonymized. Patients were randomized by the Department of Clinical Pharmacy. Treatment allocation was performed by block randomization. Before the start of

surgery, 1.6 mL of 500 μ M ICG:HSA or ICG alone was transvaginally injected by the surgeon submucosally in 4 quadrants of the cervix. Directly after injection, following surgical scrub and sterile covering of the operation field, a laparotomy was performed.

Prior to the systematic pelvic lymphadenectomy, all standard locations (along the external iliac vessels and the hypogastric artery, the common iliac artery, the obturator fossa and the lateral parametrium) were examined for NIR fluorescence using the Mini-FLARE imaging system. Both the surgeon and the Mini-FLARE operator, who was responsible for analyzing the data, were blinded to the treatment allocation. All fluorescent hotspots, containing one or more lymph nodes, were denominated as SLNs and were subsequently resected and measured for fluorescence *ex vivo*. Subsequently, the standard systemic pelvic lymphadenectomy was performed and all resected lymph nodes were also measured for fluorescence *ex vivo*. Lymphadenectomy consisted of removal of all lymph node-bearing fatty tissue along the external iliac vessels, the common iliac artery, the hypogastric artery, and from the obturator fossa¹³. Also, the area lateral to and underneath the superior vesical arteries (lateral parametrium) was cleared from the lymphatic tissue. The radical hysterectomy or abdominal trachelectomy were performed according to the standard procedure. Afterwards, all resected lymph nodes were examined by routine histopathological analysis; lymph nodes were fixed in formalin and embedded in paraffin for routine hematoxylin and eosin staining. SLNs and non-SLNs were examined separately. Additionally, a substantial part of the SLNs and clinical suspected nodes were subsequently examined using a cytokeratin staining.

Power Calculation and Statistical Analysis

The power calculation is based on data from previous studies, in which *in vitro* a threefold difference in fluorescent brightness (quantum yield) was reported between ICG alone and ICG:HSA and *in vivo* signal-to-background ratio of 10.1 ± 1.2 was observed during SLN detection by ICG:HSA^{6,11}. These data revealed that 18 patients are needed to achieve 91% power to detect non-inferiority using a one-sided, 2-sample *t* test ($\alpha = 0.025$) with a margin of equivalence of 5.0 while assuming no difference between the signal-to-background ratio (SBR) of ICG:HSA and ICG alone. For statistical analysis, SPSS statistical software package (Version 16.0, Chicago, IL) was used. To compare the SBR and the number of SLNs identified between ICG:HSA and ICG alone, a 1-sided, 2-sample *t* test was performed. $P < 0.05$ was considered significant.

RESULTS

Patient characteristics

Eighteen consecutive early-stage cervical cancer patients scheduled to undergo a pelvic lymphadenectomy were randomized to ICG:HSA or ICG alone for NIR fluorescence SLN imaging. All patients were clinically staged as FIGO stage IB1 cervical cancer. Of these 18 patients, the median age was 40 years (range, 28-67), median body mass index was 25 (21-38), and median tumor size was 1.6 cm (range, 0.3-5.0 cm). In one patient in whom preoperative pathology was not conclusive (either cervical cancer or endometrial cancer), postoperative pathological evaluation showed endometrial cancer. In all patients a complete bilateral pelvic lymphadenectomy was performed, except for one case. In this case the surgeon did not complete the lymphadenectomy, due to pathologically proven metastatic lymphatic disease by intraoperative frozen section and excessive blood loss during surgery. Patient and tumor characteristics and previous treatment were equally distributed over the treatment groups (Table 1).

NIR Fluorescence Imaging

The results of the NIR fluorescence detection of SLNs are presented in Table 2. During surgery, NIR fluorescence imaging enabled identification of 1 or more fluorescent hotspots in 14 out of 18 (78%) patients (Figure 1). In 11 patients (61%) fluorescent hotspots were identified bilaterally, whereas in 3 patients (17%) hotspots were identified unilaterally. In 4 patients (22%) no fluorescent hotspots were detected intraoperatively. Average time between injection of ICG:HSA or ICG alone and imaging was 43 ± 14 min and did not lengthen the standard of care surgery. On average, 2.8 ± 2.2 hotspots were detected intraoperatively by NIR fluorescence, yielding an average of 4.2 ± 3.7 SLNs per patient at pathological examination. An average of 24.5 (range, 9-46) lymph nodes per patient were harvested when a complete bilateral lymphadenectomy was performed.

In addition, all lymph nodes were examined for fluorescence *ex vivo* directly after surgical resection in the operating room. In 11 of 18 patients, a total of 29 additional fluorescent hotspots could be identified, which were not identified during *in vivo* NIR fluorescence imaging. When the *ex vivo* detected fluorescent hotspots and the *in vivo* detected fluorescent hotspots were combined, NIR fluorescence imaging enabled identification of 1 or more fluorescent hotspots in 16 out of 18 (89%) patients, thus in 2 more patients compared to *in vivo* identification alone. In 13

patients (72%) these were identified bilaterally, in 3 patients (17%) unilaterally, and in 2 patients (11%) there were no fluorescent hotspots detected *in vivo* or *ex vivo*.

Histological analysis showed lymph node metastases in 6 out of 18 patients of whom 4 patients had macrometastases (> 2 mm) and 2 patients had micrometastases (\leq 2 mm) ¹⁴. In 5 of 6 patients with lymph node metastases, one or more tumor positive nodes were fluorescent. Though, in 2 of these 6 patients, the fluorescent nodes were only detected *ex vivo*. Furthermore, in 1 patient, the resection specimen contained a nonfluorescent fibrotic nodule with mature fat cells, some lymphoid infiltration, and a micrometastatic lesion. No metastases were found in this patient's fluorescent nodes.

Table 1 - Patient and Tumor Characteristics

Characteristic	ICG:HSA (N = 9)		ICG alone (N = 9)		P
	N	%	N	%	
Age (median, range)	40 (28 - 67)		40 (30 - 50)		.86
Body mass index (median, range)	25 (22 - 38)		23 (21 - 34)		.13
Previous procedures	3	33	3	33	.77
No local treatment	2	23	2	23	
Local excision	3	33	4	44	
Conization	1	11	0	0	
Local excision + Neoadjuvant chemotherapy					
Histological type					.57
Squamous cell carcinoma	4	44.5	5	56.5	
Adenocarcinoma	4	44.5	4	44.5	
Endometroid adenocarcinoma	1	11	0	0	
Type of tumor excision					.26
Radical hysterectomy	6	67	8	89	
Radical trachelectomy	3	33	1	11	
Type of lymphadenectomy					.30
Complete bilateral lymphadenectomy	8	89	9	100	
Incomplete bilateral lymphadenectomy	1	11	0	0	
Tumor size (median, range)	1.4 (0.6 - 5.0)		1.8 (0.3 - 3.6)		.88

ICG:HSA, indocyanine green adsorbed to human serum albumin

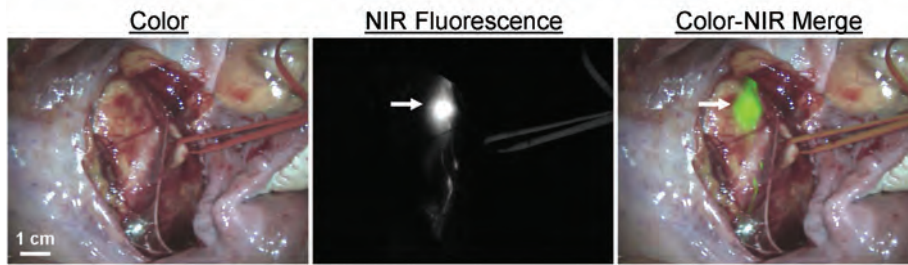


Figure 1 – NIR Fluorescence-Based SLN Mapping using ICG:HSA and Mini-FLARE: Identification of a SLN (arrow), located along the right iliac vessels, with NIR fluorescence imaging is demonstrated in a cervical cancer patient after administration of 500 μ M ICG:HSA.

Comparison between treatment groups

The primary endpoint of this study was the average brightness of the SLN, expressed in SBR. The average SBR of ICG:HSA (9.3 ± 3.6) and ICG alone (10.1 ± 4.5) were not significantly different ($P = .72$). No significant difference was observed in the average number of *in vivo* identified fluorescent hotspots between ICG:HSA and ICG alone (2.9 ± 1.7 vs 2.7 ± 2.6 , $P = .84$). Similarly, there was no significant difference in intraoperative detection rate ($P = .13$) or presence of fluorescent nodes after *ex vivo* inspection ($P = .82$).

DISCUSSION

The current 18-patient clinical study confirmed the feasibility of the SLN procedure in early-stage cervical cancer using NIR fluorescence imaging with ICG. The overall intraoperative detection rate was 78%, and in 61% of all patients fluorescent nodes could be identified bilaterally. This double-blind randomized trial did not show any advantages of ICG:HSA over ICG alone in SBR, average number of intraoperatively detected fluorescent hotspots, or percentage of patients in whom fluorescent nodes could be detected.

The recent introduction of NIR fluorescence imaging has provided new opportunities in the field of SLN mapping. Preclinical studies indicated that adsorption of ICG to HSA increases the fluorescence intensity and the hydrodynamic diameter, thereby providing improved detection and better retention in the SLN.¹¹ In the current study, ICG:HSA performed equally well as ICG alone. This is in concordance with a previous study performed by our group in which no differences were found between the use of ICG:HSA and ICG alone in SLN mapping in breast cancer patients¹⁵. In lymph

fluids a high protein constitution is found.¹⁶ A potential explanation for the lack of difference between ICG:HSA and ICG alone is that ICG rapidly binds to endogenous proteins when drained in the lymphatic system, eliminating the need for premixing ICG and HSA.

Table 2 – SLN Identification Results

Characteristic	Total (18 subjects)		ICG:HSA (9 subjects)		ICG alone (9 subjects)		P
	N	%	N	%	N	%	
Intraoperative detection rate							0.13
Bilateral	11	61	5	56	6	67	
Unilateral	3	17	3	33	0	0	
None	4	22	1	11	3	33	
Average number of intraoperative NIR hotspots ± SD	2.8 ± 2.2		2.9 ± 1.7		2.7 ± 2.6		.84
Signal-to-background ratio	9.7 ± 3.9		9.3 ± 3.6		10.1 ± 4.5		.72
Average lymph nodes in lymphadenectomy ± SD	24.5 ± 8.8		23.4 ± 4.3		25.6 ± 11.6		.62
Average number of additional hotspots <i>ex vivo</i> ± SD	1.6 ± 2.0		1.0 ± 1.3		2.2 ± 2.4		.21
Presence of fluorescent nodes							.82
Bilateral	13	72	6	67	7	78	
Unilateral	3	17	2	22	1	11	
None	2	11	1	11	1	11	
Histology							.51
negative	12	67	7	78	5	56	
ITC/micrometastasis	2	11	1	11	1	11	
macrometastasis	4	22	1	11	3	33	
False negative rate							
intraoperatively detected nodes	3/6		1/2		2/4		
all fluorescent nodes	1/6		1/2		0/4		

ICG:HSA, indocyanine green adsorbed to human serum albumin; ITC, isolated tumor cells

The detection rate in this study is in concordance with previously reported detection rates in studies using NIR fluorescence for SLN mapping in early-stage cervical cancer, which vary from 60% to 100%.⁶⁻⁹ Large studies in early-stage cervical cancer patients using radiocolloid tracers reported higher detection rates varying from 88% to 99%.¹⁷⁻²³ Possible explanations for the lower detection rate observed in this study could be the inclusions of patients with larger tumors (>2 cm) and, especially, the learning curve associated with cervical injection of the tracer and the intraoperatively exposure of tissue to maximize NIR fluorescence detection.^{17,24} Unlike the present study, our initial 9-patient study of NIR fluorescence SLN mapping in cervical cancer utilized two clinicians for all NIR lymphatic tracer injections.

Although the learning curve could be of significant effect on the intraoperative identification rate and time needed to identify the SLN, it is unlikely that the learning curve interferes with the SBR, which was used to power the present trial and to test difference between ICG alone and ICG:HSA. Assessment of the learning curve will be essential before NIR fluorescence can be compared to conventional techniques using radiocolloid tracers in a sufficient powered study.

After resection, additional fluorescent lymph nodes, which were missed during intraoperative inspection with the Mini-FLARE, were identified in the resection specimens of 11 out of the 18 patients. Intraoperative detection of these additional fluorescent nodes would have considerably improved the detection rate and the false negative rate. Difficulty in the intraoperative detection of these nodes could be based on the relatively limited tissue penetration of NIR light (several millimeters) compared to radiocolloid tracers, or the learning curve associated with positioning tissue intraoperatively to maximize NIR fluorescence detection. Moreover, radiocolloid tracers permit preoperative localization of the SLN, which assists surgical planning. Still, radiocolloids have the disadvantage that there is no real-time visualization during the operation, and detection is hampered if the SLNs are located near the point of the tracer injection. NIR fluorescence imaging is suitable for real-time identification and detection of SLNs located in the vicinity of the injection site. In addition, NIR fluorescence has as a much better tissue penetration when compared to blue dyes. Therefore, a combination of a radiocolloid and a NIR fluorescence tracer might be preferable. In a recent study, van der Poel et al. reported the successful use of such a multimodal tracer combining radioactivity and NIR fluorescence in sentinel lymph node mapping in prostate cancer patients using a NIR fluorescence laparoscope.²⁵

In conclusion, this double-blind, randomized trial showed no advantage of ICG:HSA in comparison to ICG alone for the SLN procedure in early-stage cervical cancer. Further optimization of NIR fluorescence imaging is required to improve the intraoperative detection rate to permit this technique to compete with radiocolloid tracers.

REFERENCES

1. Kashima K, Yahata T, Fujita K et al. Analysis of the complications after radical hysterectomy for stage IB, IIA and IIB uterine cervical cancer patients. *J Obstet Gynaecol Res* 2010; 36:555-559.
2. Sakuragi N. Up-to-date management of lymph node metastasis and the role of tailored lymphadenectomy in cervical cancer. *Int J Clin Oncol* 2007; 12:165-175.
3. Delgado G, Bundy BN, Fowler WC, Jr. et al. A prospective surgical pathological study of stage I squamous carcinoma of the cervix: a Gynecologic Oncology Group Study. *Gynecol Oncol* 1989; 35:314-320.
4. Gortzak-Uzan L, Jimenez W, Nofech-Mozes S et al. Sentinel lymph node biopsy vs. pelvic lymphadenectomy in early stage cervical cancer: is it time to change the gold standard? *Gynecol Oncol* 2010; 116:28-32.
5. Eiriksson L, Covens A. Sentinel lymph node mapping in cervical cancer: the future? *BJOG* 2011.
6. van der Vorst JR, Hutteman M, Gaarenstroom KN et al. Optimization of near-infrared fluorescent sentinel lymph node mapping in cervical cancer patients. *Int J Gynecol Cancer* 2011; 21:1472-1478.
7. Furukawa N, Oi H, Yoshida S et al. The usefulness of photodynamic eye for sentinel lymph node identification in patients with cervical cancer. *Tumori* 2010; 96:936-940.
8. Crane LM, Themelis G, Pleijhuis RG et al. Intraoperative multispectral fluorescence imaging for the detection of the sentinel lymph node in cervical cancer: a novel concept. *Mol Imaging Biol* 2011; 13:1043-1049.
9. Rossi EC, Ivanova A, Boggess JF. Robotically assisted fluorescence-guided lymph node mapping with ICG for gynecologic malignancies: a feasibility study. *Gynecol Oncol* 2012; 124:78-82.
10. Schaafsma BE, Mieog JS, Hutteman M et al. The clinical use of indocyanine green as a near-infrared fluorescent contrast agent for image-guided oncologic surgery. *J Surg Oncol* 2011; 104:323-332.
11. Ohnishi S, Lomnes SJ, Laurence RG et al. Organic alternatives to quantum dots for intraoperative near-infrared fluorescent sentinel lymph node mapping. *Mol Imaging* 2005; 4:172-181.
12. Mieog JS, Troyan SL, Hutteman M et al. Toward optimization of imaging system and lymphatic tracer for near-infrared fluorescent sentinel lymph node mapping in breast cancer. *Ann Surg Oncol* 2011; 18:2483-2491.
13. Pieterse QD, Kenter GG, Gaarenstroom KN et al. The number of pelvic lymph nodes in the quality control and prognosis of radical hysterectomy for the treatment of cervical cancer. *Eur J Surg Oncol* 2007; 33:216-221.
14. Hermanek P, Hutter RV, Sobin LH et al. International Union Against Cancer. Classification of isolated tumor cells and micrometastasis. *Cancer* 1999; 86:2668-2673.
15. Hutteman M, Mieog JS, van der Vorst JR et al. Randomized, double-blind comparison of indocyanine green with or without albumin premixing for near-infrared fluorescence imaging of sentinel lymph nodes in breast cancer patients. *Breast Cancer Res Treat* 2011; 127:163-170.
16. Cherrick GR, Stein SW, Leevy CM et al. Indocyanine green: observations on its physical properties, plasma decay, and hepatic extraction. *J Clin Invest* 1960; 39:592-600.
17. Altgassen C, Hertel H, Brandstadt A et al. Multicenter validation study of the sentinel lymph node concept in cervical cancer: AGO Study Group. *J Clin Oncol* 2008; 26:2943-2951.
18. Ogawa S, Kobayashi H, Amada S et al. Sentinel node detection with (99m)Tc phytate alone is satisfactory for cervical cancer patients undergoing radical hysterectomy and pelvic lymphadenectomy. *Int J Clin Oncol* 2010; 15:52-58.
19. Darlin L, Persson J, Bossmar T et al. The sentinel node concept in early cervical cancer performs well in tumors smaller than 2 cm. *Gynecol Oncol* 2010; 117:266-269.
20. Du XL, Sheng XG, Jiang T et al. Sentinel lymph node biopsy as guidance for radical trachelectomy in young patients with early stage cervical cancer. *BMC Cancer* 2011; 11:157.
21. Diaz JP, Gemignani ML, Pandit-Taskar N et al. Sentinel lymph node biopsy in the management of early-stage cervical carcinoma. *Gynecol Oncol* 2011; 120:347-352.
22. Roy M, Bouchard-Fortier G, Popa I et al. Value of sentinel node mapping in cancer of the cervix. *Gynecol Oncol* 2011; 122:269-274.

23. Lecuru F, Mathevet P, Querleu D et al. Bilateral negative sentinel nodes accurately predict absence of lymph node metastasis in early cervical cancer: results of the SENTICOL study. *J Clin Oncol* 2011; 29:1686-1691.
24. Plante M, Renaud MC, Tetu B et al. Laparoscopic sentinel node mapping in early-stage cervical cancer. *Gynecol Oncol* 2003; 91:494-503.
25. van der Poel HG, Buckle T, Brouwer OR et al. Intraoperative Laparoscopic Fluorescence Guidance to the Sentinel Lymph Node in Prostate Cancer Patients: Clinical Proof of Concept of an Integrated Functional Imaging Approach Using a Multimodal Tracer. *Eur Urol* 2011.

Chapter 8

Dose optimization for near-infrared fluorescence sentinel lymph node mapping in melanoma patients

van der Vorst JR¹, Schaafsma BE¹, Verbeek FP, Swijnenburg RJ, Hutteman M,
Liefers GJ, van de Velde CJ, Frangioni JV, Vahrmeijer AL

¹Both authors contributed equally to this work and share first authorship.

Br J Dermatol. 2013 Jan;168(1):93-8

ABSTRACT

Background

Regional lymph node involvement is the most important prognostic factor in cutaneous melanoma. Since only 20% of melanoma patients have occult nodal disease and would benefit from a regional lymphadenectomy, the sentinel lymph node (SLN) biopsy was introduced. NIR fluorescence has been hypothesized to improve SLN mapping. The objective was to assess the potential of intraoperative near-infrared (NIR) fluorescence imaging to improve SLN mapping in melanoma patients and to examine the optimal dose of indocyanine green adsorbed to human serum albumin (ICG:HSA).

Material and Methods

Fifteen consecutive cutaneous melanoma patients underwent the standard SLN procedure using ^{99m}Tc -nanocolloid and patent blue. In addition, intraoperative NIR fluorescence imaging was performed after injection of 1.6 mL of 600, 800, 1000 or 1200 μM of ICG:HSA in four quadrants around the primary excision scar.

Results

NIR fluorescence SLN mapping was successful in 93% of patients. In one patient, no SLN could be identified using either conventional methods or NIR fluorescence. A total of 30 SLNs (average 2.0, range 1-7) were detected, 30 radioactive (100%), 27 blue (73%), and 30 NIR fluorescent (100%). With regard to the effect of concentration on SBR a trend ($P = 0.066$) was found favouring the 600, 800 and 1000 μM groups over the 1200 μM group.

Conclusion

This study demonstrates feasibility and accuracy of SLN mapping using ICG:HSA. Considering safety, cost, and pharmacological characteristics, an ICG:HSA concentration of 600 μM appears optimal for SLN mapping in cutaneous melanoma, though lower doses need to be assessed.

INTRODUCTION

Regional lymph node involvement is the most important prognostic factor in cutaneous melanoma patients and complete lymph node dissection is the current standard treatment for patients with nodal metastasis.¹ Only 20% of melanoma patients have occult nodal disease and therefore will benefit from a regional lymphadenectomy.² However, the remaining 80% of patients without nodal involvement will be exposed to the risk of morbidity without offering a therapeutic advantage when performing a lymphadenectomy. The sentinel lymph node (SLN) biopsy was introduced by Morton et al.³ to obtain a minimal invasive assessment of regional nodal involvement and is now regarded as standard-of-care in staging cutaneous melanoma patients with primary lesions of at least 1 mm thick.

The SLN biopsy in melanoma patients is generally performed using a combination of radioactive colloid and blue dye. The use of this combination facilitates detection rates of over 90% and false-negative rates of approximately 5%.³⁻⁵ However, the use of radioactive colloid comes with certain disadvantages, such as the involvement of a nuclear physician, high costs, and the lack of visual information. In addition, blue dye staining can result in hampered visibility of the surgical field and results in tattooing of the injection site lasting for several months. Consequently, blue dye staining is omitted in some institutions when the primary tumour is located in the facial region. The blue dye cannot be seen through skin and fatty tissue.

The use of invisible near-infrared (NIR) light (700-900 nm) has several characteristics that can be advantageous in the SLN procedure, which include relatively high penetration into living tissue (several millimetres) and the lack of ionizing radiation.⁶ Indocyanine green (ICG) is one of only two clinically available NIR fluorescent agents and is currently the most optimal agent for SLN mapping.⁷ In several studies, intraoperative imaging systems in combination with ICG have been used for the SLN procedure for various types of cancer.⁸⁻¹³ The lymphatic channels and SLNs in cutaneous melanoma patients are often relatively superficially located. Therefore, NIR fluorescence imaging could be particularly useful for this indication. Indeed, several groups reported on the successful use of NIR fluorescence and ICG for SLN mapping in melanoma patients.¹⁴⁻¹⁸

Preclinical evidence demonstrated that premixing of ICG with human serum albumin (HSA, complex is ICG:HSA) increases the fluorescence intensity and hydrodynamic diameter of ICG, resulting in better retention in the SLN.¹⁹ The aims of the current study were to assess the use of NIR fluorescence imaging using ICG:HSA and the Mini-FLARE intraoperative imaging system for the SLN procedure in melanoma patients. Furthermore, the optimal dose of ICG:HSA to perform a NIR fluorescence SLN procedure was assessed.

MATERIAL AND METHODS

Preparation of Indocyanine Green Adsorbed to Human Serum Albumin

ICG (25 mg vials) was purchased from Pulsion Medical Systems (Munich, Germany) and resuspended in 10 mL of sterile water for injection for the 600 μM group, or in 5 mL of sterile water for injection for the 800 μM , 1000 μM and 1200 μM groups, to yield stock solutions of 3.2 mM and 6.4 mM, respectively. Various amounts of this stock solution were transferred to a 50 cc vial of Cealb (20% human serum albumin [HSA] solution; Sanquin, Amsterdam, The Netherlands) to yield ICG in HSA (ICG:HSA) at a final concentration of 600 μM , 800 μM , 1000 μM or 1200 μM .

Intraoperative NIR Fluorescence Imaging

SLN mapping was performed using the Mini-FLARE image-guided surgery system as described in detail previously.⁹ Briefly, the system consists of 2 wavelength separated light sources: a “white” LED light source, generating 26,600 lx of 400 to 650 nm light to illuminate the surgical field and an NIR LED light source, generating 7.7 mW / cm² of 760 nm fluorescence excitation light. White light and NIR fluorescence images are acquired simultaneously and displayed in real time, using custom designed optics and software. A pseudo-coloured (lime green) image of NIR fluorescence superimposed over the white light image is also displayed, to provide the NIR fluorescence signal in proper anatomical context.

Clinical Trial

The current dose escalation clinical trial was approved by the Medical Ethics Committee of the Leiden University Medical Center and was performed in concordance with the ethical standards of the Helsinki Declaration of 1975. Fifteen consecutive patients that were planned to undergo a therapeutic

re-excision and a SLN procedure for cutaneous melanoma were included in this study between April 2010 and June 2011. Exclusion criteria were pregnancy, lactation or an allergy to iodine, shellfish, or indocyanine green.

All patients gave informed consent and were anonymized. Patients received the standard-of-care SLN procedure. For our institution, this implies injections at four quadrants around the primary excision scar of 60-100 MBq ^{99m}Tc -nanocolloid on the afternoon of the day before, or the morning prior to surgery. Before the start of the operation, approximately 1 mL total of patent blue V (Guerbet, France) was injected at four quadrants around the primary excision scar. Immediately after injection of patent blue, a total of 1.6 mL of ICG:HSA was injected at the same four sites as the patent blue injections. ICG:HSA was injected at a concentration of 600, 800, 1000 and 1200 μM . In each concentration group, 3 patients were included (N = 12 patients). Subsequently, 3 patients were included at the optimal ICG:HSA concentration.

After surgical scrub, the Mini-FLARE imaging head was positioned at approximately 30 cm above the surgical field. The NIR fluorescence signal was measured percutaneously, prior to skin incision, and continuously during the surgical procedure. Throughout the procedure, the surgeon was continuously provided with real-time NIR fluorescence image guidance. When the SLN could not be found easily by NIR fluorescence, the handheld gamma probe could be used for the localization of SLNs. Relative brightness of the SLNs was determined by measuring signal-to-background ratios (SBRs); that is the NIR fluorescence signal of the SLN divided by the (auto)fluorescent signal of a directly adjacent region. Excised sentinel lymph nodes were analyzed *ex vivo* for NIR fluorescence and radioactivity and were routinely analyzed by histopathology. SLNs were fixed in formalin and embedded in paraffin for haematoxylin, eosin, and immunohistopathological staining using the S-100 and MART-1 markers at six levels, with an interval of 50-150 μm .

Statistical Analysis: For statistical analysis, SPSS statistical software package (Version 17.0, Chicago, IL) was used. Graphs were generated using GraphPad Prism Software (Version 5.01, La Jolla, CA). Signal-to-background ratios were reported as median and range. To test differences between groups, the Kruskal-Wallis one-way analysis of variance test and the Dunn's Multiple Comparison Test were used to test for differences between time and dose groups. Statistical tests were two-tailed and $P < 0.05$ was considered significant.

RESULTS

Patient and Tumour Characteristics

Fifteen consecutive patients with cutaneous melanoma undergoing SLN mapping were included in this study. Patients and tumour characteristics are described in Table 1. Median body mass index (BMI) was 24 (range 18 - 32), median age was 55 years (range 21 - 70 years), and median Breslow's depth was 1.9 mm (range 0.7 - 7 mm). In 1 patient, the melanoma was located in the head and neck region, in 4 patients at the higher extremities, in 9 patients at the trunk and in 1 patient at the lower extremities.

Intraoperative NIR Fluorescence Imaging

Average time between ICG:HSA injection and skin incision was 12.6 ± 3.6 minutes. In 14 patients, one or more SLNs were identified. A total of 30 SLNs were detected, all of which were radioactive and fluorescent (Table 2). Twenty-two out of 30 SLNs (73%) were stained blue. A typical example of NIR fluorescence imaging using the Mini-FLARE imaging system is shown in figure 1. In one patient, no SLN could be identified using either conventional methods or NIR fluorescence. Average time between skin incision and resection of the first SLN was 10.2 ± 3.9 minutes. The location of the SLNs is summarized in Table 2. In each patient, following resection of all NIR fluorescent nodes, the surgical field was systematically inspected for remaining radioactivity or blue nodes. No additional nodes were found that were not detected by NIR fluorescence. No adverse reactions associated with the use of ICG:HSA or the Mini-FLARE imaging system were observed.

The Effect of Lymphatic Tracer Dose on SLN Brightness

The effect of injected lymphatic tracer dose on fluorescence brightness was determined by comparing median SBRs between concentration groups (Fig. 2). Median SBRs of the SLNs were 12.33 (range: 10.90 – 20.92), 16.59 (range: 12.94 – 23.73), 15.47 (range: 14.87 – 18.42) and 6.76 (range: 6.14 – 10.14) for the 600, 800, 1000 and 1200 μM concentration groups, respectively. The independent samples Kruskal-Wallis Test to test for difference in signal-to-background ratios showed a trend favouring the 600,800 and 1000 μM dose groups over the 1200 μM dose group ($P = 0.066$).

Table 1 – Patient and Tumour Characteristics

Characteristic	N	%
Age (median, range)	55 (21 - 70)	
Gender (% male)		53
Body Mass Index (median, range)	24 (18 - 32)	
Skin type		
- II	8	53
- III	7	47
Breslow (median, range)	1,9 (0,7 - 7)	
Clark classification		
- 3	4	27
- 4	10	67
- N/A	1	6
Tumour localization		
- Head and neck	1	6
- Upper extremities	4	27
- Ventral trunk	4	27
- Dorsal trunk	5	34
- Lower extremities	1	6
Type of Surgery		
- Primary excision	1	6
- Re-excision	14	94

Percutaneous Visualization of Lymphatic Channels and Sentinel Lymph Nodes

Prior to the incision, the ability to identify lymphatic vessels and SLNs using NIR fluorescence was assessed. In 13 of 15 patients (87%), lymphatic vessels running away from the site of injection could be identified percutaneously (Fig. 1). In 3 of 15 patients (20%), the location of a total of 8 SLNs could be identified prior to incising the skin. These SLNs were all located in the neck and on the ventral trunk.

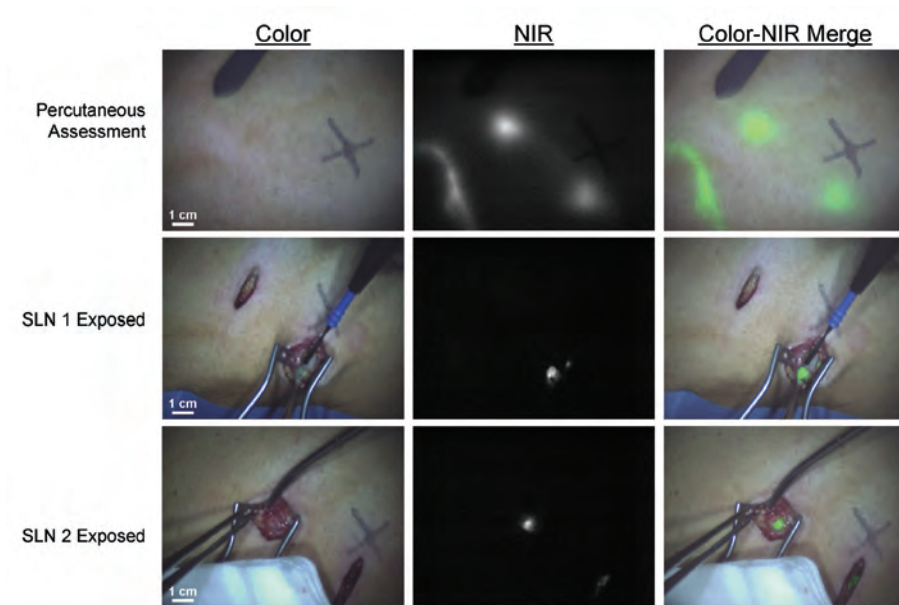


Figure 1 – Sentinel lymph node mapping using NIR fluorescence imaging in cutaneous melanoma: Lymphatic channel (arrowhead) and SLNs (arrows) can be clearly identified percutaneously (top row). Identification of the first SLN (middle row) and second SLN (bottom row) is demonstrated using NIR fluorescence imaging at 15 min after injection of 1.6 mL of 1000 μM ICG:HSA around the excision scar.

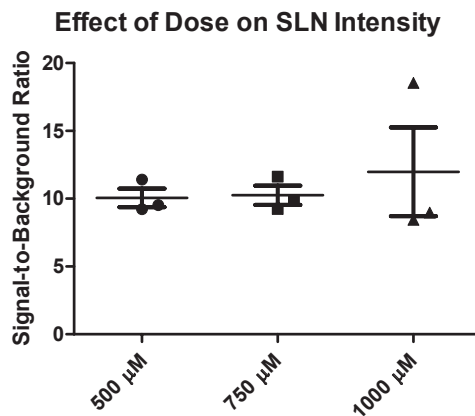


Figure 2 – Optimization of ICG:HSA dose: Signal-to-background ratio (mean \pm S.D.) of melanoma SLNs (ordinate) is plotted as a function of injected dose of ICG:HSA (abscissa). A trend was found favouring the 600, 800 and 1000 μM over 1200 μM ($P = 0.066$).

Table 2 – SLN Identification Results

Characteristic	N	%
SLN Detection		
- Number of SLNs Identified	30	
- Average Number of SLNs Identified (S.D.)	2.0 ± 1.6	
Method of Detection		
- Radioactive	30	100
- Blue	22	73
- Near-Infrared Fluorescence	30	100
Average Time between Injection of ICG:HSA and Skin Incision (S.D.)	12.6 ± 3.6	
Average Time between Skin Incision and SLN Resection (S.D.)	10.2 ± 3.9	
Pecutaneous identification		
- Lymphatic vessels (no. of patients)	13	87
- Sentinel lymph nodes (no. of nodes)	8	27
Sentinel lymph node localization		
- Axilla	18	60
- Neck	2	7
- Groin	4	13
- Ventral trunk	5	17
- Dorsal trunk	1	3
Histology*		
- Negative	11	72
- Macrometastases	1	7
- Micrometastases	1	7
- Isolated Tumour Cells and Micrometastases	1	7
Adjuvant treatment		
- None	12	80
- Axillary Lymph Node Dissection	2	13
- Follow up	1	7
Complications		
- No	15	100
- Yes	0	0

*No SLNs detected in 1 patient using both conventional techniques and NIR fluorescence

DISCUSSION

The current study demonstrates feasibility of NIR fluorescence SLN mapping using ICG:HSA and the Mini-FLARE imaging system in melanoma patients. The accuracy of the SLN procedure using NIR fluorescence was similar to that of radiocolloids and superior to that of blue dye staining. The use of both NIR fluorescence and radiocolloids lead to a 100% SLN detection rate. Whereas only 73% of all SLNs were stained blue. These results are in concordance with previous studies performed by our group on NIR fluorescence SLN mapping in breast and vulvar cancer patients.^{9,20,21}

An advantage of using NIR fluorescent light is that it is capable of penetrating several millimetres into living tissue. In cutaneous melanoma, there is a high variability in localization of the SLN mostly depending on the site of the primary tumour. Not infrequently, different SLNs can be found at completely different sites in the human body, which can lead to a prolonged search and even the need of displacing the patient on the operating table. In these cases, real-time percutaneous assessment of lymphatic drainage, from the primary tumour to the SLN will have a substantial added value. Percutaneous assessment of lymphatic vessels was possible in 87% of patients in the current study. Moreover, in 20% of patients, the SLNs could be identified through the skin. SLNs in cutaneous melanoma patients are often superficially located, making NIR fluorescence imaging highly suitable for this indication. Percutaneous visualization can be influenced by the skin type of patients, as melanin and hemoglobin determine skin color and have high scattering and absorption properties in the NIR spectral range. In this study, no differences were observed as all patients had skin type II/III. Moreover, when located deeper, for example in the axilla, no SLNs could be identified percutaneously using NIR fluorescence. The advantages of NIR fluorescence using ICG:HSA could allow more efficient detection of the SLN, which can result in less damage of healthy tissue, and possibly increase sensitivity.²² Though, in the current study, in one patient, no SLN could be identified using NIR fluorescence or the conventional technique, for which no explanation could be appointed.

For future clinical use of this new technique it is important to determine the dose of ICG:HSA that provides optimal imaging results. We observed a trend in SBR differences between the ascending concentrations of ICG:HSA leading to a decline of signal in the 1200 μM group. This is in line with previously reported results in breast cancer.⁹ A decrease of fluorescence signal with an increase in concentration

can likely be explained by fluorescence quenching.⁷ To assess the possibility of using lower concentrations for fluorescence SLN mapping in melanoma patients, a dose-finding study with concentrations ranging from 50 μM – 500 μM of ICG:HSA will be reported separately (Clinicaltrials.gov identifier: NCT01121718).

In the process of optimization of the SLN procedure using NIR fluorescence in breast cancer patients, we have previously demonstrated in a randomized trial that there is no advantage of using ICG premixed with HSA over ICG alone²⁰ and that patent blue can be omitted when NIR fluorescence is used.²³ For optimization of this technique in melanoma patients, future studies investigating the additional value of premixing ICG with HSA and the necessity to use patent blue have to be performed. Moreover, in the current study SLN localization was performed directly after tracer administration. In a previous study by our group in SLN biopsy in oral cavity and oropharyngeal cancers, rapid migration of ICG:HSA beyond the SLN was observed.²⁴ The migration beyond the SLN requires localization of SLN directly after injection of the tracer, to prevent detection of many second-tier lymph nodes.

In conclusion, our current study demonstrates the feasibility of SLN mapping in cutaneous melanoma patients using ICG:HSA and the mini-FLARE image-guided surgery system. With respect to logistical and safety issues, a dose of 600 μM of ICG:HSA seems to be optimal. NIR fluorescence has a 100% accuracy in SLN detection and adds the value of percutaneous lymphatic drainage and in some cases SLN assessment.

REFERENCES

1. Balch CM, Soong SJ, Atkins MB et al. An evidence-based staging system for cutaneous melanoma. *CA Cancer J Clin* 2004; 54:131-149.
2. Morton DL, Wanek L, Nizze JA et al. Improved long-term survival after lymphadenectomy of melanoma metastatic to regional nodes. Analysis of prognostic factors in 1134 patients from the John Wayne Cancer Clinic. *Ann Surg* 1991; 214:491-499.
3. Morton DL, Wen DR, Wong JH et al. Technical details of intraoperative lymphatic mapping for early stage melanoma. *Arch Surg* 1992; 127:392-399.
4. Thompson JF, McCarthy WH, Bosch CM et al. Sentinel lymph node status as an indicator of the presence of metastatic melanoma in regional lymph nodes. *Melanoma Res* 1995; 5:255-260.
5. Gershenwald JE, Ross MI. Sentinel-lymph-node biopsy for cutaneous melanoma. *N Engl J Med* 2011; 364:1738-1745.
6. Frangioni JV. In vivo near-infrared fluorescence imaging. *Curr Opin Chem Biol* 2003; 7:626-634.
7. Gioux S, Choi HS, Frangioni JV. Image-guided surgery using invisible near-infrared light: fundamentals of clinical translation. *Mol Imaging* 2010; 9:237-255.
8. Hojo T, Nagao T, Kikuyama M et al. Evaluation of sentinel node biopsy by combined fluorescent and dye method and lymph flow for breast cancer. *Breast* 2010; 19:210-3.
9. Mieog JS, Troyan SL, Hutteman M et al. Towards Optimization of Imaging System and Lymphatic Tracer for Near-Infrared Fluorescent Sentinel Lymph Node Mapping in Breast Cancer. *Ann Surg Oncol* 2011; 18:2483-2491.
10. Troyan SL, Kianzad V, Gibbs-Strauss SL et al. The FLARE intraoperative near-infrared fluorescence imaging system: a first-in-human clinical trial in breast cancer sentinel lymph node mapping. *Ann Surg Oncol* 2009; 16:2943-2952.
11. Murawa D, Hirche C, Dresel S et al. Sentinel lymph node biopsy in breast cancer guided by indocyanine green fluorescence. *Br J Surg* 2009; 96:1289-1294.
12. Schaafsma BE, Mieog JSD, Hutteman M et al. The clinical use of indocyanine green as a near-infrared fluorescent contrast agent for image-guided oncologic surgery. *J Surg Oncol* 2011; in press.
13. Crane LM, Themelis G, Pleijhuis RG et al. Intraoperative multispectral fluorescence imaging for the detection of the sentinel lymph node in cervical cancer: a novel concept. *Mol Imaging Biol* 2011; 13:1043-1049.
14. Fujisawa Y, Nakamura Y, Kawachi Y et al. A Custom-Made, Low-Cost Intraoperative Fluorescence Navigation System with Indocyanine Green for Sentinel Lymph Node Biopsy in Skin Cancer. *Dermatology* 2011.
15. Fujiwara M, Mizukami T, Suzuki A et al. Sentinel lymph node detection in skin cancer patients using real-time fluorescence navigation with indocyanine green: preliminary experience. *J Plast Reconstr Aesthet Surg* 2009; 62:e373-e378.
16. Tanaka R, Nakashima K, Fujimoto W. Sentinel lymph node detection in skin cancer using fluorescence navigation with indocyanine green. *J Dermatol* 2009; 36:468-470.
17. Mizukami T, Fujiwara M, Suzuki A et al. Sentinel lymph node detection by indocyanine green fluorescence imaging in skin cancer patients: technical refinement. *The Open Surgical Oncology Journal* 2010; 2:57-61.
18. Polom K, Murawa D, Rho YS et al. Skin melanoma sentinel lymph node biopsy using real-time fluorescence navigation with indocyanine green and indocyanine green with human serum albumin. *Br J Dermatol* 2011.
19. Ohnishi S, Lomnes SJ, Laurence RG et al. Organic alternatives to quantum dots for intraoperative near-infrared fluorescent sentinel lymph node mapping. *Mol Imaging* 2005; 4:172-181.
20. Hutteman M, Mieog JS, van der Vorst JR et al. Randomized, double-blind comparison of indocyanine green with or without albumin premixing for near-infrared fluorescence imaging of sentinel lymph nodes in breast cancer patients. *Breast Cancer Res Treat* 2011; 127:163-170.

21. Hutteman M, van der Vorst JR, Gaarenstroom KN et al. Optimization of near-infrared fluorescent sentinel lymph node mapping for vulvar cancer. *Am J Obstet Gynecol* 2011.
22. Fujisawa Y, Nakamura Y, Kawachi Y et al. Indocyanine green fluorescence-navigated sentinel node biopsy showed higher sensitivity than the radioisotope or blue dye method, which may help to reduce false-negative cases in skin cancer. *J Surg Oncol* 2012.
23. van der Vorst JR, Schaafsma BE, Verbeek FP et al. Randomized Comparison of Near-infrared Fluorescence Imaging Using Indocyanine Green and 99(m) Technetium With or Without Patent Blue for the Sentinel Lymph Node Procedure in Breast Cancer Patients. *Ann Surg Oncol* 2012; 19:4104-4111.
24. van der Vorst JR, Schaafsma BE, Verbeek FP et al. Near-infrared fluorescence sentinel lymph node mapping of the oral cavity in head and neck cancer patients. *Oral Oncol* 2012.

Chapter 9

Near-infrared fluorescence sentinel lymph node mapping of the oral cavity in head and neck cancer patients

van der Vorst JR, Schaafsma BE, Verbeek FP, Keereweer S, Jansen J, van der Velde LA, Langeveld A, Hutteman M, Lowik CW, van de Velde CJ, Frangioni JV, Vahrmeijer AL

Oral Oncol. 2013 Jan;49(1):15-9

ABSTRACT

Background

Elective neck dissection is frequently performed during surgery in head and neck cancer patients. The sentinel lymph node (SLN) procedure can prevent the morbidity of a neck dissection and improve lymph node staging by fine pathology. Near-infrared (NIR) fluorescence imaging is a promising technique to identify the sentinel lymph node (SLN) intraoperatively. This feasibility study explored the use of indocyanine green adsorbed to human serum albumin (ICG:HSA) for SLN mapping in head and neck cancer patients.

Material and Methods

A total of 10 consecutive patients with oral cavity or oropharyngeal cancer and a clinical N0 neck were included. After exposure of the neck, 1.6 mL of ICG:HSA (500 μ M) was injected at 4 quadrants around the tumor. During the neck dissection, levels I, II, III and IV were measured for fluorescence using the Mini-FLARE imaging system.

Results

In all 10 patients, NIR fluorescence imaging enabled visualization of one or more SLNs. A total of 17 SLNs were identified. The mean contrast between the fluorescent signal of the lymph nodes and of the surrounding tissue was 8.7 ± 6.4 . In 3 patients, of which 1 was false-negative, lymph node metastases were found. After administration of ICG:HSA, the average number of fluorescent lymph nodes significantly increased over time ($P < 0,001$).

Conclusion

This study demonstrated feasibility to detect draining lymph nodes in head and neck cancer patients using NIR fluorescence imaging. However, the fluorescent tracer quickly migrated beyond the SLN to higher tier nodes.

INTRODUCTION

In head and neck cancer patients, cervical lymph node involvement is the single most important prognostic factor.^{1,2} To obtain adequate staging and local control of the cervical region, elective neck dissections are frequently performed, even in patients with clinical and radiological N0 stage. In approximately 25% of these patients, lymph node metastases are found.³ Furthermore, micrometastases and isolated tumor cells are often missed during standard pathological workup.

To decrease the morbidity of neck dissection and to improve lymph node staging by fine pathology, the sentinel lymph node (SLN) procedure has been advocated. The SLN procedure is based on the theory that flow from a tumor travels sequentially to the first tier node (i.e. the sentinel node) and subsequently to the remaining lymph node basin. The SLN procedure is currently standard of care in breast cancer and melanoma in most centers. Although much work has been performed in head and neck cancer, the SLN procedure has not yet been established as standard of care.⁴⁻⁷ As in breast cancer, the use of radiocolloids and a blue dye can be considered the gold standard to locate the SLN. However, the disadvantages of radiocolloids are the lack of real-time intraoperative visual information and the need for a nuclear physician; and disadvantages of blue dyes include limited depth penetration and blue staining of the surgical field.

Recently, the use of near-infrared (NIR) fluorescent light has been introduced to intraoperatively to identify lymph nodes, tumors and vital structures.⁸ NIR fluorescence using the fluorescent dye indocyanine green (ICG) has been successfully used for sentinel lymph node mapping in breast cancer, melanoma, cervical cancer, and vulvar cancer.⁹⁻¹² The concept of NIR fluorescence guided SLN mapping in oropharyngeal cancer has also been reported in humans.¹³ However, in the study by Bredell et al.¹³, the interval between injection of ICG and imaging varied between 5 and 30 min, which can result in identification of higher tier nodes. Preclinical work suggests that premixing ICG with human serum albumin (complex: ICG:HSA) could improve the fluorescent properties and improves retention in the SLN due to its increased hydrodynamic diameter.¹⁴ Furthermore, the injected dose of ICG (without HSA) used by Bredell et al. was 10 mg per patient. Several clinical dose-finding studies have shown that a significant lower dose (0.5-1.0 mg ICG:HSA) can successfully be used for sentinel lymph node mapping in other indications.¹⁰⁻¹² The aim of the current study was to assess the feasibility of NIR fluorescence and ICG:HSA for SLN mapping in head and neck cancer using 1.6 ml of 500 μ M ICG:HSA and the Mini-FLARE imaging system.

MATERIAL AND METHODS

Preparation of Indocyanine Green Adsorbed to Human Serum Albumin

ICG (25 mg vials) was from Pulsion Medical Systems (Munich, Germany) and was resuspended in 10 cc of sterile water for injection to yield a 2.5-mg/ml (3.2-mM) stock solution. Of this solution, 7.8 cc was transferred to a 50-cc vial of Cealb (20% human serum albumin (HSA) solution; Sanquin, Amsterdam, The Netherlands) to yield ICG in HSA (ICG:HSA) at a final concentration of 500 μ M.

Intraoperative NIR Fluorescence Imaging

SLN mapping was performed using the Mini-FLARE image-guided surgery system as described before.¹¹ Briefly, the system consists of 2 wavelength-isolated light sources: a “white” light source, generating 26,600 lx of 400 to 650-nm light and a “near-infrared” light source, generating 7.7-mW/cm² of 760-nm light. Color video and NIR fluorescence images are simultaneously acquired and displayed in real time using custom optics and software that separate the color video and NIR fluorescence images. A pseudo-colored (lime green) merged image of the color video and NIR fluorescence images is also displayed. The imaging head is attached to a flexible gooseneck arm, which permits positioning of the imaging head virtually anywhere over the surgical field, and at extreme angles. For intraoperative use, the imaging head and imaging system pole stand are wrapped in a sterile shield and drape (Medical Technique Inc., Tucson, AZ).

Clinical Trial

The single-institution clinical trial was approved by the Medical Ethics Committee of the Leiden University Medical Center and was performed in accordance with the ethical standards of the Helsinki Declaration of 1975. A total of 10 consecutive patients with oral cavity or oropharyngeal cancer, and a clinical and radiological N0 neck were included. All patients underwent ultrasound guided cytology of lymph nodes in the neck region to assess nodal status. All patients provided informed consent and were anonymized. Exclusion criteria were pregnancy, lactation or an allergy to iodine, shellfish, or indocyanine green.

After exposure of the neck following subplatysmal flap elevation, 1.6-mL ICG:HSA (500 μ M) was injected at 4 quadrants around the tumor using a 21G, 1½ inch needle. During the neck dissection, levels I, II, III and IV were measured for fluorescence using the Mini-FLARE imaging system after injection of ICG:HSA. To

assess the occurrence of drainage to higher tier nodes and the optimal time of imaging after injection, measurements were performed at 5, 10, 15, 20, 25, 30, 45 and 60 min after injection. All first draining NIR fluorescent hotspots were considered SLNs and were marked using sutures. The neck dissections consisted of resection of level I, IIa, IIb and III and in some cases level IV. The resection of the primary tumor afterwards was performed following standard procedure. Afterwards, all resected lymph nodes were examined by routine histopathological analysis; lymph nodes were fixed in formalin and embedded in paraffin for routine hematoxylin and eosin staining. SLNs and non-SLNs were examined separately.

Statistical Analysis

For statistical analysis and to generate graphs, GraphPad Prism Software (Version 5.01, La Jolla, CA) was used. Age, body mass index (BMI) and tumor size were reported as median and range. Signal-to-background ratio (SBR) was reported as mean and standard deviation. Difference in number of lymph nodes identified between time points was tested using a repeated measures ANOVA.

RESULTS

Patient and Tumor Characteristics

Patient and tumor characteristics are detailed in Table 1. Ten patients with oral cavity or oropharyngeal tumors and a clinical and radiological stage N0 were included. Median patient age was 59.5 years (range 33-73 years), median BMI was 24 (range 19-35 kg/m²), and median primary tumor size was 2.2 cm (range 0.3-5.2 cm). Location of primary tumor was the tongue in 7 patients, tonsil region in 2 patients, and retromolar trigone in 1 patient. Four patients underwent a hemiglossectomy, 4 patients underwent a commando resection, and 2 patients underwent a pull-through resection. Nine patients underwent a unilateral neck dissection and 1 patient a bilateral neck dissection. One patient was previously treated for a laryngeal cancer and developed a second primary tumor after a disease-free period of 10 y, for which the patient was treated and included in the current study. This patient was initially treated with surgical removal of the tumor and bilateral radiotherapy of the neck region. After histological examination, 9 patients were diagnosed with a squamous cell carcinoma and 1 patient with a basal cell adenocarcinoma.

Table 1 - Patient and Tumor Characteristics

Patient no.	Age (Years)	BMI (kg/m ²)	Tumor Location	Type of Surgery	Tumor Type	Tumor Size (cm)
1	33	22	Tongue	Hemiglossectomy	Squamous	1.7
2	73	25	Tongue	Hemiglossectomy	Squamous	5.2
3	64	24	Oropharynx	Commando resection	Basal cell adenocarcinoma	1.3
4	62	22	Tongue	Hemiglossectomy	Squamous	3.3
5	58	23	Trigonum Retromolare	Commando resection	Squamous	0.3
6	55	27	Tongue	Hemiglossectomy	Squamous	1.6
7	52	32	Tongue	Hemiglossectomy	Squamous	3
8	63	35	Oropharynx	Commando resection	Squamous	4
9	53	24	Tongue	Pull through resection	Squamous	2.4
10	61	19	Tongue	Pull through resection	Squamous	2

BMI: Body Mass Index

Intraoperative NIR Fluorescence Imaging

In all patients (N = 10), NIR fluorescence imaging enabled identification of 1 or more SLNs. An example of the intraoperative identification of a SLN using NIR fluorescence is shown in Figure 1. A total of 17 SLNs were detected. On average, 1.7 ± 0.8 SLNs per patient were detected and a total of 22.9 ± 9.7 lymph nodes were resected per patient (Table 2). The average contrast between fluorescent signal of the SLN and the surrounding tissue was 8.7 ± 6.4 . In 3 patients, the identified SLNs were located in level I, in 5 patients in level IIA and in 2 patients in level III. No adverse reactions or complications occurred during the current study. Histological analysis showed that 3 out of 10 patients had metastatic disease, all in a single lymph node. In 2 cases, the tumor-positive lymph node was the NIR fluorescent SLN, and in 1 patient the tumor-positive lymph node was a non-SLN located in level 2A, which was also not NIR fluorescent. No adverse reactions occurred.

Table 2 – Results from *In Vivo* SLN Imaging

Patient no.	NIR Hotspots	Total LNs Harvested	LN+	Mean SBR	Location of NIR Hotspots
1	3	14	No	16.3	2A
2	1	26	No	21.0	1
3	1	30	No	12.0	1
4	3	35	Yes (SLN +)	3.2	1
5	2	9	No	2.6	2A
6	1	20	Yes (SLN +)	4.2	2A
7	2	24	No	5.2	3
8	1	15	No	4.2	3
9	2	17	Yes (SLN -)	5.7	2A
10	1	39	No	12.3	2A

NIR: Near Infrared, LN: Lymph Node, SBR: Signal-to-background

Intraoperative lymphatic mapping

To assess the occurrence of drainage to higher tier nodes and the optimal time of imaging after injection, NIR fluorescence was measured at several time points after injection (Fig. 2). All first draining NIR fluorescent hotspots were considered SLNs and were marked using sutures. Additional lymph nodes that became fluorescent during later imaging time-points were allocated as higher tier non-SLNs. In 7 of 10 patients SLNs could be identified within 5 min after injection. In 3 patients, SLNs were detected after 10, 15 and 30 min, respectively. Using a repeated measures ANOVA test, the average number of fluorescent lymph nodes significantly increased over time ($P < 0.001$; Fig. 3).

DISCUSSION

The current study examined the feasibility of using the Mini-FLARE imaging system and ICG:HSA for intraoperative fluorescence guided SLN mapping in head and neck cancer patients. In all patients, 1 or more SLNs could be identified during surgery, and in the majority of patients the SLN could be identified within 5 min after injection. The average contrast between fluorescence of the SLNs and background fluorescence was 8.7, which is consistent with SBRs that were reported for fluorescence SLN mapping studies using ICG:HSA in other cancer types.⁹⁻¹¹ Another important finding of the current study was that after several min, ICG:HSA

drains to second tier nodes, which can possibly result in the identification of false-positive sentinel nodes.

Bredell et al. was the first to describe the successful use of NIR fluorescence in SLN mapping in oropharyngeal cancer patients. In this study, the time between injection of ICG (without HSA) and imaging varied between 5 and 30 min. Based on the present study, this could result in identification of higher tier lymph nodes. Furthermore, the injected dose of ICG used in the previous study was 10 mg, which is considerably higher than the dose used in the present study (0.62 mg). In breast cancer patients, our group has shown that when ICG is injected in a high dose, a phenomenon known as quenching can occur, which can result in a decrease of the NIR fluorescence signal.¹¹

Based on previous preclinical results, ICG was premixed with HSA in the current study to obtain better retention in the SLN and to increase quantum yield.¹⁴ However, it still remains unclear if premixing ICG with HSA is necessary or significantly improves performance. A randomized clinical trial in breast cancer patients reported no differences between using ICG:HSA and ICG alone.⁹ However, the effect of premixing ICG with HSA is potentially indication-specific, therefore this should be examined for head and neck cancer patients.

Another approach recently presented by van der Poel et al. is combining fluorescence and radioactivity in 1 lymphatic tracer by simply premixing ^{99m}Tc-NanoColl and ICG.¹⁵ Using this multimodal tracer injected by the nuclear physician before surgery, time of surgery will probably be shortened because the dye does not have to be injected during surgery. Furthermore, preoperative SLN localization and subsequent surgical planning can be performed using a lymphoscintigraphy or a SPECT/CT exam. Heuveling et al. demonstrated SLN mapping in rabbits using Nanocolloidal albumin which was covalently conjugated to IRDye-800CW, which showed excellent retention in the SLN after 24 hr.¹⁶ However, translation of this compound to a clinical setting remains challenging due to regulatory issues.

The current study showed a relatively wide range in time between injection of ICG:HSA and identification of the SLN, which was 30 min in 1 patient. This particular patient was treated for a primary laryngeal tumor by resection and cervical radiotherapy 10 y prior to the current study, and only 1 fluorescent lymph node could be detected. After pathological workup, 15 lymph nodes were detected. Radiation can influence microvasculature and damage the capillary network, which manifests itself as telangiectatic vessels that increase over time.¹⁷ Other studies showed that repair of damaged endothelium by angiogenesis

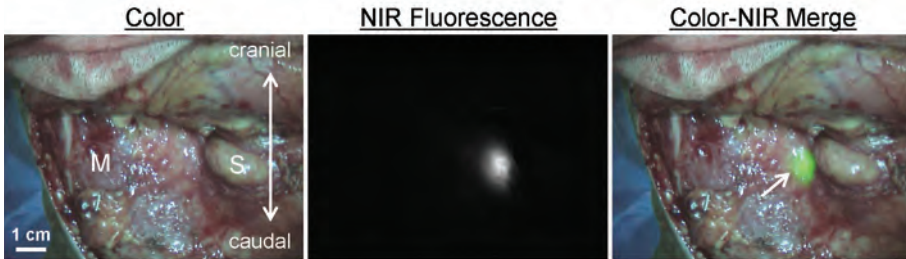


Figure 1 – Sentinel lymph node mapping using NIR fluorescence imaging in oropharyngeal cancer patients: Peritumoral injection of 1.6 mL of 500- μ M ICG:HSA identifies a SLN (arrow) in an oropharyngeal cancer patient. M = sternocleidomastoid muscle and S = submandibular gland.

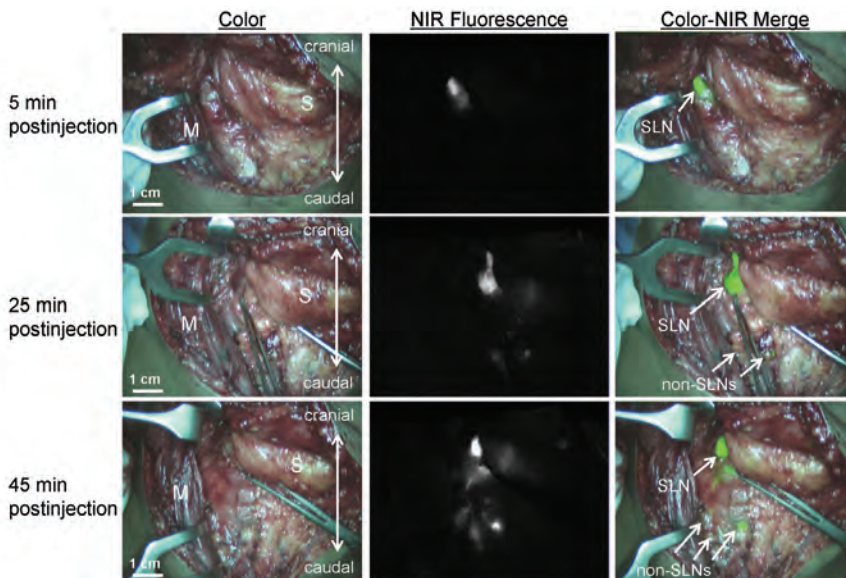


Figure 2 – Sentinel lymph node mapping in head and neck cancer over time: One SLN (arrows) can be clearly identified 5 min (top row) postinjection of 1.6 mL of 500- μ M ICG:HSA around the primary tumor. Identification of higher tier nodes was observed after 25 min (middle row), and the number of fluorescent lymph nodes increased further at 45 min postinjection (bottom row). M = sternocleidomastoid muscle and S = submandibular gland.

is inhibited by radiotherapy.¹⁸ Similar damage and aberrant repair may occur in lymphatic microvessels after radiation. Therefore, a possible explanation for the relatively long time to identify the SLN in this patient was that damage to the lymphatic microvessels perturbed drainage in the irradiated neck. Furthermore, it is known from rectal cancer studies that an average of approximately 5 times fewer nodes can be identified in resection specimens when patients are treated with neoadjuvant radiation compared to patients only treated with surgery.¹⁹ When

translating these results to head and neck cancer patients, prudence should be applied in patients pretreated with radiation since SLN mapping can be more challenging in these patients.

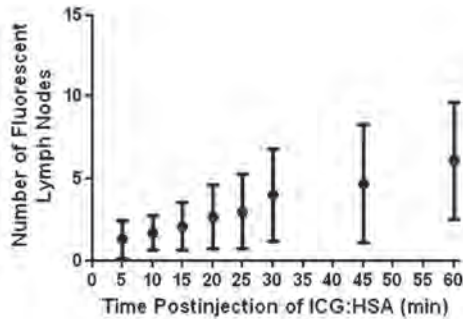


Figure 3 – Lymph node identification as a function of postinjection time: Number of fluorescent lymph nodes (mean \pm S.D.) is plotted as a function of time after injection of 500- μ M ICG:HSA. The number of fluorescent lymph nodes significantly increased over time ($P < 0.001$)

Based on standard pathology, in 1 of 3 patients with positive nodes, tumor cells were detected in a non-SLN, while the SLNs did not contain tumor. The reason for this patient being false-negatively staged remains unclear. A potential explanation could be that in case of multiple drainage patterns, a subset of SLNs can become fluorescent later, and will be incorrectly identified as higher tier lymph nodes. Future research should therefore be focused on fluorescent tracers that are retained in the first draining node(s), which makes it possible to perform imaging later after injection of the dye. Furthermore, the relatively low depth sensitivity of the current generation imaging systems (on the order of millimeters), could be an explanation for false-negative results. Another potential explanation could be the occurrence of a skip metastasis in this particular patient, which has been reported previously in head and neck cancer patients.²⁰ Since only 10 patients were included in the current study, a final potential explanation for this patient being false-negative is the learning curve associated with tracer injection and imaging. Therefore, the false-negative rate has to be assessed in larger patient series.

In conclusion, the current study successfully showed the use of NIR fluorescence and ICG:HSA for intraoperative identification of the SLN in oropharynx and oral cavity cancer patients. Optimal dosage, true false-negative rate, and optimization of lymphatic tracers and possibly multimodal hybrid tracers, are topics for future studies.

REFERENCES

1. Leemans CR, Tiwari R, Nauta JJ et al. Regional lymph node involvement and its significance in the development of distant metastases in head and neck carcinoma. *Cancer* 1993; 71:452-456.
2. Layland MK, Sessions DG, Lenox J. The influence of lymph node metastasis in the treatment of squamous cell carcinoma of the oral cavity, oropharynx, larynx, and hypopharynx: N0 versus N+. *Laryngoscope* 2005; 115:629-639.
3. Sheahan P, O'Keane C, Sheahan JN et al. Effect of tumour thickness and other factors on the risk of regional disease and treatment of the N0 neck in early oral squamous carcinoma. *Clin Otolaryngol Allied Sci* 2003; 28:461-471.
4. Alkureishi LW, Ross GL, Shoab T et al. Sentinel node biopsy in head and neck squamous cell cancer: 5-year follow-up of a European multicenter trial. *Ann Surg Oncol* 2010; 17:2459-2464.
5. Burcia V, Costes V, Faillie JL et al. Neck restaging with sentinel node biopsy in T1-T2N0 oral and oropharyngeal cancer: Why and how? *Otolaryngol Head Neck Surg* 2010; 142:592-597.
6. Civantos FJ, Zitsch RP, Schuller DE et al. Sentinel lymph node biopsy accurately stages the regional lymph nodes for T1-T2 oral squamous cell carcinomas: results of a prospective multi-institutional trial. *J Clin Oncol* 2010; 28:1395-1400.
7. Kuriakose MA, Trivedi NP. Sentinel node biopsy in head and neck squamous cell carcinoma. *Curr Opin Otolaryngol Head Neck Surg* 2009; 17:100-110.
8. Schaafsma BE, Mieog JS, Hutteman M et al. The clinical use of indocyanine green as a near-infrared fluorescent contrast agent for image-guided oncologic surgery. *J Surg Oncol* 2011; 104:323-332.
9. Hutteman M, Mieog JS, van der Vorst JR et al. Randomized, double-blind comparison of indocyanine green with or without albumin premixing for near-infrared fluorescence imaging of sentinel lymph nodes in breast cancer patients. *Breast Cancer Res Treat* 2011; 127:163-170.
10. Hutteman M, van der Vorst JR, Gaarenstroom KN et al. Optimization of near-infrared fluorescent sentinel lymph node mapping for vulvar cancer. *Am J Obstet Gynecol* 2011.
11. Mieog JS, Troyan SL, Hutteman M et al. Toward Optimization of Imaging System and Lymphatic Tracer for Near-Infrared Fluorescent Sentinel Lymph Node Mapping in Breast Cancer. *Ann Surg Oncol* 2011.
12. van der Vorst JR, Hutteman M, Gaarenstroom KN et al. Optimization of near-infrared fluorescent sentinel lymph node mapping in cervical cancer patients. *Int J Gynecol Cancer* 2011; 21:1472-1478.
13. Bredell MG. Sentinel lymph node mapping by indocyanin green fluorescence imaging in oropharyngeal cancer - preliminary experience. *Head Neck Oncol* 2010; 2:31.
14. Ohnishi S, Lomnes SJ, Laurence RG et al. Organic alternatives to quantum dots for intraoperative near-infrared fluorescent sentinel lymph node mapping. *Mol Imaging* 2005; 4:172-181.
15. van der Poel HG, Buckle T, Brouwer OR et al. Intraoperative Laparoscopic Fluorescence Guidance to the Sentinel Lymph Node in Prostate Cancer Patients: Clinical Proof of Concept of an Integrated Functional Imaging Approach Using a Multimodal Tracer. *Eur Urol* 2011.
16. Heuveling DA, Visser GW, de GM et al. Nanocolloidal albumin-IRDye 800CW: a near-infrared fluorescent tracer with optimal retention in the sentinel lymph node. *Eur J Nucl Med Mol Imaging* 2012.
17. Turesson I. Individual variation and dose dependency in the progression rate of skin telangiectasia. *Int J Radiat Oncol Biol Phys* 1990; 19:1569-1574.
18. Scharpfenecker M, Kruse JJ, Sprong D et al. Ionizing radiation shifts the PAI-1/ID-1 balance and activates notch signaling in endothelial cells. *Int J Radiat Oncol Biol Phys* 2009; 73:506-513.
19. Govindarajan A, Gonen M, Weiser MR et al. Challenging the feasibility and clinical significance of current guidelines on lymph node examination in rectal cancer in the era of neoadjuvant therapy. *J Clin Oncol* 2011; 29:4568-4573.
20. Lodder WL, Sewnaik A, den Bakker MA et al. Selective neck dissection for N0 and N1 oral cavity and oropharyngeal cancer: are skip metastases a real danger? *Clin Otolaryngol* 2008; 33:450-457.

Chapter 10

Randomized comparison of near-infrared fluorescence imaging using indocyanine green and ^{99m} technetium with or without patent blue for the sentinel lymph node procedure in breast cancer patients

van der Vorst JR, Schaafsma BE, Verbeek FP, Hutteman M, Mieog JS, Lowik CW, Liefers GJ, Frangioni JV, van de Velde CJ, Vahrmeijer AL

Ann Surg Oncol. 2012 Dec;19(13):4104-11

ABSTRACT

Background

Near-infrared (NIR) fluorescence imaging using indocyanine green (ICG) has the potential to improve sentinel lymph node (SLN) mapping of breast cancer. In the current randomized clinical trial, the value of blue dyes when used in combination with NIR fluorescence was assessed. Furthermore, the possibility to perform SLN mapping without radiotracers was preliminarily examined.

Material and Methods

Clinical trial subjects were 24 consecutive breast cancer patients scheduled to undergo SLN biopsy. All patients received standard of care using ^{99m}Tc -nanocolloid and received 1.6 mL of 500 μM ICG injected periareolarly. Patients were randomly assigned to undergo SLN biopsy with or without patent blue. To assess the need for radiocolloids to localize the SLN(s), the surgeon did not use the handheld gamma probe during the first 15 min after the axillary skin incision.

Results

SLN mapping was successful in 23 of the 24 patients. No significant difference was found in signal-to-background ratio between the patent blue group and no patent blue group (8.3 ± 3.8 vs. 10.3 ± 5.7 , respectively, $P = 0.32$). In both groups, 100% of SLNs were radioactive and fluorescent and in the patent blue group, only 84% of SLNs were stained blue. In 25% of patients, the use of the gamma probe was necessary to localize the SLN within the first 15 minutes.

Conclusion

This study shows that there is no benefit of using patent blue for SLN mapping in breast cancer patients when using NIR fluorescence and ^{99m}Tc -nanocolloid. NIR fluorescence imaging outperformed patent blue in all patients.

INTRODUCTION

Sentinel lymph node (SLN) mapping is regarded as standard of care in staging of the axilla in breast cancer patients with clinically negative axillary lymph nodes.¹ To locate the SLN, different techniques can be used. Combining a radiotracer and blue dye staining achieves the highest identification rates (95%-97%) and is therefore preferred²⁻⁵; however, both methods have several disadvantages. Radioactive colloids require involvement of a nuclear physician, do not provide visual information intraoperatively, and the time window in which they can be used is limited due to the half-life of ^{99m}Tc. Moreover, a substantial part of patients undergoes SLN mapping using only a blue dye, since radioactive isotopes are not widely available in every medical center. The percentage of patients in whom only blue dye staining is used for SLN mapping varies from 4 – 50% in developed countries.⁶⁻⁹ Blue dyes cannot be seen through skin and fatty tissue, permit only limited visualization of afferent lymphatic vessels, and in case a lumpectomy is performed, tattooing of the breast can be seen up until several months after blue dye injection.

Due to these disadvantages, optical imaging using the near-infrared (NIR) fluorescence lymphatic tracer indocyanine green (ICG) has been put forward as an alternative for, or an addition to conventional SLN mapping. Feasibility of this technique has been extensively reported in breast cancer patients¹⁰⁻¹⁶ and other cancer types.¹⁷ A previous dose-finding study performed by our group recently demonstrated that NIR fluorescence using a dose of 500 μ M ICG adsorbed to human serum albumin was most convenient.¹⁸ A follow-up double-blind randomized clinical trial demonstrated no advantages of premixing ICG with human serum albumin in comparison to ICG alone at a dose of 500 μ M for NIR fluorescence SLN mapping.¹⁹

In the clinical trials discussed above, the NIR fluorescence signal of ICG was consistently visualized earlier than the blue dye staining. In the total of 60 SLNs that were detected in the 2 studies (N = 42 patients), only 48 (80%) were stained blue, while 60 (100%) SLNs could be detected with NIR fluorescence.^{18,19} Therefore, NIR fluorescence imaging has the potential to replace blue dyes in SLN mapping in breast cancer patients. If the use of blue dye staining could be omitted, disadvantages like tattooing of the breast and blue staining of the surgical field in case of a lumpectomy could be prevented. Furthermore, the use of blue dyes may interfere with NIR fluorescence imaging by absorbing the fluorescent light

and thereby decreasing the NIR fluorescent signal. Finally, anaphylactic reactions to blue dyes, although rare, can be life threatening. Because NIR fluorescent light penetrates relatively deep into tissue (up to 0.5-1 cm), it also has the potential to replace the use of radiotracers. However, omitting the use of radiotracers may only be reserved for selected patients, for example those with a sufficiently low body mass index (BMI).

In the current randomized clinical trial, the added value of using blue dye staining when used in combination with NIR fluorescence and radiotracer was assessed. Furthermore, the possibility to perform SLN mapping without radiotracers was preliminarily explored.

METHODS

Preparation of Indocyanine Green

ICG (25 mg vials) was purchased from Pulsion Medical Systems (Munich, Germany) and was resuspended in 10 cc of sterile water for injection to yield a 2.5-mg/ml (3.2 mM) stock solution. To obtain a 500- μ M dilution of ICG, 7.8 mL of the 3.2-mM ICG solution was diluted in 42.8 mL of sterile water. In a previous study, we determined that the optimal dose of ICG lies between 400 μ M and 800 μ M¹⁸, therefore a dose of 500 μ M was chosen.

Intraoperative Near-Infrared Imaging System (Mini-FLARE™)

SLN mapping was performed using the Mini-Fluorescence-Assisted Resection and Exploration (Mini-FLARE™) image-guided surgery system, as described earlier.¹⁸ Briefly, the system consists of 2 wavelength isolated light sources: a “white” light source, generating 26,600 lx of 400 to 650 nm light, and a “near-infrared” light source, generating 7.7 mW/cm² of 760 nm light. Color video and NIR fluorescence images are simultaneously acquired and displayed in real time using custom optics and software that separate the color video and NIR fluorescence images. A pseudo-colored (lime green) merged image of the color video and NIR fluorescence images is also displayed. The imaging head is attached to a flexible gooseneck arm, which permits positioning of the imaging head at extreme angles virtually anywhere over the surgical field. For intraoperative use, the imaging head and imaging system pole stand are wrapped in a sterile shield and drape (Medical Technique Inc., Tucson, AZ).

Clinical Trial

This randomized, single-institution trial comparing NIR fluorescence SLN mapping with or without patent blue was approved by the Medical Ethics Committee of the Leiden University Medical Center and was performed in accordance with the ethical standards of the Helsinki Declaration of 1975. All patients planning to undergo a SLN procedure for invasive breast cancer or high-risk carcinoma *in situ* were eligible for participation in the trial. Patients had clinically negative axillary nodes as assessed by palpation and ultrasonography. Exclusion criteria were pregnancy, lactation or an allergy to iodine, shellfish, or indocyanine green. All patients gave informed consent and were anonymized.

As part of the SLN procedure, patients were injected periareolarly with approximately 100 MBq ^{99m}Tc-technetium-nanocolloid the day before surgery. Before the start of the operation, patients were randomly assigned to receive or not receive an injection with patent blue. Patients were randomized by the Department of Surgery and treatment allocation was performed by block randomization. For patients randomized to be injected with patent blue, 1 mL total of patent blue (Bleu Patenté V, Guerbet, Brussels, Belgium) was injected intradermally and periareolarly at 4 sites before the start of the operation. All patients were intradermally and periareolarly injected with 1.6 mL total of 500 µM ICG at 4 sites before the start of the operation. Patent blue and ICG injections were performed by the surgeon. Subsequently, gentle pumping pressure was applied to the injection site for 1 min. After surgical scrub and sterile covering of the operation field, NIR fluorescence imaging was performed with the imaging head of the Mini-FLARE™ at approximately 30 cm distance to the surgical field. The lights in the operating room were turned off and the complete procedure could be performed using the white light source of the Mini-FLARE™. Camera exposure times were between 5 to 250 ms. A SLN exhibiting a signal-to-background ratio (SBR) ≥ 1.1 *in situ* was considered positive by NIR fluorescence.

To assess the need for radiocolloids to localize the SLN(s), the surgeon did not use the handheld gamma probe during the first 15 min of the operation starting from the axillary skin incision. In case the SLN(s) were not localized using only ICG or ICG in combination with patent blue within the first 15 min, the surgeon was allowed to use the handheld gamma probe for SLN localization.

Routine histopathological frozen analysis of SLNs was performed during surgery. After frozen section, SLNs were fixed in formalin and embedded in paraffin for routine hematoxylin and eosin staining and immunohistopathological staining

for AE1/AE3 at 3 levels, with an interval of 150 to 250 μm , according to the Dutch guidelines for SLN analysis. Patients underwent an axillary lymph node dissection if the SLN was found to contain metastases. If micrometastases ($< 0.2 \text{ mm}$) or isolated tumor cells were found, no axillary lymph node dissection was performed.

Power Calculation and Statistical Analysis

To show non-inferiority, a power calculation based on data from our previous studies^{18,19} revealed that 24 patients are needed to achieve 91% power to detect a difference of 5.0 in SBR between the 2 groups with the null hypothesis that the mean SBR of each group is $10.0 \pm$ the standard deviation of 3.5 and the alternative hypothesis that the mean of the no blue dye group is 15.0 with a significance level of 0.05 using a two-sided two-sample *t* test. For statistical analysis, SPSS statistical software package (Version 16.0, Chicago, IL) was used. To compare patient characteristics, SBR and the number of SLNs identified between the patent blue group and no patent blue group, the independent-sample *t* test and chi-square test were used. $P < 0.05$ was considered significant.

RESULTS

Patient and Tumor Characteristics: Twenty-four consecutive breast cancer patients undergoing SLN mapping using ^{99m}Techneium-nanocolloid and ICG were randomized to be injected with or without patent blue. The median age of the included patients was 59 years (range: 39-75) and the median BMI was 24 kg/m^2 (range: 19-47). BMI was significantly higher in the no patent blue group ($P = 0.042$). Other patient, tumor, and treatment characteristics were equally distributed over the treatment groups (Table 1). The average time between injection of ICG and the skin incision was not significantly different between treatment groups and was $15.2 \pm 3.0 \text{ min}$ and $13.2 \pm 3.0 \text{ min}$ for the patent blue and no patent blue patient groups, respectively. No adverse reactions associated with the use of ICG or the Mini-FLARE imaging system occurred. No postoperative complications of the sentinel lymph node procedure were observed.

Table 1 – Patient and Tumor Characteristics

Characteristic	Patent Blue (N = 12)		No Patent Blue (N = 12)		P
	N	%	N	%	
Age in years (Median, Range)	54 (39-75)		67 (48-71)		0.15
Body Mass Index (median, range)	23.5 (19-34)		28 (20-47)		0.042*
Skin Type					0.62
- II*	2	17	2	17	
- III*	10	83	10	83	
Previous Procedure of Breast					0.54
- Excision fibroadenoma	1	8	0	0	
- Neoadjuvant Chemotherapy	2	17	1	8	
- Neoadjuvant Hormonal Therapy	0	0	1	8	
Multifocality	0	0	1	8	0.31
Tumor side					0.41
- Left	6	50	7	59	
- Right	6	50	5	42	
Tumor localization					0.69
- Upper Outer	7	59	7	59	
- Lower Outer	0	0	0	0	
- Lower Medial	0	0	0	0	
- Upper Medial	3	25	3	25	
- Central	2	17	2	17	
Type of Operation					0.36
- Mastectomy	2	17	3	25	
- Wide Local Excision	9	75	9	75	
- SNB Only	1	8	0	0	
Pathological Tumor Size in mm (Median, Range)	15 (5-35)		16 (5-50)		0.12
Histological Type					1
- Infiltrating Ductal type Adenocarcinoma	10	83	10	83	
- Infiltrating Lobular type Adenocarcinoma	1	8	1	8	
- Ductal Carcinoma In Situ	1	8	1	8	
Histological Grade					0.56
- I	4	33	3	25	
- II	4	34	3	25	
- III	3	2	5	42	
- No grading possible (DCIS)	1	8	1	8	

*Skin type II: White: usually burns easily; tans minimally (Northern European), *Skin type III: III. White (average): some-times burns; tans gradually to light brown (Central European)

Intraoperative NIR Fluorescence Imaging: In 23 of 24 patients, at least one SLN (Figure 1) was identified (Table 2). In one patient included in the no patent blue group, no SLN could be detected, even when using the gamma probe. A total of 19 and 18 SLNs were resected in the patent blue and no patent blue groups, respectively. In the patent blue group, 19 of 19 (100%) of SLNs were NIR fluorescent, 17 of 19 (89%) SLNs were radioactive and 16 of 19 (84%) SLNs were blue. In the no patent blue group, 18 of 18 (100%) SLNs were NIR fluorescent and 18 of 18 (100%) of SLNs were radioactive. The afferent lymphatics were visualized percutaneously in 83% and 75% of patients in the patent blue and no patent blue patient groups, respectively. No significant difference was observed. In all patients that were administered with patent blue, the NIR fluorescence signal in the SLN was detected before patent blue was visualized.

Average brightness of the SLN, expressed in signal-to-background ratio (SBR), was 8.3 ± 3.8 and 10.3 ± 5.7 for the patent blue and the no patent blue group, respectively (Figure 2; Table 2). No significant difference in SBR was observed between the treatment groups ($P = 0.32$). Average time between skin incision and SLN identification was 12.4 ± 7.7 min and 18.1 ± 18.9 min for the blue dye and no blue dye patient groups, respectively. No significant difference was observed ($P = 0.35$). In one patient in the no patent blue group, time between skin incision and SLN detection was 66.91 min. This patient received neoadjuvant chemotherapy, and the SLN was located in the area next to the latissimus dorsi muscle. Excluding this outlier, average time between skin incision and SLN identification was 12.4 ± 7.7 min and 13.2 ± 10.3 for the patent blue and no patent blue treatment groups, respectively ($P = 0.83$).

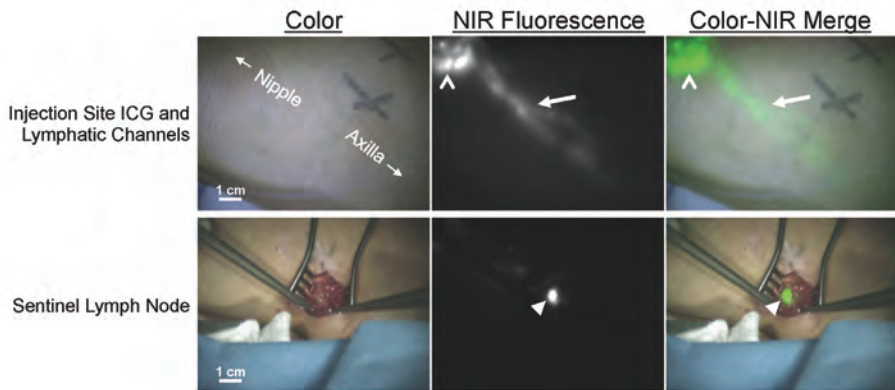


Figure 1 - NIR fluorescence imaging during sentinel lymph node mapping in a breast cancer patient: In the upper row, the periareolar injection site (open arrowhead) and an afferent lymphatic channel (arrow) are clearly visualized. In the lower row, identification of the SLN (arrowhead) with NIR fluorescence imaging is demonstrated 10 min after incision. Camera exposure times were 30 ms (top row) and 100 ms (bottom row). Scale bars represent 1 cm. Patent blue was omitted in this patient.

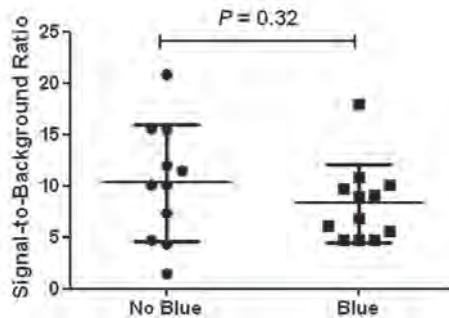


Figure 2 – Difference in brightness of SLNs between treatment groups: Signal-to-background ratios (mean \pm S.D.) of breast SLNs are plotted. The SBRs of blue and no blue patient groups were not significantly different.

To assess the need for radiotracers to localize the SLN(s), the surgeon did not use the handheld gamma probe during the first 15 min starting from skin incision. After the first 15 min, the use of the handheld gamma probe was necessary to locate the SLN(s) in 2 patients in the patent blue group and 4 patients in the no patent blue group. In all other patients, the handheld gamma probe was only used to verify the SLN for radioactivity *ex vivo* and to verify if any SLNs were missed. The average BMI of patients in whom the gamma probe was needed for SLN identification (33.1 ± 9.9) was significantly higher than in patients in whom the gamma probe could be omitted (24.4 ± 5.4 ; $P < 0.01$; Figure 3).

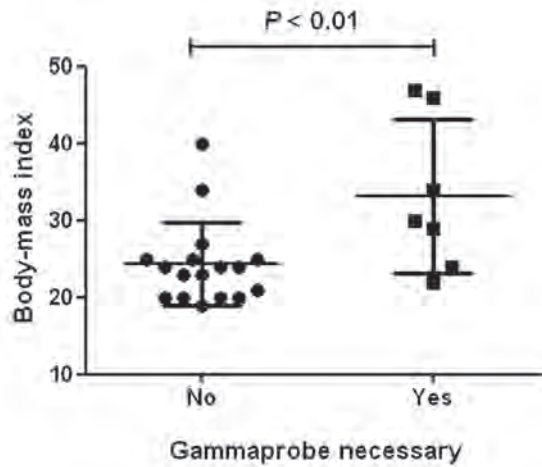


Figure 3 - Influence of body-mass index on the necessity to use the gammaprobe: The BMI of patients was plotted. The average BMI of patients in whom the gamma probe was needed for SLN identification (33.1 ± 9.9) was significantly higher than in patients in whom the gamma probe could be omitted (24.4 ± 5.4) ($P < 0.01$).

DISCUSSION

NIR fluorescence imaging has been extensively described as a tool for the SLN procedure in various types of cancer. In previous work, we demonstrated that a dose of $500 \mu\text{M}$ of ICG, without premixing with human serum albumin, was optimal to perform NIR fluorescence SLN mapping in breast cancer 18,19. In the current randomized clinical trial, the added value of patent blue staining, when used in combination with NIR fluorescence, was assessed in breast cancer patients undergoing the SLN procedure. Regarding time to identify the SLN, no significant difference between the 2 treatment groups was observed. In one patient in the no patent blue group, the SLN mapping lasted 67 min. A possible explanation for this relatively long time to locate the SLN could be that this patient was treated with neoadjuvant chemotherapy (NAC). It has been proposed that NAC alters the lymphatic drainage network, thereby possibly hampering the accuracy of the SLN procedure.²⁰ This could possibly be an explanation for the difficult identification of the SLN in one of our patients. However, in the current study, 2 more patients were treated with NAC and in those patients time between skin incision and SLN identification was in concordance with the average time between skin incision and SLN identification that was observed in all other patients (approximately 13 min).

Table 2 – SLN Identification Results

Characteristic	Total (N = 24)		Patent Blue (N = 12)		No Patent Blue (N = 12)		P
	N	%	N	%	N	%	
Number of SLNs Identified	37		19		18		
Number of SLNs Identified per Patient							0.54
- No SLN	1	4	0	0	1	8	
- One SLN	12	50	7	58	5	42	
- Two SLNs	9	38	4	33	5	42	
- Three SLNs	1	4	1	8	0	0	
- Four SLNs	1	4	0	0	1	8	
Average Number of SLNs Identified (SD)	1.5 ± 0.8		1.6 ± 0.7		1.5 ± 1.0		0.81
Method of Detection							
- Radioactive	35	95	17	89	18	100	
- Blue	16	84	16	84	0	0	
- Fluorescent	37	100	19	100	18	100	
Signal-to-Background Ratio	9.2 ± 4.8		8.3 ± 3.8		10.3 ± 5.7		0.32
Percutaneous Lymph Drainage Visualization							0.84
- Yes	12	50	6	50	6	50	
- Partially	7	29	4	33	3	25	
- No	5	21	2	17	3	25	
Average Time between Injection and Skin Incision (min, SD)	14.8 ± 3.3		15.2 ± 3.0		13.8 ± 3.9		0.17
Average Time between Skin Incision and SLN Resection (min, SD)	12.2 ± 7.9		12.4 ± 7.7		18.1 ± 18.9		0.35
Histology sentinel lymph node							0.10
- Negative	16	67	6	50	10	83	
- Isolated Tumor Cells	4	17	4	33	0	0	
- Micrometastases	2	8	0	0	2	17	
- Macrometastases	2	8	2	17	0	0	
Axillary Lymph Node Dissection							0.14
- No	22	92	10	83	12	100	
- Yes	2	8	2	17	0	0	

A meta-analysis of studies that examined the SLN procedure in patients treated with NAC included 1273 patients and reported an identification rate of 90% and a false-negative rate of 12%²¹; additionally, a more recent meta-analysis reported similar results.²² These results are not significantly different from meta-analyses of SLN biopsy in patients who are naïve to chemotherapy.²³ Nonetheless, results of SLN biopsy after NAC remain conflicting. The prospective multicenter German SENTINA trial is currently accruing patients to evaluate the accuracy of the SLN procedure after NAC.

Comparing the patent blue and no patent blue patient groups, brightness of the SLNs was higher in the no patent blue group (difference in SBR is 2.0); however, this difference was not significant. Furthermore, in the patent blue group, only 84% of NIR fluorescent SLNs were stained blue, which is in concordance with previous studies.^{18,19} These results indicate that NIR fluorescence using ICG can replace blue dye staining, which would have several advantages. First, the use of blue dyes stains the surgical field in an unnatural color that persists over the course of several months after surgery. Second, blue dyes cannot be visualized when covered by overlying tissue, while ICG can be detected through millimeters to a centimeter of overlying tissue. Third, in many cases, ICG can be seen percutaneously, which allows lymphatic mapping before surgery, which possibly decreases time to identify the SLN.

An obvious next step in the optimization of the SLN procedure would be to evaluate the need for radiotracers. Although radiotracers have superior tissue penetration, they expose caregivers and patients to ionizing radiation and they can only be detected using a gamma probe, which does not provide the surgeon with visual information. Furthermore, the time window for SLN identification is limited due to the short half-life (6 hours) of ^{99m}Tc. To explore the necessity of intraoperative radiotracers in addition to NIR fluorescence, the surgeon was not allowed to use the gamma probe during the first 15 min of the surgery. In 6 of 24 patients (25%), the surgeon could not identify the SLN within the first 15 min and in one patient, no SLN could be detected at all. In the current study, average BMI of patients in whom the gamma probe was used for SLN identification was significantly higher than in patients in whom the gamma probe was not necessary. These results are in concordance with previous studies that showed a significant correlation between time to identify the SLN and BMI^{24,25}. Furthermore, when only patent blue is used for SLN mapping, the SLN detection rate is significantly higher in patients with a BMI < 30 compared to patients with a BMI > 30²⁶. This suggests

that BMI plays an important role in selecting those patients whom are eligible for NIR fluorescence SLN mapping without the use of radiotracers. However, the current study was not powered to compare NIR fluorescence and radiocolloids and this has to be addressed in a future sufficiently powered clinical trial. Furthermore, since larger series will be required to determine the safety and SLN identification rate when radiotracers are omitted, the use of NIR fluorescence imaging using ICG as a lymphatic tracer is at present particularly attractive to hospitals unable to work with radioactive isotopes.

Another approach within the field of SLN mapping is combining fluorescence and radioactivity in one lymphatic tracer by simply premixing ICG and ^{99m}Tc -NanoColl (complex: ICG- ^{99m}Tc -NanoColl) which has been performed in prostate cancer patients.¹⁷ Using this multimodal tracer injected by the nuclear physician before surgery, time of surgery will probably be shortened because no dye injection and massage is needed in the surgical theatre. A clinical trial in breast cancer patients using this hybrid multimodal radiocolloid is currently ongoing in our center.

In conclusion, this randomized trial showed no advantage of using patent blue for the SLN procedure in breast cancer when NIR fluorescence and radiotracers are used. Combining these results with previous work, a dose of 500 μM ICG injected in a total of 1.6 ml is recommended for NIR fluorescence SLN mapping in breast cancer patients and patent blue can be omitted.

REFERENCES

1. Cox CE, Pendas S, Cox JM et al. Guidelines for sentinel node biopsy and lymphatic mapping of patients with breast cancer. *Ann Surg* 1998; 227:645-651.
2. Goyal A, Newcombe RG, Chhabra A et al. Factors affecting failed localisation and false-negative rates of sentinel node biopsy in breast cancer--results of the ALMANAC validation phase. *Breast Cancer Res Treat* 2006; 99:203-208.
3. Krag DN, Anderson SJ, Julian TB et al. Technical outcomes of sentinel-lymph-node resection and conventional axillary-lymph-node dissection in patients with clinically node-negative breast cancer: results from the NSABP B-32 randomised phase III trial. *Lancet Oncol* 2007; 8:881-888.
4. Zavagno G, De Salvo GL, Scalco G et al. A Randomized clinical trial on sentinel lymph node biopsy versus axillary lymph node dissection in breast cancer: results of the Sentinella/GIVOM trial. *Ann Surg* 2008; 247:207-213.
5. Straver ME, Meijnen P, van Tienhoven G et al. Sentinel Node Identification Rate and Nodal Involvement in the EORTC 10981-22023 AMAROS Trial. *Ann Surg Oncol* 2010; 17:1854-61.
6. Sonoo H, Noguchi S. Results of questionnaire survey on breast cancer surgery in Japan 2004-2006. *Breast Cancer* 2008; 15:3-4.
7. Davis KG, Schriver JP. Prevalence of teaching sentinel lymph node biopsy for breast cancer in general surgery residency programs. *Curr Surg* 2002; 59:420-422.
8. Keshtgar M, Aresti N, Macneil F. Establishing axillary Sentinel Lymph Node Biopsy (SLNB) for early breast cancer in the United Kingdom: a survey of the national training program. *Eur J Surg Oncol* 2010; 36:393-398.
9. Quan ML, Hodgson N, Lovrics P et al. National adoption of sentinel node biopsy for breast cancer: lessons learned from the Canadian experience. *Breast J* 2008; 14:421-427.
10. Kitai T, Inomoto T, Miwa M et al. Fluorescence navigation with indocyanine green for detecting sentinel lymph nodes in breast cancer. *Breast Cancer* 2005; 12:211-215.
11. Murawa D, Hirche C, Dresel S et al. Sentinel lymph node biopsy in breast cancer guided by indocyanine green fluorescence. *Br J Surg* 2009; 96:1289-1294.
12. Tagaya N, Yamazaki R, Nakagawa A et al. Intraoperative identification of sentinel lymph nodes by near-infrared fluorescence imaging in patients with breast cancer. *Am J Surg* 2008; 195:850-853.
13. Hirche C, Murawa D, Mohr Z et al. ICG fluorescence-guided sentinel node biopsy for axillary nodal staging in breast cancer. *Breast Cancer Res Treat* 2010; 121:373-8.
14. Hojo T, Nagao T, Kikuyama M et al. Evaluation of sentinel node biopsy by combined fluorescent and dye method and lymph flow for breast cancer. *Breast* 2010; 19:210-3.
15. Troyan SL, Kianzad V, Gibbs-Strauss SL et al. The FLARE intraoperative near-infrared fluorescence imaging system: a first-in-human clinical trial in breast cancer sentinel lymph node mapping. *Ann Surg Oncol* 2009; 16:2943-2952.
16. Sevick-Muraca EM, Sharma R, Rasmussen JC et al. Imaging of lymph flow in breast cancer patients after microdose administration of a near-infrared fluorophore: feasibility study. *Radiology* 2008; 246:734-741.
17. van der Poel HG, Buckle T, Brouwer OR et al. Intraoperative Laparoscopic Fluorescence Guidance to the Sentinel Lymph Node in Prostate Cancer Patients: Clinical Proof of Concept of an Integrated Functional Imaging Approach Using a Multimodal Tracer. *Eur Urol* 2011.
18. Mieog JS, Troyan SL, Hutteman M et al. Toward Optimization of Imaging System and Lymphatic Tracer for Near-Infrared Fluorescent Sentinel Lymph Node Mapping in Breast Cancer. *Ann Surg Oncol* 2011.
19. Hutteman M, Mieog JS, van der Vorst JR et al. Randomized, double-blind comparison of indocyanine green with or without albumin premixing for near-infrared fluorescence imaging of sentinel lymph nodes in breast cancer patients. *Breast Cancer Res Treat* 2011; 127:163-170.
20. Kuerer HM, Hunt KK. The rationale for integration of lymphatic mapping and sentinel node biopsy in the management of breast cancer patients receiving neoadjuvant chemotherapy. *Semin Breast Dis* 2002; 5:80-87.
21. Xing Y, Foy M, Cox DD et al. Meta-analysis of sentinel lymph node biopsy after preoperative chemotherapy in patients with breast cancer. *Br J Surg* 2006; 93:539-546.

22. van Deurzen CH, Vriens BE, Tjan-Heijnen VC et al. Accuracy of sentinel node biopsy after neoadjuvant chemotherapy in breast cancer patients: a systematic review. *Eur J Cancer* 2009; 45:3124-3130.
23. Fraile M, Rull M, Julian FJ et al. Sentinel node biopsy as a practical alternative to axillary lymph node dissection in breast cancer patients: an approach to its validity. *Ann Oncol* 2000; 11:701-705.
24. Aliakbarian M, Memar B, Jangjoo A et al. Factors influencing the time of sentinel node visualization in breast cancer patients using intradermal injection of the radiotracer. *Am J Surg* 2011; 202:199-202.
25. Pritsivelis C, Garcia Mendonca CA, Pinheiro Pessoa MC et al. Failure predictors of the sentinel lymph node in patients with breast cancer using Tc-99m sulfur colloid and periareolar injection. *Q J Nucl Med Mol Imaging* 2007; 51:189-193.
26. Nos C, Freneau P, Guilbert S et al. Sentinel lymph node detection for breast cancer: which patients are best suited for the patent blue dye only method of identification? *Ann Surg Oncol* 2001; 8:438-443.

Part III:

Clinical translation:
Solid tumor imaging

Chapter 11

Near-infrared fluorescence-guided resection of colorectal liver metastases

van der Vorst JR¹, Schaafsma BE¹, Hutteman M, Verbeek FP, Liefers GJ, Hartgrink HH, Smit VJ, Frangioni JV, van de Velde CJ, Vahrmeijer AL

¹Both authors contributed equally to this work and share first-authorship.

Cancer. 2013 Sep 15;119(18):3411-8

ABSTRACT

Background

The fundamental principle of oncologic surgery is the complete resection of malignant cells. However, small tumors are often difficult to find during surgery using conventional techniques. Our objectives were to determine if optical imaging, using a contrast agent already approved for other indications, could improve hepatic metastasectomy with curative intent, to optimize dose and timing, and to determine the mechanism of contrast agent accumulation.

Material and Methods

We exploited the high tissue penetration of near-infrared (NIR) light using the FLARE™ image-guided surgery system and the NIR fluorophore indocyanine green (ICG) in a clinical trial of 40 patients undergoing hepatic resection for colorectal cancer metastases.

Results

A total of 71 superficially located (< 6.2 mm beneath the liver capsule) colorectal liver metastases were identified and resected using NIR fluorescence imaging. Median tumor-to-liver ratio (TLR) was 7.0 (range 1.9-18.7) and no significant differences between time-points or doses were found. ICG fluorescence was seen as a rim around the tumor, which we show to be entrapment around CK7-positive hepatocytes compressed by the tumor. Importantly, in 5 of 40 patients (12.5%, 95% CI: 5.0-26.6), additional small and superficially located lesions were detected using NIR fluorescence, and were otherwise undetectable by preoperative computed tomography (CT), intraoperative ultrasound (IOUS), visual inspection, and palpation.

Conclusion

We conclude that NIR fluorescence imaging, even when utilizing a non-targeted, clinically available NIR fluorophore, is complementary to conventional imaging and able to identify missed lesions by other modalities.

INTRODUCTION

Prognosis and survival of colorectal cancer patients depends primarily on the occurrence of distant metastases, which occur most frequently in the liver.¹ A resection with curative intent can offer patients with colorectal liver metastases a 5-year survival rate of 36% to 60%.²⁻⁵ Despite improvements in preoperative imaging modalities, surgical techniques, and chemotherapy regimens, intrahepatic recurrence rates vary from 11% to 37.5% after hepatic metastasectomy, and 65% to 85% of these recurrences appear within 2 years after resection.^{2,6-9} A possible explanation for this high intrahepatic recurrence rate is that some hepatic metastases are already present at the time of liver resection, but were undetected by the technology typically available in the community setting, namely, preoperative imaging, intraoperative ultrasound (IOUS), and inspection/palpation by the surgeon. For example, it is known that small and superficially located liver metastases are difficult to identify using available imaging modalities such as preoperative computed tomography (CT), MRI, and IOUS.¹⁰⁻¹²

Near-infrared (NIR) fluorescence imaging using indocyanine green (ICG) is a promising technique to intraoperatively visualize the contrast between liver metastases and normal liver tissue in real time.¹³⁻¹⁵ This type of optical imaging is relatively inexpensive and is quickly becoming widely available. Unlike visible light, which is used to excite fluorophores such as fluorescein, NIR light can penetrate several millimeters into tissue and through blood. ICG is excreted exclusively into the bile after intravenous injection; it has been hypothesized that colorectal liver metastases can be visualized due to passive accumulation of ICG caused by hampered biliary excretion, which results in a fluorescent rim around the metastases. However, the mechanism of ICG accumulation has not yet been explored.

Recently, Ishizawa et al.¹³ described the intraoperative detection of colorectal liver metastasis using NIR fluorescence imaging after intravenous injection of 0.5 mg/kg ICG, 1 to 14 days prior to surgery, as part of an ICG-retention liver function test. The dose and interval between ICG injection and surgery are key determinants of the remaining background fluorescence signal in the liver and the fluorescent rim surrounding the tumor. In a preclinical study in rats performed by our group, the influence of injection time prior to surgery and dose of ICG pertaining to the contrast between the fluorescent rim around the hepatic metastases and normal liver tissue (tumor-to-liver ratio) was examined.¹⁶ In this preclinical study, the highest tumor-to-liver ratio (TLR) was reached when ICG was injected 72 h prior

to surgery. Furthermore, this study demonstrated that even small liver metastases (≈ 1 mm) could be identified using NIR fluorescence. In the current study, these preclinical results were translated to a clinical trial in patients with colorectal liver metastases in order to optimize intraoperative identification of liver metastases using ICG. Furthermore, the mechanism of ICG accumulation in the transition area between tumor and normal liver tissue was investigated, and the value added by NIR fluorescence imaging was determined.

MATERIAL AND METHODS

Preparation and Administration of Indocyanine Green

ICG (25 mg vials) was purchased from Pulsion Medical Systems (Munich, Germany) and resuspended in 10 cc of sterile water for injection to yield a 2.5-mg/ml (3.2 mM) stock solution. Of this stock solution 4 or 8 mL, corresponding to doses of 10 or 20 mg, were administered intravenously.

Clinical Trial

The study was approved by the Local Medical Ethics Committee of the Leiden University Medical Center and was performed in accordance with the ethical standards of the Helsinki Declaration of 1975. All patients were evaluated for hepatic treatment by a multidisciplinary specialized liver unit (Surgeon, Oncologist, Interventional radiologist and an experienced abdominal radiologist). From 2010 to 2012, a total of 40 patients with suspected colorectal liver metastases, based on a preoperative 4-phase CT-scan (Toshiba Aquilion 64, Tokyo, Japan) of the thorax and abdomen with a slice thickness of 5 mm, who were planned to undergo curative intended liver resection were included. All patients provided informed consent. Exclusion criteria were pregnancy, lactation or an allergy to iodine, shellfish or indocyanine green.

Patients received 10 mg or 20 mg of ICG diluted in a total volume of 4 mL and 8 mL, respectively, as an intravenous bolus at 24 or 48 h prior to surgery on an inpatient base. This resulted in 4 groups of 4 patients per group (N = 16 patients). Subsequently, 24 patients were included at the optimal combination of ICG dose and injection time. After mobilization of the liver, first visual inspection, palpation, and IOUS were performed to determine the number and location of the liver metastases. To evaluate the additional benefit of NIR fluorescence imaging, all

liver segments were imaged using the Mini-FLARE™ imaging system, which has been described previously.¹⁷ Directly following liver resection, resection specimens were delivered to the Department of Pathology, where the specimens were sliced into 5 to 7 mm thick slices and examined by an experienced pathologist for NIR fluorescence using the Mini-FLARE™ imaging system.

Fluorescence Microscopy

Based on macroscopic evaluation and *ex vivo* fluorescence imaging, tissue was acquired from the transition zone between the tumor and the normal liver from multiple patients. Excised tissue was snap-frozen and sectioned at 5 μm for fluorescence and regular microscopy. Sections were measured for fluorescence using the Nuance multispectral imager (CRi, Woburn, MA) mounted on a Leica DM IRE2 inverted microscope (Leica, Wetzlar, Germany). Subsequently, these slides were stained with hematoxylin and eosin. Consecutive slides were stained for the presence of CD31 (Dako, M0823), CK7 (Dako, M7018) and CD68 (Dako, M0814) to correlate fluorescence to blood vessels, bile ducts and macrophages, respectively. White light images were subsequently merged with fluorescence images.

Statistical Analysis

For statistical analysis, SPSS statistical software package (Version 17.0, Chicago, IL) was used. Tumor-to-liver (TLR) signal, rim fluorescence, and background fluorescence were reported as median and range. Tumor size was reported as mean with standard deviation. To test differences between groups, the Kruskal-Wallis one-way analysis of variance test was used to test for differences between time and dose groups. Statistical tests were 2-tailed and $P < 0.05$ was considered significant. 95% binomial confidence intervals of the percentage of patients in whom additional metastases were identified were calculated using the Adjusted Wald Method by GraphPad QuickCalcs (GraphPad Software, La Jolla, CA).

RESULTS

Study Subjects:

Patient and tumor characteristics of the 40 patients are listed in Table 1. None of the patients suffered from hepatitis or liver cirrhosis, and 22 patients received neoadjuvant chemotherapy. In 7 patients, no liver resection was performed due to invasion of tumor into the portal vein (N = 3), the presence of additional irresectable liver metastases (N = 2), or the appearance of lymph node metastases (N = 2). Nevertheless, these patients were included for TLR, rim fluorescence, and background fluorescence analysis.

Table 1 – Study subject characteristics (N = 40).

Characteristic	Median [Range] or (%)
Age	63 [45 - 77]
BMI	25 [19 - 38]
Sex	Male: 21 (52.5%) Female: 19 (47.5%)
Primary tumor location	
- Colon	21 (52.5%)
- Sigmoid	5 (12.5%)
- Rectum	13 (32.5%)
- Anus	1 (2.5%)
Neo-adjuvant chemotherapy	22 (55.0%)
Type of resection	
- Hemihepatectomy	6 (15.0%)
- Metastasectomy / segmentectomy	19 (47.5%)
- Metastasectomy / segmentectomy + RFA	7 (17.5%)
- RFA only	1 (2.5%)
- No resection	7 (17.5%)

Abbreviations: BMI: body mass index; RFA: radiofrequency ablation.

Optimization of ICG Dose and Injection Timing (N=16 patients)

To determine the effect of ICG dosage and post injection imaging time, patients were allocated to 2 dose groups and imaged at 2 time-points after ICG administration, resulting in 4 groups containing 4 patients per group. Fluorescence intensity of the rim around the liver metastases was significantly higher than the fluorescent signal in the liver ($P < 0.001$). Median tumor-to-liver ratio (TLR) in all 16 patients was 7.3 (range: 1.9-18.7). Median TLRs were 5.0 (range: 2.2-15.4), 6.7 (range: 2.7-9.2), 10.5

(range: 1.9- 18.7), 8.0 (range: 7.0-9.3) for the 10 mg at 24 hr, 20 mg at 24 hr, 10 mg at 48 hr and 20 mg at 48 hr patient group, respectively. Median rim fluorescence (normalized pixel value) was 530.1 (range: 257.89-823.0), 938.4 (range: 902.3-1239.1), 648.6 (range: 137.1-1929.36), 608.5 (range: 507.6-688.1) for the 10 mg at 24 hr, 20 mg at 24 hr, 10 mg at 48 hr and 20 mg at 48 hr patient group, respectively. Median background fluorescence (normalized pixel value) was 98.3 (range: 53.6-127.6), 209.1 (range: 96.1-356.5), 64.6 (range: 53.4-112.4), and 77.4 (range: 67.5-96.2) for the 10 mg at 24 hr, 20 mg at 24 hr, 10 mg at 48 hr, and 20 mg at 48 hr patient group, respectively. Using the independent samples Kruskal-Wallis Test, no significant differences in signal-to-background ratios ($P = 0.70$), rim fluorescence ($P = 0.67$) and background fluorescence were observed ($P = 0.08$). Since no differences in TLRs were observed between the various groups, the optimal dose was determined by clinical and logistical preferences (the minimal dose of 10 mg of ICG administered 24 h prior to surgery).

Intraoperative Detection of Colorectal Liver Metastases (N=40):

Subsequently, 24 more patients were included to assess the added value of NIR fluorescence imaging during resection of colorectal liver metastases. Results of liver metastases detection are summarized in Table 2. Using a combination of preoperative CT scanning, IOUS, visual inspection, and/or palpation, a total of 100 lesions were identified as suspected colorectal liver metastases. After resection, 3 of these lesions were histologically proven to be benign, for a net detection of 97 metastatic lesions by conventional imaging. NIR fluorescence imaging (Figure 1) detected a total of 71 lesions proven histologically to be metastases, all of which were ≤ 6.2 mm from the surface of the liver capsule. However, only 66 of the 71 lesions identified using NIR fluorescence overlapped with conventional imaging (Table 2 and Figure 2). Most important, in 5 patients (12.5 %, 95% CI 5.0 – 26.6), superficially located, otherwise occult liver metastases were detected using NIR fluorescence only, but not by conventional imaging (i.e., preoperative CT, IOUS, intraoperative visualization, and intraoperative palpation) (Figure 1). Sensitivity of the preoperative CT scanning, intraoperative visual inspection/palpation in combination with IOUS, and NIR fluorescence imaging were 75%, 95% and 73%, respectively. In 3 patients, an additional wedge resection was performed to resect these metastases, and in 2 patients the preoperatively planned metastasectomy was extended to resect the additional metastases. In these 5 patients, the total number of metastases (including the occult metastases detected only by NIR

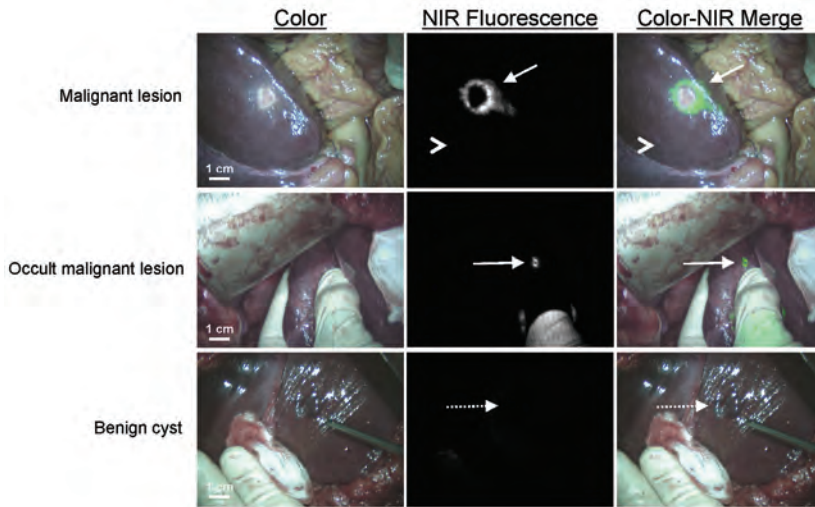


Figure 1 – NIR fluorescence imaging of colorectal liver metastases: A colorectal liver metastasis (arrow) is clearly identified by a rim around the tumor *in vivo* (top row), 24 h after injection of 10-mg ICG. Normal liver tissue (arrowhead) shows minimal background uptake of ICG. In 5 patients, small, superficial, otherwise occult metastases (middle row, arrow) were identified by NIR fluorescence imaging. Benign lesions (bottom row, dashed arrow) could be differentiated from malignant lesions by a lack of a fluorescent rim around the lesion.

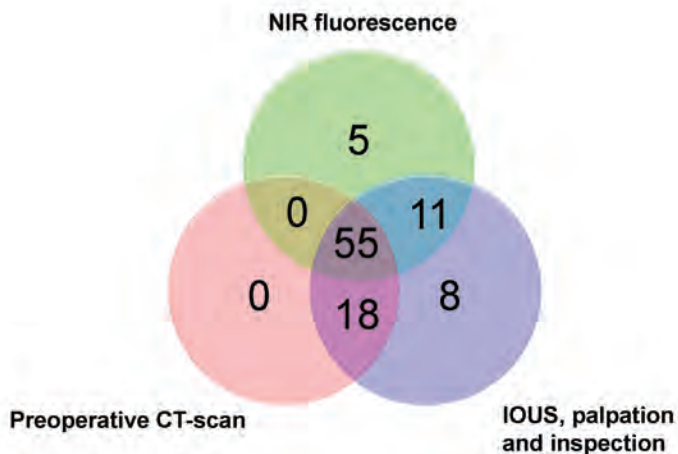


Figure 2 – Methods of detection of colorectal liver metastases: Venn diagram showing how the 97 hepatic metastases were detected as a function of each modality alone or in combination.

fluorescence) were 4, 3, 3, 2 and 2. After resection, these lesions were found to be 2, 3, 4, 6, and 9 mm in diameter. Histopathological examination confirmed these lesions to be colorectal liver metastases. One of these 5 occult lesions, which was 9

Table 2 – Methods of detection.

Modality	Number of hepatic metastases identified* (%)	Number of patients	Size of metastases (mm)
Preoperative CT-scan	73 (75)	39	29.9 ± 19.1
IOUS, palpation and inspection	92 (95)	40	26.3 ± 19.5
NIR fluorescence	71 (73)	37	29.0 ± 29.8
Preoperative CT-scan, IOUS, inspection palpation and/or NIR fluorescence	97 (100)	40	24.5 ± 19.7

* Liver metastases were confirmed by histology or in the case of nonresected lesions by clinical appearance, IOUS, and CT.

mm in diameter, was labeled as a complicated cyst based on IOUS and CT, whereas the clear NIR fluorescent ring around the lesion suggested that it was a liver metastasis. Twenty-six liver metastases (27%) identified by conventional imaging could not be detected using NIR fluorescence and all were deeper than 8 mm from the liver surface. All fluorescent liver metastases presented a fluorescent rim around the tumor. The overall (N=40) median TLR was 7.0 (range, 1.9 – 18.7). The use of neoadjuvant chemotherapy did not significantly influence the TLR (7.5 ± 5.1 vs. 7.1 ± 2.9 , $P = 0.77$). In addition to liver metastases, a total of 8 hemangiomas, 13 cysts, and 4 bile duct hamartomas were identified in 13 patients. These hemangiomas, cysts, and bile duct hamartomas did not show a NIR fluorescent signal or rim (Figure 1). Thus, NIR fluorescence imaging might help differentiate malignant liver lesions from some benign lesions. As might be expected based on the mechanism of ICG contrast (described below), extrahepatic tumor-positive lymph nodes were not fluorescent (data not shown).

Ex Vivo Detection of Colorectal Liver Metastases

Liver resection specimens were sliced in 5 to 7-mm slices and subsequently the slices were imaged with the Mini-FLARE imaging system. In all patients for whom a liver resection was performed (N = 33), *ex vivo* NIR fluorescence imaging was performed. All known metastases were identified *ex vivo* by a clear fluorescent ring around the lesion.

Immunohistochemistry and Fluorescence Microscopy

Fluorescence signal was located in liver tissue directly surrounding the tumor and was located both intracellularly and extracellularly (Figure 3B). In liver tissue,

in the area near the tumor, compressed hepatocytes and increased ductular transformation, periportal fibrosis, and presence of Kupffer cells were observed. Immunohistochemical analysis showed a close relation between fluorescence and CK7 staining (Figure 3C). CK7 is expressed by immature hepatocytes in the areas of ductular transformation. No relation was found between fluorescence and the presence of Kupffer cells (CD68) and blood vessels (CD31).

DISCUSSION

The main objective of this study was to evaluate the potential of intra-operative NIR fluorescence imaging to improve oncologic resection of colorectal metastases to liver. As confirmed by pathological analysis, all superficially located (< 6.2 mm beneath the liver surface) metastases were identified using NIR fluorescence. Additionally, in 5 patients, occult metastases were detected using NIR fluorescence only and were missed by conventional detection methods (Figure 2). Moreover, this study provides increased understanding of the mechanism responsible for the rim fluorescence and increases the understanding of the effect of different administration time-points and doses of ICG on tumor detection. This is crucial for the implementation of this technique and interpretation of results in future studies.

An important recent study using visible wavelength optical imaging showed real-time identification of ovarian cancer metastases.¹⁸ Because of the relatively low tissue penetration of visible light, this technology is limited to tumors already on the surface of anatomical structures. Even when using NIR fluorescence imaging, however, penetration depth is still a major issue. The penetration depth of NIR fluorescence light is highly dependent on the optical properties, i.e., absorption and scatter, of the tissue being imaged. Liver is highly absorbing compared to other tissues, such as breast and subcutaneous tissue of axilla, resulting in higher attenuation (i.e., lower signal).¹⁹ In the current study, 26 metastases that were located 8 mm or more beneath the liver capsule could not be identified using NIR fluorescence. Preoperative CT scanning and IOUS are more appropriate for deeper lesions and did successfully identify these 26 lesions. However, superficially located, small occult metastases are known to be difficult to detect using IOUS, inspection, and palpation.^{10,11} Although IOUS is still required to identify deep (≥ 6 mm) metastases in the liver, our results suggest that NIR fluorescence imaging is complementary and helps to find small, superficially located liver metastases.

The use of NIR fluorescence imaging to detect liver metastases is dependent on the clearance of ICG by the liver. To optimize the use of this technique, it is necessary to examine the influence of ICG dose and timing of ICG administration prior to surgery. In the current study, differences in dose and timing did not significantly influence the TLR. A previously performed study in rats by our group showed an optimal TLR in the group where ICG was administered at 72 h prior to surgery.¹⁶ In the current clinical study, liver signal at 24 to 48 h postinjection of 10-mg ICG was comparable to preinjection baseline level which we measured in a previous study in patients undergoing a pancreatoduodenectomy, eliminating the need to test other time-points.²⁰ Therefore, NIR fluorescence imaging at 72 h after ICG administration was not performed. Other clinical work performed by Ishizawa et al. suggested an interval between administration of ICG and liver surgery of at least 2 days to lower background fluorescence and to obtain adequate TLRs.¹³

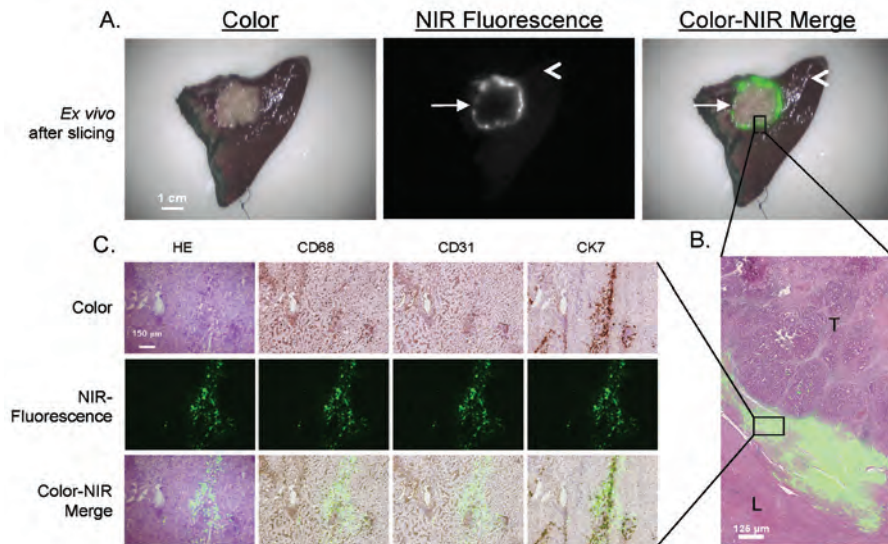


Figure 3 – Pathologic examination of the tumor border:

- A. After resection and slicing of the same specimen, the rim around the tumor can be visualized *ex vivo*.
- B. Shown are hematoxylin and eosin (HE) staining with a pseudo-colored green NIR fluorescence overlay of a 20 μm tissue section of a colorectal liver metastasis using a 5 X objective. The fluorescent rim in stromal tissue appears in the transition zone between tumor (T) and normal liver tissue (L).
- C. Shown is liver tissue located in the fluorescent rim of a colorectal liver metastasis. Consecutive frozen sections (5 μm) are stained with hematoxylin and eosin (HE) and for CD68, CD31, and CK7. Microscopic color images (left column), NIR fluorescence images (middle column), and a pseudo-colored green merge (right column) were obtained (100X zoom). The NIR fluorescence signal is mainly located intracellularly and shows a high correlation with CK7 staining.

However, in latter study a substantially higher dose of ICG (0.5 mg/kg; \approx 35 mg per subject) was administered. In the current study, a relatively low dose of ICG (0.13-0.26 mg/kg) was used and it was therefore possible to reach acceptable TLRs and sufficiently low background liver fluorescence at 24 h after administration of 10 mg ICG, which is safe and desirable from a logistical point of view.

Because no clinical data on lesion detection rates and standard deviation of the measurements were available prior to the study, a formal sample size calculation was not possible. However, we have provided 95% coincidence intervals for the 12.5% of patients in which additional lesions were detected only by NIR fluorescence (95% CI: 5.0-26.6). Well-powered future studies can now be designed based on these data.

The detection rate of additional occult liver metastases during surgery is strongly dependent on the preoperative and intraoperative imaging modalities used. In the current study preoperative CT and IOUS were acquired to assess the extent of the disease. However, multiple novel imaging instruments are available for improved preoperative and intraoperative assessment of occult liver metastases. MRI benefits from increased soft tissue contrast and the availability of hepatocyte-specific contrast agents, which yields a higher sensitivity compared to CT for the detection of subcentimeter liver metastases and in case of neoadjuvant chemotherapy^{21,22}. Moreover, FDG-PET or PET-CT has been shown to be of additional value to detect extrahepatic disease²¹. However, the sensitivity of detection of occult liver metastases using PET is not higher than CT²¹. Despite the possible higher detection rate using MRI, it can be expected that lesions missed during preoperative imaging, can be detected during IOUS or palpation, which will therefore not significantly alter the finding of the current study. Next to preoperative imaging modalities, novel modalities for intraoperative assessment of occult liver metastases, such as contrast enhanced IOUS, have been introduced to improve sensitivity^{23,24}. However, NIR fluorescence has been shown to add value when used in combination with contrast enhanced IOUS as well²³.

An important aspect of our study is that it can be readily translated to the community setting. First, it utilizes a contrast agent already FDA-approved for other indications. Second, multiple optical imaging systems are now available commercially and are comparable in size, cost, and upkeep to an IOUS instrument. And, finally, unlike PET, MRI, and other emerging imaging technologies that require significant infrastructure investment and high operational costs, cart-based optical imaging is potentially viable in any clinical setting.

Although the false-positive rate in the current study was zero, previous studies have reported that non-malignant lesions (large regenerative nodules and atypical hyperplastic nodules) display ICG uptake.^{13,14} The pattern of uptake appears to be important. In large regenerative nodules and atypical hyperplastic nodules, NIR fluorescence is seen throughout the tumor (not rim only). In the benign lesions (hemangiomas, cysts, and bile duct hamartomas) of our study, no fluorescence rim was seen. Clearly, larger clinical trials will be needed to determine the true false-positive rate and pattern of uptake of ICG as a function of benign lesion histology.

Using fluorescence microscopy, we observed intracellular accumulation of ICG in and around CK7-positive cells directly surrounding the tumor, and being compressed by it. The architecture of the liver parenchyma is often changed by the presence of hepatic metastases leading to compression of hepatic parenchyma, inflammatory infiltrate, ductular transformation, and increased presence of immature hepatocytes.²⁵⁻²⁷ It is known that immature hepatocytes often have impaired expression of their organic anion transporters, which are essential for the transport of many organic anions, including ICG.²⁸⁻³² For example, in the absence of multidrug resistance P-glycoprotein 2, the biliary excretion of ICG can be reduced by 90%.³³ Therefore, the pattern of rim fluorescence could be explained by the presence of immature hepatocytes in the liver tissue surrounding the tumor that have taken up ICG, but exhibit impaired biliary clearance.

As in other areas of surgery, the use of laparoscopy is expanding to liver surgery. Minor liver resections such as left lateral hepatectomies are being performed laparoscopically as standard-of-care in several centers.³⁴ NIR fluorescence may also be of great value in laparoscopic surgery because palpation of the liver is not possible and the surgeon can only rely on visual inspection, IOUS, and preoperative imaging. To implement NIR fluorescence in laparoscopic liver surgery, laparoscopic NIR fluorescence camera systems are currently being developed and tested.³⁵⁻³⁷

In conclusion, this study demonstrated identification of otherwise undetectable cancer metastases in 12.5% of patients and suggests that intraoperative NIR fluorescence imaging is complementary to conventional techniques for the detection of liver metastases from colorectal cancer and has great potential for laparoscopic procedures.

REFERENCES

1. Manfredi S, Lepage C, Hatem C et al. Epidemiology and management of liver metastases from colorectal cancer. *Ann Surg* 2006; 244:254-259.
2. Abdalla EK, Vauthey JN, Ellis LM et al. Recurrence and outcomes following hepatic resection, radiofrequency ablation, and combined resection/ablation for colorectal liver metastases. *Ann Surg* 2004; 239:818-825.
3. Choti MA, Sitzmann JV, Tiburi MF et al. Trends in long-term survival following liver resection for hepatic colorectal metastases. *Ann Surg* 2002; 235:759-766.
4. Pawlik TM, Izzo F, Cohen DS et al. Combined resection and radiofrequency ablation for advanced hepatic malignancies: results in 172 patients. *Ann Surg Oncol* 2003; 10:1059-1069.
5. Rees M, Tekkis PP, Welsh FK et al. Evaluation of long-term survival after hepatic resection for metastatic colorectal cancer: a multifactorial model of 929 patients. *Ann Surg* 2008; 247:125-135.
6. Wei AC, Greig PD, Grant D et al. Survival after hepatic resection for colorectal metastases: a 10-year experience. *Ann Surg Oncol* 2006; 13:668-676.
7. Pawlik TM, Scoggins CR, Zorzi D et al. Effect of surgical margin status on survival and site of recurrence after hepatic resection for colorectal metastases. *Ann Surg* 2005; 241:715-22, discussion.
8. Karanjia ND, Lordan JT, Fawcett WJ et al. Survival and recurrence after neo-adjuvant chemotherapy and liver resection for colorectal metastases: a ten year study. *Eur J Surg Oncol* 2009; 35:838-843.
9. Fong Y, Cohen AM, Fortner JG et al. Liver resection for colorectal metastases. *J Clin Oncol* 1997; 15:938-946.
10. Leen E, Ceccotti P, Moug SJ et al. Potential value of contrast-enhanced intraoperative ultrasonography during partial hepatectomy for metastases: an essential investigation before resection? *Ann Surg* 2006; 243:236-240.
11. Sahani DV, Kalva SP, Tanabe KK et al. Intraoperative US in patients undergoing surgery for liver neoplasms: comparison with MR imaging. *Radiology* 2004; 232:810-814.
12. Nomura K, Kadoya M, Ueda K et al. Detection of hepatic metastases from colorectal carcinoma: comparison of histopathologic features of anatomically resected liver with results of preoperative imaging. *J Clin Gastroenterol* 2007; 41:789-795.
13. Ishizawa T, Fukushima N, Shibahara J et al. Real-time identification of liver cancers by using indocyanine green fluorescent imaging. *Cancer* 2009; 115:2491-2504.
14. Gotoh K, Yamada T, Ishikawa O et al. A novel image-guided surgery of hepatocellular carcinoma by indocyanine green fluorescence imaging navigation. *J Surg Oncol* 2009; 100:75-79.
15. Verbeek FP, van der Vorst JR, Schaafsma BE et al. Image-guided hepatopancreatobiliary surgery using near-infrared fluorescent light. *J Hepatobiliary Pancreat Sci* 2012; 19:626-637.
16. van der Vorst JR, Hutteman M, Mieog JS et al. Near-Infrared Fluorescence Imaging of Liver Metastases in Rats using Indocyanine Green. *J Surg Res* 2011.
17. Mieog JS, Troyan SL, Hutteman M et al. Toward optimization of imaging system and lymphatic tracer for near-infrared fluorescent sentinel lymph node mapping in breast cancer. *Ann Surg Oncol* 2011; 18:2483-2491.
18. van Dam GM, Crane LM, Themelis G et al. Intraoperative tumor-specific fluorescence imaging in ovarian cancer by folate receptor-alpha targeting: first in-human results. *Nat Med* 2011; Sep 18;17(10):1315-9.
19. Stolik S, Delgado JA, Perez A et al. Measurement of the penetration depths of red and near infrared light in human "ex vivo" tissues. *J Photochem Photobiol B* 2000; 57:90-93.
20. Hutteman M, van der Vorst JR, Mieog JS et al. Near-Infrared Fluorescence Imaging in Patients Undergoing Pancreaticoduodenectomy. *Eur Surg Res* 2011; 47:90-97.
21. Frankel TL, Gian RK, Jarnagin WR. Preoperative imaging for hepatic resection of colorectal cancer metastasis. *J Gastrointest Oncol* 2012; 3:11-18.
22. van Kessel CS, Buckens CF, van den Bosch MA et al. Preoperative imaging of colorectal liver metastases after neoadjuvant chemotherapy: a meta-analysis. *Ann Surg Oncol* 2012; 19:2805-2813.
23. Uchiyama K, Ueno M, Ozawa S et al. Combined use of contrast-enhanced intraoperative ultrasonography and a fluorescence navigation system for identifying hepatic metastases. *World J Surg* 2010; 34:2953-2959.

24. Takahashi M, Hasegawa K, Arita J et al. Contrast-enhanced intraoperative ultrasonography using per-fluorobutane microbubbles for the enumeration of colorectal liver metastases. *Br J Surg* 2012; 99:1271-1277.
25. Irie T, Tsuchida Y, Terahata S et al. Rim enhancement in colorectal metastases at CT during infusion hepatic arteriography. Does it represent liver parenchyma or live tumor cell zone? *Acta Radiol* 1997; 38:416-421.
26. Marchal GJ, Pylyser K, Tshibwabwa-Tumba EA et al. Anechoic halo in solid liver tumors: sonographic, microangiographic, and histologic correlation. *Radiology* 1985; 156:479-483.
27. Vermeulen PB, Colpaert C, Salgado R et al. Liver metastases from colorectal adenocarcinomas grow in three patterns with different angiogenesis and desmoplasia. *J Pathol* 2001; 195:336-342.
28. Oshima H, Kon J, Ooe H et al. Functional expression of organic anion transporters in hepatic organoids reconstructed by rat small hepatocytes. *J Cell Biochem* 2008; 104:68-81.
29. de Graaf W, Hausler S, Heger M et al. Transporters involved in the hepatic uptake of (99m)Tc-mebrofenin and indocyanine green. *J Hepatol* 2011; 54:738-745.
30. Cui Y, Konig J, Leier I et al. Hepatic uptake of bilirubin and its conjugates by the human organic anion transporter SLC21A6. *J Biol Chem* 2001; 276:9626-9630.
31. Yang YM, Tian XD, Zhuang Y et al. Risk factors of pancreatic leakage after pancreaticoduodenectomy. *World J Gastroenterol* 2005; 11:2456-2461.
32. Ros JE, Roskams TA, Geuken M et al. ATP binding cassette transporter gene expression in rat liver progenitor cells. *Gut* 2003; 52:1060-1067.
33. Huang L, Vore M. Multidrug resistance p-glycoprotein 2 is essential for the biliary excretion of indocyanine green. *Drug Metab Dispos* 2001; 29:634-637.
34. Chang S, Laurent A, Tayar C et al. Laparoscopy as a routine approach for left lateral sectionectomy. *Br J Surg* 2007; 94:58-63.
35. Matsui A, Tanaka E, Choi HS et al. Real-time intra-operative near-infrared fluorescence identification of the extrahepatic bile ducts using clinically available contrast agents. *Surgery* 2010; 148:87-95.
36. van der Poel HG, Buckle T, Brouwer OR et al. Intraoperative Laparoscopic Fluorescence Guidance to the Sentinel Lymph Node in Prostate Cancer Patients: Clinical Proof of Concept of an Integrated Functional Imaging Approach Using a Multimodal Tracer. *Eur Urol* 2011; 60:826-33.
37. Ishizawa T, Bandai Y, Kokudo N. Fluorescent cholangiography using indocyanine green for laparoscopic cholecystectomy: an initial experience. *Arch Surg* 2009; 144:381-382.

Chapter 12

Near-infrared fluorescence imaging in patients undergoing pancreaticoduodenectomy

Hutteman M¹, van der Vorst JR¹, Mieog JS, Bonsing BA, Hartgrink HH, Kuppen PJ,
Lowik CW, Frangioni JV, van de Velde CJ, Vahrmeijer AL

¹Both authors contributed equally to this work and share first authorship.

Eur Surg Res. 2011;47(2):90-7

ABSTRACT

Background

Intraoperative visualization of pancreatic tumors has the potential to improve radical resection rates. Intraoperative visualization of the common bile duct and bile duct anastomoses could be of added value. In this study, we explored the use of indocyanine green (ICG) for these applications, and attempted to optimize injection timing and dose.

Material and Methods

Eight patients undergoing a pancreaticoduodenectomy were injected intravenously with 5 or 10 mg ICG. During and after injection, the pancreas, tumor, common bile duct, and surrounding organs were imaged in real-time using the Mini-FLARE™ near-infrared (NIR) imaging system.

Results

No clear tumor-to-pancreas contrast was observed, except for incidental contrast in one patient. The common bile duct was clearly visualized using NIR fluorescence, within 10 minutes after injection, with a maximal contrast between 30 to 90 min after injection. Patency of biliary anastomoses could be visualized due to biliary excretion of ICG.

Conclusion

No useful tumor demarcation could be visualized in pancreatic cancer patients after intravenous injection of ICG. However, the common bile duct and biliary anastomoses were clearly visualized during the observation period. Therefore, these imaging strategies could be beneficial during biliary surgery in cases where the surgical anatomy is aberrant or difficult to identify.

INTRODUCTION

Pancreatic cancer is the fourth leading cause of cancer-related mortality in the United States, with an incidence of approximately 38,000 cases and an estimated 34,000 deaths. The overall 5-year survival rate is very low (< 5%).¹ Approximately 10% to 15% of patients are eligible for surgical resection, which is presently the only potentially curative treatment option. Even after curative resection, the reported 5-year survival rates are disappointing and vary from 10% to 17%.²⁻⁵ Several factors, such as tumor size, lymph node status, tumor grade, and blood vessel invasion are correlated with prognosis. Involvement of tumor margins is an important prognostic factor, as reported survival for R0 (radical) resections (20.3 months) is twice that of R1 resections (10.3 months).⁶ For preoperative staging and determination of resectability, the imaging procedure of choice is a multiphase, multidetector helical computed tomography (CT) with intravenous administration of a contrast agent combined with an endoscopic ultrasonography.⁷

During pancreatic surgery, assessment of the extent of the pancreatic tumor is made based on visual inspection and palpation, sometimes in conjunction with intraoperative ultrasonography.^{8,9} Intraoperative tumor identification remains challenging, partly because the surrounding pancreatic tissue is frequently inflamed. Local recurrence rates of 72% to 86% are reported¹⁰⁻¹², which in part could be caused by inadequate intraoperative evaluation of the location and extent of the tumor.

Near-infrared (NIR) fluorescence imaging is a promising technique to facilitate intraoperative, real-time, visual information.¹³⁻¹⁵ In order to detect tumors using NIR fluorescence, contrast agents that target tumor-specific characteristics can be used to selectively label tumor cells.¹⁶⁻¹⁹ Novel NIR fluorescent agents have been developed that target tumor-specific cell surface marker¹⁶⁻²⁰, enzymatic activity^{17,19,21}, or increased glucose metabolism.²² However, these tumor-specific agents are not yet available for clinical use. The only NIR fluorescent contrast agents currently available, methylene blue and indocyanine green (ICG), are not tumor-specific. However, the enhanced permeability and retention (EPR) effect can potentially be used to obtain accumulation of non-targeted contrast agents in tumors.^{23,24} Due to newly formed, more porous blood vessels, molecules can passively accumulate into the surrounding tissue. Furthermore, poorly developed lymphatics in the tumor result in an increased retention. Previous studies showed breast carcinomas and liver tumors could be identified noninvasively with NIR

fluorescence using ICG based on the EPR effect.²⁵⁻²⁸ The aim of our study was to assess the applicability of NIR fluorescence imaging using ICG to provide a clear tumor-to-background contrast in oncologic pancreatic surgery.

Because ICG is almost exclusively excreted into the bile, it can also be used for intraoperative NIR fluorescence exploration of the biliary anatomy.²⁹⁻³¹ This can be useful in patients with a difficult laparoscopic cholecystectomy, due to an aberrant biliary anatomy or an acute cholecystitis, for example. Furthermore, ICG can potentially be used to assess anastomosis patency in patients undergoing bile duct reconstruction. This is a well-suited setting to study both biliary anatomy and anastomosis patency intraoperatively, as the common bile duct can be visualized for a long time during pancreaticoduodenectomy.

MATERIAL AND METHODS

Intraoperative Near-Infrared Imaging System (Mini-FLARE™)

Intraoperative imaging was performed using the hand-held Fluorescence-Assisted Resection and Exploration (Mini-FLARE™) image-guided surgery system as described by Mieog et al (manuscript accepted for publication). This system consists of two wavelength isolated light sources: a “white” light source, generating 26,600 lx of 400-650 nm light and a NIR light source, generating 7.7 mW/cm² of 760 nm light. Color video and NIR fluorescence images are simultaneously acquired and displayed in real-time using custom optics and software that separate the color video and NIR fluorescence images. A pseudo-colored (lime green) merged image of the color video and NIR fluorescence images is also displayed. The imaging head is attached to a flexible gooseneck arm, which permits positioning of the imaging head virtually anywhere over the surgical field, even at extreme angles. For intraoperative use, the imaging head and imaging system pole stand are wrapped in a sterile shield and drape (Medical Technique Inc., Tucson, AZ).

Preparation and Administration of Indocyanine Green

ICG (25 mg vials) was purchased from Pulsion Medical Systems (Munich, Germany) and resuspended in 10 cc of sterile water for injection to yield a 2.5 mg/ml (3.2 mM) stock solution. Of this stock solution 2 or 4 mL, corresponding with doses of 5 or 10 mg, was administered.

Clinical Trial

The study was approved by the Local Medical Ethics Committee of the Leiden University Medical Center and was performed in accordance with the ethical standards of the Helsinki Declaration of 1975. A total of 8 consecutive patients with suspected ampullary or pancreatic head carcinoma planned to undergo curative resection were included. All patients provided informed consent. Exclusion criteria included pregnancy, lactation or an allergy to iodine, shellfish, or indocyanine green. The surgical technique used in our center implies a standard pancreaticoduodenectomy with resection of peripancreatic tissues and lymph nodes. Following resection, reconstruction is performed with pancreaticojejunostomy, choledochojejunostomy, and pylorojejunostomy for pylorus preserving pancreaticoduodenectomy or a gastrojejunostomy as part of Whipple's procedure. After opening the omental bursa, performing the Kocher maneuver, and exploration of the hepatoduodenal ligament, the pancreatic tumor was fully exposed. The Mini-FLARE imaging system was positioned 30 centimeters above the surgical field. Next, 4 patients were intravenously administered 5 mg ICG diluted in 2 mL sterile water as a bolus and 4 patients were intravenously administered 10 mg ICG diluted in 4 mL sterile water as a bolus. All operating room lights, with the exception of the white light and NIR light of the Mini-FLARE imaging system, were dimmed. The NIR fluorescence measurements of the pancreatic tumor, pancreas, duodenum, stomach, liver, gall bladder, and common bile duct were recorded at the time of injection ($T=0$), 45 seconds and 3-, 10-, 30-, 60-, 90-, 120-, 180- min post-injection. At each measurement, camera exposure times were set appropriately to prevent the NIR fluorescence signal from reaching saturation. Bile duct imaging ended at 90 min because the bile duct was resected at this time as part of the pancreaticoduodenectomy. Furthermore, imaging of the choledochojejunostomy was performed to assess leakage and patency. Fluorescent intensity of these structures was quantified using the custom Mini-FLARE software. To calculate tumor-to-pancreas ratios, tumor and healthy pancreas regions of interest were manually drawn, guided by palpation. Signal-to-background ratios (SBR) for the common bile duct were manually drawn, and a background region of interest was drawn on direct surrounding tissue.

Statistical Analysis

For statistical analysis and graph design, GraphPad Prism Software (Version 5.01, La Jolla, CA) and SPSS (Version 17.0, Chicago, IL) were used. All data were reported as mean \pm standard deviation or median and range. To compare the signal-to-background ratios between the two concentration groups, T-tests were used. Repeated-measures ANOVAs were used to test differences between time points. All statistical tests were two-tailed and $P < 0.05$ was considered significant.

RESULTS

Patient and tumor characteristics

Patient and tumor characteristics are listed in Table 1. Eight patients undergoing surgery for a suspected ampullary or pancreatic head carcinoma were included in the study. In one patient, the common bile duct was cut several minutes after ICG administration and therefore measurements beyond 3 min were excluded from the analysis. Four patients underwent a complete Whipple procedure, three patients underwent a pylorus preserving pancreaticoduodenectomy, and one patient had an irresectable tumor, resulting in a biopsy without further resection.

Tumor Imaging

Directly after injection, superficial arterial flow of ICG was identified by NIR fluorescence on the surface of the pancreas followed by venous drainage. In the 5-mg patient group ($N = 4$), a mean tumor-to-pancreas ratio of 0.89 ± 0.25 was observed. In the 10-mg patient group ($N = 4$), a mean tumor-to-pancreas ratio of 1.22 ± 0.39 was observed (Figure 1a). Time had no significant effect on tumor-to-pancreas ratio ($P = 0.899$). Tumor-to-pancreas ratios were significantly higher in the 10-mg group, when compared to 5-mg group ($P = 0.002$). In one patient (patient 5, 10-mg dose group), a clear NIR fluorescent hotspot was observed on the pancreas (Figure 1b). Histological analyses confirmed that the signal corresponded to tumor tissue surrounding the pancreatic duct. Other than this incidental finding, no contrast was observed.

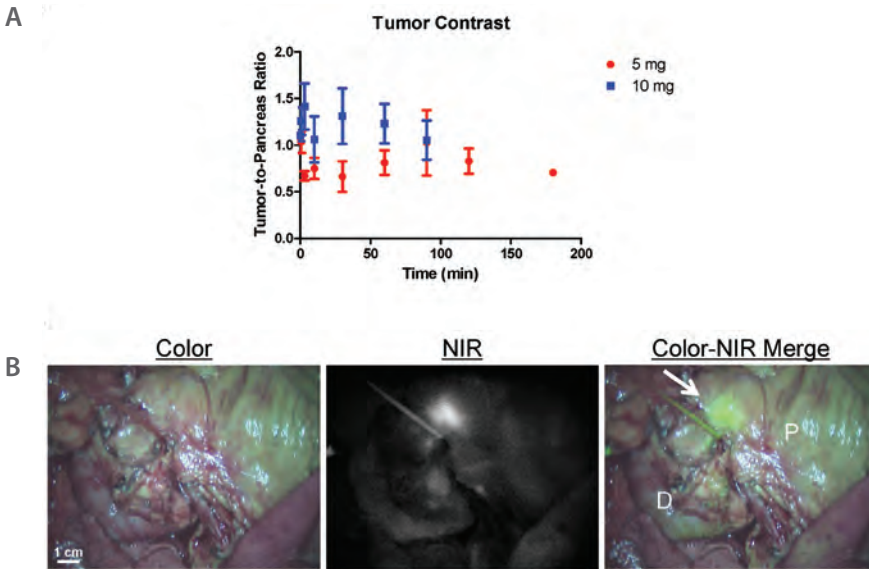


Figure 1 - Tumor-to-Pancreas Contrast using NIR Fluorescence and ICG:
 A. Tumor-to-pancreas ratios (mean \pm SD) of the pancreatic tumors over time, per dose group.
 B. Color video (left panel), NIR fluorescence (middle panel) and a color-NIR overlay (right panel) of intraoperative imaging of the pancreas. In this example, clear contrast (arrow) is shown between pancreatic tumor and normal pancreatic tissue (P), 20 min after administration of 10 mg of ICG. However, this was an incidental finding in one patient. The duodenum is marked with the letter D.

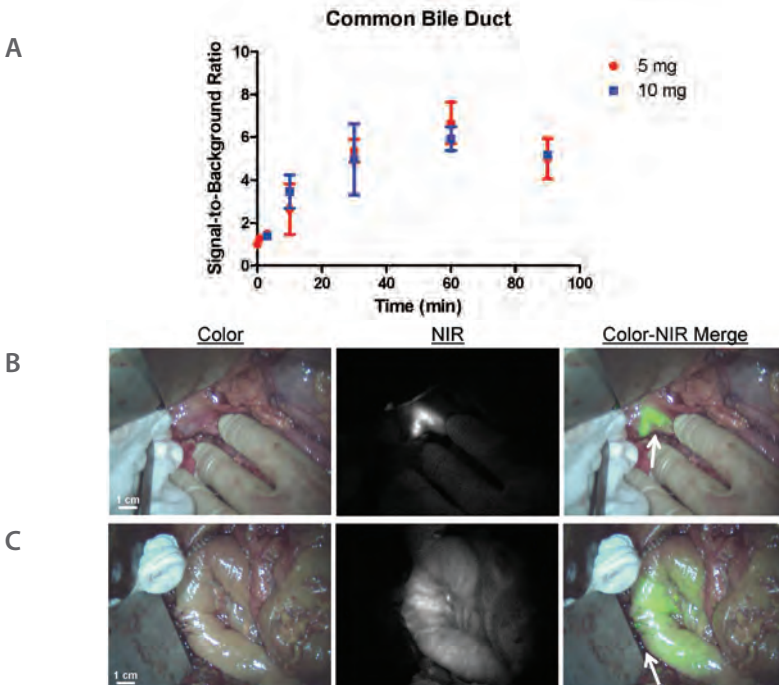


Figure 2 - Intraoperative Imaging of the Common Bile Duct using NIR Fluorescence and ICG:

- A. Signal-to-background ratios (mean \pm SD) of the common bile duct over time, per dose group. Signal-to-background ratios (SBR) for the common bile duct were calculated. A background region-of-interest was drawn on direct surrounding tissue.
- B. Color video (left panel), NIR fluorescence (middle panel) and a color-NIR overlay (right panel) of intraoperative imaging of the common bile duct in a patient who underwent a cholecystectomy during previous surgery, 30 min after administration of 5 mg ICG. A clear contrast is shown between common bile duct (arrow) and surrounding tissue.
- C. Color video (left panel), NIR fluorescence (middle panel) and a color-NIR overlay (right panel) of a choledochojejunostomy (arrow), 30 min after completion of the anastomosis. NIR fluorescence signal of excreted ICG is visualized intraluminally in the jejunum, indicating anastomotic patency and absence of leakage.

Imaging of the Common Bile Duct using NIR Fluorescence

Within 10 min after administration of ICG, the common bile duct, cystic duct, and common hepatic duct could clearly be identified by NIR fluorescence (Figure 2a and b) in all patients. The NIR fluorescence signal of the liver outshined the left and right hepatic ducts and therefore prevented a clear visualization. The fluorescent signal of the bile ducts lasted until 90 min postinjection, at which point the bile duct was resected, along with the head of the pancreas and the duodenum, as part of the pancreaticoduodenectomy. No difference was observed between the 5-mg and 10-mg groups ($P = 0.849$). Time significantly influenced signal-to-background ratio ($P = 0.002$). An optimum was found between 30 and 90 min postinjection, with a maximum mean signal-to-background ratio of 6.24 ± 1.32 at 60 min postinjection. After completion of the choledochojejunostomy, anastomotic patency could be confirmed by visualizing the NIR fluorescence signal passing the anastomosis into the jejunum (Figure 2c).

DISCUSSION

The first objective of this study was to exploit the EPR effect^{23,24} to induce retention of the non-targeted probe ICG in pancreatic tumors. However, in all but one patient, no useful intraoperative tumor-to-pancreas ratios in pancreatic cancer patients were observed using NIR fluorescence and ICG. In one patient, a clear hotspot was observed on the pancreas, which corresponded with the resected adenocarcinoma. No pathological characteristics were observed that could account for this phenomenon. Several factors might explain the observed lack of contrast in all other patients. Healthy pancreas tissue showed a relatively high uptake of ICG, whereas tumor tissue showed similar uptake. As washout of NIR fluorescence signal was comparable in both healthy pancreas tissue and tumor

Table 1 - Patient Characteristics

Pt	Age (y)	Sex	Weight (kg)	Length (cm)	BMI	AP (U/L)	gGT (U/L)	ASAT (U/L)	ALAT (U/L)	Tumor size (cm)	Tumor location	Surgery	T	N	M	R	Vasc inv	Perin inv	Pathology
1	39	M	90	186	26	261	86	92	155	n/a	Head	Bypass	3	+	-	n/a	n/a	n/a	Poorly diff. AC
2	76	V	64	164	24	97	72	21	16	4.7	Ampulla	Whipple	3	-	-	R0	-	+	Poorly diff. AC
3	45	M	65	179	20	118	274	20	19	4	Head	PPPD	3	+	-	R1	-	+	Well diff. AC
4	32	M	88	188	25	114	66	48	78	-	-	Whipple	-	-	-	-	-	-	No malignancy
5	74	V	75	169	26	72	46	69	40	6	Head	Whipple	2	+	-	R1	-	-	AC
6	61	V	73	176	24	674	1472	280	292	1.7	Head	PPPD	3	+	-	R0	-	+	AC
7	46	V	89	170	31	42	11	59	39	1.8	Head	Whipple	1	+	-	R1	-	-	Neuroendocrine
8	62	M	68	180	21	71	64	21	23	2.3	Duodenum	PPPD	-	-	-	R0	-	-	Adenomatous polyp

AC: Adenocarcinoma, AP, alkaline phosphatase; gGT, gamma-glutamyltransferase; ASAT, aspartate transaminase, ALAT, alanine transaminase; Vasc. inv, vascular invasion; Perin inv, perineural invasion; n/a, not available due to irresectable tumor; PPPD, pylorus-preserving pancreaticoduodenectomy, Pt- patient

Biodistribution of ICG

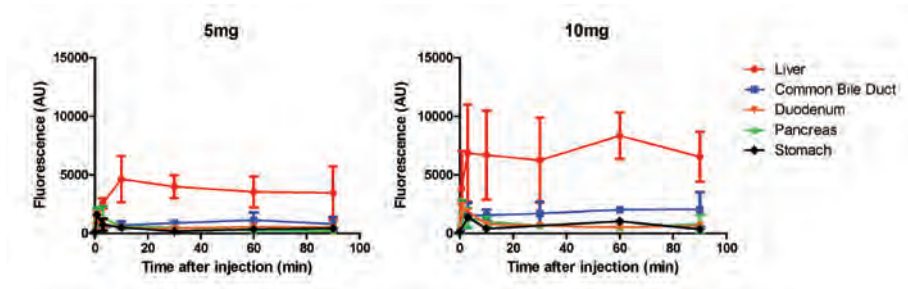


Figure 3 - Biodistribution of ICG in Organs Exposed During Pancreaticoduodenectomy: Shown are NIR fluorescence intensities of organs exposed during pancreaticoduodenectomy. Measurements of the duodenum were taken over an area not containing bile. Intensities are shown over time for both 5 mg (left panel) and 10 mg (right panel) groups.

tissue, no EPR effect could be visualized. This is possibly the result of different tumor biology of pancreatic cancer when compared to breast cancer, in which the EPR effect has been observed in previous studies. Several earlier studies reported a lower perfusion of tumor tissue in comparison with healthy pancreas tissue^{32,33}, which might decrease availability of ICG for a potential EPR effect of the tumor. Furthermore, previous studies that reported an EPR effect of ICG in breast tumors used detection methods (laser scanning or optical tomography), that may detect lower concentrations of ICG but require post-processing, and are therefore not applicable for real-time intraoperative imaging.^{26,27}

Novel NIR fluorescent probes are being developed to increase signal penetration depth and decrease background uptake. For multiple applications within cancer surgery, it is imperative to design improved tumor targeting probes. Tumor targeting can be accomplished by conjugating a fluorophore to a targeting ligand such as antibodies or peptides, for example.^{16,19,21,22} It is expected that several of those tumor targeted probes will be available for first-in-human trials within the coming years.

The second objective of this study was to evaluate the biodistribution of ICG and its clearance by the liver into the bile. Patients undergoing a pancreaticoduodenectomy are well suited for this study, as the bile ducts and abdominal organs can be studied for a relatively long time. As stated before, iatrogenic common bile duct injury occurs in patients undergoing cholecystectomy. A non-invasive imaging modality that can visualize the common bile duct intraoperatively could potentially reduce the incidence of common bile duct injury

in these patients. For example, this technique can help the surgeon identify vital structures during difficult laparoscopic cholecystectomies in patients with acute cholecystitis or aberrant biliary anatomy. This technique could potentially prevent the need to convert to an open procedure.

In this study, the common bile duct was identified using NIR fluorescence imaging after ICG administration in all patients. This is in concordance with preclinical data, described by Matsui et al.³⁰ and in clinical studies of patients undergoing cholecystectomy.^{29,31} A useful contrast between the common bile duct and surrounding tissue was observed starting at 10 min postinjection. The optimal timing of ICG administration prior to imaging lies between 30 and 90 min. In this interval, mean SBRs of 5 to 6 were observed. Ideally, background fluorescence levels of all surrounding organs should be minimal. In this study, the liver signal remained high throughout the imaging interval. Although this did not prevent a contrast being observed between common bile duct and surrounding tissues, future studies should focus on optimal timing to minimize background fluorescence, especially when studying the liver. Indeed, in a separate study, in which patients with colorectal liver metastases were injected intravenously with 10 mg ICG at 24 hours prior to liver surgery, liver fluorescence decreased to background levels, while bile duct imaging was still possible. However, compared to the fluorescent intensity observed in the present study, the bile duct signal was significantly decreased by 88 %.³⁴ Therefore, novel NIR fluorescent agents should be developed that are excreted into bile, with minimal liver uptake, thereby reducing background fluorescence and increasing the ability to visualize bile ducts. In contrast to most other imaging systems, the Mini-FLARE imaging system used in this study can display the NIR fluorescence signal in relation to the surgical anatomy, by simultaneously displaying color video and NIR fluorescence. This feature is of added benefit in performing true image-guided surgery. The Mini-FLARE can only be used during open surgery. However, most cholecystectomies are performed by laparoscopy. In order to enable intraoperative NIR fluorescence imaging during laparoscopic surgery, laparoscopic camera systems are currently being developed and tested.^{31,35,36} Furthermore, as with all novel techniques, large clinical studies are necessary to prove the added value of NIR fluorescence imaging in patients undergoing a cholecystectomy. These trials can use the data presented in this study to select the optimal time of imaging after ICG administration.

This study showed that no useful tumor demarcation could be visualized in pancreatic cancer patients using intraoperative NIR fluorescence imaging after ICG

administration. Furthermore, our study showed the ability to visualize the common bile duct after ICG administration and demonstrated the influence of time on signal-to-background ratio. Moreover, patency of the jejunal-biliary anastomosis could be visualized. For a translation to clinical practice, larger trials should be executed. This is dependent on broad availability of commercial intraoperative NIR fluorescence imaging systems. When these imaging systems become available for use in the clinic in the coming years, the true value of this technique can be assessed.

REFERENCES

1. Jemal A, Siegel R, Ward E et al. Cancer statistics, 2008. *CA Cancer J Clin* 2008; 58:71-96.
2. Yeo CJ, Sohn TA, Cameron JL et al. Periampullary adenocarcinoma: analysis of 5-year survivors. *Ann Surg* 1998; 227:821-831.
3. Sohn TA, Yeo CJ, Cameron JL et al. Resected adenocarcinoma of the pancreas-616 patients: results, outcomes, and prognostic indicators. *J Gastrointest Surg* 2000; 4:567-579.
4. Cleary SP, Gryfe R, Guindi M et al. Prognostic factors in resected pancreatic adenocarcinoma: analysis of actual 5-year survivors. *J Am Coll Surg* 2004; 198:722-731.
5. Conlon KC, Klimstra DS, Brennan MF. Long-term survival after curative resection for pancreatic ductal adenocarcinoma. Clinicopathologic analysis of 5-year survivors. *Ann Surg* 1996; 223:273-279.
6. Garcea G, Dennison AR, Pattenden CJ et al. Survival following curative resection for pancreatic ductal adenocarcinoma. A systematic review of the literature. *JOP* 2008; 9:99-132.
7. Miura F, Takada T, Amano H et al. Diagnosis of pancreatic cancer. *HPB (Oxford)* 2006; 8:337-342.
8. Shin LK, Brant-Zawadzki G, Kamaya A et al. Intraoperative ultrasound of the pancreas. *Ultrasound Q* 2009; 25:39-48.
9. Sun MR, Brennan DD, Kruskal JB et al. Intraoperative ultrasonography of the pancreas. *Radiographics* 2010; 30:1935-1953.
10. Griffin JF, Smalley SR, Jewell W et al. Patterns of failure after curative resection of pancreatic carcinoma. *Cancer* 1990; 66:56-61.
11. Sperti C, Pasquali C, Piccoli A et al. Recurrence after resection for ductal adenocarcinoma of the pancreas. *World J Surg* 1997; 21:195-200.
12. Westerdahl J, Andren-Sandberg A, Ihse I. Recurrence of exocrine pancreatic cancer--local or hepatic? *Hepatogastroenterology* 1993; 40:384-387.
13. Keereweer S, Kerrebijn JD, van Driel PB et al. Optical Image-guided Surgery-Where Do We Stand? *1. Mol Imaging Biol* 2011; 13:199-207.
14. Frangioni JV. New technologies for human cancer imaging. *J Clin Oncol* 2008; 26:4012-4021.
15. Gioux S, Choi HS, Frangioni JV. Image-guided surgery using invisible near-infrared light: fundamentals of clinical translation. *Mol Imaging* 2010; 9:237-255.
16. Lee SB, Hassan M, Fisher R et al. Affibody molecules for in vivo characterization of HER2-positive tumors by near-infrared imaging. *Clin Cancer Res* 2008; 14:3840-3849.
17. Jiang T, Olson ES, Nguyen QT et al. Tumor imaging by means of proteolytic activation of cell-penetrating peptides. *Proc Natl Acad Sci U S A* 2004; 101:17867-17872.
18. Hutteman M, Mieog JS, van der Vorst JR et al. Intraoperative near-infrared fluorescence imaging of colorectal metastases targeting integrin $\alpha(v)\beta(3)$ expression in a syngeneic rat model. *Eur J Surg Oncol* 2011; 37:252-257.
19. Mieog JS, Hutteman M, van der Vorst JR et al. Image-guided tumor resection using real-time near-infrared fluorescence in a syngeneic rat model of primary breast cancer. *Breast Cancer Res Treat* 2010.
20. Gleysteen JP, Newman JR, Chhieng D et al. Fluorescent labeled anti-EGFR antibody for identification of regional and distant metastasis in a preclinical xenograft model. *Head Neck* 2008; 30:782-789.
21. Weissleder R, Tung CH, Mahmood U et al. In vivo imaging of tumors with protease-activated near-infrared fluorescent probes. *Nat Biotechnol* 1999; 17:375-378.
22. Zhou H, Luby-Phelps K, Mickey BE et al. Dynamic near-infrared optical imaging of 2-deoxyglucose uptake by intracranial glioma of athymic mice. *PLoS One* 2009; 4:e8051.
23. Matsumura Y, Maeda H. A new concept for macromolecular therapeutics in cancer chemotherapy: mechanism of tumoritropic accumulation of proteins and the antitumor agent smancs. *Cancer Res* 1986; 46:6387-6392.
24. Maeda H, Wu J, Sawa T et al. Tumor vascular permeability and the EPR effect in macromolecular therapeutics: a review. *J Control Release* 2000; 65:271-284.

25. Hagen A, Grosenick D, Macdonald R et al. Late-fluorescence mammography assesses tumor capillary permeability and differentiates malignant from benign lesions. *Opt Express* 2009; 17:17016-17033.
26. Intes X, Ripoll J, Chen Y et al. In vivo continuous-wave optical breast imaging enhanced with Indocyanine Green. *Med Phys* 2003; 30:1039-1047.
27. Alacam B, Yazici B, Intes X et al. Pharmacokinetic-rate images of indocyanine green for breast tumors using near-infrared optical methods. *Phys Med Biol* 2008; 53:837-859.
28. Ishizawa T, Fukushima N, Shibahara J et al. Real-time identification of liver cancers by using indocyanine green fluorescent imaging. *Cancer* 2009; 115:2491-2504.
29. Tagaya N, Shimoda M, Kato M et al. Intraoperative exploration of biliary anatomy using fluorescence imaging of indocyanine green in experimental and clinical cholecystectomies. *J Hepatobiliary Pancreat Surg* 2009; 17:595-600.
30. Matsui A, Tanaka E, Choi HS et al. Real-time intra-operative near-infrared fluorescence identification of the extrahepatic bile ducts using clinically available contrast agents. *Surgery* 2010; 148:87-95.
31. Ishizawa T, Bandai Y, Ijichi M et al. Fluorescent cholangiography illuminating the biliary tree during laparoscopic cholecystectomy. *Br J Surg* 2010; 97:1369-1377.
32. Reuter SR, Redman HC, Bookstein JJ. Differential problems in the angiographic diagnosis of carcinoma of the pancreas. *Radiology* 1970; 96:93-99.
33. Komar G, Kauhanen S, Liukko K et al. Decreased blood flow with increased metabolic activity: a novel sign of pancreatic tumor aggressiveness. *Clin Cancer Res* 2009; 15:5511-5517.
34. Verbeek FP, Schaafsma BE, Tummers QR et al. Optimization of near-infrared fluorescence cholangiography for open and laparoscopic surgery. *Surg Endosc* 2013.
35. Matsui A, Tanaka E, Choi HS et al. Real-time, near-infrared, fluorescence-guided identification of the ureters using methylene blue. *Surgery* 2010; 148:78-86.
36. Aoki T, Murakami M, Yasuda D et al. Intraoperative fluorescent imaging using indocyanine green for liver mapping and cholangiography. *J Hepatobiliary Pancreat Surg* 2009; 17:590-594.

Chapter 13

Intraoperative near-infrared fluorescence imaging of parathyroid adenomas using low-dose methylene blue

van der Vorst JR¹, Schaafsma BE¹, Verbeek FP, Swijnenburg RJ, Hutteman M,
Hamming JF, Kievit J, Frangioni JV, van de Velde CJ, Vahrmeijer AL

¹Both authors contributed equally to this work and share first authorship.

Head Neck. 2013 May 29

ABSTRACT

Background

Intraoperative identification of parathyroid adenomas can be challenging. We hypothesized that low-doses methylene blue (MB) and near-infrared fluorescence (NIRF) imaging could be used to identify parathyroid adenomas intraoperatively.

Material and Methods

MB was injected intravenously after exploration at a dose of 0.5 mg/kg into 12 patients who underwent parathyroid surgery. NIRF imaging was performed using the Mini-FLARE™ imaging system.

Results

In 10 of 12 patients, histology confirmed a parathyroid adenoma. In 9 of these patients, NIRF could clearly identify the parathyroid adenoma during surgery. Seven of these 9 patients had a positive preoperative ^{99m}Tc-sestamibi SPECT scan. Importantly, in two patients, parathyroid adenomas could be identified only using NIRF.

Conclusion

This is the first study to show that low-dose MB can be used as NIRF tracer for identification of parathyroid adenomas, and suggests a correlation with preoperative ^{99m}Tc-sestamibi SPECT scanning.

INTRODUCTION

Primary hyperparathyroidism is a common endocrine disorder caused by overproduction of parathyroid hormone (PTH) by adenomatous or hyperplastic parathyroid glands. In hyperparathyroidism patients, resection of these glands is the only curative treatment. The wide variability of the anatomical location, shape, and number of parathyroid glands makes successful parathyroid surgery challenging. Various preoperative imaging modalities contribute to detailed surgical planning, which is particularly important when using a minimally invasive surgical approach.¹⁻³ Currently, a combination of a cervical ultrasonography (US) and a ^{99m}Tc-sestamibi planar scan, whether or not combined with a single-photon emission computed tomography (SPECT) 3D scan, is most often used for preoperative localization. However, only few intraoperative imaging modalities are available. Despite that the current success rate of parathyroidectomy exceeds 95% without any intraoperative imaging adjuncts in the hands of experienced surgeons,^{1,4} intraoperative imaging tools could aid in the localization of difficult localized parathyroid adenoma and in addition possibly reduce time of surgery.⁵

For intraoperative localization, radioguided parathyroidectomy using ^{99m}Tc-sestamibi has been reported.^{6,7} This technique, however, lacks real-time visual information. High-dose methylene blue (MB), used as a blue dye, was introduced by Dudley and colleagues in 1971⁸ for the intraoperative identification of parathyroid adenomas by a simple peripheral infusion.^{6,9,10} reporting sensitivity and specificity of 79% and 93% respectively.^{10,11} However, a major disadvantage of using MB is that the high dose (7.5 mg/kg) required for visualization of blue color by the human eye brings a substantial risk of serious adverse events, such as toxic metabolic encephalopathy.¹² A different, recently introduced, technique is the use of visible fluorescence and aminolevulinic acid (ALA) to identify parathyroid glands, which was successfully tested in clinical studies.¹³⁻¹⁵ However, ALA can cause phototoxic reactions for which patients have to be shielded from direct light exposure for 48 hours. Furthermore, sub-surface detectability using ALA is minimal due to high absorption and scatter of visible light in living tissue. Therefore, novel and improved intraoperative imaging modalities to aid the surgeon in localization of the parathyroid glands are needed during parathyroid surgery.

Near-infrared (NIR) fluorescence imaging is a promising technique that also facilitates intraoperative, real-time, visual information.¹⁶⁻¹⁸ This technique is based on the use of exogenous NIR fluorescent contrast agents that can be detected

by intraoperative imaging systems to visualize specific tissues. Advantage of this technique are its high sensitivity and high tissue penetration of approximately 5 millimeters. As such, it has wide applications, including sentinel lymph node mapping in several tumor types.¹⁹⁻²² MB, which was used for parathyroid adenoma identification as stated above, has the advantageous property that it becomes a moderate-strength fluorophore emitting at ≈ 700 nm when diluted to levels that are almost undetectable to the human eye. When lower doses of MB can still provide clear identification of parathyroid adenomas using NIR fluorescence, this could significantly reduce the risk for adverse events.²³ The aim of this study was to assess feasibility of using low-dose MB for intraoperative NIR fluorescence-guided detection of parathyroid adenomas. Furthermore, the concordance between preoperative ^{99m}Tc-sestamibi-SPECT scanning and intraoperative NIR fluorescence was preliminarily assessed.

MATERIAL AND METHODS

Clinical Study

This study was approved by the Medical Ethics Committee of the Leiden University Medical Center and was performed in accordance with the ethical standards of the Helsinki Declaration of 1975. All patients planning to undergo a resection of a parathyroid adenoma for primary hyperparathyroidism or parathyromatosis were eligible for participation in the study. Exclusion criteria were pregnancy or lactation, the use of serotonin reuptake inhibitors, serotonin, and noradrenalin reuptake inhibitors and/or tricyclic antidepressants, severe renal failure, G6PD-deficiency, or an allergy to MB. All patients gave informed consent and were anonymized. Patients received standard of care diagnostic work-up, which for our center implied a preoperative ^{99m}Tc-sestamibi-SPECT, which was sometimes combined with a low-dose computed tomography (CT) scan for preoperative surgical planning. If indicated a preoperative cervical US was performed. After subplatysmal dissection, retraction, draping and initial surgical exploration of the suspected parathyroid adenoma in the neck region, 0.5 mg/kg of MB (concentration 10 mg/ml) was infused intravenously over 5 min. Subsequently, NIR fluorescence imaging of the neck region was performed using the Mini-FLARE NIR fluorescence imaging system, which has been described previously.²⁰ In one patient a thoracotomy was performed after SPECT-CT localization of the parathyroid adenoma in pericardium.

After resection of the putative parathyroid adenoma, an intraoperative PTH assay was performed. Post-operative histopathological examination was obtained, which served as gold standard for parathyroid adenoma identification. Parathyroid tissue was snap frozen and sectioned at 10 μm for fluorescence microscopy.

Fluorescence Microscopy

Snap frozen tissue was sectioned at 10 μm for fluorescence microscopy, which was performed on a Zeiss LSM 700 Confocal Laser Scanning Microscope and a Zeiss HBO 100 Microscope Illuminating System (Jena, Germany) using a 633 nm laser for excitation and a 650 nm high pass emission filter. Subsequently, tissue sections were stained with hematoxylin and eosin (H&E).

Statistical Analysis

For statistical analysis, SPSS statistical software package (Version 16.0, Chicago, IL) was used. Signal-to-background ratios were calculated by dividing the fluorescent signal in the parathyroid adenoma by fluorescent signal of surrounding healthy tissue. Patient age and body mass index (BMI) were reported in median and range and signal-to-background was reported in mean and standard deviation. To compare fluorescent signal in the parathyroid adenoma with fluorescent signal in the thyroid gland, the independent-sample *t* test was used. $P < 0.05$ was considered significant.

RESULTS

Study Subjects

Patient characteristics and histological results of the 12 patients included are listed in Table 1. Median patient age was 58 years (range 17 – 78 years), median BMI was 26 (range 18 – 34 kg/m^2). Eleven patients were planned for surgery for primary hyperparathyroidism and 1 patient suffered from parathyromatosis. Prior to the study, one patient underwent a total thyroid resection, one patient a parathyroid adenoma resection, and one patient had undergone previous parathyroid surgery 3 times as well as a thymectomy. During the current study, a resection of the putative diseased tissue was performed in all patients. Histopathological examination showed a solitary parathyroid adenoma in 7 patients, two parathyroid adenomas in 1 patient, small parathyroid fragments in 1 patient, a parathyroid carcinoma in

1 patient and a thyroid carcinoma with a synchronous parathyroid adenoma in 2 patients. Average maximum diameter of the resected lesions was 15.7 ± 8.7 mm.

Preoperative Imaging

In all patients, a preoperative ^{99m}Tc -sestamibi-SPECT scan was performed which was combined with a low-dose CT-scan in 10 patients. In 8 of 12 patients, the ^{99m}Tc -sestamibi-SPECT scan could identify the parathyroid adenoma. In 9 of 12 patients a preoperative ultrasonography was performed, which was positive in 4 patients. Preoperative imaging results are summarized in Table 2.

Intraoperative NIR Fluorescence Imaging

Intraoperative NIR fluorescent guidance was provided by the Mini-FLARE imaging system and MB, which clearly identified a hyperparathyroid adenoma in 9 patients (Figs. 1 and 2). Of these patients, the average signal-to-background ratio (SBR) was 6.1 ± 4.1 . Importantly, in 2 of these 9 NIR fluorescence-positive patients, the parathyroid adenoma was not identified using the ^{99m}Tc -sestamibi-SPECT scan or preoperative ultrasound. In 3 of 12 patients, no intraoperative fluorescent signal could be detected. In two of these patients, no parathyroid adenoma was found during histological examination (parathyromatosis and a necrotic parathyroid carcinoma). In one patient a normal parathyroid adenoma, which contained extensive fibrosis and bleeding, was identified. In other words, in 9 of 10 patients diagnosed with a parathyroid adenoma, the adenoma could be identified using NIR fluorescence. No significant difference was observed between parathyroid fluorescence and thyroid fluorescence (322.6 ± 272.1 vs. 220.2 ± 186.7 , $P = 0.25$). During the course of the study, no adverse events were observed.

In 9 of 12 patients, preoperative results using ^{99m}Tc -sestamibi overlapped with intraoperative NIR fluorescence. In 1 patient in whom the ^{99m}Tc -sestamibi-scan was positive, no fluorescent signal could be obtained. This patient was found to have a parathyroid carcinoma. In 2 patients in whom the ^{99m}Tc -sestamibi-scan was negative, NIR fluorescence could identify the parathyroid adenoma. In 3 of 9 patients in whom an ultrasonography was performed, results overlapped with NIR fluorescence. The overlap between different imaging modalities and the location of the parathyroid glands is schematically shown in Figure 3.

Table 1 – Patient and surgical characteristics

Subject	Gender	Age	BMI	Disease	Previous treatment	Preop calcium (mmol/L)	Preop PTH (pmol/L)	Surgical procedure	Histology	Max diameter (mm)
1	F	67	34	PH	No	1.48	17.7	PAR right, thyroid biopsy, thyroidal cystectomy	Parathyroid adenoma	8
2	F	78	24	PH	Total thyroid resection	NA	17.8	PAR right, resection of thyroidal nodule right, parathyroid gland resection left	Parathyroid adenoma	9
3	F	58	27	PH	PAR	2.98	NA	Intermediastinal PAR, thymectomy	Parathyroid adenoma	20
4	M	48	31	PT	Parathyroid surgery (3x); thymectomy	2.76	8.7	Resection of 8 tissue fragments	Parathyromatosis	fragments < 21 mm
5	F	17	24	PH	No	2.71	11.4	Thyroid biopsy, subtotal parathyroidectomy	Parathyroid adenoma	11
6	M	58	26	PH	No	3.15	9.6	PAR left, resection suspected lymph nodes, resection left thyroid	Parathyroid adenoma, thyroid carcinoma	30
7	F	44	30	PH	No	2.7	231	PAR right, hemithyroidectomy right	Parathyroid carcinoma	30
8	F	60	23	PH	No	2.59	16.7	PAR left	Parathyroid adenoma	7
9	M	78	23	PH	No	2.78	23.8	PAR right	Parathyroid adenoma	22
10	F	52	33	PH	No	2.77	34.3	PAR right, hemithyroidectomy right, resection suspected nodes left, thymectomy	Parathyroid adenoma, (2) thyroid carcinoma	8;4
11	F	49	18	PH	No	3.00	47.7	PAR retrosternal	Parathyroid adenoma	15
12	F	64	32	PH	No	2.59	14.5	PAR left	Parathyroid adenoma	15

BMI: Body-mass index; Preop: preoperative, PH: primary hyperparathyroidism; PT: parathyromatosis; PAR: parathyroid adenoma resection

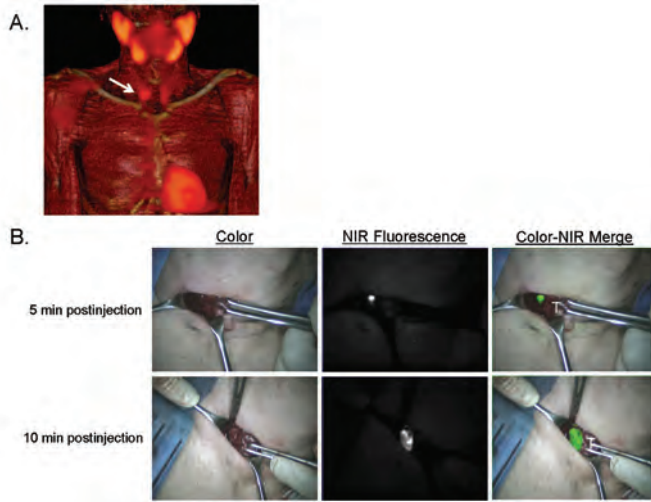


Figure 1 – Preoperative surgical planning and intraoperative NIR fluorescence-guided resection of a parathyroid adenoma located in the neck:

A: 3D SPECT-CT image 2 h postinjection of ^{99m}Tc -sestamibi with visualization of a parathyroid adenoma located at the right side of the neck (arrow).

B: During minimally-invasive parathyroid surgery, a parathyroid adenoma is identified using NIR fluorescence imaging, 5 and 10 minutes postinjection of 0.5 mg/kg MB. T= thyroid tissue.

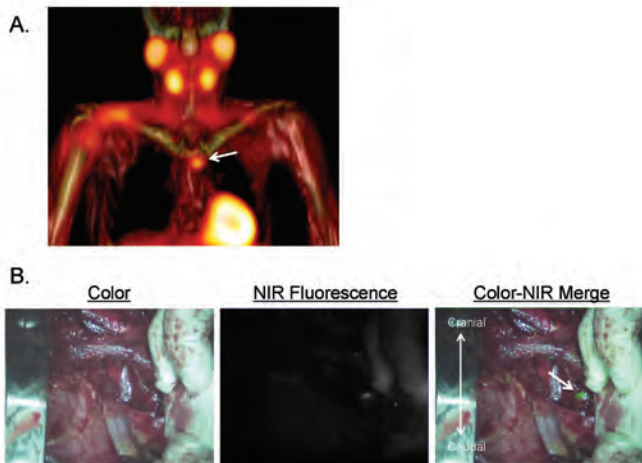


Figure 2 – Preoperative surgical planning and intraoperative NIR fluorescence-guided resection of a parathyroid adenoma located in the mediastinum:

A: 3D SPECT-CT image 2 h postinjection of ^{99m}Tc -sestamibi with visualization of a parathyroid adenoma located paratracheally in the mediastinum (arrow).

B: A parathyroid adenoma located paratracheally in the mediastinum is identified using NIR fluorescence imaging, 10 minutes postinjection of 0.5 mg/kg MB.

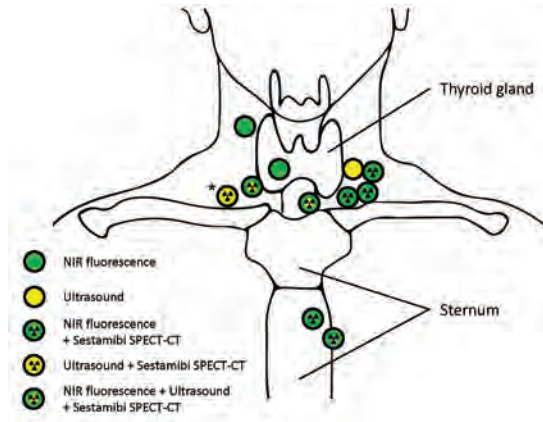


Figure 3 – Schematic overview of parathyroid adenoma location and corresponding detection methods: Shown is the location of all parathyroid adenomas (N = 10) and one parathyroid carcinoma (N = 1, Asterix) and corresponding imaging modalities with which they were identified. The patient with parathyromatosis was excluded from this scheme.

Fluorescence Microscopy

700 NIR fluorescence signal of methylene blue was located within oncocytic cells as confirmed using H&E staining of the same specimen (Fig. 4).

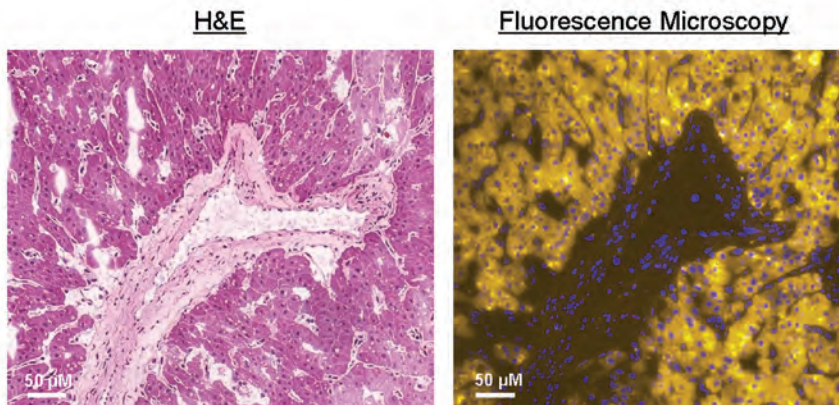


Figure 4 – Histopathological evaluation and fluorescence microscopy:

Shown are 40X H&E staining (left) of the resected specimen, which shows oncocytic cells with monotone round nuclei surrounding a blood vessel. The right image shows the same section stained with 4',6-diamidino-2-phenylindole (DAPI) nuclear staining (blue), with the 700 nm NIR fluorescence from MB pseudo-colored in yellow. The NIR fluorescent signal is located in the oncocytic cells.

Table 2 –Identification of parathyroid adenomas

Subject #	Sestamibi-SPECT-CT	Preoperative Ultrasound	PTH decrease Post-resection	NIR fluorescence detection	SBR
1	-	-	+	+	5.48
2	+	-	+	+	9.59
3	+	-	+	+	4.37
4	-	-	-	-	n/a
5	+*	NP	+	+	2.68
6	-	+	+	-	n/a
7	+*	+	+	-	n/a
8	+	+	+	+	4.45
9	+	+	+	+	5.50
10	-	-	+	+	1.91
11	+	NP	+	+	5.21
12	+	NP	+	+	15.33

PTH: parathyroid hormone; n/a: not applicable; NIR: Near-infrared; NP: Not performed; SBR: signal-to-background ratio; *: SPECT without CT was performed

DISCUSSION

The primary objective of the current study was to test the feasibility of NIR fluorescence with low-dose MB (0.5 mg/kg; 15 times lower than the dose used for macroscopic identification) to identify parathyroid adenomas during surgery. Furthermore, concordance between ^{99m}Tc -sestamibi SPECT and intraoperative NIR fluorescence imaging results was assessed. Two patients were not diagnosed with a parathyroid adenoma. A clear identification of parathyroid adenomas using NIR fluorescence was found in 9 of 10 patients who were histologically diagnosed with a parathyroid adenoma. Furthermore, a high overlap between imaging results of ^{99m}Tc -sestamibi SPECT and NIR fluorescence was observed.

In 3 of 12 patients, no clear identification of the lesion could be obtained using NIR fluorescence. In one of these patients, histopathological examination revealed a parathyroid carcinoma. This carcinoma was described as a highly necrotic lesion, which presumably hampered MB uptake in this lesion. Alternatively, carcinoma may not take up MB like benign lesions. One patient suffered from extended cervical parathyromatosis and in this patient all parathyroid glands were already surgically removed in the past. In this patient, the parathyroid tissue could not be demarcated from the surrounding tissue, however no adenomas were

present. In one patient with a large parathyroid adenoma, in whom no adequate SBR could be obtained, the adenoma contained extensive fibrosis and bleeding. The extensive fibrosis and bleeding could have hampered uptake of MB in the adenoma, which might also explain the negative ^{99m}Tc -sestamibi SPECT scan.

A potential pitfall using the technology we describe is the background signal in the thyroid gland. It is known from data acquired in patients undergoing ^{99m}Tc -sestamibi radioscintigraphy that adenomatous and hyperplastic parathyroid tissue show more avid uptake of ^{99m}Tc -sestamibi, although initially this activity can be obscured by uptake from the adjacent thyroid gland. The observation that abnormal parathyroid tissue commonly retains ^{99m}Tc -sestamibi longer than thyroid gland tissue has led to the widespread use of delayed imaging.²⁴ Therefore, an early (15-30 min.) and delayed (2-3 hr.) imaging sequence is performed. Furthermore, a window of 4 hours between administration and imaging was also used in the clinical studies that used ALA for parathyroid identification.^{13,15} In the current study, high thyroid gland uptake of MB was observed. We hypothesize that a similar delayed imaging protocol could improve the contrast between thyroid gland and parathyroid gland tissue.

Although conventional preoperative imaging modalities (^{99m}Tc -sestamibi scan and US) achieve an accurate preoperative localization of the adenoma in most cases (sensitivity approximately 80% for both techniques), intraoperative identification can be challenging.²⁵ In this perspective, time needed to intraoperatively localize the adenoma may decrease using NIR fluorescence and MB. The comparable biological characteristics of MB and sestamibi, both lipophilic and cationic, resulted in a high concordance between the outcome of ^{99m}Tc -sestamibi scans and NIR fluorescence detection in 7 of 9 patients in the current study. The results of the ^{99m}Tc -sestamibi SPECT-CT may therefore help predict those patients that will most likely benefit from NIR fluorescence intraoperative imaging.

The current study was the first to show that low-dose MB and NIR fluorescence can be used for the intraoperative detection of parathyroid adenomas after a simple peripheral infusion. Though this technique will not replace the detailed and thorough anatomical knowledge and experience of surgeons, which are the key factors for successful parathyroidectomy. Due to the significantly lower doses MB that can be used, this technique can provide valuable additional information during surgery in a safe manner, provided that proper exclusion criteria are followed. However, optimization of MB dose, timing of injection, clinical outcome and patient benefit need to be studied in larger clinical trials.

REFERENCES

1. Udelsman R. Six hundred fifty-six consecutive explorations for primary hyperparathyroidism. *Ann Surg* 2002; 235:665-670.
2. Grant CS, Thompson G, Farley D et al. Primary hyperparathyroidism surgical management since the introduction of minimally invasive parathyroidectomy: Mayo Clinic experience. *Arch Surg* 2005; 140:472-478.
3. Lew JI, Solorzano CC. Surgical management of primary hyperparathyroidism: state of the art. *Surg Clin North Am* 2009; 89:1205-1225.
4. Norman J, Lopez J, Politz D. Abandoning unilateral parathyroidectomy: why we reversed our position after 15,000 parathyroid operations. *J Am Coll Surg* 2012; 214:260-269.
5. Patel CN, Salahudeen HM, Lansdown M et al. Clinical utility of ultrasound and 99mTc sestamibi SPECT/CT for preoperative localization of parathyroid adenoma in patients with primary hyperparathyroidism. *Clin Radiol* 2010; 65:278-287.
6. Harrison BJ, Triponez F. Intraoperative adjuncts in surgery for primary hyperparathyroidism. *Langenbecks Arch Surg* 2009; 394:799-809.
7. Flynn MB, Bumpous JM, Schill K et al. Minimally invasive radioguided parathyroidectomy. *J Am Coll Surg* 2000; 191:24-31.
8. Dudley NE. Methylene blue for rapid identification of the parathyroids. *Br Med J* 1971; 3:680-681.
9. Han N, Bumpous JM, Goldstein RE et al. Intra-operative parathyroid identification using methylene blue in parathyroid surgery. *Am Surg* 2007; 73:820-823.
10. Orloff LA. Methylene blue and sestamibi: complementary tools for localizing parathyroids. *Laryngoscope* 2001; 111:1901-1904.
11. Raffaelli M. Systematic review of intravenous methylene blue in parathyroid surgery (*Br J Surg* 2012; 99: 1345-1352). *Br J Surg* 2012; 99:1352.
12. Kartha SS, Chacko CE, Bumpous JM et al. Toxic metabolic encephalopathy after parathyroidectomy with methylene blue localization. *Otolaryngol Head Neck Surg* 2006; 135:765-768.
13. Prosst RL, Weiss J, Hupp L et al. Fluorescence-guided minimally invasive parathyroidectomy: clinical experience with a novel intraoperative detection technique for parathyroid glands. *World J Surg* 2010; 34:2217-2222.
14. Prosst RL, Gahlen J, Schnuelle P et al. Fluorescence-guided minimally invasive parathyroidectomy: a novel surgical therapy for secondary hyperparathyroidism. *Am J Kidney Dis* 2006; 48:327-331.
15. Prosst RL, Willeke F, Schroeter L et al. Fluorescence-guided minimally invasive parathyroidectomy: a novel detection technique for parathyroid glands. *Surg Endosc* 2006; 20:1488-1492.
16. Keereweer S, Kerrebijn JD, van Driel PB et al. Optical Image-guided Surgery-Where Do We Stand? *Mol Imaging Biol* 2010.
17. Frangioni JV. New technologies for human cancer imaging. *J Clin Oncol* 2008; 26:4012-4021.
18. Gioux S, Choi HS, Frangioni JV. Image-guided surgery using invisible near-infrared light: fundamentals of clinical translation. *Mol Imaging* 2010; 9:237-255.
19. Hutteman M, Choi HS, Mieog JS et al. Clinical Translation of Ex Vivo Sentinel Lymph Node Mapping for Colorectal Cancer Using Invisible Near-Infrared Fluorescence Light. *Ann Surg Oncol* 2010; Epub ahead of print.
20. Mieog JS, Troyan SL, Hutteman M et al. Towards Optimization of Imaging System and Lymphatic Tracer for Near-Infrared Fluorescent Sentinel Lymph Node Mapping in Breast Cancer. *Ann Surg Oncol* 2011; 18:2483-2491.
21. Hutteman M, van der Vorst JR, Gaarenstroom KN et al. Optimization of near-infrared fluorescent sentinel lymph node mapping for vulvar cancer. *Am J Obstet Gynecol* 2011.
22. Crane LM, Themelis G, Pleijhuis RG et al. Intraoperative Multispectral Fluorescence Imaging for the Detection of the Sentinel Lymph Node in Cervical Cancer: A Novel Concept. *Mol Imaging Biol* 2010.
23. Majithia A, Stearns MP. Methylene blue toxicity following infusion to localize parathyroid adenoma. *J Laryngol Otol* 2006; 120:138-140.

24. Taillefer R, Boucher Y, Potvin C et al. Detection and localization of parathyroid adenomas in patients with hyperparathyroidism using a single radionuclide imaging procedure with technetium-99m-sestamibi (double-phase study). *J Nucl Med* 1992; 33:1801-1807.
25. Cheung K, Wang TS, Farrokhyar F et al. A meta-analysis of preoperative localization techniques for patients with primary hyperparathyroidism. *Ann Surg Oncol* 2012; 19:577-583.

Chapter 14

Near-infrared fluorescence imaging of a solitary fibrous tumor of the pancreas using methylene blue

van der Vorst JR, Vahrmeijer AL, Hutteman M, Bosse T, Smit VT, van de Velde CJ,
Frangioni JV, Bonsing BA

World J Gastrointest Surg. 2012 Jul 27;4(7):180-4

ABSTRACT

A 67-year-old female presented with unexplained abdominal pain. A contrast-enhanced CT scan of the abdomen incidentally revealed a mass in the uncinate process of the pancreas. This mass was resected and based on histopathological findings, diagnosed as a solitary fibrous tumor of the pancreas. A solitary fibrous tumor is an extremely rare benign mesenchymal tumor that in 65% of cases affects the visceral pleura but can also affect extra-pleural sites. The intraoperative demarcation of pancreatic tumors, such as a solitary fibrous tumor, can be challenging. In this report, the first clear intraoperative identification of a solitary fibrous tumor of the pancreas using near-infrared fluorescence and methylene blue in a human was shown.

INTRODUCTION

Pancreatic tumors are most often adenocarcinomas, but can also be rare neuroendocrine tumors and even rarer benign mesenchymal tumors. Diagnostic workup of pancreatic tumors is typically performed using contrast-enhanced Doppler ultrasound (US), helical computed tomography (CT), enhanced magnetic resonance imaging (MRI), and endoscopic US (EUS). However, during pancreatic surgery, tumor localization and assessment of the extent of disease is presently made using visual inspection and palpation, and in some cases, intraoperative US. Inadequate intraoperative tumor identification can lead to recurrent disease and/or the need for re-exploration.

Near-infrared (NIR) fluorescence imaging is a promising technique to facilitate intraoperative, real time, visual identification of tumors,^{1,2} which uses tumor-specific fluorescent contrast agents.³⁻⁶ Although several targeted NIR fluorophores have shown promise in preclinical model systems, there are no tumor-specific contrast agents presently available for clinical use. In fact, the only 2 NIR fluorescent contrast agents available clinically, and approved for other indications, are the 700 nm fluorophore methylene blue (MB) and the 800 nm fluorophore indocyanine green (ICG); both agents are classified as non-specific with respect to targeting. MB and ICG have been clinically used for decades. MB is used in parathyroid surgery⁷ and for the treatment of septic shock⁸. ICG is used to assess the clearance capacity of the liver⁹ and for angiographies¹⁰ and has been used off label for NIR fluorescence sentinel lymph node mapping.¹¹

Although the enhanced permeability and retention (EPR) effect can potentially be used to accumulate non-targeted contrast agents in tumors,^{12,13} a recent clinical study by our group suggested that intravenously injected ICG did not result in improved identification of adenocarcinoma of the pancreas from this effect.¹⁴ In a different preclinical study by our group, it appeared that intravenous injection of MB into transgenic mice resulted in high sensitivity detection of insulinomas and a pancreatic neuroendocrine tumor.¹⁵ The optimal dose of MB in that study was 1 to 2 mg/kg. Based on these results, a clinical study was initiated in which patients with a suspected neuroendocrine tumor of the pancreas were administered 1.0 mg/kg MB intraoperatively and the pancreas was imaged using an optimized NIR fluorescence imaging system.

CASE REPORT

A 67-year-old female presented with unexplained abdominal pain. The patient did not have jaundice or other symptoms of obstruction. A contrast-enhanced CT scan of the abdomen incidentally revealed a mass of 1.6 x 2.8 cm in the uncinate process of the pancreas (Fig. 1; dashed outline). The mass showed hyperattenuation during the arterial phase of contrast administration. Static total body and SPECT / low-dose CT scans using In-111-Octreotide showed a normal distribution in the body and no uptake in the pancreatic mass (data not shown). Moreover, no hormonal hypersecretion was observed. Family history of multiple endocrine neoplasia syndrome was negative. A non-functioning neuroendocrine tumor was suspected and the patient was planned for resection. During surgery, directly after exposure of the uncinate process, NIR fluorescence imaging of the pancreatic mass using MB was performed. Afterwards, the lesion was enucleated (Fig. 1) while sparing the pancreatic duct and processed for histology. No surgical complications or adverse events were reported and the patient was released from the hospital 7 days postoperatively.

Intraoperative NIR Fluorescence Imaging System

NIR fluorescence imaging was performed using the Mini-FLARE™ image-guided surgery system as described in detail previously (Fig 2)¹⁶. Briefly, the system consists of 2 wavelength separated light sources: a “white” LED light source, generating 26,600 lx of 400 to 650 nm light to illuminate the surgical field and an NIR LED light source, generating 7.7 mW / cm² of 670 nm fluorescence excitation light. White light and NIR fluorescence images are acquired simultaneously and displayed in real time, using custom designed optics and software. A pseudo-colored (neon red) image of NIR fluorescence superimposed over the white light image is also displayed, to provide the NIR fluorescence signal in the proper anatomical context.

Intraoperative NIR Fluorescence Imaging and Fluorescence Microscopy

The current study was approved by the Medical Ethics Committee of the Leiden University Medical Center and was performed in accordance with the ethical standards of the Helsinki Declaration of 1975. One patient with a suspected pancreatic neuroendocrine tumor was included and gave written informed consent. In this patient, a dose of 1.0 mg/kg MB (64 mg in 6.4 ml of water; 10 mg/ml final stock solution concentration) was infused intravenously over 5 min directly

after exposure of the uncinata process. After the start of infusion, NIR fluorescence imaging of the pancreatic mass and the pancreas was performed approximately every 30 seconds for a period of 20 min. *Ex vivo* NIR fluorescence imaging of the sliced resection specimen was performed at the pathology department. NIR fluorescence imaging using the Mini-FLARE™ system enabled clear visualization of the pancreatic lesion (Fig. 3A). After the infusion time of 5 min, a tumor-to-background ratio of ≈ 3 was reached and was stable for the next 15 min (Fig. 3B). No adverse effects occurred.

Histopathology

Part of the excised tissue was fixed in formalin and embedded in paraffin for hematoxylin and eosin (H&E) and immunohistopathological staining, and part of the excised tissue was snap frozen for fluorescence microscopy. Macroscopically, a clearly defined well-circumscribed pale tan firm nodule was seen. Sections showed an unencapsulated, circumscribed tumor, consisting of a spindle cell proliferation with hypercellular areas alternating with hypocellular foci (Fig. 4A). The hypercellular areas are made up of spindle shaped cells without cytological atypia. There is no cellular pleomorphism, mitoses or necrosis. Furthermore, deposition of abundant hyalinized collagen was identified (sometimes keloid-like) and the stroma contained several vessels, a few of which were dilated and hemangiopericytic. Several normal pancreatic acinar elements are embedded within the mass. No islets of Langerhans were identified within the lesion. Additional, immunohistochemical staining shows that the tumor cells were positive for CD34, CD99, and Bcl2 (Fig. 4A). CD117 and b-catenin were negative (data not shown). Based on these histopathological findings the tumor was diagnosed as a solitary fibrous tumor (SFT) of the pancreas.

Fluorescence Microscopy

Snap frozen tissue was sectioned at 6 μm for fluorescence microscopy and additionally stained with a blue 4',6-diamidino-2-phenylindole (DAPI) nuclear staining. Fluorescence microscopy was performed on a Zeiss LSM 700 Confocal Laser Scanning Microscope and a Zeiss HBO 100 Microscope Illuminating System (Jena, Germany) using a 633 nm laser for excitation and a 650 nm high pass emission filter. Subsequently, tissue sections were stained with H&E and overlay images of NIR fluorescence were created. Fluorescence signal was located in remnants of the exocrine pancreatic tissue, encapsulated by the tumor tissue (Fig 4B).



Figure 1: Presurgical and intraoperative visualization of the pancreatic mass (dashed outline)

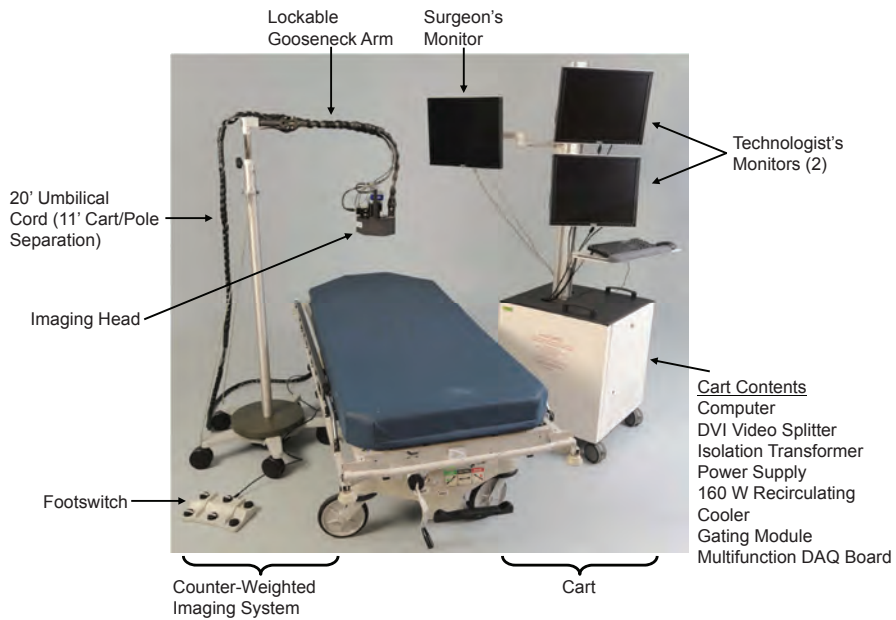


Figure 2: The Mini-FLARE imaging system

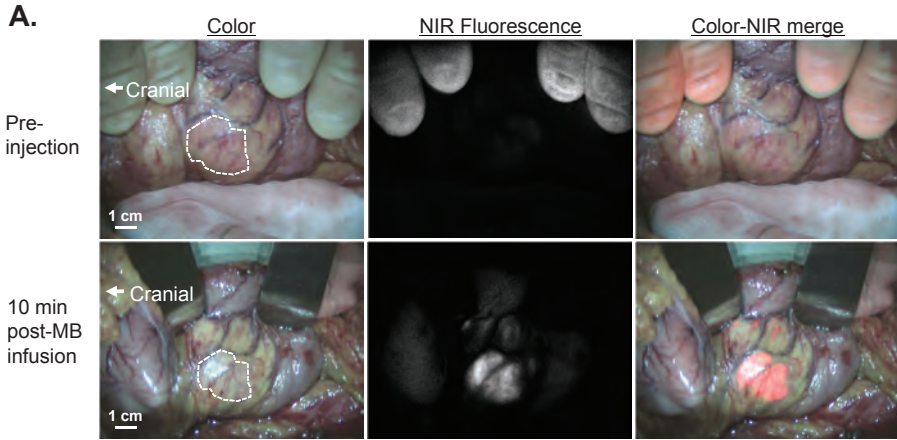


Figure 3A: Intraoperative near-infrared (NIR) fluorescence imaging

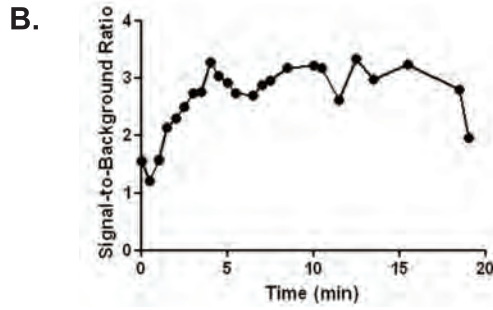


Figure 3B: Signal-to-background ratio of the solitary fibrous tumor

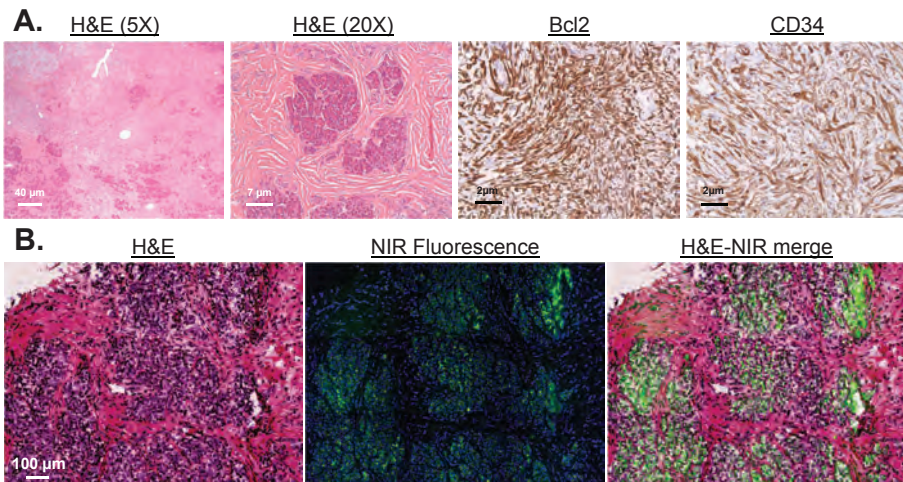


Figure 4A: Histopathological evaluation

Figure 4B: Fluorescence microscopy

DISCUSSION

Despite the availability of many preoperative imaging modalities, intraoperative identification and demarcation of pancreatic tumors remains challenging. In this report, the first clear identification of a SFT of the pancreas using NIR fluorescence and MB in a human was shown. A SFT is an extremely rare benign mesenchymal tumor that in 65% of cases affects the visceral pleura but can also affect extra-pleural sites. Until now, 9 cases of a SFT affecting the pancreas have been reported.¹⁷⁻²⁵ In these cases, patients were asymptomatic or complained of abdominal pain.

Although the current study was initiated to assess the ability to intraoperatively detect neuroendocrine tumors using NIR fluorescence and MB, the unexpected findings in this patient with a SFT in the pancreas are encouraging. Although SFTs mimic neuroendocrine tumor radiologically, it remains unknown whether MB will provide strong contrast in other non-adenocarcinoma pancreatic tumors. SFTs, like neuroendocrine tumors, typically show a hypervascular, hyperenhancing mass using contrast-enhanced CT, and because MB is a phenothiazine derivative that acts as a perfusion tracer, it remains likely that future clinical testing will confirm what has been seen preclinically in neuroendocrine tumors.¹⁵ Our clinical study enrolling patients with a suspected neuroendocrine tumor remains open to accrual. Moreover, NIR fluorescence imaging using methylene blue could potentially be translated to patients with other diseases giving hypervascular lesions, such as hyperparathyroidism and angiodysplasia of the gut. A clinical trial in hyperparathyroidism patients using methylene blue and NIR fluorescence is currently ongoing in our center.

In conclusion, the current study demonstrated the first in human NIR fluorescence imaging of a SFT in the pancreas using MB, a registered and approved pharmaceutical. Larger series will be needed to confirm this result.

REFERENCES

1. Vahrmeijer AL, Frangioni JV. Seeing the invisible during surgery. *Br J Surg* 2011; 98:749-750.
2. Gioux S, Choi HS, Frangioni JV. Image-guided surgery using invisible near-infrared light: fundamentals of clinical translation. *Mol Imaging* 2010; 9:237-255.
3. Lee SB, Hassan M, Fisher R et al. Affibody molecules for in vivo characterization of HER2-positive tumors by near-infrared imaging. *Clin Cancer Res* 2008; 14:3840-3849.
4. Jiang T, Olson ES, Nguyen QT et al. Tumor imaging by means of proteolytic activation of cell-penetrating peptides. *Proc Natl Acad Sci U S A* 2004; 101:17867-17872.
5. Hutteman M, Mieog JS, van der Vorst JR et al. Intraoperative near-infrared fluorescence imaging of colorectal metastases targeting integrin $\alpha(v)\beta(3)$ expression in a syngeneic rat model. *Eur J Surg Oncol* 2011; 37:252-257.
6. Mieog JS, Hutteman M, van der Vorst JR et al. Image-guided tumor resection using real-time near-infrared fluorescence in a syngeneic rat model of primary breast cancer. *Breast Cancer Res Treat* 2010.
7. Han N, Bumpous JM, Goldstein RE et al. Intra-operative parathyroid identification using methylene blue in parathyroid surgery. *Am Surg* 2007; 73:820-823.
8. Paciullo CA, McMahon HD, Hattton KW et al. Methylene blue for the treatment of septic shock. *Pharmacotherapy* 2010; 30:702-715.
9. Fan ST. Liver functional reserve estimation: state of the art and relevance for local treatments: the Eastern perspective. *J Hepatobiliary Pancreat Sci* 2010; 17:380-384.
10. Hassenstein A, Meyer CH. Clinical use and research applications of Heidelberg retinal angiography and spectral-domain optical coherence tomography - a review. *Clin Experiment Ophthalmol* 2009; 37:130-143.
11. Schaafsma BE, Mieog JS, Hutteman M et al. The clinical use of indocyanine green as a near-infrared fluorescent contrast agent for image-guided oncologic surgery. *J Surg Oncol* 2011; 104:323-332.
12. Hagen A, Grosenick D, Macdonald R et al. Late-fluorescence mammography assesses tumor capillary permeability and differentiates malignant from benign lesions. *Opt Express* 2009; 17:17016-17033.
13. Maeda H, Wu J, Sawa T et al. Tumor vascular permeability and the EPR effect in macromolecular therapeutics: a review. *J Control Release* 2000; 65:271-284.
14. Hutteman M, van der Vorst JR, Mieog JS et al. Near-Infrared Fluorescence Imaging in Patients Undergoing Pancreaticoduodenectomy. *Eur Surg Res* 2011; 47:90-97.
15. Winer JH, Choi HS, Gibbs-Strauss SL et al. Intraoperative Localization of Insulinoma and Normal Pancreas Using Invisible Near-Infrared Fluorescent Light. *Ann Surg Oncol* 2009.
16. Mieog JS, Troyan SL, Hutteman M et al. Towards Optimization of Imaging System and Lymphatic Tracer for Near-Infrared Fluorescent Sentinel Lymph Node Mapping in Breast Cancer. *Ann Surg Oncol* 2011; 18:2483-2491.
17. Sugawara Y, Sakai S, Aono S et al. Solitary fibrous tumor of the pancreas. *Jpn J Radiol* 2010; 28:479-482.
18. Chetty R, Jain R, Serra S. Solitary fibrous tumor of the pancreas. *Ann Diagn Pathol* 2009; 13:339-343.
19. Ishiwatari H, Hayashi T, Yoshida M et al. [A case of solitary fibrous tumor of the pancreas]. *Nippon Shokakibyō Gakkai Zasshi* 2009; 106:1078-1085.
20. Kwon HJ, Byun JH, Kang J et al. Solitary fibrous tumor of the pancreas: imaging findings. *Korean J Radiol* 2008; 9 Suppl:S48-S51.
21. Srinivasan VD, Wayne JD, Rao MS et al. Solitary fibrous tumor of the pancreas: case report with cytologic and surgical pathology correlation and review of the literature. *JOP* 2008; 9:526-530.
22. Miyamoto H, Molena DA, Schoeniger LO et al. Solitary fibrous tumor of the pancreas: a case report. *Int J Surg Pathol* 2007; 15:311-314.
23. Gardini A, Dubini A, Saragoni L et al. [Benign solitary fibrous tumor of the pancreas: a rare location of extra-pleural fibrous tumor. Single case report and review of the literature]. *Pathologica* 2007; 99:15-18.
24. Chatti K, Nouria K, Ben RM et al. [Solitary fibrous tumor of the pancreas. A case report]. *Gastroenterol Clin Biol* 2006; 30:317-319.
25. Luttges J, Mentzel T, Hubner G et al. Solitary fibrous tumour of the pancreas: a new member of the small group of mesenchymal pancreatic tumours. *Virchows Arch* 1999; 435:37-42.

Part IV

Chapter 15

Summary and Future Perspectives

SUMMARY

Complete surgical resection of a tumor still is the single most important prognostic factor in most types of cancer. Many preoperative imaging modalities are being used to diagnose and stage patients and to finalize the surgical planning. However, during surgery only a limited number of tools can be used to identify tumors, and more importantly to differentiate between normal tissue and tumor tissue. Since it can be extremely challenging to assess the resection margins during surgery, irradical resections unfortunately still occur in a substantial part of patients. Near-infrared (NIR) fluorescence imaging has the potential to be of major impact on surgical treatment and surgical treatment in surgical oncology in particular. Intraoperative real-time visualization of tumors and lymph nodes can hopefully decrease the number of irradical resections and improve surgical outcome parameters such as time of surgery and surgical complications (**chapter 1**).

This thesis focus on preclinical validation of novel fluorescent contrast agents for solid tumor imaging (**Part I**), the clinical introduction of NIR fluorescence sentinel lymph node imaging in several cancer types using indocyanine green (**Part II**) and the clinical translation of NIR fluorescence imaging using clinically available fluorescent contrast agents for solid tumor imaging (**Part III**).

Part 1: Pre-clinical validation of near-infrared image guided surgery

Chapter 2 describes the preclinical optimization of intraoperative visualization of colorectal liver metastases using NIR fluorescence and indocyanine green (ICG). ICG has shown to passively accumulate around liver metastases, however optimal conditions in terms of injection time and dose were never tested. Several different time-points of ICG administration prior to surgery and several different dose groups were tested in an experimental syngeneic liver metastases rat model. All metastases could be identified after ICG injection. The highest tumor-to-liver ratio was obtained when ICG was administered 72 hours prior to surgery.

In head and neck surgery, positive resection margins severely impact patient outcome. Intraoperative assessment of resection margins could be of great value and has the potential to decrease the number of irradical resections. Since most head and neck cancers show high levels of EGFr expression, **chapter 3** describes the successful use of the EGFr –targeting nanobody 7D12 in an experimental orthotopic tongue

cancer mouse model. All tumors could be clearly identified and most importantly, the negative control nanobody showed no fluorescent uptake in the tumor.

Chapter 4 describes the use of the zwitterionic fluorophore ZW800-1 which was conjugated to the tumor specific peptide cRGD (targeting integrins) and to the α -specific peptide cRAD. These probes were injected in mice bearing subcutaneous and orthotopic HT-29 human colorectal tumors. Both subcutaneous and orthotopic tumors could be clearly identified using cRGD-ZW800-1. A significantly higher signal-to-background ratio (SBR) was observed in mice injected with cRGD-ZW800-1 compared to mice injected with cRAD-ZW800-1 or ZW800-1 alone when measured at 24 h after probe administration. The clearance of cRGD-ZW800-1 permitted visualization of the ureters and also generated minimal background fluorescence in the gastrointestinal tract.

Part 2: Clinical translation: Sentinel lymph node imaging

In vulvar cancer patients, SLN mapping is standard of care to obtain nodal staging. Typically, a blue dye and radiocolloids are being used, which have certain disadvantages. In **chapter 5**, the use of NIR fluorescence imaging was tested in vulvar cancer patients using different doses of ICG premixed with human serum albumin (complex ICG:HSA). In this study, a high identification rate of 100% was demonstrated. SLN mapping in vulvar cancer patients is in particular an interesting indication since the lymph nodes are often located superficially which enables NIR fluorescence imaging to percutaneously identify the SLN.

In cervical cancer, sentinel lymph node biopsies are not yet standard of care due to disappointing identification rates and high false-negative rates. In **chapter 6**, NIR fluorescence and ICG:HSA was used for sentinel lymph node mapping in cervical cancer patients. Three dose levels (1.6 ml of 500, 750 and 1000 μ M ICG:HSA) were tested. A high intraoperative identification rate of 100% was observed, no false negative cases were observed and no significant differences between dose groups could be identified. NIR fluorescence therefore has the potential to be used for SLN mapping in cervical cancer patients and can thereby possibly prevent a total lymphadenectomy in a large number of patients. However, this has to be assessed in larger clinical trials.

In-vitro and preclinical studies showed that premixing ICG with HSA increased fluorescent yield and increased hydrodynamic diameter, which possibly results in better retention in the SLN.¹ However, a randomized clinical study in breast cancer patients showed no differences between using ICG alone and

ICG:HSA.² This can possibly be explained by the physiologically available proteins in lymph fluid, which eliminate the need of premixing with HSA. In **chapter 7**, a randomized study is described, which tested the need of premixing ICG with HSA in cervical cancer patients. Based on **chapter 6**, a dose level of 500 μ M ICG (1.6 ml) alone or ICG:HSA was used. No significant differences could be observed between the ICG alone group and the ICG:HSA group. These results show that ICG alone can be used for SLN mapping in cervical cancer patients.

In **chapter 8**, the use of NIR fluorescence and ICG:HSA at different dose levels was tested in a clinical trial in melanoma patients. In all patients (N = 15), the SLN could be identified using NIR fluorescence. Thereby, SLNs could be percutaneously identified using NIR fluorescence in several cases. Using NIR fluorescence in melanoma patients, time of surgery could possibly be decreased. Furthermore, NIR fluorescence outperformed blue dye staining and the benefit of using patent blue needs to be assessed in future larger clinical trials.

The SLN procedure is not standard of care in oral cavity and oropharynx cancer patients. NIR fluorescence imaging using ICG:HSA was tested in patients which were planned for surgery for oral cavity or oropharynx carcinoma in **chapter 9**. Since standard of care in our center includes a complete neck dissection, a perfect platform is created to test the flow to higher tier lymph nodes using ICG:HSA. In all patients, a SLN could be identified during surgery and one false-negative case was observed. This can be explained by multiple drainage patterns, resulting in a subset of SLNs becoming fluorescent later, being incorrectly identified as higher tier lymph nodes. Future research should therefore be focused on fluorescent tracers that are retained in the first draining node(s), which makes it possible to perform imaging later after injection of the dye.

Previous clinical studies showed that SLN mapping in breast cancer patients can be performed using NIR fluorescence and that 1.6 ml 500 μ M of ICG alone is most optimal to use. In chapter 10, the need to use patent blue when using NIR fluorescence and radiocolloids has been assessed in a randomized trial. The results of this study show that patent blue can be omitted when NIR fluorescence and radiocolloids are used. In all cases, the SLN was identified with NIR fluorescence earlier than with patent blue. Furthermore, to preliminarily assess the needs of radiocolloids for SLN mapping in breast cancer patients the gamma probe was not used during the first 15 minutes of the operation. To identify the SLN, the gamma probe was still needed in 25% of patients. However, the body mass index of patients in whom the gamma probe was needed to identify the SLN

was significantly higher compared to the body mass index of patients in whom the SLN could be identified using only NIR fluorescence (33.1 ± 9.9 vs. 24.4 ± 5.4). These results suggest that BMI might be used eventually to select those patients in whom SLN mapping can be performed without the use of radiocolloids.

In summary, this thesis shows that a dose of $500\mu\text{M}$ of ICG administered as a volume of 1.6 ml without the need of premixing with HSA is optimal to use for the sentinel lymph node procedure in various cancer types that were studied in this thesis. Another recently developed approach is combining radioactive colloids with indocyanine green in one multimodal tracer.^{3,4} The advantage of this approach is the necessity of only one injection. Moreover, rather than visualizing lymph flow with fluorescence imaging, the hybrid approach individually illuminates the very nodes identified on lymphoscintigrams and SPECT/CT and thus combines preoperative results with intraoperative findings.

Part 3: Clinical translation: Solid tumor imaging

Chapter 11 was performed to clinically translate the results from **chapter 2**. In this study, ICG was injected prior to surgery to intraoperatively identify colorectal liver metastases using NIR fluorescence imaging. In 40 patients, median tumor-to-liver ratios of 7.0 (range 1.9-18.7) were observed. No differences in tumor-to-liver ratios were observed between dose and time groups. Therefore, the lowest tested dose of 10 mg is recommended. In 12.5 % (95 % CI: 5.0 -26.6) of patients, additional metastases, which would otherwise be missed, could be identified and resected using NIR fluorescence. Furthermore, it was shown that ICG accumulated in CK7-positive immature hepatocytes. It is known that immature hepatocytes often have impaired expression of their organic anion transporters, which are essential for the transport of many organic anions, including ICG. Consequently, the biliary excretion of ICG in immature hepatocytes can be reduced by 90%. Therefore, the pattern of rim fluorescence could be explained by the presence of immature hepatocytes in the liver tissue surrounding the tumor that have taken up ICG, but exhibit impaired biliary clearance.

In **chapter 12**, an attempt was made to use ICG to explore the enhanced permeability and retention (EPR) effect to intraoperatively identify pancreatic tumors. Even after a macroscopically curative resection of pancreatic tumors, tumor cells might be observed by microscopy at one or more edges of the resected specimen in 17–74%.⁵⁻⁷ Better visualization of pancreatic tumors during

surgery could therefore decrease the number of irradical resections. The EPR effect, which is based on leaky vessels and hampered lymphatic drainage and results in passive accumulation of agents in tumors has been described extensively. Since no tumor-specific contrast agents are yet available clinically, ICG was injected intravenously with the objective to explore the EPR effect in pancreatic cancer patients. However, no adequate contrast between tumor and normal pancreatic tissue could be observed in all but one patient, unfortunately. This is possibly the result of different tumor biology of pancreatic cancer when compared to other cancer types. Several earlier studies reported a lower perfusion of tumor tissue in comparison with healthy pancreas tissue, which might decrease availability of ICG for a potential EPR effect of the tumor.^{8,9} Concluding, pancreatic cancer is not a suitable tumor type to exploit the EPR effect. On the other hand, results will not be distorted by the EPR effect when using tumor-targeting fluorescent agents.

The intraoperative identification of parathyroid adenomas can be challenging, which results in surgical complications and reoperations. In the past, methylene blue has been used to macroscopically stain parathyroid glands during surgery. However, since high doses were necessary for visual identification and toxicity could occur, this was stopped. As methylene blue is a medium-strength fluorophore when diluted to doses invisible to the human eye, **chapter 13** describes the use of NIR fluorescence and low-dose methylene blue in parathyroid surgery. In 10 of 12 patients, histology confirmed a parathyroid adenoma and in 9 of these patients, NIRF could clearly identify the parathyroid adenoma during surgery. Seven of these 9 patients had a positive preoperative ^{99m}Tc-sestamibi SPECT scan. Importantly, in two patients, parathyroid adenomas could be identified only using NIRF. This is the first study to show that low-dose MB can be used as NIRF tracer for identification of parathyroid adenomas, and suggests a correlation with preoperative ^{99m}Tcsestamibi SPECT scanning.

As discussed in the **chapter 13**, based on an unknown mechanism, methylene blue accumulates in neuro-endocrine tissue. This mechanism could be used to identify neuro-endocrine tumors of the pancreas by injecting methylene blue during surgery. **Chapter 14** describes a case study in which methylene blue was intravenously injected in a patient suffering from an extremely rare solitary fibrous tumor of the pancreas. In this case, the pancreatic tumor could be clearly identified during surgery and maximum tumor-to-background ratio of approximately 3 was observed.

FUTURE PERSPECTIVES

NIR fluorescent contrast agents

The clinical availability of the fluorescent contrast agents indocyanine green and methylene blue, which were used in part II and III of this thesis resulted in a fast introduction of NIR fluorescence imaging in cancer surgery. Thereby, it significantly contributed to the practical knowledge of using NIR fluorescence imaging during surgery. However, both these agents cannot be conjugated to other molecules without changing their chemical structure, which will result in the necessity to conduct phase 0 and 1 clinical trials. Moreover, fluorescent brightness of both ICG and MB are by far not optimal. In order to determine the true clinical benefit of this technique, development and clinical assessment of contrast agents tailored to specific applications are essential. In this perspective, the development of novel targeted probes starts with clinically-compatible fluorophores. Although several fluorophores have been studied and tested preclinically, to date only two fluorophores made it towards the process of clinical translation. IRDye 800CW (LI-COR Biosciences, Lincoln, NE) and ZW800-1 (The FLARE Foundation, Wayland, MA) are both small molecules which are easily conjugatable to targeting ligands. Initial toxicity studies of both compounds showed no toxicity and the purely renal clearance of ZW800-1, and the combined renal and hepatic clearance of IRDye 800CW, enable these agents to be used for imaging of ureters and bile ducts.

Combining these NIR fluorophores with clinically available antibodies could usher in a new generation of NIR fluorescent contrast agents. As recently reviewed by Scheuer and colleagues¹⁰ clinically approved targeted antibodies are available for various tumors and tumor markers, for example bevacizumab (Genentech, San Francisco, CA) against the vascular endothelial growth factor A, cetuximab against the epidermal growth factor receptor (Bristol-Myers Squibb, New York City, NY, and Eli Lilly, Indianapolis, IN), and trastuzumab against the human epidermal growth factor receptor 2 (Genentech, San Francisco, CA). Indeed, van Dam and colleagues are currently accruing patients in the first clinical trial using bevacizumab conjugated to IRDye 800CW.¹¹ Next to antibodies, which have several disadvantages such as their large size and long circulation time, other smaller targeting molecules have been advocated and even successfully translated into the clinic. Cyclic arginine-glycine-aspartic acid (cRGD) has been extensively used clinically in positron emission tomography studies mostly in glioblastoma patients.¹²⁻¹⁴ cRGD conjugated to ZW800-1 (cRGD-ZW800-1) was first described by Choi et al^{15,16} and was preclinically

used to clearly visualize orthotopic colon tumors in mice (*unpublished data*). Another approach to overcome the drawbacks of intact antibodies is the use of smaller antigen binding fragments such as nanobodies (chapter 3 of this thesis).¹⁷

Imaging system development and optimization

During the last decade, many different imaging systems, designed and developed by both academic and industry groups, for open, laparoscopic, thoracoscopic, and robotic surgery were used for NIR fluorescence imaging studies.^{4,18-24} The optics, usability, fluorescence excitation source and power and cost are key issues in imaging system design. There should be a balance between maximizing the fluence rate of the excitation light, which increases tissue penetration depth and minimizing undesirable effects such as skin/eye exposure, irreversible photochemical bleaching of the NIR fluorophore, and tissue heating. To avoid these issues and to avoid the need to wear laser goggles, fluence rates are mostly limited to the 10-25 mW/cm² range. A few imaging systems are able to acquire multiple wavelengths of light at the same time.^{19,23} This enables the visualization of the targeted tissue in relation to the surrounding tissue anatomy. For example, tumor identification and nerve visualization in pelvic surgery for rectal cancer would be extremely beneficial. Furthermore, using software based correction techniques, it is also possible to discriminate between multiple contrast agents emitting at a nearly similar wavelength.^{25,26} NIR fluorescence imaging can also be of particular benefit in laparoscopic and robot assisted surgery, in which there exists diminished tactile feedback. NIR fluorescence-capable fiberscopic systems are now readily available for these applications.^{4,27,28} Further technical developments of these laparoscopic NIR imaging systems are in progress aiming to improve the real-time intraoperative display of NIR fluorophores.

Limitations and leverage

The major disadvantage of using NIR fluorescence and reason for it being an adjunct rather than a substitute of other imaging modalities is the limited penetration depth. NIR fluorescence imaging (which uses reflectance-based systems) is not able to visualize structures that are located more than 5 mm to 1 cm beneath the tissue surface. Therefore, the field of intraoperative imaging is moving towards combining imaging modalities. Imaging modalities based on radioactive tracers, such as preoperative PET and SPECT, and intraoperative gamma probes and gamma cameras, have depth sensitivity to several cm but cannot provide real-time and precise visualization. Intraoperative ultrasound imaging also has superior depth penetration when compared with NIR fluorescence, but requires tissue contact and has problems visualizing smaller and superficial lesions. Combining NIR fluorescence imaging with these modalities leverages the key benefits, whilst overcoming the limited penetration depth of NIR light.

Conclusion and path to routine patient care

NIR fluorescence image-guidance during cancer surgery has the potential to change patient management by visualizing tissue demarcation in real-time, thereby increasing the completeness of surgery and decreasing the morbidity associated with damage to normal structures. As stated before, the limited penetration depth will make NIR fluorescence imaging complementary to existing techniques rather than replacing them. However, results of studies using the first generation imaging systems and clinically available contrast agents are extremely promising and feasibility has been proven in many clinical studies. That leaves the main question, when will it become part of routine patient care? As we know from other promising imaging techniques that made it to wide clinical implementation, such as magnetic resonance imaging and computed tomography, adaptation had to satisfy two major criteria; changing patient management and being clinically realistic. Thus, it needs to have a significant impact on patient care and it cannot disrupt normal workflow. Thereby, since insurance companies and governments try to streamline (reign in) health care, a novel imaging modality also needs to make patient care faster, better, and cheaper. NIR fluorescence imaging has the ability to meet all criteria as the surgeon can possibly identify the targeted tissue faster and it will not disrupt normal workflow, as the surgical field will not be hampered. If NIR fluorescence imaging will increase the number of radical resections and decrease complication rates, then healthcare costs can and will be significantly reduced, but most importantly, patient care and prognosis will be improved.

REFERENCES

1. Ohnishi S, Lomnes SJ, Laurence RG et al. Organic alternatives to quantum dots for intraoperative near-infrared fluorescent sentinel lymph node mapping. *Mol Imaging* 2005; 4:172-181.
2. Hutteman M, Mieog JS, van der Vorst JR et al. Randomized, double-blind comparison of indocyanine green with or without albumin premixing for near-infrared fluorescence imaging of sentinel lymph nodes in breast cancer patients. *Breast Cancer Res Treat* 2011; 127:163-170.
3. Brouwer OR, Klop WM, Buckle T et al. Feasibility of Sentinel Node Biopsy in Head and Neck Melanoma Using a Hybrid Radioactive and Fluorescent Tracer. *Ann Surg Oncol* 2011; 19:1988-1994.
4. van der Poel HG, Buckle T, Brouwer OR et al. Intraoperative laparoscopic fluorescence guidance to the sentinel lymph node in prostate cancer patients: clinical proof of concept of an integrated functional imaging approach using a multimodal tracer. *Eur Urol* 2011; 60:826-833.
5. Jamieson NB, Foulis AK, Oien KA et al. Positive mobilization margins alone do not influence survival following pancreaticoduodenectomy for pancreatic ductal adenocarcinoma. *Ann Surg* 2010; 251:1003-1010.
6. Raut CP, Tseng JF, Sun CC et al. Impact of resection status on pattern of failure and survival after pancreaticoduodenectomy for pancreatic adenocarcinoma. *Ann Surg* 2007; 246:52-60.
7. Verbeke CS. Resection margins in pancreatic cancer. *Surg Clin North Am* 2013; 93:647-662.
8. Reuter SR, Redman HC, Bookstein JJ. Differential problems in the angiographic diagnosis of carcinoma of the pancreas. *Radiology* 1970; 96:93-99.
9. Komar G, Kauhanen S, Liukko K et al. Decreased blood flow with increased metabolic activity: a novel sign of pancreatic tumor aggressiveness. *Clin Cancer Res* 2009; 15:5511-5517.
10. Scheuer W, van Dam GM, Dobosz M et al. Drug-based optical agents: infiltrating clinics at lower risk. *Sci Transl Med* 2012; 4:134ps11.
11. US National Library of Medicine. VEGF-targeted Fluorescent Tracer Imaging in Breast Cancer. *Clinicaltrials.gov* [online] NCT01508572. 2014.
12. Beer AJ, Haubner R, Goebel M et al. Biodistribution and pharmacokinetics of the alphavbeta3-selective tracer 18F-galacto-RGD in cancer patients. *J Nucl Med* 2005; 46:1333-1341.
13. Beer AJ, Niemeyer M, Carlsen J et al. Patterns of alphavbeta3 expression in primary and metastatic human breast cancer as shown by 18F-Galacto-RGD PET. *J Nucl Med* 2008; 49:255-259.
14. Beer AJ, Kessler H, Wester HJ et al. PET Imaging of Integrin alphaVbeta3 Expression. *Theranostics* 2011; 1:48-57.
15. Choi HS, Nasr K, Alyabyev S et al. Synthesis and in vivo fate of zwitterionic near-infrared fluorophores. *Angew Chem Int Ed Engl* 2011; 50:6258-6263.
16. Choi HS, Gibbs SL, Lee JH et al. Targeted zwitterionic near-infrared fluorophores for improved optical imaging. *Nat Biotechnol* 2013; 31:148-153.
17. Sabrina Oliveira, Guus A.M.S.van Dongen, Marijke Stigter-van Walsum et al. Rapid Visualization of Human Tumor Xenografts through Optical Imaging with a Near-infrared Fluorescent Anti-Epidermal Growth Factor Receptor Nanobody. *Molecular Imaging* 2011.
18. Hirche C, Engel H, Kolios L et al. An experimental study to evaluate the fluobeam 800 imaging system for fluorescence-guided lymphatic imaging and sentinel node biopsy. *Surg Innov* 2013; 20:516-523.
19. Troyan SL, Kianzad V, Gibbs-Strauss SL et al. The FLARE intraoperative near-infrared fluorescence imaging system: a first-in-human clinical trial in breast cancer sentinel lymph node mapping. *Ann Surg Oncol* 2009; 16:2943-2952.
20. Yamauchi K, Nagafuji H, Nakamura T et al. Feasibility of ICG fluorescence-guided sentinel node biopsy in animal models using the HyperEye Medical System. *Ann Surg Oncol* 2011; 18:2042-2047.
21. Spinoglio G, Piora F, Bianchi PP et al. Real-time near-infrared (NIR) fluorescent cholangiography in single-site robotic cholecystectomy (SSRC): a single-institutional prospective study. *Surg Endosc* 2013; 27:2156-2162.
22. Mieog JS, Hutteman M, van der Vorst JR et al. Image-guided tumor resection using real-time near-infrared fluorescence in a syngeneic rat model of primary breast cancer. *Breast Cancer Res Treat* 2010.

23. Crane LM, Themelis G, Pleijhuis RG et al. Intraoperative multispectral fluorescence imaging for the detection of the sentinel lymph node in cervical cancer: a novel concept. *Mol Imaging Biol* 2011; 13:1043-1049.
24. Yamashita S, Tokuishi K, Anami K et al. Video-assisted thoracoscopic indocyanine green fluorescence imaging system shows sentinel lymph nodes in non-small-cell lung cancer. *J Thorac Cardiovasc Surg* 2011; 141:141-144.
25. Themelis G, Yoo JS, Ntziachristos V. Multispectral imaging using multiple-bandpass filters. *Opt Lett* 2008; 33:1023-1025.
26. Kumar AT, Chung E, Raymond SB et al. Feasibility of in vivo imaging of fluorescent proteins using lifetime contrast. *Opt Lett* 2009; 34:2066-2068.
27. Borofsky MS, Gill IS, Hemal AK et al. Near-infrared fluorescence imaging to facilitate super-selective arterial clamping during zero-ischaemia robotic partial nephrectomy. *BJU Int* 2013; 111:604-610.
28. van der Pas MH, Ankersmit M, Stockmann HB et al. Laparoscopic sentinel lymph node identification in patients with colon carcinoma using a near-infrared dye: description of a new technique and feasibility study. *J Laparoendosc Adv Surg Tech A* 2013; 23:367-371.

Nederlandse samenvatting
List of Publications
Curriculum Vitae
Dankwoord

NEDERLANDS SAMENVATTING

Complete chirurgische resectie van een tumor is nog steeds de belangrijkste prognostische factor in de meeste typen kanker. Beeldvormende technieken worden preoperatief vaak ingezet om patiënten te diagnosticeren, te stadiëren en om een chirurgisch plan te maken. Echter, tijdens de operatie kan maar een zeer beperkt aantal hulpmiddelen gebruikt worden om tumoren op te sporen en nog belangrijker, de grens tussen tumor en normaal weefsel aan te duiden. Daar het vaak erg lastig is om de resectiemarges tijdens de operatie te bepalen komen irradicale resecties helaas nog in een substantieel deel van patiënten voor. Nabij-infrarood (NIR) fluorescentie zou in potentie een grote impact kunnen hebben op de chirurgische behandeling van tumoren. Intraoperatieve beeldvorming van tumoren en lymfeklieren in real-time kan het aantal irradicale resectie hopelijk verminderen en de chirurgische outcome verbeteren.

Dit proefschrift richt zich op de preklinische validatie van nieuwe fluorescente contrastmiddelen voor intraoperatieve imaging van solide tumoren (**Deel 1**), de klinische introductie van NIR fluorescentie binnen de schildwachtklier (SLN) procedure in verschillende kankertypen met indocyanine groen (ICG) (**Deel 2**) en de klinische translatie van NIR fluorescente beeldvorming van solide tumoren met klinisch beschikbare contrastmiddelen (**Deel 3**).

Deel 1: preklinische validatie van nabij-infrarood fluorescente beeldgeleide chirurgie

Hoofdstuk 2 beschrijft de preklinische optimalisatie van intraoperatieve visualisatie van colorectale levermetastasen met NIR fluorescentie en indocyanine groen. ICG accumuleert passief rondom levermetastasen, echter de optimale condities wat betreft tijdstip van injecteren en dosis werden nooit onderzocht. In een syngene levermetastasen ratmodel werden verschillende momenten van injecteren en verschillende dosisgroepen met elkaar vergeleken. Alle metastasen werden geïdentificeerd middels NIR fluorescentie en ICG. De hoogste tumor-lever ratio werd bereikt in de groep waar ICG 72 uur voor de operatie werd geïnjecteerd. Tussen verschillende dosisgroepen werd geen significant verschil gevonden.

In de hoofd-halschirurgie hebben positieve resectiemarges een enorme invloed op de overleving van patiënten. Intraoperatieve beoordeling van resectievlakken zou van grote waarde zijn en zou het aantal radicale resecties kunnen verminderen. Daar tumoren in het hoofd-halsgebied vaak een hoge epithelial growth factor receptor (EGFr) expressie vertonen werd in **hoofdstuk 3** het EGFr-targeting nanobody 7D12 getest in een orthotopisch tongcarcinoom muismodel. Alle tumoren konden duidelijk worden geïdentificeerd het negatieve controle nanobody vertoonde geen opname in de tumor.

Hoofdstuk 4 beschrijft het gebruik van de fluorescente stof ZW800-1, welke werd geconjugeerd aan het tumorspecifieke peptide cRGD (target integrines) en het specifieke cRAD. Deze probes werden geïnjecteerd in muizen met humane subcutane en orthotopische HT-29 colontumoren. Zowel de subcutane als orthotopische tumoren konden duidelijk worden geïdentificeerd met cRGD-ZW800-1. Een significant hogere signaal-tot-achtergrond ratio werd gemeten in muizen geïnjecteerd met cRGD-ZW800-1 vergeleken met muizen geïnjecteerd met cRAD-ZW800-1 of ZW800-1 alleen. Deze metingen werden verricht na 24 uur. De renale klaring van cRGD-ZW800-1 maakte het mogelijk om de ureteren intraoperatief te identificeren met NIR fluorescentie.

Deel 2: klinische translatie: schildwachtklier procedure

In patiënten met een vulvacarcinoom wordt de SLN procedure standaard uitgevoerd. De conventionele techniek beschrijft het gebruik van een blauwe kleurstof en radiocolloïden. **Hoofdstuk 5** beschrijft het gebruik van NIR fluorescentie in vulvacarcinoom patiënten met verschillende doseringen ICG gemixt met humaan serum albumine (complex: ICG:HSA). In deze studie werd een hoge identificatieratio van 100% bereikt. De SLN procedure is in deze patiëntenpopulatie bij uitstek interessant daar de klieren meestal oppervlakkig gelegen zijn en veelal percutaan gedetecteerd konden worden.

In patiënten met een cervixcarcinoom wordt de SLN procedure niet standaard uitgevoerd wegens tegenvallende identificatie percentages en hoge percentages fout-negatieve patiënten. In **hoofdstuk 6** werd NIR fluorescentie en ICG:HSA (in drie dosis groepen) gebruikt voor de SLN procedure in patiënten met een cervixcarcinoom. Een hoog intraoperatief identificatie percentage van 100% en geen fout-negatieve patiënten werden geobserveerd. Er werden geen significante verschillen tussen dosisgroepen gevonden. Hoewel het nog onderzocht moet

worden in grotere studies zou NIR fluorescentie gebruikt kunnen worden voor de SLN procedure in patiënten met cervixcarcinoom en zou hiermee in de toekomst veel patiënten een complete lymfadenectomie bespaard kunnen worden.

In-vitro en preklinische studies laten zien dat het mixen van ICG met HSA de fluorescente eigenschappen verbetert en de hydrodynamische diameter vergroot. Hierdoor wordt wellicht een betere retentie in de eerste echilon lymfeklier bewerkstelligt. In **hoofdstuk 7** wordt een gerandomiseerde studie beschreven die het nut van het mixen van ICG met HSA onderzoekt in patiënten met een cervixcarcinoom. Op data verkregen uit **hoofdstuk 6** werd een dosis van 500 μ M ICG (1.6 ml) gebruikt. Er werden geen significante verschillen tussen de ICG alleen groep en de ICG gemixt met HSA groep gevonden.

In **hoofdstuk 8** werd het gebruik van NIR fluorescentie en ICG:HSA in verschillende doseringen getest in patiënten met een melanoom. In alle 15 patiënten kon de SLN (vaak percutaan) geïdentificeerd worden. Verder liet het gebruik van NIR fluorescentie et ICG:HSA betere resultaten zien dan het gebruik van patent blauw.

De SLN procedure wordt niet standaard uitgevoerd in patiënten met tumoren in de mondholte of oropharynx. NIR fluorescentie met behulp van ICG:HSA werd getest in patiënten die werden geopereerd aan een tumor in de mondholte of oropharynx in **hoofdstuk 9**. Omdat deze patiëntenpopulatie standaard een volledige halsklierdissectie ondergaat ontstond er een ideaal platform om doorstroming van ICG:HSA naar hogere echilon klieren te testen. In alle patiënten werd tenminste 1 SLN geïdentificeerd waarbij 1 fout-negatieve patiënt geobserveerd werd. Daarbij werd geobserveerd dat ICG:HSA relatief snel doorstroomde naar hogere echilon klieren.

Eerdere studies lieten zien dat de SLN procedure in borstkanker patiënten uitgevoerd kan worden met NIR fluorescentie en dat het gebruik van 1.6 ml 500 μ M ICG alleen de meest optimale condities creëert. In **hoofdstuk 10** werd het nut van het gebruik van patent blauw naast NIR fluorescentie en het radiocolloid onderzocht in een gerandomiseerde studie. Deze studie laat zien dat patent blauw weggelaten kan worden wanneer het radiocolloid in combinatie met ICG:HSA gebruikt wordt. Verder werd de gammaprobe in deze studie de eerste 15 minuten niet gebruikt om de noodzaak van het gebruik van radiocolloiden te testen. Om de SLN te vinden was de gammaprobe nog noodzakelijk in 25% van de patiënten. Wel bleken deze patiënten een significant hogere body-mass index te hebben, iets wat in de toekomst zou kunnen helpen bij de selectie van patiënten waarbij het gebruik van radiocolloiden niet meer nodig is.

Samengevat beschrijft dit proefschrift dat een dosis van 500 μ M ICG toegediend als een volume van 1.6 ml zonder het premixen van HSA optimaal is voor de SLN procedure in verschillende typen kanker. Een andere recentelijk ontwikkelde aanpak is het combineren van de radiocolloïden met ICG in 1 multimodale tracer. Het voordeel van deze aanpak is de noodzaak van enkel een injectie in plaats van twee. Daarnaast kan de data van preoperatieve beeldvormende modaliteiten als de lymfoscintigrafieën en de SPECT/CT gerelateerd worden met intraoperatieve bevindingen.

Deel 3: Klinische translatie: beeldvorming van solide tumoren

Hoofdstuk 11 beschrijft de klinische translatie van **hoofdstuk 2**. In deze studie werd ICG voor de operatie intraveneus toegediend om colorectale levermetastasen intraoperatief te identificeren middels NIR fluorescentie. In 40 patiënten werd een mediane ratio tussen signaal in de tumor en signaal in de lever van 7.0 (bereik 1.9 – 18.7) geobserveerd. Er werden geen verschillen gevonden tussen dosisgroepen en het moment van injectie had geen invloed op de resultaten. Hierdoor werd de laagst geteste dosis van 10mg ICG aanbevolen. In 12.5% van de patiënten werd een additionele metastasen gevonden, welke anders gemist zou zijn. Immunohistochemische kleuringen lieten zien dat ICG ophoopt in immature hepatocyten gelegen rondom de metastasen.

In **hoofdstuk 12** werd getracht het enhanced-permeability and retention (EPR) effect te gebruiken en met ICG en NIR fluorescentie pancreas tumoren te identificeren. Het EPR-effect is gebaseerd op lekkende bloedvaten en verminderde lymfe afvoer, waardoor er passieve accumulatie in tumoren ontstaat. Helaas bleek het met ICG niet mogelijk een adequaat contrast tussen tumor en omliggend pancreasweefsel te bereiken.

De intraoperatieve identificatie van bijschildklieradenomen kan erg uitdagend zijn en resulteert soms in chirurgische complicaties en re-operaties. In het verleden werd methyleen blauw (MB) gebruikt voor macroscopische identificatie van bijschildklieradenomen. Echter, omdat er hoge doseringen nodig voor een goed signaal in het adenoom en dit een risico op toxiciteit met zich mee bracht is het gebruik van MB gestopt. Omdat MB een gemiddeld sterke fluorescente stof is wanneer verdund tot doses die onzichtbaar zijn met blote oog werd in **hoofdstuk 13** het gebruik hiervan in patiënten met een bijschildklieradenoom onderzocht. In 10 van de 12 patiënten bevestigde histologisch onderzoek een bijschildklieradenoom.

In 9 van deze 10 patiënten kon MB en NIR fluorescentie het bijschildklieradenoom intraoperatief duidelijk identificeren. Zeven van deze 9 patiënten had een positieve preoperatieve ^{99m}Tc -sestamibi SPECT scan. In 2 patiënten in deze studie werd het bijschildklieradenoom enkel met NIR fluorescentie gevonden.

Zoals besproken in **hoofdstuk 13**, gebaseerd op een onbekend mechanisme, hoopt MB zich op in neuro-endocrien weefsel. **Hoofdstuk 14** beschrijft het succesvol gebruik van MB en NIR fluorescentie in een patiënt met een solitaire fibreuze tumor van het pancreas.

CONCLUSIE

NIR fluorescentie geleide chirurgie heeft de potentie patiëntenzorg te verbeteren door de demarcatie van tumor en normaal weefsel tijdens de operatie in beeld te brengen. Hiermee zou het aantal irradicale resecties verminderd en de morbiditeit geassocieerd met schade aan vitale structuren beperkt kunnen worden. Dan rest nog 1 vraag, wanneer zal het deel uit gaan maken van de standaard zorg? Zoals we weten van andere veelbelovende beelvormende technieken die brede klinische implementatie hebben gekend, zoals de magnetic resonance imaging (MRI) en computed tomography (CT), zal moeten voldaan worden aan 2 criteria: het kunnen veranderen van patiëntenzorg en klinisch realistisch zijn. Dus, impact op patiëntenzorg zonder de normale workflow te beïnvloeden. Daar overheden en verzekeringsmaatschappijen voortdurend bezig zijn de zorg te 'stroomlijnen' dient een nieuwe techniek daarnaast patiëntenzorg ook snelle, effectiever, goedkoper en beter te maken. Mijns inziens heeft NIR fluorescentie de potentie aan al deze criteria te voldoen en ik verwacht dat de techniek spoedig breed geïmplementeerd zal worden.

LIST OF PUBLICATIONS

Tummers QR, Verbeek FP, Schaafsma BE, Boonstra MC, **van der Vorst JR**, Liefers GJ, van de Velde CJ, Frangioni JV, Vahrmeijer AL, Towards real-time detection of positive margins in breast cancer: intraoperative near-infrared fluorescence imaging using methylene blue, *Eur J Surg Oncol*, *in press*, 2014

Verbeek FP*, **van der Vorst JR***, Tummers QR, Boonstra MC, de Rooij KE, Lowik CW, Valentijn AR, van de Velde CJ, Choi HS, Frangioni JV, Vahrmeijer AL, Near-infrared fluorescent imaging of both colorectal cancer and ureters using a low- dose integrin targetted probe, *Ann Surg Oncol*, 2014 Feb 11.

Verbeek FP, Schaafsma BE, Tummers QR, **van der Vorst JR**, van der Made WJ, Baeten CI, Bonsing BA, Frangioni JV, van de Velde CJ, Vahrmeijer AL, Swijnenburg RJ, Optimization of near-infrared fluorescence cholangiography for open and laparoscopic surgery, *Surg Endosc*. 2013 Nov 14

van Driel PB*, **van der Vorst JR***, Verbeek FP, Oliveira S, Snoeks TJ, Keereweer S, Frangioni JV, van Bergen Henegouwen PM, Vahrmeijer AL, Lowik CW, Intraoperative fluorescence delineation of head and neck cancer with a fluorescent anti-epidermal growth factor receptor nanobody, *Int J Cancer*. 2013 Nov 13

Vahrmeijer AL, Hutteman M, **van der Vorst JR**, van de Velde CJ, Frangioni JV, Image-guided cancer surgery using near-infrared fluorescence, *Nat Rev Clin Oncol*. 2013 Sep;10(9):507-18

van der Vorst JR*, Schaafsma BE*, Hutteman M, Verbeek FP, Liefers GJ, Hartgrink HH, Smit VJ, Frangioni JV, van de Velde CJ, Vahrmeijer AL, Near-infrared fluorescence imaging of colorectal liver metastases patients using indocyanine green, *Cancer*. 2013 Sep 15;119(18):3411-8

van der Vorst JR*, Schaafsma BE*, Verbeek FP, Swijnenburg RJ, Hutteman M, Hamming JF, Kievit J, Frangioni JV, van de Velde CJ, Vahrmeijer AL, Intraoperative near-infrared fluorescence imaging of parathyroid adenomas using low-dose methylene blue, *Head Neck*. 2013 May 29.

Schaafsma BE, Verbeek FP, Rietbergen DD, van der Hiel B, **van der Vorst JR**, Tummers QR, Liefers GJ, Frangioni JV, van de Velde CJ, van Leeuwen FW, Vahrmeijer AL, Combined radio- and fluorescence-guided sentinel lymph node biopsy in breast cancer, *Br J Surg*. 2013 Jul;100(8):1037-44.

Wong CY, de Vries MR, Wang Y, **van der Vorst JR**, Rothuizen TC, van Zonneveld AJ, Roy-Chaudhury P, Rabelink TJ, Quax PH, Rotmans JI, A novel murine model of arteriovenous fistula failure; unravelling vascular remodeling and intimal hyperplasia, *J Vasc Surg*. 2014 Jan;59(1):192-201

Verbeek FP, **van der Vorst JR**, Schaafsma BE, Swijnenburg RJ, Gaarenstroom KN, Elzevier HW, van de Velde CJ, Frangioni JV, Vahrmeijer AL, Intraoperative near-infrared fluorescence-guided identification of the ureters using low-dose methylene blue: a first-in-human experience, *J Urol*. 2013 Aug;190(2):574-9

Deneuve S, Rivera C, Carrabin N, Mieog JS, Malyshec N, **van der Vorst JR**, Mordant P, Quality of life of surgical oncology residents and fellows across Europe, 2013, *J of Surg Educ*

Schaafsma BE, Verbeek FP, Peters AW, **van der Vorst JR**, de Kroon CD, van Poelgeest MI, Trimbos JB, van de Velde CJ, Frangioni JV, Vahrmeijer AL, Gaarenstroom KN, Randomized comparison of lymphatic tracers for near-infrared fluorescence sentinel lymph node biopsy in vulvar cancer, *BJOG*. 2013 May;120(6):758-64

Schaafsma BE, Verbeek FP, **van der Vorst JR**, Hutteman M, Kuppen PJ, Frangioni JV, van de Velde CJ, Vahrmeijer AL, Ex vivo sentinel lymph node mapping in colon cancer combining both blue dye staining and near-infrared fluorescence imaging, *J Surg Res*. 2013 Jul;183(1):253-7

van der Vorst JR*, Schaafsma BE*, Verbeek FP, Swijnenburg RJ, Hutteman M, Liefers GJ, van de Velde CJ, Frangioni JV, Vahrmeijer AL, Dose optimization for near-infrared fluorescence sentinel lymph node mapping in melanoma patients, *Br J Dermatol*. 2013 Jan;168(1):93-8

van der Vorst JR, Schaafsma BE, Verbeek FP, Keereweer S, Jansen J, van der Velde LA, Langeveld A, Hutteman M, Lowik CW, van de Velde CJ, Frangioni JV, Vahrmeijer AL, Near-Infrared Fluorescence Sentinel Lymph Node Mapping of the Oral Cavity in Head and Neck Cancer Patients, *Oral Oncol*. 2013 Jan;49(1):15-9.

van der Vorst JR, Vahrmeijer AL, Hutteman M, Bosse T, Smit VT, van de Velde CJ, Frangioni JV, Bonsing BA, Near-infrared fluorescence imaging of a solitary fibrous tumor of the pancreas using methylene blue, *World J Gastrointest Surg*. 2012 Jul 27;4(7):180-4.

Schaafsma BE*, **van der Vorst JR***, Gaarenstroom KA, Peters AA, Verbeek FP, de Kroon CD, Trimbos JB, Poelgeest MI, Frangioni JV, Vahrmeijer AL, Randomized Comparison of Near-Infrared Fluorescence Lymphatic Tracers for Sentinel Lymph Node Mapping of Cervical Cancer, *Gynecol Oncol*. 2012 Oct;127(1):126-30.

Verbeek FP, **van der Vorst JR**, Schaafsma BE, Hutteman M, van Leeuwen F, Bonsing BA, van de Velde CJ, Frangioni JV, Vahrmeijer AL, Image-guided hepatopancreatobiliary surgery using near-infrared fluorescent light, *J Hepatobiliary Pancreat Sci*. 2012 Nov;19(6):626-37

van der Vorst JR, Schaafsma BE, Verbeek FP, Hutteman M, Mieog JS, Lowik CW, Liefers GJ, Frangioni JV, van de Velde CJ, Vahrmeijer AL, Randomized comparison of near-infrared fluorescence imaging using indocyanine green and ^{99m}Tc with or without patent blue for the sentinel lymph node procedure in breast cancer patients, *Ann Surg Oncol*. 2012 Dec;19(13):4104-11

van Dam RM, Wong-Lun-Hing EM, van Breukelen GJ, Stoot JH, **van der Vorst JR**, Bemelmans MH, Olde Damink SW, Lassen K, Dejong CH, The ORANGE II-Trial: an international multicentre randomised controlled trial of optimised surgical recovery after left lateral hepatic sectionectomy: open versus laparoscopic surgery within an enhanced recovery (ERAS) programme, *Trials*. 2012 May 6;13:54.

van der Vorst JR*, Hutteman M*, Gaarenstroom K, Peters AA, Mieog JS, Schaafsma BE, Kuppen PJ, Frangioni JV, van de Velde CJ, Vahrmeijer AL, Optimization of Near-Infrared Fluorescent Sentinel Lymph Node Mapping in Cervical Cancer Patients, *Int J of Gyn Can*, 2011, *Int J Gynecol Cancer*. 2011 Nov;21(8):1472-8.

Hutteman M*, **van der Vorst JR***, Gaarenstroom K, Peters AA, Mieog JS, Schaafsma BE, Kuppen PJ, Frangioni JV, van de Velde CJ, Vahrmeijer AL, Optimization of Near-Infrared Fluorescent Sentinel Lymph Node Mapping in Vulvar Cancer Patients, *Am J Obstet Gynecol.* 2012 Jan;206(1):89.e1-5.

Hutteman M*, **van der Vorst JR***, Mieog JS, Bonsing BA, Hartgrink HH, Kuppen PJ, Lowik CW, Frangioni JV, van de Velde CJ, Vahrmeijer AL, Near-infrared fluorescence imaging in patients undergoing a pancreatoduodenectomy, *Eur Surg Res.* 2011;47(2):90-7.

Schaafsma BE, Mieog JS, Hutteman M, **van der Vorst JR**, Kuppen PJ, Lowik CW, Frangioni JV, van de Velde CJ, Vahrmeijer AL, The clinical use of indocyanine green as a near-infrared fluorescent contrast agent for image-guided oncologic surgery, *J Surg Oncol.* 2011 Sep 1;104(3):323-32

van der Vorst JR, Hutteman M, Mieog JS, de Rooij KE, Kaijzel EL, Löwik CW, Putter H, Kuppen PJ, Frangioni JV, van de Velde CJ and Vahrmeijer AL, Near-Infrared Fluorescence Imaging of Liver Metastases in Rats using Indocyanine Green, *J Surg Res.* 2012 May 15;174(2):266-71

Mieog JS, Troyan SL, Hutteman M, Donohoe KJ, **van der Vorst JR**, Stockdale A, Liefers GJ, Choi HS, Gibbs-Strauss SL, Putter H, Gioux S, Kuppen PJ, Ashitate Y, Löwik CW, Smit VT, Oketokoun R, Ngo LH, van de Velde CJ, Frangioni JV, Vahrmeijer AL, Toward optimization of imaging system and lymphatic tracer for near-infrared fluorescent sentinel lymph node mapping in breast cancer, *Ann Surg Oncol.* 2011 Sep;18(9):2483-91

Hutteman M, Mieog JS, **van der Vorst JR**, Liefers GJ, Putter H, Lowik CW, Frangioni JV, van de Velde CJ, Vahrmeijer AL, Randomized, double-blind comparison of indocyanine green with or without albumin premixing for near-infrared fluorescence imaging of sentinel lymph nodes in breast cancer patients, *Breast Cancer Res Treat.* 2011 May;127(1):163-70.

Hutteman M, Mieog JS, **van der Vorst JR**, Dijkstra J, Kuppen PJ, van der Laan AM, Tanke HJ, Kaijzel EL, Que I, van de Velde CJ, Löwik CW and Vahrmeijer AL, Intraoperative near-infrared fluorescence imaging of colorectal metastases targeting integrin $\alpha\beta 3$ expression in a syngeneic rat model, *Eur J Surg Oncol*, 2011 Mar; 37(3):252-7.

Hutteman M, Choi HS, Mieog JS, **van der Vorst JR**, Ashitate Y, Kuppen PJK, van Groningen MC, Löwik CW, Smit VT, van de Velde CJ, Frangioni JV and Vahrmeijer AL, Clinical Translation of Ex Vivo Sentinel Lymph Node Mapping for Colorectal Cancer using Invisible Near-Infrared Fluorescence Light, *Ann Surg Oncol*, 2011 Apr;18(4):1006-14.

Mieog JS, Hutteman M, **van der Vorst JR**, Kuppen PJ, Que I, Dijkstra J, Kaijzel EL, Prins F, Löwik CW, Smit VT, van de Velde CJ, Vahrmeijer AL, Image-guided tumor resection using real-time near-infrared fluorescence in a syngeneic rat model of primary breast cancer, *Breast Cancer Res Treat*. 2011 Aug;128(3):679-89

van der Vorst JR, van Dam RM, van Stiphout RS, van den Broek MA, Hollander IH, Kessels F, Dejong CH, Virtual Liver Resection and Volumetric Analysis of the Future Liver Remnant using Open Source Image Processing Software. *World J Surg*. 2010 Oct;34(10):2426-33

Mieog JS, Vahrmeijer AL, Hutteman M, **van der Vorst JR**, Drijfhout van Hooff M, Dijkstra J, Kuppen PJ, Keijzer R, Kaijzel EL, Que I, van de Velde CJ, Lowik CW, Novel intraoperative near-infrared fluorescence camera system for optical image-guided cancer surgery. *Mol Imaging*. 2010 Aug;9(4):223-31.

Keereweer S, Kerrebijn JD, van Driel PB, Xie B, Kaijzel EL, Snoeks TJ, Que I, Hutteman M, **van der Vorst JR**, Mieog JS, Vahrmeijer AL, van de Velde CJ, Baatenburg de Jong RJ, Löwik CW, Optical Image-Guided Surgery - Where Do We Stand? *Mol Imaging Biol*. 2011 Apr;13(2):199-207.

***shared first authorship**

CURRICULUM VITAE

Joost Renier van der Vorst werd geboren op 15 maart 1984 in Geldrop. Na het behalen van het VWO-diploma in 2002 aan het Lorentz Casimir Lyceum te Eindhoven startte hij met de studie Geneeskunde aan de Universiteit van Maastricht. Gedurende zijn studie werkte hij mee aan diverse onderzoeken naar leverchirurgie bij de afdeling Heelkunde van het Academisch Ziekenhuis Maastricht onder leiding van Prof. dr. C.H.C. Dejong. Zijn co-assistentenschappen deed hij onder meer bij de afdeling Gynaecologie in het Kalafong ziekenhuis in Pretoria, Zuid-Afrika. In 2009 studeerde hij af. Aansluitend startte hij zijn promotieonderzoek bij de afdeling Heelkunde aan het Leids Universitair Medisch Centrum (promotor: Prof. dr. C.J.H. van de Velde, co-promotor: Dr. A.L. Vahrmeijer) waarvan de resultaten in dit proefschrift zijn beschreven. Gedurende zijn promotieonderzoek werkte hij als research fellow aan het Beth Israel Deaconess Medical Center, Harvard Medical School te Boston, Verenigde Staten, onder leiding van Prof. J.V. Frangioni. Sinds 2010 zit hij in het bestuur van de European Society of Surgical Oncology (ESSO) Young Surgeons Club, waarvan hij sinds 2012 voorzitter is. Sinds 2012 zit hij tevens in het bestuur van de Education and Training Committee van de ESSO. In 2011 verkreeg hij een ZonMw assistent-geneeskunde in opleiding tot klinisch onderzoeker (AGIKO) stipendium. Van januari 2013 tot juli 2013 werkte hij als arts-assistent niet in opleiding (ANIOS) Heelkunde in het Medisch Centrum Haaglanden te den Haag en per 1 juli 2013 is hij in opleiding tot chirurg in het Groene Hart Ziekenhuis te Gouda (opleider: Dr. R.F. Schmitz).

DANKWOORD

Allereerst ben ik alle patiënten die hebben meegewerkt aan de klinische studies zeer dankbaar. De realisatie van dit proefschrift is een *team-effort* geweest en ik wil iedereen die hierbij geholpen heeft hartelijk danken. Er is bij de totstandkoming van dit proefschrift een aantal mensen die ik in het bijzonder wil noemen.

Prof. van de Velde, vanaf onze eerste kennismaking in 2009 was ik onder de indruk van uw drive en doortastendheid. Ondanks de '*hatrick*' van afspraken die ik vergeten ben dank ik u voor uw begeleiding, geduld en de vele deuren die u voor me geopend heeft.

Dr. Vahrmeijer, beste Alexander, je rust, zakelijk inzicht en mensenkennis zijn uitzonderlijk, jij leerde me dat het soms (lees: vaak) verstandiger en effectiever is om om de muur heen te lopen dan er doorheen te willen gaan. Ik blijf me verbazen over hoe je een groep jonge, ongeremde honden elke dag weer op een natuurlijke wijze in het gareel houdt.

Prof. Frangioni, dear John, thank you for the warm welcome and the guidance you gave me during my research fellowship at your lab in Boston, it was a great experience which I will never forget.

Dan bedank ik het Green Team, een begrip in het LUMC, een dynamische groep mannen die ervoor zorgde dat het promoveren voor mij zelfs nog een paar jaar langer had mogen duren.

Sven, pater familias, je energie en vrolijkheid werkte aanstekelijk, dank voor je altijd teambuilde initiatieven. Dat wij samen een nieuw ESSO-hoofdstuk zijn begonnen vind ik schitterend!

Merlijn, Hut, ik heb je zien evolueren van oermens tot *uomo universale*, in slechts 3 jaar! Dat we beiden geen 'normale' promotie hebben gehad en dat dit onze band enkel heeft versterkt ben je ongetwijfeld met me eens. Wat hebben we samen een mooie tijd gehad, dank daarvoor!

Bob, hoewel we totaal verschillende persoonlijkheden zijn, vulden we elkaar uitstekend aan en hebben we jarenlang zij aan zij het fort bewaakt. Ik heb enorm met je gelachen, een hoop prijzen met je uitgedeeld en vond het prachtig om ook in de kliniek een tijd met je te werken.

Floris, begonnen als groene onervaren student, maar ontpopt tot een waardig onderzoeker, leid je nu de J3-104. Wat heb je het allemaal snel voor elkaar gebokst! Succes met je co-schappen en ik hoop snel tot ziens bij de chirurgie.

Rutger-Jan, een jaar heb je als *senior researcher* mogen proeven aan het Green Team, je was een uitstekende aanvulling op de groep en bracht een hoop nieuwe plannen en energie!

Quirijn, Q'tje. Je voldoet met je gigantische drive en neusje voor nieuw mogelijkheden prima aan de *green light criteria*. Ik heb er alle vertrouwen in dat je de klus gaat klaren.

Mark, korporaal, chef pre-kliniek, met jouw vechtlust weet ik zeker dat de pre-kliniek hoogtij zal vieren!

Noor, Charlotte en Hein, alle ogen zijn op jullie gericht nu! Ik vind het mooi om te zien dat de trein onder jullie leiding net zo hard doordendert als toen.

Dit proefschrift is alleen tot stand kunnen komen dankzij hulp van velen. Graag wil ik de volgende groepen mensen bedanken voor hun inzet en hulp: chirurgen, gynaecologen, urologen, KNO-artsen en hun arts-assistenten van het LUMC. Verder dank ik het Heelkunde research lab, mede-promovendi, de proefdierversorgers, anesthesie- en ok-medewerkers, de afdelingen LKEB, Pathologie, Moleculaire Celbiologie, Radiologie en de trial apotheek. Ik dank de co-auteurs voor hun immer kritische blik en nieuwe input.

De assistenten en chirurgen van het Medisch Centrum Haaglanden dank ik voor een schitterend begin van mijn klinische carrière. Het vervolg in het Groene Hart Ziekenhuis is, met dank aan de poli-dames, (SEH)-verpleegkundigen, OK-assistentes, assistenten en chirurgen, een feestje gebleken.

Mijn paranimfen, Jan Ten Bosch, Jantje, wat ben er ik ontzettend trots op hoe je het leven aanpakt en wat heb ik stiekem veel van je geleerd. Ik besef dat de vriendschap die wij hebben meer dan bijzonder is. Het gevoel dat ik, wat er ook gebeurt, altijd op je terug kan vallen is iets dat ik koester. Rick van de Langenberg, Face, de knapste van het stel, mijn *partner in crime*. De zomer van 2007 is een schoolvoorbeeld van wat we samen hebben meegemaakt. Het lijkt alsof de vriendschap alleen nog maar hechter wordt. Thijs van Herpt, T_, jij maakt het viertal compleet, zonder jou geen HS. Elke keer als ik je zie geniet ik weer met volle teugen van je.

Vrienden, jullie zorgen ervoor dat ik altijd met een lach opsta en met een lach ga slapen. Wappie Semi's, Nondejuke, 2003, Koninkies, MELT'13, De échte Boston, 44, Tiki wiki, Lalalalorentz, de Javakade en de ZA posse; ik prijs mezelf elke dag heel gelukkig met zo'n mooie groep mensen om me heen.

Oma, zonder dat je het misschien weet geef je me enorm veel energie. Dat jij me op je 91^e met je iPad nog *facetimes* is op z'n minst bijzonder te noemen. Het is een geruststellende gedachte dat jij tijdens de verdediging achter me zit.

Laurens en Myrthe, heerlijk hebben jullie het samen en daar ben ik als grote (schoon) broer weer intens gelukkig mee. Laus je inzet de laatste 5 jaar laten zien dat je het altijd al in je hebt gehad, ben enorm trots op wat je hebt bereikt.

Papa en mama, het creëren van een veilige thuishaven, waar alles kan en niets teveel is geeft me nog steeds veel rust. Jullie onvoorwaardelijke liefde, steun en vertrouwen betekenen alles voor me. Zonder jullie was ik nooit zo ver gekomen.

